Springer Theses
Recognizing Outstanding Ph.D. Research

Taotao Zou

Anti-Cancer N-Heterocyclic Carbene Complexes of Gold(III), Gold(I) and Platinum(II)

Thiol "Switch-on" Fluorescent Probes, Thioredoxin Reductase Inhibitors and Endoplasmic Reticulum Targeting Agents

Springer

Springer Theses

Recognizing Outstanding Ph.D. Research

Aims and Scope

The series "Springer Theses" brings together a selection of the very best Ph.D. theses from around the world and across the physical sciences. Nominated and endorsed by two recognized specialists, each published volume has been selected for its scientific excellence and the high impact of its contents for the pertinent field of research. For greater accessibility to non-specialists, the published versions include an extended introduction, as well as a foreword by the student's supervisor explaining the special relevance of the work for the field. As a whole, the series will provide a valuable resource both for newcomers to the research fields described, and for other scientists seeking detailed background information on special questions. Finally, it provides an accredited documentation of the valuable contributions made by today's younger generation of scientists.

Theses are accepted into the series by invited nomination only and must fulfill all of the following criteria

- They must be written in good English.
- The topic should fall within the confines of Chemistry, Physics, Earth Sciences, Engineering and related interdisciplinary fields such as Materials, Nanoscience, Chemical Engineering, Complex Systems and Biophysics.
- The work reported in the thesis must represent a significant scientific advance.
- If the thesis includes previously published material, permission to reproduce this must be gained from the respective copyright holder.
- They must have been examined and passed during the 12 months prior to nomination.
- Each thesis should include a foreword by the supervisor outlining the significance of its content.
- The theses should have a clearly defined structure including an introduction accessible to scientists not expert in that particular field.

More information about this series at http://www.springer.com/series/8790

Taotao Zou

Anti-Cancer N-Heterocyclic Carbene Complexes of Gold(III), Gold(I) and Platinum(II)

Thiol "Switch-on" Fluorescent Probes, Thioredoxin Reductase Inhibitors and Endoplasmic Reticulum Targeting Agents

Doctoral Thesis accepted by
The University of Hong Kong, Hong Kong, China

Springer

Author
Dr. Taotao Zou
Department of Chemistry
The University of Hong Kong
Hong Kong
China

Supervisor
Prof. Chi-Ming Che
Department of Chemistry
The University of Hong Kong
Hong Kong
China

ISSN 2190-5053 ISSN 2190-5061 (electronic)
Springer Theses
ISBN 978-981-10-0656-2 ISBN 978-981-10-0657-9 (eBook)
DOI 10.1007/978-981-10-0657-9

Library of Congress Control Number: 2016932333

Printed on acid-free paper

This Springer imprint is published by SpringerNature
The registered company is Springer Science+Business Media Singapore Pte Ltd.

Parts of this thesis have been published in the following journal articles:

1. **Zou**, **T**; Lum, C T; Lok, C-N; Zhang, J-J; Che, C-M, "Chemical biology of anticancer gold(III) and gold(I) complexes", *Chem. Soc. Rev.*, **2015**, 44, 8786–8801.
2. **Zou**, **T**; Lum, C T; Lok, C-N; To, W-P; Low, K-H; Che, C-M, "A binuclear gold(I) complex with mixed bridging diphosphine and bis(N-heterocyclic carbene) ligands shows favorable thiol reactivity and inhibits tumor growth and angiogenesis in vivo", *Angew. Chem. Int. Ed.*, **2014**, 53, (23), 5810–5814.
3. **Zou**, **T**; Lum, C T; Chui, S S-Y; Che, C-M, "Gold(III) complexes containing N-heterocyclic carbene ligands: thiol "switch-on" fluorescent probes and anti-cancer agents", *Angew. Chem. Int. Ed.*, **2013**, 52, (10), 2930–2933.
4. **Zou**, **T**; Lok, C-N; Fung, Y M E; Che, C-M, "Luminescent organoplatinum(II) complexes containing bis(N-heterocyclic carbene) ligands selectively target the endoplasmic reticulum and induce potent photo-toxicity", *Chem. Commun.*, **2013**, 49, (47), 5423–5425.

Supervisor's Foreword

This thesis describes the scientific achievements of Dr. Taotao Zou, which were made during his doctoral program in Department of Chemistry, the University of Hong Kong. Dr. Zou has achieved outstanding research outputs on metal-based medicines during his Ph.D. studies. He has done exceptional works in the areas of bioinorganic chemistry and anticancer metal medicines; particularly his works on anticancer gold(III), gold(I), and platinum(II) complexes would have long-lasting impact. As his Ph.D. supervisor, I like to introduce two important findings from his doctoral work. One is the first use of the strategies of gold(III) to gold(I) reduction to develop fluorescent thiol "switch-on" probes and anticancer gold(I) prodrugs/precursors, and the other is the development of a dinuclear gold(I) complex to combat cancers in vivo with minimal side effects.

The reduction of 4-coordinated Au^{3+} to 2-coordinated Au^{+} by thiols is well documented in the literature. Owing to the low-energy $5d_{x^2-y^2}$ orbital of Au^{3+}, most gold(III) complexes are non-emissive in solutions. By taking the advantage of these properties of Au(III) complexes, Dr. Zou has synthesized a class of non-emissive Au(III) complexes containing highly fluorescent N^N^N and NHC ligands. In these complexes, the NHC ligand could stabilize the reduced Au(I) species from further reduction to Au(0). The $[Au^{III}(N^N^N)(NHC)]^{+}$ complex was readily reduced by GSH to form $[Au^{I}(NHC)(GS)]$, accompanied by the release of the fluorescent $H_2N^N^N$ ligand, therefore acting as a fluorescent "switch-on" probe for thiols. In addition, the anticancer activity of Au(I) is attributed to its ability to inhibit thiol enzymes; thus, the Au(III) complexes could also serve as precursors/prodrugs, activated by metal reduction, to deliver anticancer active Au(I) species.

The major shortcoming of most anticancer active Au(I) complexes is the lack of in vivo antitumor activity due to their high thiol reactivity which leads to many off-target binding interactions with blood thiols. Dr. Zou prepared a dinuclear gold(I) complex bearing mixed diphosphine and bis(NHC) ligands. This dinuclear Au(I) complex displays a favorable stability that conveys potent thioredoxin reductase inhibition without being attacked by blood thiols. This complex significantly inhibited tumor growth in two independent mouse models with no

observable side effects. The dinuclear Au(I) complex also exhibited antiangiogenesis activity in a tumor model and inhibited sphere formation of cancer stem cells in vitro. In toxicology studies, neither systemic anaphylaxis in guinea pigs nor localized irritation in rabbits was observed.

The findings from both projects have been published in the top journal *Angew. Chem. Int. Ed.* with one highlighted as a very important paper. I hope that these research works could stimulate more researchers to work on and push anticancer gold complexes to clinical status.

Hong Kong, China
December 2015

Prof. Chi-Ming Che

Acknowledgments

First of all, I would like to show my greatest appreciation to my supervisor, Prof. Chi-Ming Che, a nice, patient, wise, creative, and hard-working pioneer in the field of inorganic chemistry. It is he that opened my door to the area of bioinorganic chemistry. He is easily accessible and talked with me quite frequently. I am sure he has influenced and will influence my whole life.

Special thanks to Prof. Raymond Wai-Yin Sun, Dr. Chun-Nam Lok, and Dr. Jie-Sheng Huang. Professor Sun initiated my research and gave me many helpful suggestions. Dr. Lok is an excellent bioexpert who has taught me a great deal of bioknowledge and designed most of the bioassays; he has also assisted to revise my publications. Dr. Huang is a careful and unselfish teacher who has taught me how to write excellent papers and also helped to revise the papers.

Another person I would like to thank is Dr. (Michelle) Ching Tung Lum. Dr. Lum assisted to conduct most of the animal studies and also taught me the mouse experiment. She is also very helpful in the biological studies as well as in the daily life.

Dr. Yungen Liu and Dr. (Kevin) Wai-Pong To helped me solve lots of problems I met during the synthesis works. Dr. Kam-Hung Low and Stephen Sin-Yin Chui have helped me perform the single crystal X-ray diffraction analysis. Dr. Yi Man Eva Fung and Dr. Kwan-Ming Ng have assisted to carry out high-resolution mass spectrometry analyses. I do appreciate their kind help.

I will also thank other labmates: Dr. Wai-Lun Kwong, Dr. Kai Li, Dr. Jing-Jing Zhang, Dr. Iris Wing-Shan Lin, Dr. Songhai Tian, Ms. (May) Sin Ki Fung, Mr. (Ken) Ka-Chung Tong, Dr. Tommy Tsz-Him Fong, Dr. Faisal Mehmood, Ms. Di Hu, Mr. Chen Yang, Dr. Vanessa Kar-Yan Lo, Dr. (Jessica) Kar-Yee Lam, Mr. (Kelvin) Chun-Wai Tse, Dr. Annapureddy Rajasekar Reddy, Dr. Siu-Man Law, Mr. Wai-Man Chan, Mr. Ka-Pan Shing, Dr. Anna On-Yee Chan, Mr. Lui Lui Tsai, Ms. Yin Ming Ng, Ms. Pui Ki Wan. Dr. (Andy) Faan-Fung Hung, Dr. Xinshan Xiao, Dr. Xiaoyong Chang, Dr. Pui Keong Chow, Dr. Glenna So Ming Tong, and all other members in Prof. Che's group. Their kind accompany, friendly talk, and good advices have impressed me so much in these years.

Finally, my sincere thanks will be devoted to my family. My parents supported my Ph.D. study just as what they have done during the past twenty more years. I do hope they will keep in good health forever. My wife, Ms. Bei Cao who I married during Ph.D. study, should be awarded with my deepest appreciation. Her accompany, encouragement, and tolerance have contributed to my successful accomplishment of Ph.D. study.

Contents

Chapter 1
Introduction

1.1 Inorganic Medicines

Inorganic chemistry plays an essential role in human life. As depicted in Fig. 1.1, there are 24 known essential elements, but the possible biological roles of some other elements (e.g., Cr, B) in life science remain to be understood. For those bioactive metal ions, their biological properties can be significantly affected by their coordinating ligands. Similarly, the biological activities of metallodrugs are affected both by the metal ion and by the coordinating ligand(s). Coordination of appropriate ligand(s) to metal ions can adjust the reduction potentials and/or ligand exchange reactions with biomolecules, thereby regulating the important biological processes. In general, the binding interactions between metallodrug and biomolecules can be categorized into the following two types: (i) non-covalent interactions (i.e., hydrogen bonding and van der Waals interaction) with bond energies below 60 kJ mol^{-1} and (ii) covalent bonding interactions or, more exactly, coordination bonding interactions with bond energies of 50–150 kJ mol^{-1}, which are lower than that of organic covalent bonds (C–C bond is 300–400 kJ mol) [1].

While organic drugs usually obey Lipinski's rule of five, there have not been many examples of inorganic drugs closely adhering to this rule. In most cases, inorganic drugs are considered as prodrugs, usually undergoing redox reactions or ligand exchange reactions prior to affecting their biomolecular target(s). In this regard, knowledge on the thermodynamics and kinetics of the reactions of metallodrugs in biological media is beneficial in elucidating their mechanisms of action(s).

Presently, there are examples of inorganic medicines clinically used to treat diseases. These therapeutics include platinum and arsenic compounds used in the treatment of cancers; compounds of silver, bismuth, mercury, and antimony for treating infectious diseases; and compounds of gold and manganese to treat arthritis.

T. Zou, *Anti-Cancer N-Heterocyclic Carbene Complexes of Gold(III), Gold(I) and Platinum(II)*, Springer Theses, DOI 10.1007/978-981-10-0657-9_1

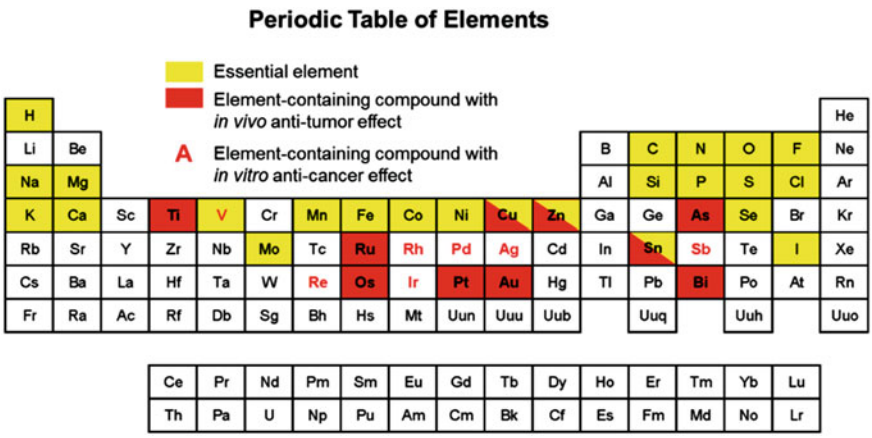

Fig. 1.1 Periodic table showing the essential elements and element-containing compounds with anticancer activities

The most seminal contribution of inorganic drugs was reported by Rosenberg and coworkers on the anticancer activities of cisplatin [*cis*-diamminedichloridoplatinum(II)] in the 1960s. Nowadays, new cisplatin derivatives have been widely used to treat many cancers such as ovarian cancer, lymphomas, and testicular cancer. In particular, the cure rate for testicular cancer was reported to increase from 10 to ~85 % after cisplatin treatment [2]. However, wide application of cisplatin is hampered by acquired or intrinsic resistance as well as side effects. Arsenic trioxide is another successful anticancer drug used to treat acute promyelocytic leukemia with a cure rate exceeding 80 % when used in combination with all-*trans*-retinoic acid [3]. An orally active formulation of arsenic trioxide has been developed [4]. Ruthenium-containing drugs, including NAMI-A and KP1019, are now in clinical trials with promising prospects since dose-dependent toxicity has not been observed [5]. Titanium-based drugs such as $[Cp_2TiCl_2]$ and budotitane previously entered into clinical trial studies, but the outcomes were not satisfactory because of the formulation problems and/or suboptimal drug responses [6]. Other promising anticancer agents with in vivo antitumor properties (Fig. 1.2) include complexes of gold (e.g., gold(III)-porphyrin [7], $[Au^{I}(dppe)_2]^+$ [8]), osmium (e.g., organometallic half-sandwich $[Os^{VI}(N)(sap)(OH_2)Cl]$ [9]), tin (IST-FS 35 [10]), gallium (Ganite®, $Ga(NO_3)_3$ [11]), copper ($[Cu(N^S)Cl_2]$ [12]), zinc (ZnHPT [13]), bismuth ($Bi(DEDT)_3$ [14]), and molybdenum (polyoxomolybdate, PM-8 [15]).

In general, drug development follows the following protocol: drug design, synthesis, in vitro cytotoxicity evaluation, mechanism studies, in vivo animal studies, and phase I–III clinical trials (Fig. 1.3). This thesis was aimed at the study of gold(III)-, gold(I)-, and platinum(II) complexes, which are anticancer active. The ultimate objective is to develop effective, metal-based, antitumor agents through rational design, in vitro cytotoxicity evaluation, mechanism studies, and in vivo antitumor studies in animal models.

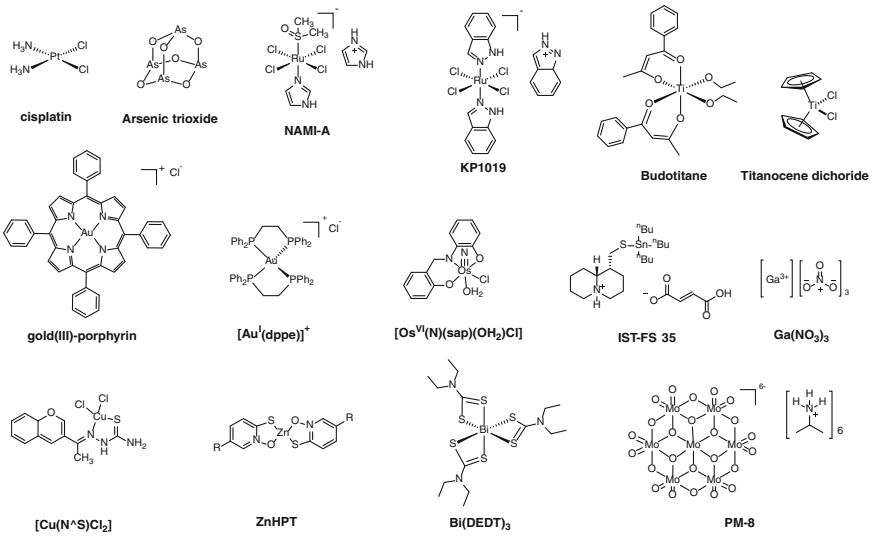

Fig. 1.2 Inorganic anticancer agents with promising in vivo antitumor effects

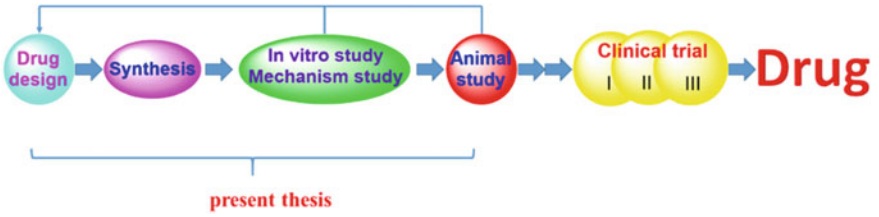

Fig. 1.3 General processes involved in drug development

1.2 Lessons from Cisplatin and Its Derivatives

1.2.1 Overview of Platinum Drugs

Cisplatin was first discovered by Michele Peyrone in 1845, but its therapeutic application was not revealed until more than 100 years later by Rosenberg and coworkers when this group occasionally observed that the electrolyzed products from a platinum electrode inhibited the division of *Escherichia coli* [16]. In 1969, Rosenberg et al. reported that this platinum compound could potently inhibit tumor growth in animal models [17]. Subsequent clinical trials quickly pushed cisplatin toward approval for anticancer treatment by US Food and Drug Administration (FDA) in 197 [18]. In order to decrease the side effects of cisplatin, second-generation (carboplatin, nedaplatin) and third-generation (oxaliplatin, lobaplatin, heptaplatin) derivatives of cisplatin have been developed and now used

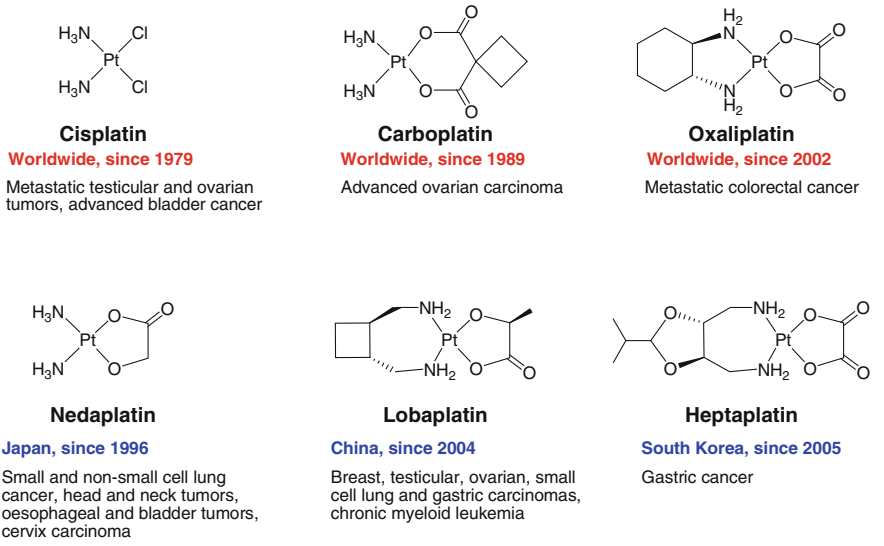

Fig. 1.4 Structures and applications of anticancer platinum drugs

worldwide (Fig. 1.4). The use of less labile bidentate dicarboxylic ligands renders the platinum compounds more stable, thereby reducing the dose-limiting toxicity of cisplatin. Besides enhanced stability, the third-generation platinum compounds possess modified amine groups that can overcome, at least partly, drug resistance issues. Indeed, oxaliplatin can be used to treat some cisplatin-/carboplatin-resistant cancers and some relapsed or refractory cancers [19].

In addition, several new derivatives of platinum compounds are present in clinical trial studies (Fig. 1.5). For example, picoplatin, containing 2-methyl pyridine group, was found to display reduced binding affinity toward intracellular glutathione (GSH). Thus, this compound may overcome the drug resistance caused by the increased intracellular thiol concentrations. Cationic, trinuclear triplatin tetranitrate compounds show higher cellular uptake and higher binding affinity toward DNA than cisplatin. Satraplatin is a Pt(IV) compound. It is less reactive and is suitable for oral administration. When present in blood, this Pt(IV) complex is reduced to the reactive Pt(II) species. Satraplatin, in combination with other anticancer drugs, has entered into various phases of clinical trials.

1.2.2 Anticancer Mechanism of Cisplatin

The generally accepted mechanisms of the anticancer action of cisplatin involve four parts: cellular uptake, activation by aquation, binding of Pt(II) with guanine of DNA, and DNA damage-associated apoptosis (Fig. 1.6).

Fig. 1.5 Anticancer platinum agents that are currently in clinical trial studies

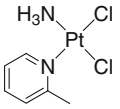

Picoplatin

Plase III: Refractory or resistant small cell lung cancer
Plase II: Metastatic colorectal cancer
Plase II: Metastatic castration-resistant prostate cancer
Plase II: Refractory or resistant ovarian cancer

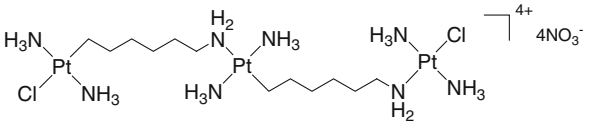

Triplatin tetranitrate

Plase II: Gastric and oesophageal adenocarcinoma

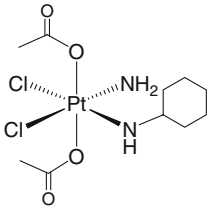

Satraplatin

Phase II: Metastatic castraterefractory prostate cancer
Phase II: Metastatic androgenindependent prostate cancer

Cisplatin enters into cancer cells through passive diffusion or, more likely, through cellular transporters such as copper transporter 1 (CTR1) and organic cation transporters (OCTs) [20]. A decrease of CTR1 expression has been correlated with lower cellular cisplatin accumulation in ovarian cancer cell lines, and this was attributed to acquired resistance problems [20]. Meanwhile, the increased expression of copper efflux transporters (ATP7A and ATP7B) was also suggested to be associated with drug resistance, suggesting that these molecules may be involved with the export of intracellular cisplatin [20].

After entering cells, cisplatin undergoes stepwise hydrolysis to form $[Pt(NH_3)_2(OH_2)_2]^{2+}$ due to the lower concentration of intracellular chloride ions. The hydrolyzed $[Pt(NH_3)_2(OH_2)_2]^{2+}$ has a low lipophilicity and hence cannot readily diffuse out of the cells, allowing it to bind to its targets (primarily DNA). If cisplatin

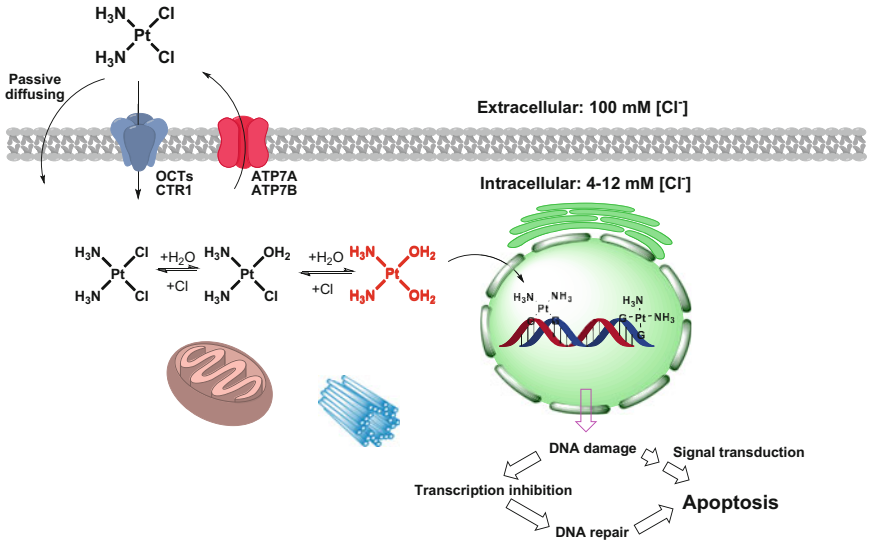

Fig. 1.6 A brief summary of anticancer mechanisms of action of cisplatin

hydrolyzes too early, e.g., forming $[Pt(NH_3)_2(OH_2)_2]^{2+}$ in the blood, it will bind to serum proteins, which will hamper effective uptake at the tumor sites.

$[Pt(NH_3)_2(OH_2)_2]^{2+}$ can covalently bind to guanine (N7) of DNA and, to a lesser extent, adenine; such binding interaction(s) will destabilize, distort, and unwind the DNA structure. Cisplatin preferentially forms intrastrand 1,2-cross-links rather than interstrand cross links (Fig. 1.7). Patients treated with cisplatin were found to have 60–65 % 1,2-d(GpG), 20–25 % 1,2-d(ApG), ~2 % 1,3-d(GpXpG), ~2 % monofunctionalized adduct of G, and ~2 % interstrand G–G cross-linking with platinum [18, 21].

Binding of Pt(II) ions with DNA will activate a variety of signal-transduction pathways, including cell cycle arrest, DNA damage recognition and repair, and finally apoptosis initiation.

Adenine has a structure similar to guanine, raising the question as to why cisplatin prefers to bind guanine N7 rather than adenine N7. Based on density functional theory (DFT) calculations, the strong hydrogen bond between an ammine (or water, as the hydrogen bond donor) of Pt and O6 (acceptor) of guanine stabilizes the Pt–N7 bond of the Pt–G adduct. Formation of a hydrogen bond between an ammine (or water) of Pt and amine at C6 of adenine is energetically unfavorable in the product (Fig. 1.8a–d) and in the transition state (Fig. 1.8e) [22]. Meanwhile, a strong orbital interaction between the unfilled $5d_{x^2-y^2}$ of Pt and the N7 lone electron pair of guanine O6 has been shown [22]. As a result, cisplatin can bind more favorably to the N7 of guanine both thermodynamically and kinetically, which is consistent with the findings of a number of experiments [23–26].

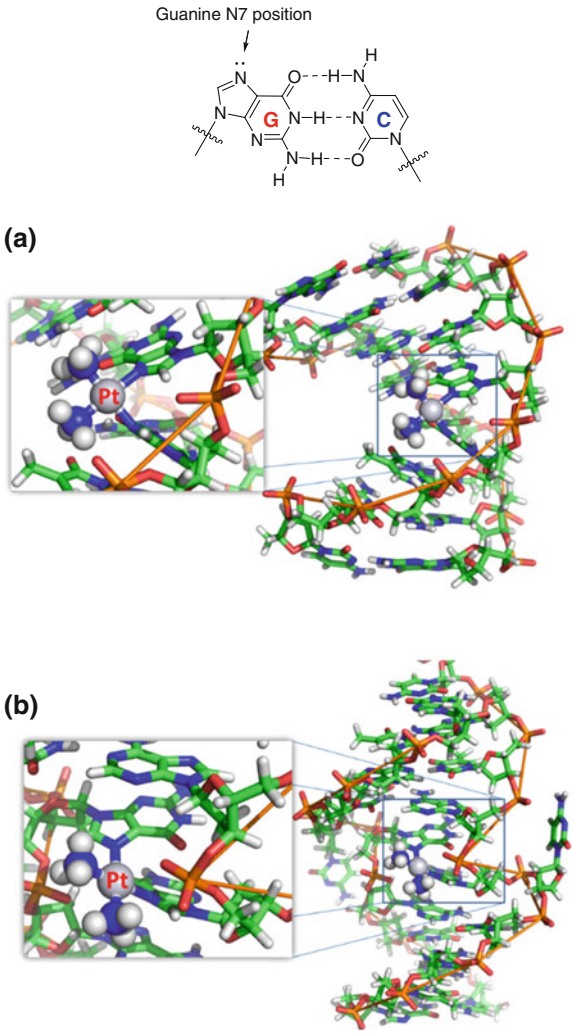

Fig. 1.7 Binding of platinum drugs with DNA at the N7 of guanine. **a** Binding of cisplatin with 1,2-d(GpG) (PDB code: 1AU5). **b** Binding of cisplatin with interstrand GG (PDB code: 1DDP)

In addition to DNA, the interaction of cisplatin with proteins is an important consideration. Pt(II) ions tend to bind soft base atoms such as sulfur (i.e., the sulfur atoms in cysteine and methionine); however, cisplatin is observed to exhibit Pt–N binding rather than Pt–S binding. Does Pt–S binding play an important role in the anticancer mechanism of action? In fact, once administrated to animals or humans, cisplatin is exposed to cysteine-containing proteins in blood and on cell membranes as well as intracellular peptides/proteins that contain cysteine/methionine residues. This would permit the rapid formation of Pt–S bonds prior to entering the tumor cell nucleus. Based on competition studies, Pt was found to be easily transferred from Pt–S adducts to guanine (N7) of DNA. The half-life of Pt–N7 binding is a few

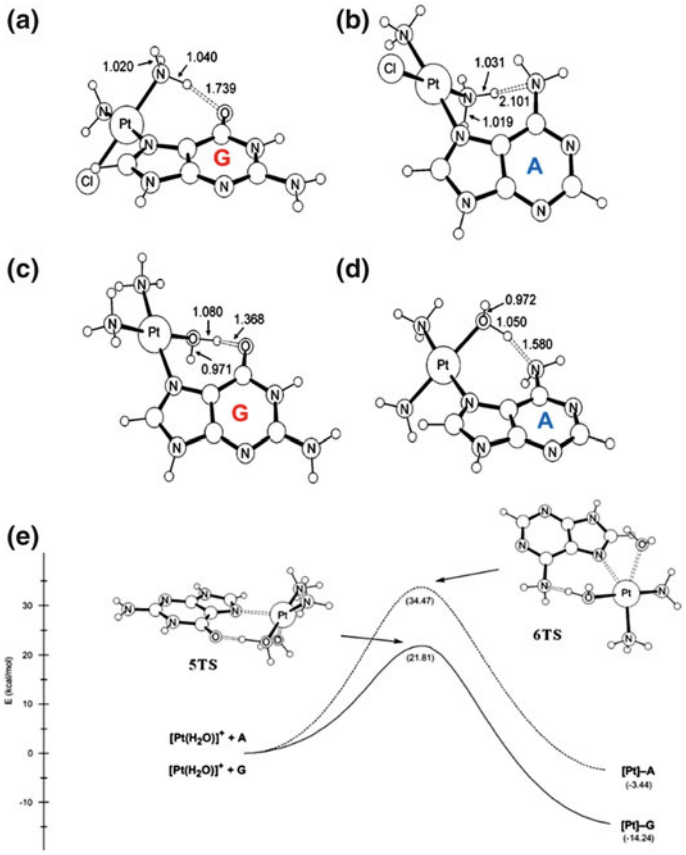

Fig. 1.8 Interaction between the hydrolyzed product of cisplatin and guanine or adenine. *cis*-$[Pt(NH_3)_2Cl(H_2O)]^+$ binds to **a** guanine or **b** adenine, and *cis*-$[Pt(NH_3)_2(H_2O)_2]^{2+}$ binds to **c** guanine or **d** adenine. The ammine forms a stronger hydrogen bond with guanine than with adenine as revealed by the hydrogen bond length. **e** Comparison of the reaction profile between *cis*-$[Pt(NH_3)_2(H_2O)_2]^{2+}$ and A or G. Reproduced with permission [22]. Copyright© 2003, American Chemical Society

hours, which is long enough to ensure that Pt remains in the nucleus so as to affect important cellular processes such as DNA replication and repair. Thus, the reaction between S atoms and Pt(II) is kinetically favored, while Pt–N interaction is thermodynamically favored; platinum-protein binding via a Pt–S bond is more likely to be involved prior to the ultimate platinum–DNA-binding interaction [27].

Notably, the exact target/mechanism of cisplatin remains elusive. Besides targeting DNA, cisplatin was also reported to trigger cell apoptosis independent of DNA damage. For example, Shoshan and coworkers reported that cisplatin could target the endoplasmic reticulum (ER) and induce ER stress, which could activate ER-specific caspase 12 and trigger cell apoptosis [28]. Dimanche-Boitrel and

coworkers found that cisplatin could trigger the redistribution of death receptor CD95 into the lipid rafts of plasma membranes, leading to CD95-mediated cell death [29].

1.2.3 Transplatin and Its Analogues

It is noteworthy that *trans*-dichlorodiammineplatinum(II) (transplatin) is inactive toward cancer cells. The inactivity of transplatin is mainly due to the ligand *trans*-effect together with altered binding interactions of Pt(II) with biomolecules: (1) Transplatin can significantly bind to serum albumin in the blood, while cisplatin shows lower binding affinity; (2) transplatin can readily form a monofunctional adduct with DNA, but its conversion into a bifunctional adduct is less efficient; (3) the monofunctional adduct between transplatin and DNA cannot be recognized by high mobility group (HMG) proteins, but the recognition of cisplatin bound DNA (specially for 1,2-GG intrastrand cross-link) by these proteins is a pivotal mechanism accounting for the cytotoxicity of cisplatin [30].

Interestingly, replacement of ammine by organic amines or bulky amine/imine resulted in anticancer active *trans*-platinum complexes having in vitro cytotoxicity comparable to cisplatin [30]. Figure 1.9 depicts some of the reported anticancer active *trans*-platinum complexes containing aromatic or aliphatic amine ligands. Unlike simple transplatin, these anticancer active *trans*-platinum complexes display different biological properties possibly owing to the steric effects of coordinated amine ligand(s) (and hence affecting the kinetics/thermodynamics). For example, the serum albumin-binding profile of *trans*-platinum analogues may be similar to cisplatin but with lower binding affinity. Active *trans*-platinums can form bifunctional interstrand cross-links with conformations similar to cisplatin-like DNA interstrand cross-links. In addition, *trans*-platinum analogues can induce DNA-protein linkages as in the example of ternary topoisomerase-Pt-DNA

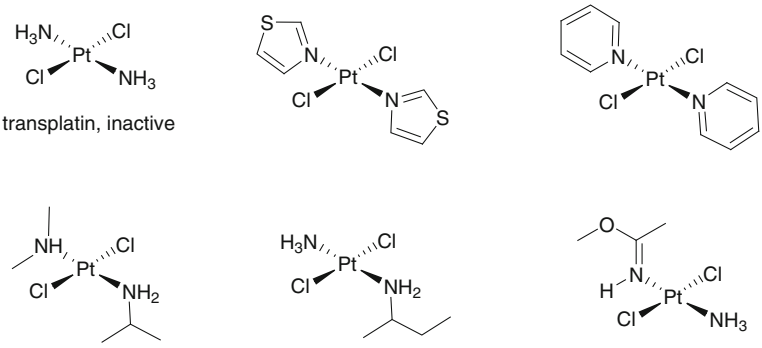

Fig. 1.9 Transplatin and its anticancer active analogues

formation, leading to a different cell death pathway than that of cisplatin. Recently, *trans*-platinum complexes have also been found to target zinc fingers proteins [31].

1.2.4 Cisplatin Resistance and Side Effect Problems

One major problem hampering the wide application of cisplatin is drug resistance (either acquired or intrinsic). Ultimately, drug resistance is caused by inadequate binding of cisplatin to DNA and/or failure to trigger cell death after DNA binding. The former can be attributed to the following: (1) low expression of the transporter (s) responsible for cisplatin uptake (especially copper transporter); (2) non-specific binding of cisplatin with cellular cysteine (including the abundant glutathione)- and methionine (e.g., metallothionein)- containing peptides/proteins; (3) active cisplatin export by the ATP-dependent glutathione S-conjugate export pump (GS-X pump) and copper exporters such as ATP7A and ATP7B (Fig. 1.10).

Of equal importance is the side effect issue. For many cancers, patients may only respond partially toward cisplatin but with severe side effects, including nephrotoxicity, neurotoxicity, toxicity toward sensory systems, emetogenicity, and immunological side effects, thus limiting the usage of high treatment dosages.

Currently, various strategies are being developed to resolve these problems such as by using nanotechnologies to deliver platinum drugs or the development of new generation of platinum drugs. Metal complexes with anticancer mechanisms of

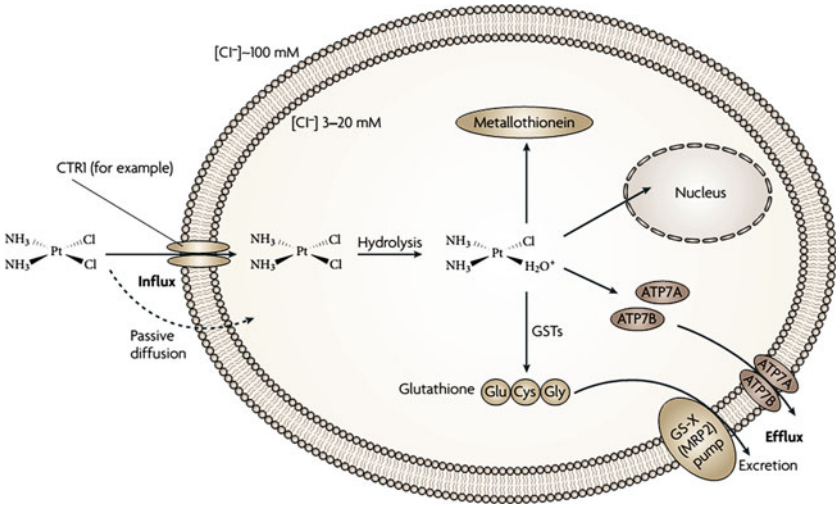

Fig. 1.10 Resistance of cisplatin due to inadequate delivery of active Pt(II) species to the molecular target. Reproduced with permission [18]. Copyright© 2007, Nature Publishing Group

action other than DNA targeting are also emerging as alternative metal-based medicines able to tackle the problems of drug resistance and side effects seen in cisplatin therapy.

1.3 The Chemistry and Anticancer Properties of Gold

1.3.1 The Chemical Properties of Gold Complexes [32]

The physiologically accessible oxidation states of gold are 0, +1, and +3. Colloidal gold and gold(I) complexes are well-known therapeutic agents. Recently, gold nanoparticles have been widely studied as drug nanocarriers. The +1 oxidation state is by far most widely investigated in gold chemistry, owing to the broad applications of gold(I) complexes in materials science, catalysis, and medicinal chemistry. The Au^{3+} ion is not biologically stable because of its high reduction potential; however, its stability can be significantly increased if strong electron-donating and/or multidentate ligands are used.

1.3.1.1 Gold(I) Complexes

Gold(I) complexes are usually two-coordinated and tend to aggregate through intermolecular gold(I)–gold(I) interactions (aurophilicity; bond strength is similar to that of a hydrogen bond), forming dimers, trimers, and even polymers.

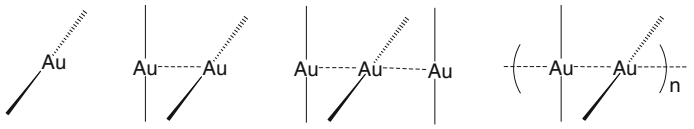

The auxiliary ligands include phosphine (P), thiolate (S^-), cyanide (CN^-), N-heterocyclic carbene (NHC), halide (X^-), carbanion (C^-), various N-ligands, and others. Polynuclear complexes can be obtained by using multidentate ligands.

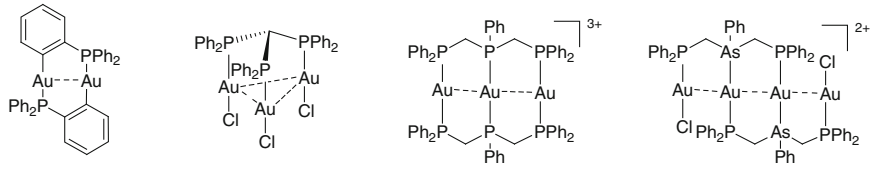

There are many examples of three- and four-coordinated gold(I) complexes which are stable.

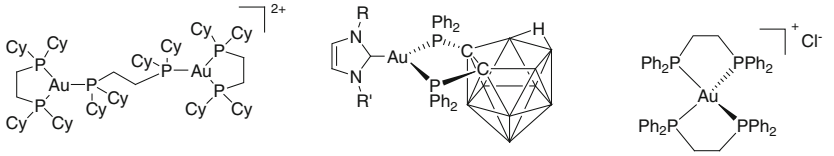

[Au(THT)Cl] (THT = tetrahydrogen thiophene) and [Au(DMS)Cl] (DMS = dimethyl sulfide) are precursors usually used in the synthesis of gold(I) complexes. These precursors can be obtained from the reduction of gold(III) salts:

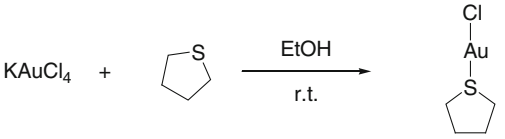

1.3.1.2 Gold(III) Complexes

The Au^{3+} ion is four-coordinated and has a high reduction potential. In the literature, most of the anticancer active gold(III) complexes are coordinated with multidentate N-ligands or ligands having strong electron-donating C-donor atom(s) (see the following figure). Gold(III) complexes containing other ligands with P, S, and even O donor atoms can be stable.

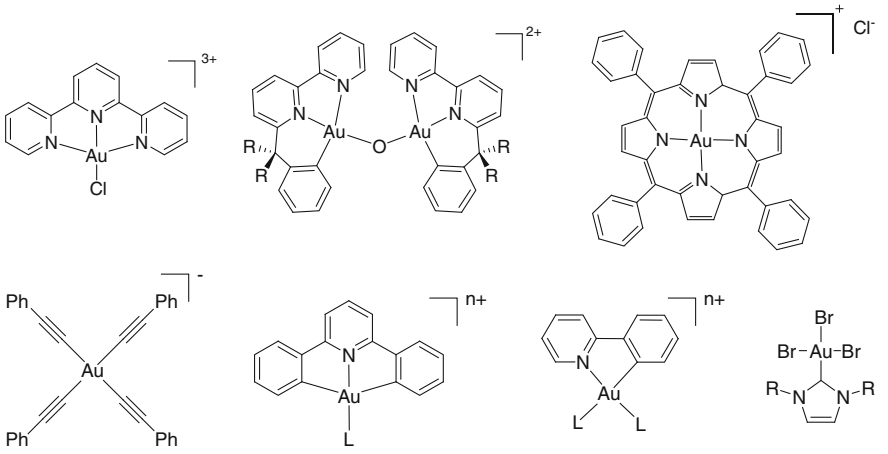

Gold(III) complexes are usually prepared by the following methods

1. Transmetalation with mecury(II) precursors.

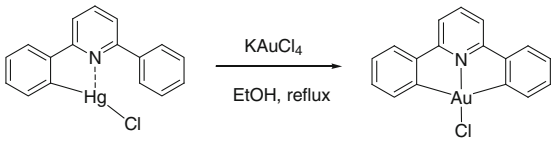

2. Direct electrophilic substitution reactions with gold(III) salts

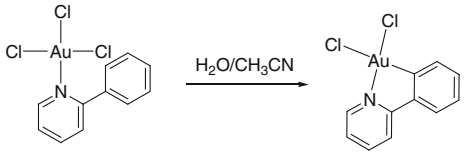

3. Ligand substitution reactions.

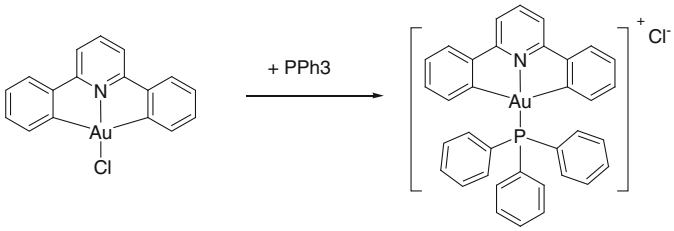

4. Oxidation of gold(I) complexes

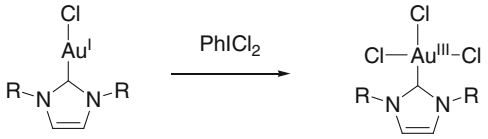

1.3.2 Gold Complexes Inhibit Thiol-Containing Enzyme Activities

In biological systems, both Au^{+} and Au^{3+} ions prefer to bind to soft, SH-/SeH-containing peptides/proteins. As many important biological processes, such as redox balance and protein degradation, are regulated by enzymes having cysteine/selenocysteine (Cys/Sec) residues in their active sites, both substitution reactive gold(I) complexes and gold(III) complexes could serve as inhibitors by blocking the active cysteine residues. Biological enzyme/proteins having cysteine thiols in the active site include redox enzymes (e.g., thioredoxin reductase, glutathione reductase, glutathione peroxidase), cysteine proteases (e.g., cathepsin,

caspase), transcription factors (e.g., NF-κB, IKK), deubiquitinases, and membrane water/glycerol channel protein (aquaporin 3) [33, 34]. These enzymes are often overexpressed in cancer cells; thus, the inhibition of their activities could be promising therapeutic strategies for cancer treatment. Currently, direct structural evidence showing the binding interaction of gold(I) complexes with thiol enzymes is indeed present in the literature.

1.3.2.1 Inhibition of Disulfide Reductase

Glutathione reductase (GR) and thioredoxin reductase (TrxR) are two key enzymes that regulate cellular redox balance-associated cell growth [35]. Both enzymes contain cysteine thiols (TrxR also contains selenocysteine) in the redox-active sites. Various gold(I) complexes have been identified to potently inhibit TrxR activity with IC_{50} values in the low nanomolar range. The first crystal structure of a gold–GR adduct was reported by Becker and coworkers in 2006 [36]. Two nearly linear S_{cys}–Au^{I}–S_{cys} coordinations and S_{cys}–Au^{I}–$P_{phosphole}$ coordinations have been identified by crystallography (Fig. 1.11). Later, crystal structures of other disulfide reductase-gold adducts were solved, showing similar binding interactions (e.g., thioredoxin–glutathione reductase with auranofin [37] (Fig. 1.12) and

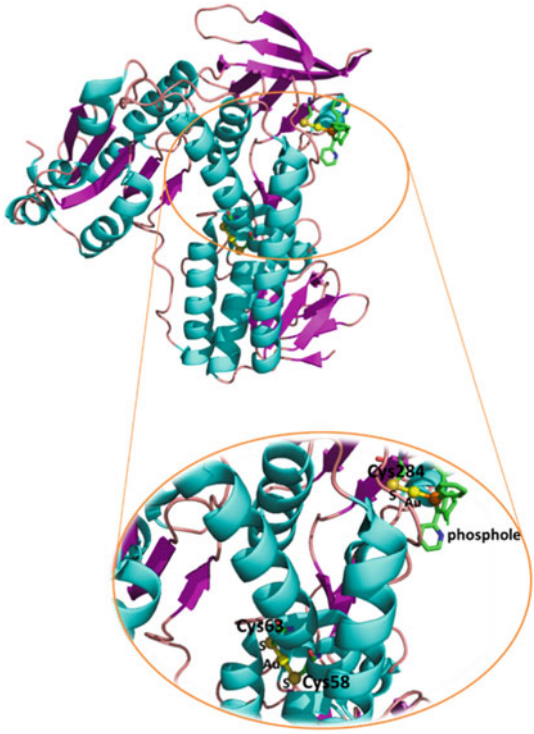

Fig. 1.11 Crystal structure of GR bound to gold–phosphole. PDB code: 2AAQ [36]

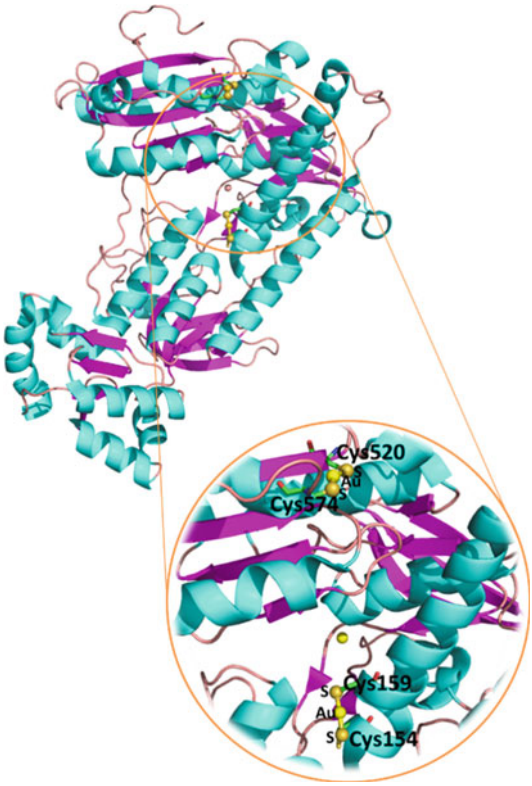

Fig. 1.12 Crystal structure of TGR bound to a Au^+ ion. PDB code: 3H4 K (Au^+ was from auranofin) [37]

trypanothione reductase with auranofin [38] (Fig. 1.13). The inhibition of such enzymes was confirmed by enzyme assays [33, 34]. These crystal structures lend strong support to the claims that gold(I) complexes can serve as tight-binding inhibitors of disulfide reductases via formation of a covalent Au–S bond in the active site.

In the literature, the selenium-containing TrxR is the most widely investigated anticancer target of gold(I) complexes. This is attributed to the low pK_a value of Se. TrxR is a flavoenzyme (containing FAD) that functions as a homodimer (Fig. 1.14a, Rat TrxR hexamer, PDB code: 3EAN [39]). The C-terminal active site (–Se–S–) can be reduced to –SeH, –SH by NADPH; the reduced TrxR then reduces Trx which can further reduce protein disulfide (Fig. 1.14b, c). Notably, TrxR is mainly localized in the cytosol (TrxR1) as well as in the mitochondria (TrxR2) and is the only enzyme that can reduce Trx.

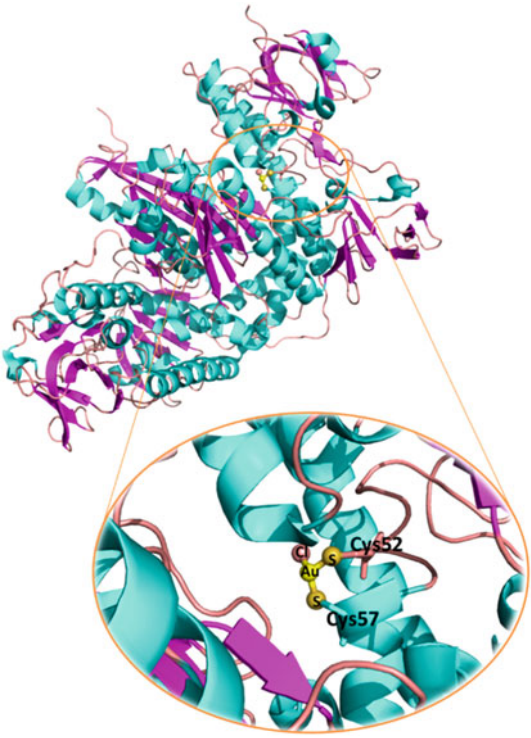

Fig. 1.13 Crystal structure of TR bound to a Au^{+} ion. PDB code: 2YAU. (Au^{+} was from auranofin) [38]

1.3.2.2 Inhibition of Cysteine Protease

Besides acting as redox regulators, cysteine thiols can also act as nucleophiles upon deprotonation. For example, cathepsin cysteine protease contains a cysteine thiol in the active site that is involved in protein turnover in the lysosome [33]. The catalytic mechanism of action is depicted below. The adjacent histine could deprotonate –SH to give nucleophilic $–S^{-}$. In the literature, auranofin and gold thiomalate were reported to significantly inhibit the activities of cathepsin K and S [33]. The crystal structure of the gold thiomalate–cathepsin K adduct shows a linear S_{cys}–Au^{I}–$S_{thiomalate}$ coordination, where the thiomalate group is stabilized by the surrounding amino acids via formation of hydrogen bonds with the thiomalate group (Fig. 1.15).

1.3.2.3 Inhibition of Other Thiol-Containing Enzymes

Protein tyrosine phosphatase. Similar to cysteine proteases, protein tyrosine phosphatase (PTP) also contains, in its catalytic site, a nucleophilic cysteine that is

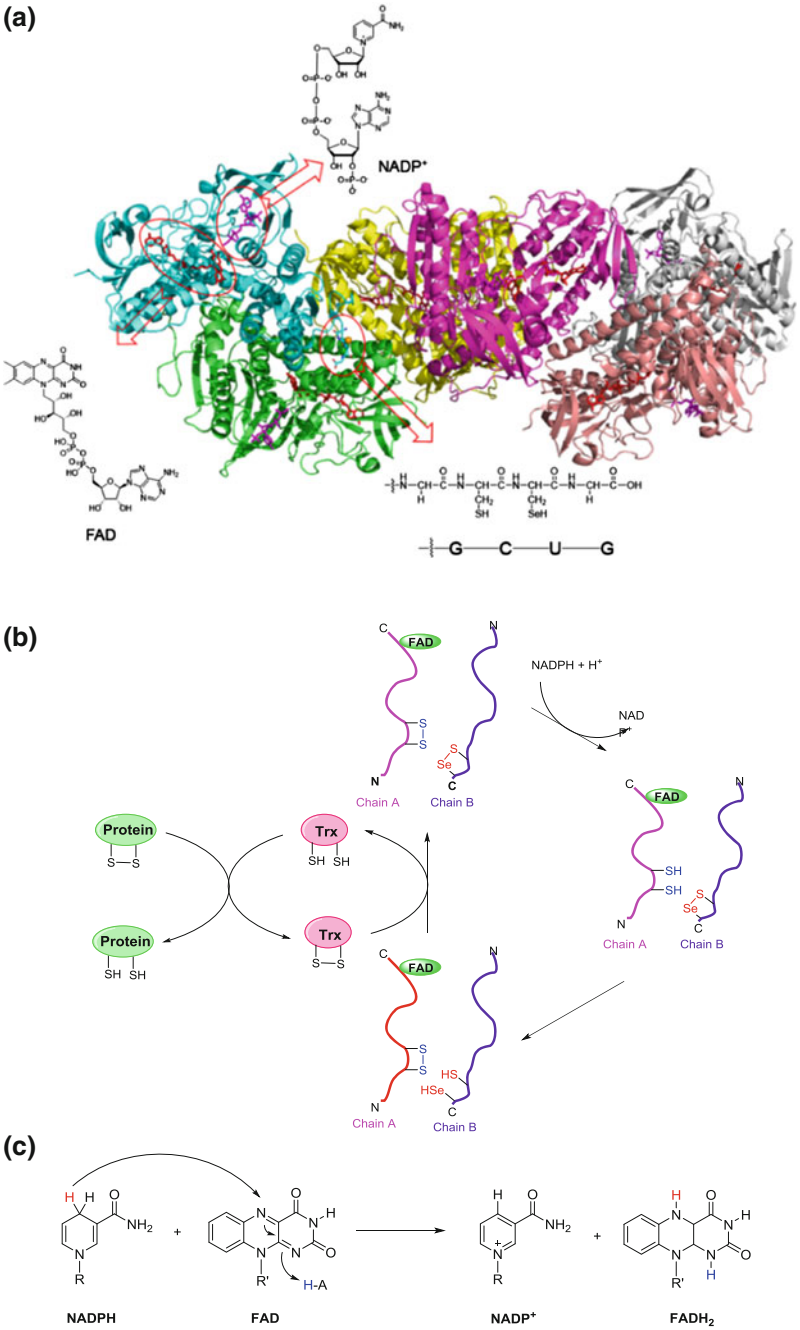

Fig. 1.14 **a** Crystal structure of TrxR containing FAD and $NADP^+$ cofactors. **b** Catalytic cycle of NADPH–TrxR–Trx oxidoreduction. **c** Reaction of NADPH with FAD

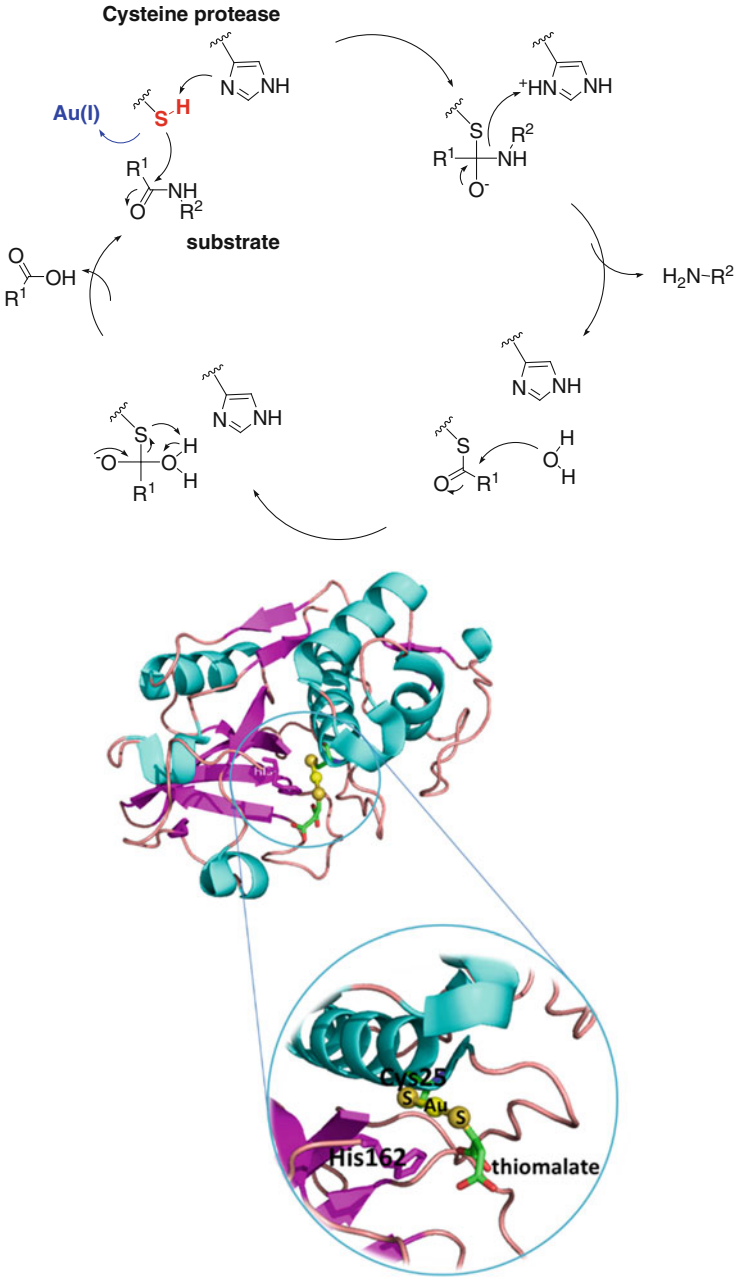

Fig. 1.15 Crystal structure of cathepsin K bound with gold–thiolate. PDB code: 2ATO. (Au^+ was from gold(I)–thiolate)

able to remove phosphate groups from phosphorylated tyrosine residues of proteins (see the scheme below). PTPs regulate important signaling pathways including cell growth, differentiation, T-cell signaling, immune response, and survival. Notably, the cysteine residue in the active site of PTP has a rather low pKa (~4.7); the cysteine thiol is deprotonated at physiological pH and thus blocked by the labile Au^{+} ion. A library of [$Au(PR_3)Cl$] complexes was screened for PTP inhibitory activity by Barrios and coworkers [40]. All the [$Au(PR_3)Cl$] complexes examined showed IC_{50} values (1.5–33 μM).

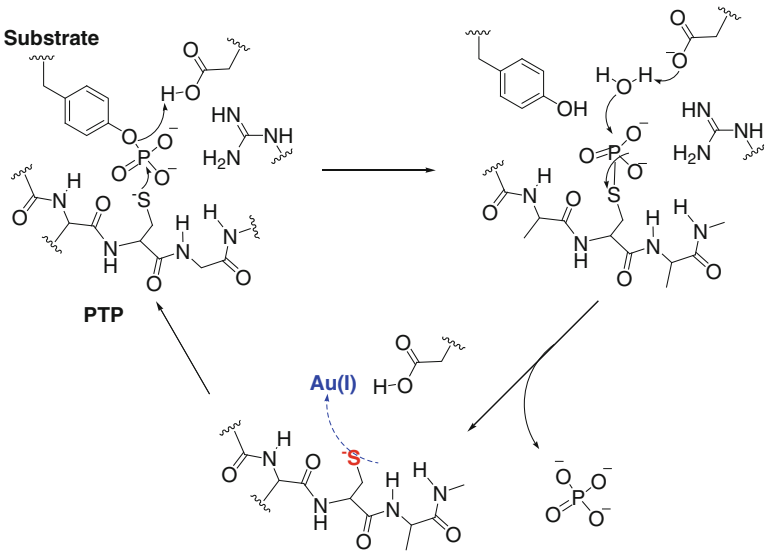

IκB Kinase. IκB kinase (IKK) is able to phosphorylate N-terminal serine residues of IκB, a cytosolic protein that inhibits the activity of nuclear factor-κB (NF-κB). The phosphorylation of IκB will cause dissociation of IκB from NF-κB and activation of NF-κB activity. As NF-κB is a transcription factor that regulates the expression of various genes involved in inflammatory diseases and cancers, the deactivation of NF-κB through inhibition of IKK activity could be a promising therapeutic methodology (see the scheme). Since there is an active cysteine residue in IKK, its catalytic activity can be inhibited by substitution reactive gold complexes such as aurothiomalate, aurothioglucose, or $AuCl_3$ [41].

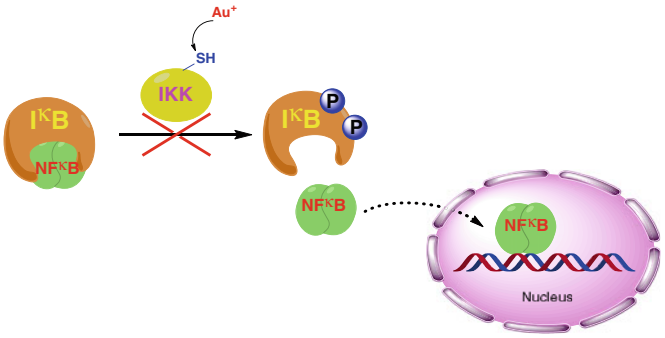

Other enzymes. The utility of cysteine residues lies in their redox (SH to S–S) or nucleophilic reactivity. The enzymatic activities can be blocked by covalent binding interactions of Se/S groups with Au^{+} ion. Besides the aforementioned enzymes, the activities of other thiol enzymes such as glutathione peroxidase (GPx) or iodothyronine deiodinase (ID) can also be inhibited by gold(I) complexes.

Most gold(I) complexes can inhibit thiol-containing enzymes. In fact, gold(III) complexes can be tight-binding inhibitors in addition to their Au–S binding property. Au(III) can be reduced to Au(I) under physiological conditions. Alternatively, those gold(III) complexes having favorable stability can also directly bind to cysteine residues through ligand exchange reactions. For example, the activities of deubiquitinase [42] and membrane water/glycerol channel protein (aquaporin 3) [43, 44] were inhibited by gold(III) complexes through Au^{III}–S_{cys} binding interactions.

1.3.2.4 Inhibition via Au–His Binding

Though the soft Au^{+} ion preferentially binds to the soft sulfur/selenium of cysteine/selenocysteine, there are examples of Au^{+} ions tightly binding to the N in histidine rather than the S of cysteine. Sadler and coworkers reported the crystal structure of the [Au(PEt_3)Cl]-cyclophilin 3 (Cyp3) adduct. Cyp3 contains four free cysteine residues, and Cys163 and Cys168 are accessible to Au^{+} ions. Surprisingly, there has been no Au^{I}–S_{cys} bond identified in the crystal structure. Instead, the [Au(PEt_3)]$^{+}$ moiety binds to the histidine residue (Fig. 1.16a). Meanwhile, the findings of chymotrypsin-coupled assays that involved no cysteines but histidine residues in the catalytic site revealed the presence of a Au–N_{His} binding interaction, correlating with potent inhibition of Cyp-3 PPIase activity by [Au(PEt_3)Cl] [45]. Recently, Messori and coworkers also reported several crystal structures showing Au^{I}–N_{His} binding interactions in a ribonuclease A-gold adduct (Fig. 1.16b) [46] and hen egg white lysozyme–gold adduct [47].

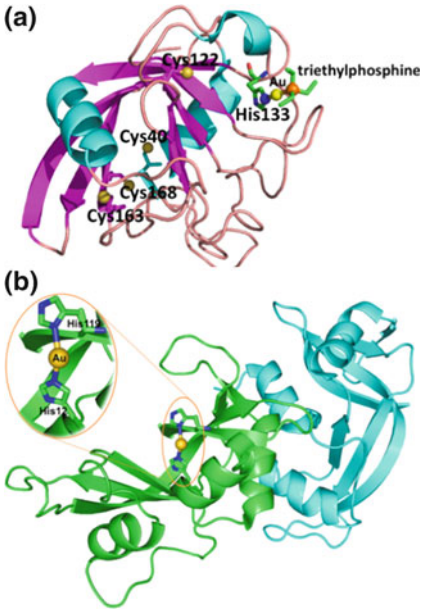

Fig. 1.16 **a** Crystal structure of cyclophilin 3 bound to gold–PEt_3. PDB code: 1E3B. (Au^+ was from [$Au(PEt_3)Cl$]) [45]. **b** Crystal structure of RNase bound to gold. PDB code: 4MXF (Au^+ was from Auoxo6) [46]

1.3.3 Current Status of Gold(I) Anticancer Agents

1.3.3.1 Gold(I)–Phosphine Complexes

[$Au(dppe)_2$]Cl Berners-Price et al. described an anticancer, four-coordinated Au(I) complex [$Au(dppe)_2$]Cl (dppe = bis(diphenylphosphino)ethane). This complex is rather stable in the presence of cellular thiols, including GSH, GSSG, and bovine serum albumin (BSA). [$Au(dppe)_2$]Cl is effective at inhibiting tumor growth in both leukemia and several solid tumors [8]. Unfortunately, toxicity to the heart, liver, and lung in dogs and rabbits was identified. The toxicity was caused by mitochondrial dysfunction due to the high lipophilicity of [$Au(dppe)_2$]Cl. Later studies showed that the replacement of the phenyl substituents with 2-pyridyl groups gave [$Au(d2pype)_2$]Cl that carries an intermediate lipophilicity. [$Au(d2pype)_2$]Cl is active in colon 38 tumors in mice [48]. This group further extended the d2pype group (five member ring) to d2pypp (six member ring) leading to the synthesis of [$Au(d2pypp)_2$]Cl. Unlike its five member ring precursor, [$Au(d2pypp)_2$]Cl displays increased thiol reactivity and can inhibit TrxR activity. [$Au(d2pypp)_2$]Cl also exhibited cytotoxicity toward breast cancer cells but not normal breast cells [48].

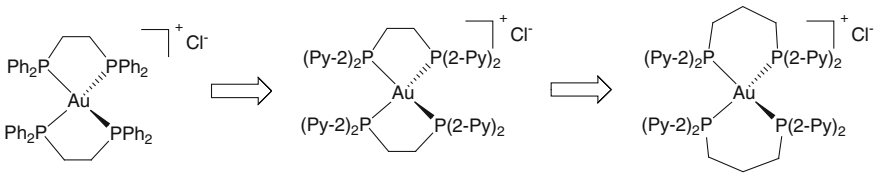

[Au^{I}(dppe)]Cl **[Au^{I}(dppe)]Cl** **[Au^{I}(dppp)]Cl**

[Au[P(CH$_2$OH)$_3$]$_4$]Cl. Katti and coworkers reported another anticancer active four-coordinated gold(I) complex, [Au[P(CH$_2$OH)$_3$]$_4$]Cl. In vitro cytotoxicity studies indicated that [Au[P(CH$_2$OH)$_3$]$_4$]Cl inhibited the proliferation of prostate cancer (LNCaP, PC-3), human colon carcinoma (HCT-15), and human gastric carcinoma (HCT-15) cells. In vivo antitumor studies on mice bearing syngeneic meth/A cells treated three times with [Au[P(CH$_2$OH)$_3$]$_4$]Cl at a dose range of 25–125 mg/kg led to a statistically significant increase of survival time. No mortality resulted from these treatments [49].

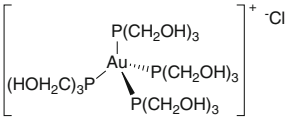

{Au[P(CH$_2$OH)$_3$]}Cl

Induction of autophagy. Autophagy is a cellular process that utilizes lysosomes to degrade unnecessary or dysfunctional components in cells. Recently, Che and coworkers reported the induction of autophagy by several multinuclear gold(I)–phosphine complexes (see below). HeLa cells treated with these gold–phosphine complexes exhibited signs of autophagosome accumulation, including the formation of RFP/GFP-LC3 vesicles, upregulation of LC3-II protein, and numerous vacuoles found in the cytoplasm. The initiation of autophagy can ultimately lead to cell death [50].

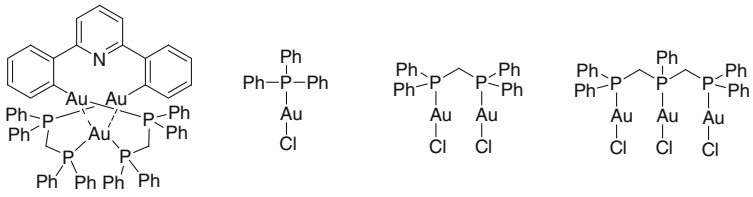

[Au$_3^-$(CNC)(μ-dppm)$_2$]Cl **Au(PPh$_3$)Cl** **Au$_2$(μ-dppe)Cl$_2$** **Au$_3$(μ-dpmp)Cl$_3$**

1.3.3.2 Clinically Used Antiarthritis Drugs with Anticancer Properties

Lorber and coworkers reported in vivo antitumor activity of auranofin and found that this antiarthritis drug could increase the survival of mice inoculated with lymphocytic leukemia P388 cells in a concentration (and dose frequency)-dependent manner [51]. Later studies by Mirabelli and coworkers indicated that the in vivo antitumor activity of auranofin is quite limited. Intraperitoneal injection (i.p.) of this gold(I) complex could neither prolong life span nor inhibit tumor growth in several subcutaneously (s.c.)-implanted solid tumor models. Meanwhile, the antitumor activity of auranofin in mice bearing P388 leukemia is only effective in i.p.-implanted P388 leukemia through i.p. injection of auranofin; the drug is inactive in i.v.-implanted mice when administered by either i.p., i.v., or s.c. [52]. Such ineffectiveness may be caused by the high reactivity of auranofin with thiols in blood, leading to the formation of gold–serum albumin adducts, thus limiting the bioavailability of gold drugs for the tumor tissue. Auranofin can readily react with Cys-34 of serum albumin (the equivalent concentration of free thiol is $\sim$0.4 mM in blood), and over 80 % of auranofin is covalently bound to serum albumin [53, 54].

The in vivo effects of another antiarthritis gold(I) drug, aurothiomalate (ATM, see below), was investigated [55]. Treatment of mice (s.c.) bearing syngenic Meth/A cells with ATM at 30 mg/kg per day or oral administration (p.o.) at 70 mg/kg per day significantly increased the survival. In 2006, Fields and coworkers reported that both aurothioglucose (ATG) and ATM can strongly disrupt the interaction of protein kinase Cι (PKCι) with its downstream effector Par6. Administration of ATG at 200 mg/kg every one or two days for 14 days significantly suppressed the tumor growth in mice bearing human non-small-cell lung cancer A549 cells. The antitumor activity was related to cytostatic effects, rather than the cytotoxic effects, of ATG [56].

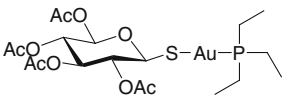

Auranofin

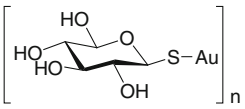

Aurothioglucose

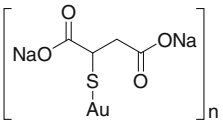

Aurothiomalate

1.3.3.3 Gold(I)–NHC Complexes as Anticancer Agents

Several properties of N-heterocyclic carbenes, such as their strong donating ability, low toxicity, and easy functionalization to tune lipophilicity and reactivity, render NHCs excellent auxiliary ligands. The anticancer activity of Au(I)–NHC complexes has been extensively studied. The initial work was done by Berners-Price and coworkers who developed a series of linear, mononuclear $[Au(NHC)_2]^+$ complexes having a wide range of lipophilicity. These $[Au(NHC)_2]^+$ complexes induced

mitochondrial membrane permeabilization (MMP) in isolated rat liver mitochondria [57] and inhibited the activity of TrxR [58]. A two-step inhibition mechanism with a stepwise ligand exchange reaction was proposed, based on ^{1}H NMR studies (see below). The rate constants were observed to depend on steric hindrance of NHC ligands, and selenium-containing Sec could react faster with $[Au(NHC)_2]^+$ than sulfur-containing Cys. Some of the complexes displayed selective cytotoxicity toward breast cancer cells and not to normal breast cells [58].

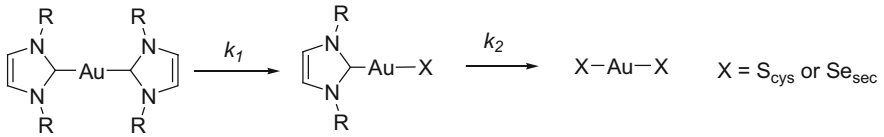

Ott and coworkers reported another type of gold(I)–NHC complex: [Au(NHC)Cl] with 1,3-diethylbenzimidazol-2-ylidene type NHCs. [Au(NHC)Cl] was found to potently inhibit the TrxR activity and mitochondrial respiration, induce the formation of reactive oxygen species (ROS) apoptosis, and strongly affect the cellular metabolism [59]. This group also compared the reactivities of [Au(NHC)L] complexes having different ligands (L = Cl, NHC, or PPh_3). All the [Au(NHC)L] complexes bind to serum albumin with rates slower than that of auranofin. [Au(NHC)Cl] was observed to react with serum albumin relatively quickly with ~60 % bound after 6 h; [Au(NHC)(PPh_3)]I reacted more slowly with albumin but faster than $[Au(NHC)_2]I$ as <20 % of $[Au(NHC)_2]I$ was bound to albumin after 6 h, with the amount bound never exceeding 50 % within 24 h. Similarly, the EC_{50} values for TrxR inhibition are 0.36, 0.66, and 4.89 μM for [Au(NHC)Cl], [Au(NHC)(PPh_3)]I, and $[Au(NHC)_2]I$, respectively [60].

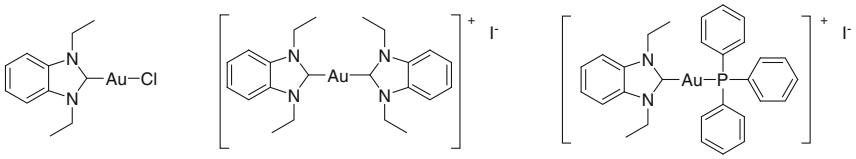

[Au(NHC)Cl] **$[Au(NHC)_2]I$** **[Au(NHC)(PPh_3)]I**

1.3.3.4 Gold(I)–Alkyne Complexes as Anticancer Agents

A class of [Au(PPh_3)(alkyne)] complexes was recently examined by Ott and coworkers [61]. These complexes selectively inhibited TrxR activity in the structurally analogous enzyme GR and had strong inhibitory effects on tumor cell metabolism and mitochondrial respiration. Similar to the gold(I)–phosphine–

thiolate complex, [Au(PPh_3)(alkyne)] also potently inhibited the formation of blood vessels in a zebrafish embryo model [62]. Chui et al. reported a dinuclear [$Au_2(PPh_3)_2$(bis-alkyne)] complex that exhibited cytotoxicity in the micromolar range toward the cancer cell lines Hep3B, SKHep-1, and MDA-MB-231. In vivo studies revealed that administration of the dinuclear gold(I) complex at 2.5 mg/kg per day (i.p.) for nine successive days could significantly inhibit tumor growth in mice bearing Hep3B without adverse effects in the liver or kidney [63].

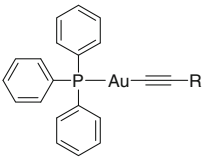

[Au(PPh_3)(acetylene)]

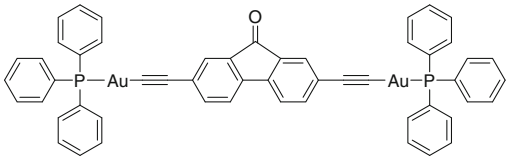

[$Au_2(PPh_3)_2$(bis-acetylene)]

1.3.3.5 Gold(I)–Thiourea Complexes as Anticancer Agents

Che and coworkers described both the anticancer activity and the TrxR inhibition mechanism of gold(I)–thiourea ([Au^I–TU_2]$^+$). [Au^I–TU_2]$^+$ inhibits TrxR activity at low nanomolar levels in a two-step, tight-binding inhibition mechanism [64]. The IC_{50} values of [Au^I–TU_2]$^+$ toward HeLa, HepG2, SUNE1, and NCI-H460 cytotoxicity are in the range of 3.7–17.4 μM. Administration of [Au^I–TU_2]$^+$ at 100 mg/kg (i.p.) twice a week in mice bearing NCI-H460 (non-small cell lung cancer) xenografts led to a 38 % inhibition of tumor growth after 28 days.

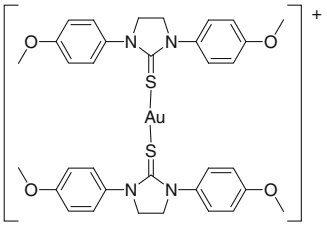

[$Au^I(TU)_2$]$^+$

1.3.4 Current Status of Anticancer Gold(III) Complexes

1.3.4.1 Gold(III)–Porphyrin Complexes as Anticancer Agents

The low stability of gold(III) complexes in biological media is a major obstacle that hampers their development as therapeutic anticancer drugs. Che and coworkers identified a gold(III) complex of 5,10,15,20-tetraphenyl-1*H*,20*H*-porphyrin (gold-**1a**) that exhibits high stability in a physiological, reducing environment, and has potent in vitro cytotoxicity toward different cancer cell lines, including cisplatin-resistant ones [7, 65].

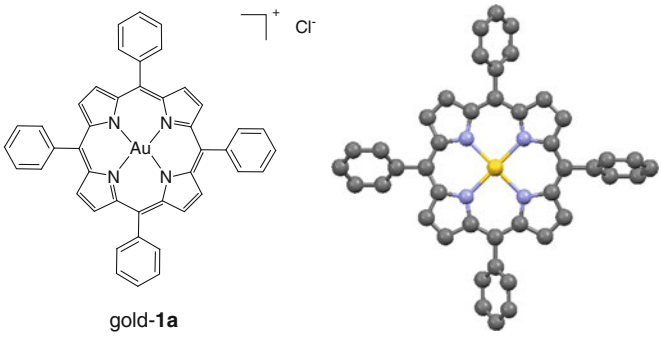

gold-**1a**

Gold-**1a** can induce apoptosis via Bcl-2 protein suppression and mitochondrial dysfunction; the complex can block the cell cycle at the G0–G1 phase, activate p38, and inhibit TrxR activity. Gold-**1a** is antitumor active in different animal models, including hepatocellular carcinoma (HCC) [66, 67], colon cancer [68], neuroblastoma [69] nasopharyngeal carcinoma (NPC) [66], and melanoma [70]. Notably, gold-**1a** is the first gold complex reported to be anticancer active in cancer stem cells (CSCs) [71]. To investigate for possible side effects, pharmaceutical safety tests of gold-**1a** have been performed. An acute toxicity study suggests a safe treatment dosage of <3 mg/kg (i.v.). This gold(III) complex did not cause blood vessel irritation or significant genotoxicity as revealed by blood vessel irritation tests in rabbits and in vivo mutagenicity tests on mice [71]. In addition, an analogue of gold-**1a** with a hydroxyl group at the para-position of the phenyl ring of TPP (gold-**2a**) exhibited improved solubility and cytotoxicity (IC_{50} was as low as 1 nM). Intraductal injection of gold-**2a** significantly inhibited breast tumor growth in mouse models. The anticancer activity of gold-**2a** is possibly related to the attenuation of the class I histone deacetylase (HDAC) and histone acetylation at the promoter of Wnt/β-catenin signaling molecules.

1.3.4.2 Cyclometalated Gold(III) Complexes Bearing Tridentate C-Deprotonated C^N^C Ligands as Anticancer Agents

In 2006, Che and coworkers reported the use of a tridentate dianionic C^N^C (H_2C^N^C = 2,6-diphenylpyridine) ligand to stabilize the Au^{3+} ion. The $[Au^{III}(C^N^C)L]^{n+}X$ complexes were redox stable in the presence of cellular reducing agents during a 72-h incubation (despite that ligand exchange of $-S^-$ with the auxiliary L ligand may occur).

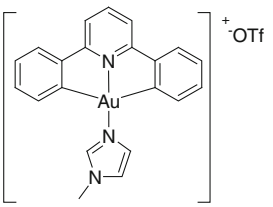

$[Au^{III}(CNC)MeIm\text{-}1]^+$

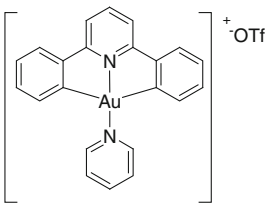

$[Au^{III}(CNC)Py]^+$

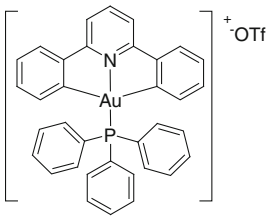

$[Au^{III}(CNC)Py]^+$

The anticancer activity of the $[Au^{III}(CNC)L]^{n+}X$ was found to vary significantly with differing L ligands. The $[Au^{III}(CNC)]^+$ moiety serves as carrier of the toxic L ligand and/or can inhibit thiol enzymes (e.g., TrxR) directly. A noteworthy example is the dinuclear $[Au_2(CNC)_2(dppp)](OTf)_2$ complex containing a bridging bis (diphenylphosphino)propane (dppp) ligand that displays potent in vitro and in vivo anticancer activities.

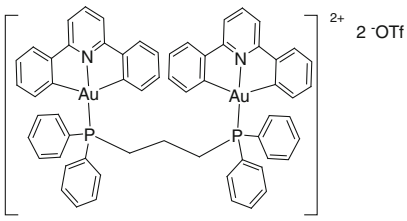

$[Au_2(CNC)_2(dppp)](OTf)_2$

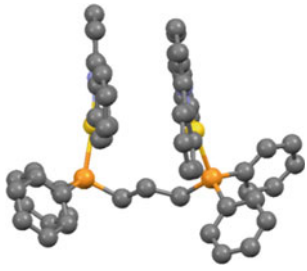

The cytotoxic IC_{50} values of $[Au_2(CNC)_2(dppp)](OTf)_2$ are in the range of 0.043–0.21 μM depending on cancer cell lines. Toward normal lung fibroblast CCD-19Lu cells, it is less cytotoxic with an IC_{50} value of 1.6 μM [72]. Importantly, $[Au_2(CNC)_2(dppp)](OTf)_2$ exhibited in vivo antitumor activity in various animal models. Administration of $[Au_2(CNC)_2(dppp)](OTf)_2$ at 10 mg/kg (i.p.) twice per week led to a 77 % tumor growth inhibition in a mouse PLC cancer model. Administration of the gold(III) complex at 4 mg/kg (i.p.) twice per week also elicited a 38.6 % inhibition of tumor growth in mice bearing H22 hepatocarcinoma

and 48.9 % inhibition in mice bearing S180 sarcoma. The in vivo activity of $[Au_2(CNC)_2(dppp)](OTf)_2$ on rats was further examined. The survival of rats could be increased from 30 to 40 days or 43 days upon administration of the gold(III) complex at dosages of 0.5 or 0.75 mg/kg, respectively, twice per week for four weeks. After 14 days, the tumor size in rats treated with $[Au_2(CNC)_2(dppp)](OTf)_2$ at 0.5 mg/kg was significantly smaller than that of the non-treatment control group. The possible side effects of $[Au_2(CNC)_2(dppp)](OTf)_2$ were examined by pharmaceutical safety tests. The LD_{50} (median lethal dose) in nude mice was 13.7 mg/kg (i.v.) after 14 days. The minimal lethal dose was found to be 9.0–13.5 mg/kg (i.v.). Therefore, $[Au_2(CNC)_2(dppp)](OTf)_2$ can suppress tumor growth at a relatively safe dose. Mechanistic studies, according to transcriptomics, connectivity map analyses, and other biological assays, suggested that induction of endoplasmic reticulum (ER) stress and TrxR inhibition were the possible anticancer mechanisms of action. Meanwhile, TNF-related apoptosis-inducing ligand (TRAIL), a ligand for death receptor 5 (DR5), displayed a synergistic property with $[Au_2(CNC)_2(dppp)](OTf)_2$ in the anticancer effects [72].

Despite that the anticancer activities of $[Au^{III}(CNC)L]^{n+}X$ complexes are closely related to the toxicity of the auxiliary L ligand, the use of non-toxic NHC ligands that have strong donor strengths was found to increase in vitro cytotoxicity.

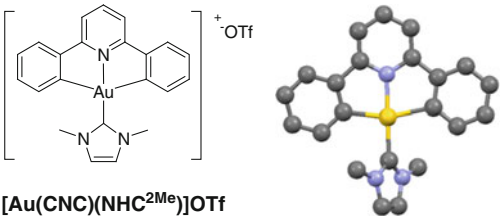

[Au(CNC)(NHC^{2Me})]OTf

$[Au^{III}(CNC)(NHC^{2nBu})]OTf$ displayed potent cytotoxicity toward HeLa cells with an IC_{50} of 0.084 μM, which is two orders of magnitude lower than that of $[Au^{III}(CNC)(MeIm\text{-}1)]$ and $[Au^{III}(CNC)(Py)]$ (8.0 and 8.2 μM, respectively). Mechanistic studies revealed that $[Au^{III}(CNC)(NHC^{2Me})]OTf$ can intercalate into DNA (binding constant $K = 5.4 \times 10^5\ M^{-1}$). The $[Au^{III}(CNC)(NHC^{2Me})]OTf$ complex inhibited the activity of topoisomerase I (TopoI) via suppression of TopoI-mediated relaxation of supercoiled DNA. Treatment of nude mice bearing PLC tumors with this gold(III) complex at 10 mg/kg (i.p.) per week for 28 days significantly suppressed tumor growth (47 %) with no observed side effects [73].

1.3.4.3 Cyclometalated Gold(III) Complexes Bearing C-Deprotonated C^N and C^N^N Ligands as Anticancer Agents

Buckley et al. in 1996 first reported the use of C-deprotonated multidentate ligands to stabilize Au^{3+} ions. The cyclometalated gold(III) complexes have the general formula of $[AuX_2(damp)]$ (dmap = o-$C_6H_4CH_2NMe_2$, X = Cl, OAc or

X_2 = dithiocarbamate, malonate) [74, 75] with [$AuCl_2$(damp)] displaying the highest cytotoxicity in cancer cell lines of breast, colon, bladder, rectum, and ovary. Administration of this complex at 12 mg/kg elicited a 60 % tumor growth inhibition. This promising in vivo activity initiated further development of organogold (III) complexes containing other C-deprotonated C^N and C^N^N ligands. For example, [$Au(AcO)_2$(damp)] inhibited the activity of cysteine cathepsin B at submicromolar concentrations [76]. Messori et al. developed a series of gold(III) complexes bearing a 2-(2-phenylpropan-2-yl)pyridine (py^{dmb}-H) or 6-(2-phenyl propan-2-yl)-2,2′-bipyridine ($bipy^{dmb}$) ligand [77]. These gold(III) complexes are stable against reduction and potently inhibited the activity of TrxR, possibly by progressive oxidative damage of cysteine and selenocysteine residues in the enzyme's active site [78]. The [Au(C^N)(dtc)] (HC^N = *N*,1,1,1-tetraphenyl-λ^5-phosphinimine) complex developed by Contel and coworkers is cytotoxic toward T-cell leukemia Jurkat cells but displays a lower cytotoxicity in normal lymphocyte PBMC cells. The cytoxicity may be the result of mitochondrial dysfunction induced by ROS and Bax/Bak activation [79, 80].

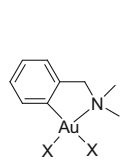

[AuX_2(damp)]

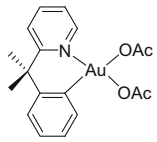

[Au(py^{dmb}-H)$(OAc)_2$]

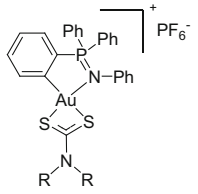

[Au(C^N)(dtc)]

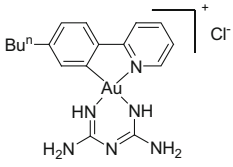

[Au(^{nBu}C^N)(biguanide)]Cl

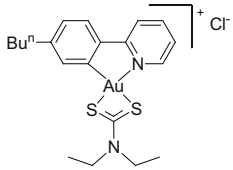

[Au(^{nBu}C^N)(dedt)]Cl

Che and coworkers recently developed two classes of organogold(III) complexes with C-deprotonated C^N (HC^N = 2-phenylpyridine) ligands. Gold(III) complex, [Au(^{nBu}C^N)(biguanide)]Cl containing a biguanide ligand, is water soluble and cannot be readily reduced by intracellular GSH, instead forming gold(III)-GSH adducts [81]. This complex displays selective cytotoxicity toward various cancer cell lines (2.1–17.1 μM) compared to normal CCD-19Lu cells (32.8 μM). Mechanism studies revealed that ER swelling/stress is a possible cause of cytotoxicity. This was confirmed by oligonucleotide microarray analysis and Western blotting assays. Another gold(III) complex [Au(^{nBu}C^N)(dedt)]Cl containing the

same C^N ligand and a dithiocarbamate ligand (dedt) selectively inhibited the proliferation of MCF-7 cells but not non-tumorigenic, immortalized MIHA (liver) cells [42]. This complex can covalently bind to thiol-containing peptides/proteins (e.g., deubiquitinases) as revealed by ESI-MS analysis. Oligonucleotide microarray analysis and purified enzyme-/cell-based assays lend support that deubiquitinases could be targets of [Au(^{nBu}C^N)(dedt)]Cl.

1.3.4.4 Gold(III) Complexes Containing Bidentate N^N and Tridentate N^N^N Ligands as Anticancer Agents

In the early 2000s, Messori et al. described the anticancer activity of gold(III) complexes containing bipyridine (bipy) and terpyridine (terpy) ligands [82].

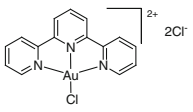

[Au(terpy)Cl]Cl_2

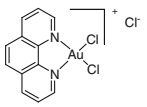

[Au(phen)Cl_2]Cl

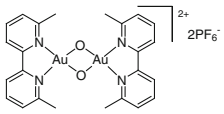

[Au(bipy^{2Me})(μ-O)$_2$]$(PF_6)_2$

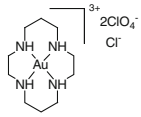

[Au(cyclam)](ClO_4)Cl

These complexes elicited in vitro effects against cancer cells, including cisplatin-resistant cancer cell lines. Compared to organogold(III) complexes, they are less stable in the presence of reducing agents, including ascorbic acid, and can cause oxidative damage to biomolecules [83]. Thiol-containing enzymes, including TrxR [35], the copper chaperone Atox-1 [84], and aquaporin [43, 44], have all been identified as potential targets of these anticancer gold(III) complexes. It is noteworthy that the highly stable [Au(cyclam)]$(ClO_4)_2$Cl exhibited no toxicity at concentrations as high as 100 μM.

1.3.4.5 Gold(III) Complexes Containing Dithiocarbamate Ligand as Anticancer Agents

Previously, the dithiocarbamate ligand was utilized as chemoprotective agent capable of protecting cisplatin from protein thiols without affecting platinum–DNA interaction. Fregona and coworkers reported the use of dithiocarbamate ligands to stabilize Au^{3+} ions. The gold(III) dithiocarbamate complex [Au^{III}(DMDT)Br_2] suppressed the activity of purified 20S proteasomes or 26S proteasomes in MDA-MB-231 breast cancer cells [85]. The complex can also significantly inhibit the activity of TrxR via irreversible binding of gold to the catalytic site [86]. Administration of [Au^{III}(DMDT)Br_2] at 1 mg/kg/d (s.c.) for 29 days caused a 50 % inhibition of tumor growth in mice bearing MDA-MB-231 cells. This effect was accompanied by a 40 % inhibition of proteasomal, chymotrypsin-like activity of the

tumor tissue [85]. Treatment of mice bearing PC3 prostate tumor xenografts with this gold(III) complex at 1 mg/kg/d for 19 days resulted in an 85 % suppression of tumor growth with no detectable side effects [87].

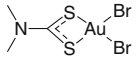

$[Au^{III}(DMDT)Br_2]$

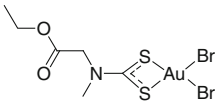

$[Au^{III}(ESDT)Br_2]$

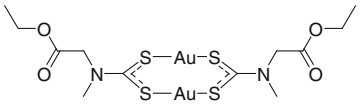

$[Au^{I}_2(ESDT)_2]$

1.4 The Chemistry and Anticancer Properties of Platinum

1.4.1 The Chemical Properties of Platinum Complexes

The accessible oxidation states of platinum in biological systems are Pt(II) and Pt (IV). While Pt^{2+} and Au^{3+} ions are both isoelectronic, the Pt^{2+} ion has a much lower reduction potential than Au^{3+}. Thus, Pt(II) complexes are usually more redox stable than their gold(III) counterparts toward physiological reducing agents. In general, Pt^{2+} ions will bind to soft atoms such as sulfur, but tight binding with hard atoms such as N has also been observed as in the case of cisplatin. Pt(IV) has a d^6 octahedral coordination geometry and can be reduced to d^8 Pt(II) with a planar coordination geometry. Pt(IV) complexes can thus serve as Pt(II) prodrugs.

1.4.1.1 Pt(II) Complexes

The most intriguing characteristics of Pt(II) complexes are their luminescent and anticancer properties. Luminescent Pt(II) complexes containing multidentate π-ligands are useful biological probes to detect nucleic acids and proteins, or act as cell imaging agents. Similar to gold(I) complexes, platinum(II) complexes undergo intermolecular aggregation forming supramolecular polymers via Pt(II)–Pt(II) and π–π interactions, which lend interesting luminescent properties arising from triplet metal–metal to ligand charge transfer (^{3}MMLCT). The anticancer mechanisms of action of platinum(II) complexes can involve covalent interactions (e.g., cisplatin binding to guanine) and/or non-covalent interactions (e.g., inert platinum complexes bind to proteins based on ionic bond and/or hydrophobic interactions) with biomolecules as discussed in Sect. 1.4.2 below.

One important consideration in the design of anticancer platinum complexes is the ligand *trans*-effect. The order of *trans*-effects is as follows:

$$CN^-, CO, C_2H_4 > PR_3H^- > CH_3^- > C_6H_5^- > NO_2^- > SCN^- > I^- > Br^- > Cl^- > NH_3, py > OH^- > H_2O$$

For σ bonds, *trans*-effects can be explained as follows: Both the ligands (L_1 and L_2) form bonds with the $6p_x$ orbital and the $5d_{x^2-y^2}$ orbital of Pt(II) ions. When a Pt–L_2 bond is strong, the electron density in the $6p_x$ and $5d_{x^2-y^2}$ orbitals of the Pt(II) ion increases, thereby resulting in a weakening of the Pt–L_1 bond.

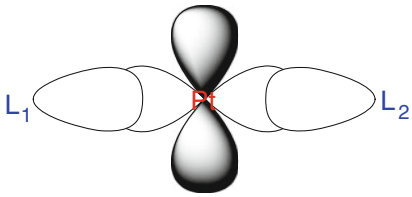

1.4.1.2 Pt(IV) Complexes

Platinum(IV) complexes can be readily generated through the oxidation of platinum (II) counterparts. Recently, Pt(IV) complexes have been receiving increasing attention as Pt(II) prodrugs, being activated by intracellular reduction by glutathione and/or ascorbic acid.

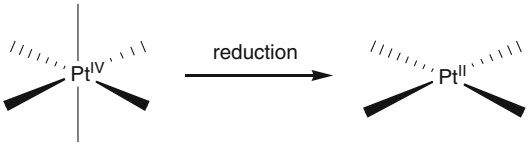

The two axial coordination sites provide opportunities for structural modification, yielding tumor cell-specific Pt(IV) prodrugs by functionalization with tumor-targeting groups or generating synergistic effects by linkage to another drug. For example, Lippard and coworkers used a single-strand carbon nanotube attached to one axial site of Pt(IV) with another axial ligand having tumor-targeting folic acid unit. Such complex could specifically recognize tumor cells and release anticancer active Pt(II) species in the intracellular environment [88]. Sadler and coworkers used an azide ligand to form complexes with Pt(IV). The Pt(IV)–azide complex is stable toward intracellular reducing agents and can be selectively reduced to Pt(II) species upon photoirradiation [89, 90]. Recently, Sadler reported another Pt(IV) complex (*trans*,*trans*,-*trans*-[$Pt(N_3)_2(OH)_2(MA)(Py)$]) that could generate reactive singlet oxygen ($^1O_2$) upon incubation with 5′-guanosine monophosphate (5′-GMP) under light irradiation [91]. Yeow, Xing [92], and Ma, Yang, and Lin [93] independently reported that these upconversion nanoparticles could be utilized to deliver Pt(IV)-azide that can be activated by NIR light. Dhar and coworkers described Pt(IV) complexes containing axial ligands with an anti-inflammatory aspirin unit. Aspirin has the potential to minimize the

nephrotoxicity induced by cisplatin. The antitumor activity of the Pt(IV)–aspirin conjugate is also more effective than the simple combination of cisplatin and aspirin [94]; Pastorin, Ang, and coworkers utilized a Pt(IV)-based strategy for the ratiometric delivery of doxorubicin and cisplatin. This Pt(IV) complex was selectively delivered to tumor tissue using a multiwalled, carbon nanotube as the vehicle [95]. All these results support the potential of Pt(IV) prodrugs as viable anticancer drugs.

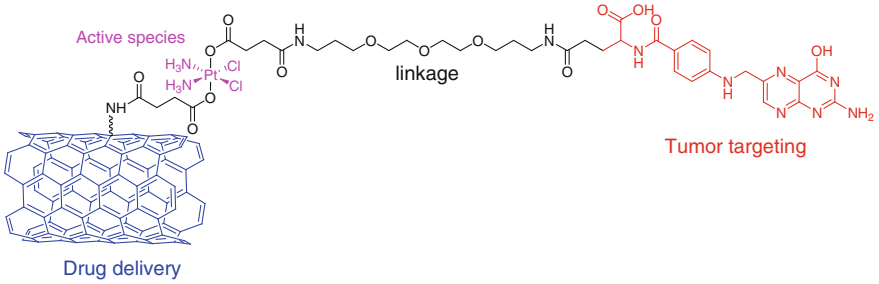

Lippard and coworkers
J. Am. Chem. Soc. **2008**, *130*, 11467-11476.

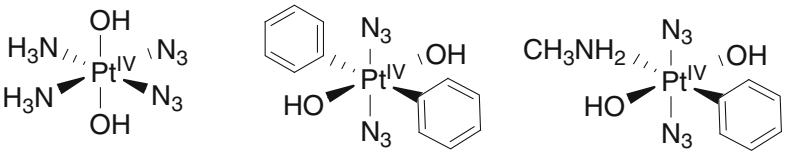

Sadler and coworker,
Angew. Chem. Int. Ed. **2003**, *42*, 335-339; **2010**, *49*, 8905-8908; **2013**, *52*, 13633-13637

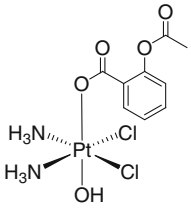

Dhar, *Angew. Chem. Int. Ed.* **2014**, *53*, 1963-1967.

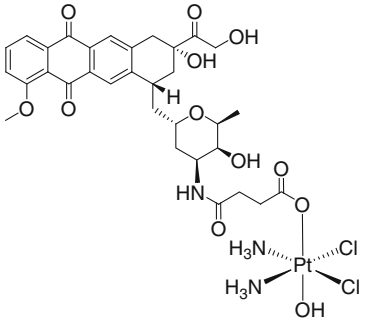

Ang, *Chem. Sci.* **2014**, DOI: 10.1039/C3SC53106F

1.4.2 *Physiologically Stable Platinum(II) Complexes as Anticancer Agents*

Owing to the square planar coordination geometry of Pt(II), platinum(II) complexes containing π-conjugated ligand(s) can bind to DNA via intercalation or groove bindings. Over the past decades, notable advancements in our understanding of this DNA binding have been made by several groups, including those of Lippard, Che, and others. The binding interactions between Pt(II) complexes and DNA can lead to DNA damage as well as cell cytotoxicity. Recently, examples of platinum(II) complexes that target G-quadruplex DNA and DNA topoisomerases have been reported. In addition, platinum(II) complexes showing potent anticancer properties with non-DNA biomolecular targets have also been reported.

1.4.2.1 Platinum(II) Complexes Target Nucleic Acids

Double-stranded DNA. Lippard first reported that $[Pt(terpy)L]^+$ (terpy = 2,2′:6′,2″-terpyridine, L = Cl or SCH_2CH_2OH) can strongly bind to DNA through intercalation [96]. Wang et al. solved the X-ray structure of the complex formed between $[Pt(terpy)(SCH_2CH_2OH)]^+$ and CpG base pairs providing direct, structural evidence to support the DNA intercalation binding mode of Pt(II) complexes (Fig. 1.17) [97]. These investigations have led to numerous studies on the DNA-binding interactions of $[Pt(terpy)L]^+$ complexes with substituted terpy and L ligands. In general, the binding constants of $[Pt(terpy)L]^+$ complexes are in the range of 3.0×10^3 – 1.8×10^7 M^{-1} [98].

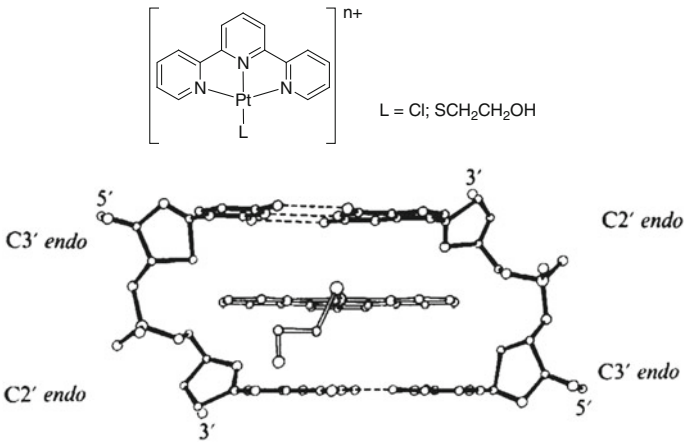

Fig. 1.17 Chemical structures of platinum(II)–terpy complexes that act as DNA intercalators (*top*) and crystal structure of the adduct formed between $[Pt(terpy)(SCH_2CH_2OH)]^{2+}$ and GpC (*bottom*). The crystal structure is reproduced from Ref. [97], Copyright© 1978, Nature Publishing Group

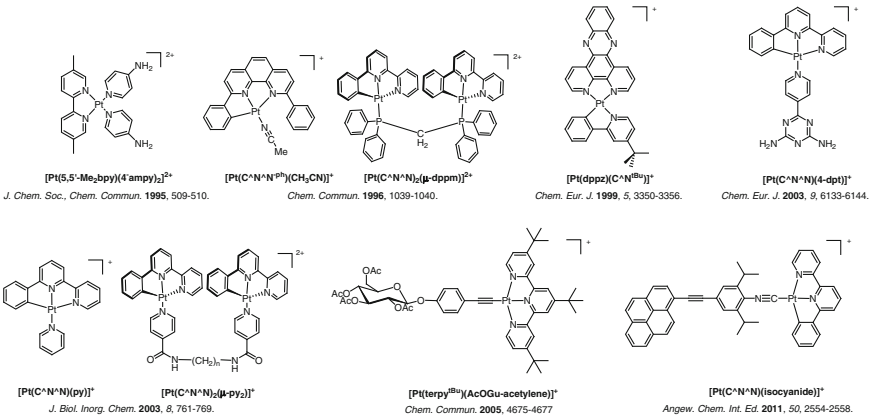

Fig. 1.18 Platinum(II) complexes that target dsDNA, as reported by Che and coworkers

Che and coworkers made use of the luminescent properties of platinum(II) complexes to develop luminescent DNA probes (Fig. 1.18). In 1995, a luminescent platinum(II) complex $[Pt(5,5'\text{-}Me_2bpy)(4\text{-}ampy)]^+$ was reported to bind DNA with the binding accompanied by an enhancement of emission intensity and increase in emission lifetime [99]. Later, the mononuclear and dinuclear cyclometalated platinum(II) complexes, $[Pt(C\text{^}N\text{^}N^{-Ph})(CH_3CN)]^+$ and $[[Pt(C\text{^}N\text{^}N)]_2(\mu\text{-dppm})]^{2+}$, were shown to intercalate between DNA base pairs accompanied by a more than 100-fold emission enhancement [100]. A notable example is $[Pt(dppz)(C\text{^}N^{tBu})]^+$ which binds to DNA through intercalation, an interaction that can elicit in vitro cytotoxicity in cancer cells. It is noteworthy that emission enhancement is normally observed in the binding reactions between DNA and monomeric luminescent platinum(II) complexes—the intercalation leads to an increase in the rigidity of the luminescent platinum(II) complex, decreasing solvent quenching of the emissive excited state. Emission enhancement upon binding of $[Pt(dppz)(C\text{^}N^{tBu})]^+$ with DNA is also accompanied by a significant redshift in the emission peak maximum (from 558 to 650 nm) that is attributed to exciplex emission arising from π–π interactions between the metal complex and DNA base pairs [101]. Besides intercalation, a cyclometalated platinum(II) complex $[Pt(C\text{^}N\text{^}N)(4\text{-dpt})]^+$ bearing a 2,4-diamino-6-(4-pyridyl)-1,3,5-triazine (dpt) ligand can interact with DNA through both intercalation and groove binding interactions. This platinum(II) complex shows specificity toward dA-dT DNA. More importantly, $[Pt(C\text{^}N\text{^}N)(4\text{-dpt})]^+$ shows cytotoxicity at least one order of magnitude lower toward normal cells than cancer cells [102]. The dinuclear Pt(II) complex $[[Pt(C\text{^}N\text{^}N)]_2(\mu\text{-py})]^{2+}$ reported in 2003 shows a much higher DNA-binding affinity than the mononuclear $[Pt(C\text{^}N\text{^}N)(py)]^+$. Both complexes show similar cytotoxicity, and this is attributed to the influence of non-DNA-binding interactions with cellular components [103].

By incorporation of a bulky *tert*-butyl group into the planar terpy ligand in order to reduce DNA intercalation, the complex [Pt(terpy^{tBu})(AcOGlu-acetylene)]$^+$ can still strongly bind to DNA. A groove binding mode which is similar to that of the commercial Hoechst 33342 dye was proposed [104]. A more recent work by Che and coworkers coordinated a large, bulky isocyanide ligand to Pt(II) so as to block the interaction between DNA and the transcription factor cAMP response element binding protein (CREB). This [Pt(C^N^N)(isocyanide)]$^+$ complex was observed to display a high binding affinity (groove binding) toward CREB gene sequence DNA and could interfere with the binding of CREB to DNA as revealed in both cell-free and cell-based assays [105].

Bierbach and coworkers combined the DNA-targeting ability of classic Pt(II) drugs and non-covalent intercalating ability of planar organic ligands in the design of new anticancer platinum(II) compounds [106]. A platinum–acridine hybrid agent, [PtCl(en)(ACRAMTU)](NO$_3$)$_2$ (en = ethane-1,2-diamine, ACRAMTU = 1-[2-(acridin-9-ylamino)ethyl]-1,3-dimethyl thiourea), was prepared and found to show high binding affinity toward DNA. According to the crystal structure, the acridine intercalates between DNA base pairs, while the Pt(II) ion binds to guanine N7. A recent study using post-labeling with fluorescent dyes by click chemistry confirmed the cellular localization of [PtCl(en)(ACRAMTU)]$^{2+}$ in the nucleus [107].

In addition to the above, several platinum(II) complexes supported by bidentate or tridentate N-ligands, including [Pt(en)(bpy)]$^{2+}$ (bpy = bipyridine) [108], [Pt(N^N)(phen)]$^{2+}$ (N^N = cyclohexane-1,2-diamine, phen^{2Me} = 5,6-dimethyl-1,10-phenanthroline) [109], [Pt(1C3)(dien)]$^{2+}$ (1C3 = 1-[(3-aminopropyl)amino]-anthracene-9,10-dione, dien = N^1-(2-aminoethyl)ethane-1,2-diamine) [110], and [Pt(en)(Py^R)$_2$]$^{2+}$ (Py^R = 1-(argiomethyl)-4-(2-(pyridin-4-yl)ethyl)pyridin-1-ium) [111], have been reported to display potent DNA intercalating activity (Fig. 1.19).

Targeting G-quadruplex DNA. DNA/RNA sequences rich in G bases can self-assemble into G-quadruplexes through hydrogen bonding interactions. Stabilization of G-quadruplexes can suppress the activity of telomerase, an enzyme that maintains the length of telomeres in cancer cells, allowing the cancer cells to divide indefinitely. In view of the planar coordination geometry of Pt(II) complexes, Che and coworkers developed several G-quadruplex stabilizing agents and probes. Modification of the metallointercalator [Pt(dppz)(C^N^{tBu})]$^+$ to [Pt(dppz^{COO})(C^N)] resulted in selective binding of the latter complex to a G-quadruplex rather than to dsDNA. The binding between [Pt(dppz^{COO})(C^N)] and the G-quadruplex is accompanied by up to 293-fold increase in emission intensity with a binding constant of $\sim 10^7$ M^{-1}. This Pt(II) complex also inhibits human telomerase activity with an IC$_{50}$ value in the submicromolar range [112]. Platinum(II) complexes bearing the Schiff base ligand [Pt(ONNO)] [113] or tridentate 2,6-bis-(benzimidazol-2-yl)pyridine (BPB) ligand [Pt(BPB)(R)]$^+$ [114] can also stabilize G-quadruplexes and inhibit the expression of the *c-myc* oncogene in cancer cells.

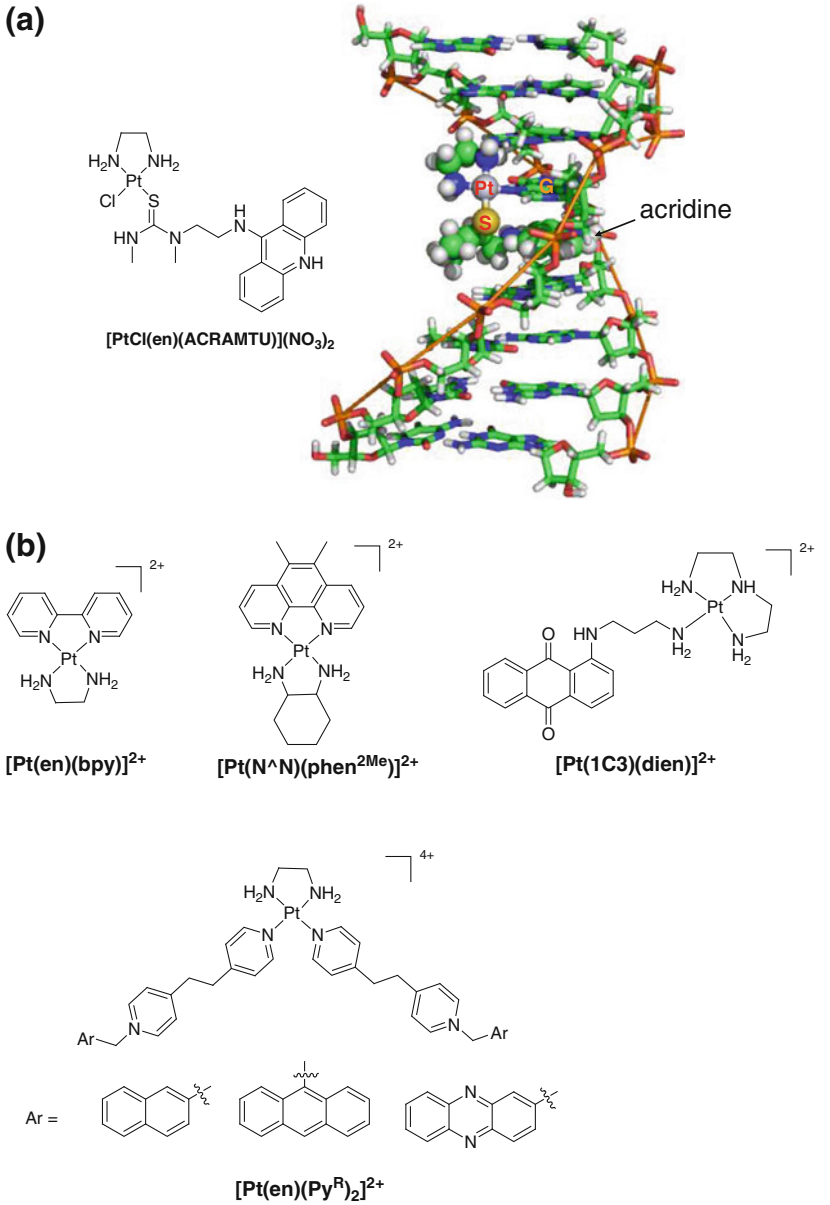

Fig. 1.19 DNA-targeting platinum(II) complexes reported by other groups. **a** A dual DNA metalating and intercalating Pt(II) complex developed by Bierbach and coworkers. **b** other forms of Pt(II)-based DNA intercalators

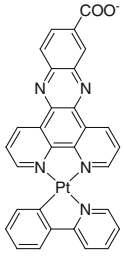

[Pt(dppz^{COO})(CN)]

J. Am. Chem. Soc. **2009**, *131*, 1835-1846.

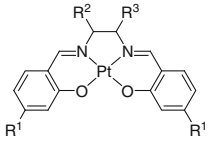

[Pt(ONNO)]

Chem. Eur. J. **2009**, *15*, 13008-13021.

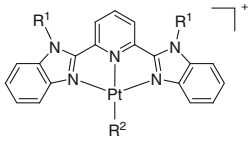

[Pt(BPB)(R)]$^+$

Chem. Eur. J. **2010,** *16*, 6900-6911.

Sleiman and coworkers recently reported an interesting series of platinum(II)–phenanthroimidazole complexes bearing cationic side chains. These Pt(II) complexes selectively bind to a G-quadruplex in the *c-Kit* promoter. Cytotoxicity studies using telomerase-proficient cell lines revealed that these complexes do not induce cytotoxicity through a telomere-targeting mechanism. mRNA analysis revealed a specific interaction of the complexes at the *c-Kit* promoter region, suggesting an alternative pathway for the observed anticancer activities [115].

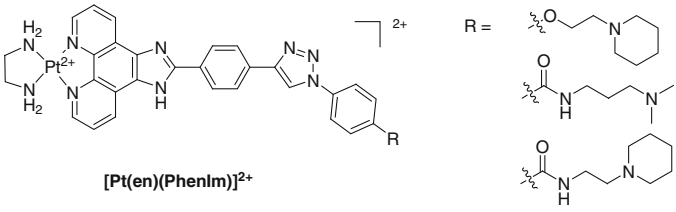

[Pt(en)(Phenlm)]$^{2+}$

Targeting DNA topoisomerases. Che and coworkers reported the use of DNA binding as a criterion to identify new platinum(II) complexes that can act as inhibitors of topoisomerase (Topo) activity. Topo is capable of controlling the overwinding and underwinding of DNA during the DNA replication processes. Platinum(II) complexes containing tridentate C-deprotonated C^N^N or terpy and nucleo-base containing alkyne ligands were found to display potent inhibition of TopoII (which cleaves both strands of DNA). [Pt(C^N^N)(alkyne)] can intercalate into DNA, while [Pt(terpy^{tBu})(alkyne)]$^+$ was reported to bind to DNA via groove binding; the topoII inhibition could be caused by either of these two DNA-binding modes [116]. The cyclometalated platinum(II) complexes [Pt(C^N)(isocyanide)$_2$]$^+$ (containing isocyanide ligands) were reported to inhibit TopoIIα activity via stabilizing the covalent TopoIIα-DNA cleavage complex, with a potency higher than a clinical TopoIIα inhibitor (etoposide, Vp-16) [117].

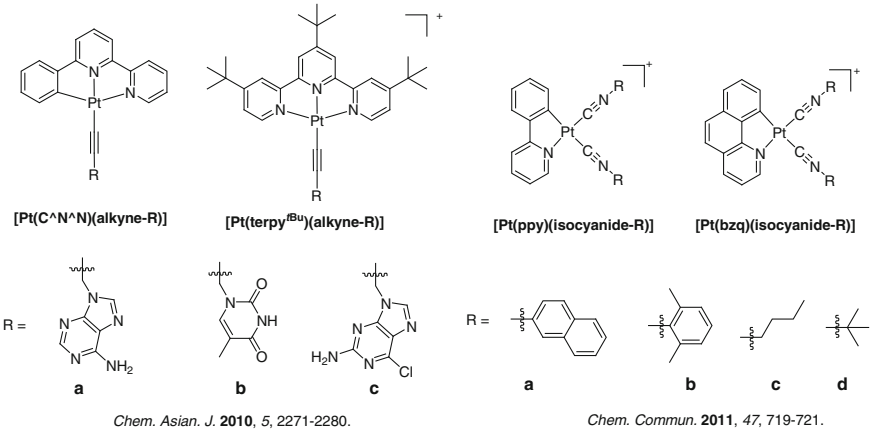

Chem. Asian. J. **2010**, *5*, 2271-2280. *Chem. Commun.* **2011**, *47*, 719-721.

1.4.2.2 Platinum Complexes with Non-DNA Targets

Targeting cytoplasmic structures. Though the square planar coordination geometry of platinum(II) complexes favors DNA binding, coordination of auxiliary bulky ligands, such as N-heterocyclic carbene to Pt(II), can switch the target of binding to non-DNA species. The $[Pt(C^N^N)(NHC)]^+$ complex containing an N-heterocyclic carbene ligand is strongly emissive but displays low DNA-binding affinity. Fluorescent microscopic analysis indicated that this complex selectively accumulates in mitochondria. It is noteworthy that $[Pt(C^N^N)(NHC)]^+$ is the first example of a transition metal complex that can suppress the expression of survivin (a member of the apoptosis inhibitor [IAP] family) as revealed by Western blotting analysis. $[Pt(C^N^N)(NHC)]^+$ selectively inhibited cancer cell growth in vitro and inhibited tumor growth in mice bearing NCI-H460 tumors [118].

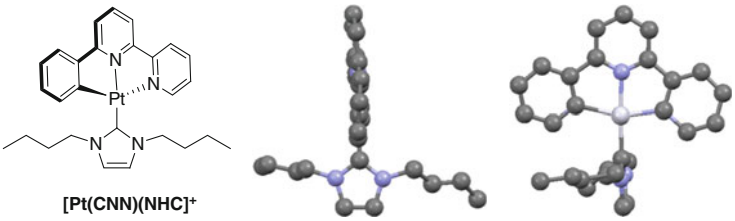

Proteasome inhibitors. Dou, Rashidi, Hemmateenejad, and coworkers reported that the complexes [Pt(bpy)(dppm)]Cl and [Pt(bpy)(dppa)]Cl, both containing diphosphine ligands, elicited proteasome inhibition. [Pt(bpy)(dppm)]Cl showed a higher inhibitory activity toward purified 20S proteasomes, while [Pt(bpy)(dppa)Cl] was more potent against purified 26S proteasomes. These two complexes could also

inhibit cancer cell growth in vitro and tumor growth in vivo; the tumor inhibition was attributed to suppression of proteasome activity [119].

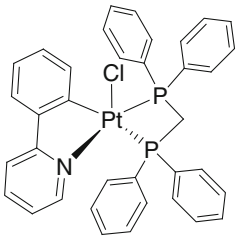

[Pt(ppy)(dppm)Cl]$^+$

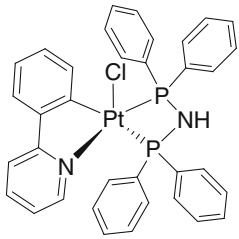

[Pt(ppy)(dppa)Cl]$^+$

1.5 The Chemistry of N-Heterocyclic Carbene Ligands

N-Heterocyclic carbenes (NHC) were first studied as analogues of phosphine ligands. Since the initial discovery of Chugaev-type diamino carbenes that can be obtained from the reaction of isocyanides and primary amines, various heterocyclic carbene ligands have been developed. The most intriguing properties of NHC ligands are their strong electron donor strength and ease of functionalization. The former property can be harnessed to stabilize metal ions in applications where stability is a key issue, such as in the development of metal-based medicines. Up to now, metal complexes bearing NHC ligands have been applied in various areas including luminescent materials [120], catalysis [121], and medicinal chemistry [122].

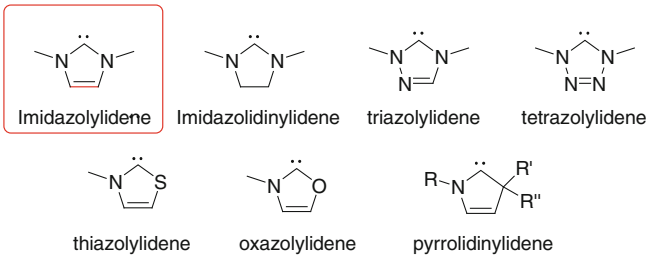

1.5.1 Electronic Properties of NHC Ligands

N-heterocyclic carbenes are strong σ-donor ligands. Their electron donor ability is stronger than the classical phosphine ligands.

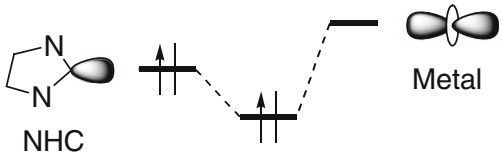

σ donating (σ to d)

N-heterocyclic carbene can also act as a π-accepting ligand that can accept electron density from metal ions.

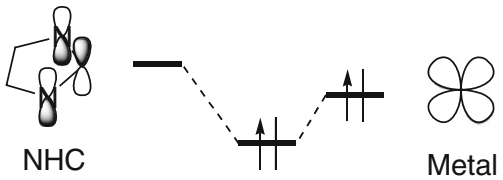

π* accepting (d to π*)

1.5.2 Steric Effects of NHC Ligands

The N-substituents of NHC ligands are responsible for the steric effects of these ligands upon metal coordination. The percentage of buried volume, $\%V_{Bur,}$ is used as a standard value to describe the percentage of volume occupied by the NHC ligand in the first coordination sphere of the metal ion. The commonly used NHC ligands and corresponding $\%V_{Bur}$ are depicted in the following figure [123]. Silver-NHC complexes having different N-substituents have been investigated by Ortiz et al. [124]. The steric effect may hinder attack (i.e., hampering ligand exchanging) from other ligands.

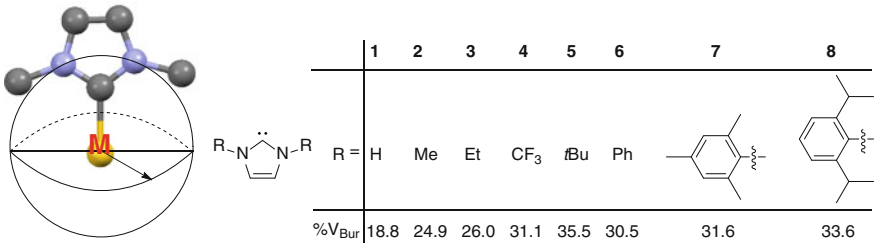

1.5.3 *Synthesis of NHC Ligands [125]*

Imidazolium compounds are a common type of precursors of NHC ligands. In general, there are three routes to synthesize the precursors of NHC ligands. Route 1 starts from imidazole, and both symmetric and asymmetric NHC precursors can be generated. But this route is confined to those compounds having alkyl substituents that are introduced through a nucleophilic exchange reaction of imidazole with RX. For the synthesis of aryl-substituted NHC carbenes, the cyclization of α-diimine (route 2) or diazobutadiene (route 3) with formaldehyde is a commonly used step. Again, both symmetric and asymmetric NHC precursors can be prepared this way.

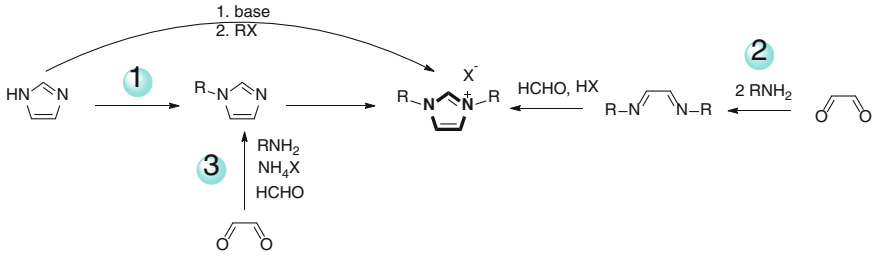

Fürstner et al. recently reported a general synthetic route to form substituted imidazolium salts, in which case two N-substituents, C4- and C5-substitutents, can be easily modified [126].

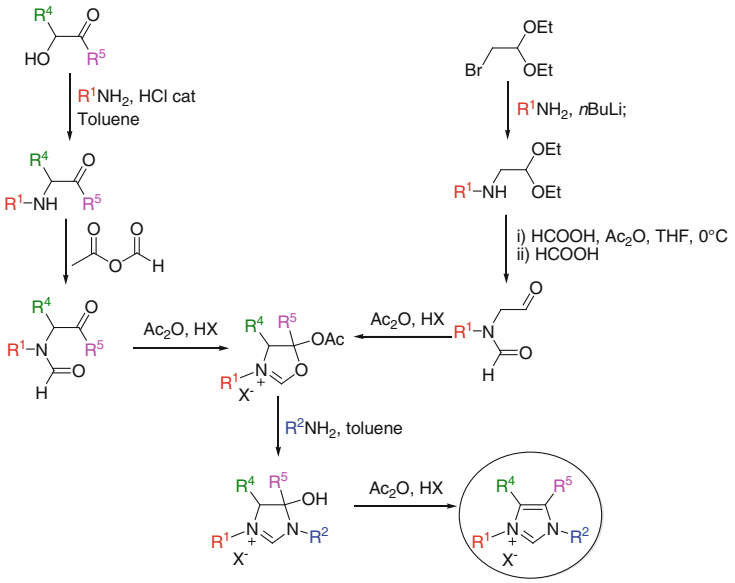

In general, the synthesis (that uses different amines) of unsymmetrical NHCs having multiple components usually gives a mixture of NHC precursors, half of which are asymmetric precursors. Baslé, Mauduit, and coworkers reported that multicomponent synthesis of unsymmetrical N-heterocyclic carbene precursors bearing a cycloalkyl moiety gave products in high yields and selectivity [127].

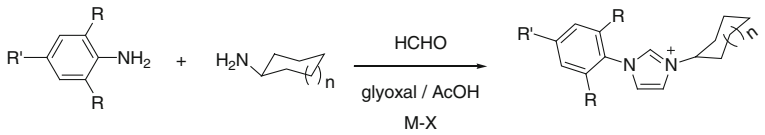

1.5.4 Synthesis of Metal–NHC Complexes

Due to the high reactivity of NHC ligands, the metal–C_{NHC} bond is usually formed by the reaction of a metal compound/salt/ion with NHC in situ generated from its precursor. The widely used strategies to form M–C_{NHC} bonds are direct deprotonation of imidazolium compounds and transmetalation reactions:

- Deprotonation by using strong base (e.g., KO^{t}Bu, NEt_3).

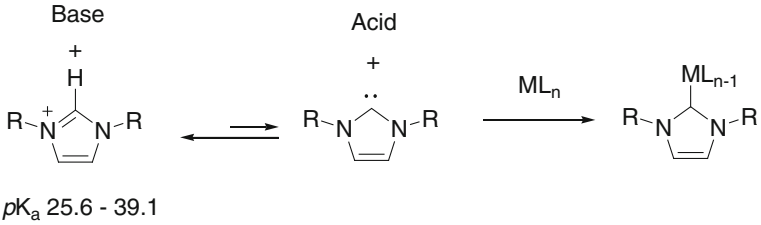

- Transmetalation with Ag–NHC precursors. This kind of reaction generally proceeds under mild conditions as heat, inert atmosphere, and/or strong bases are not required. AgX is insoluble and can be easily removed by filtration. Various metal–NHC complexes (e.g., Cu, Ni, Pd, Au, Pt, Rh, Ir, Ru) can be obtained by transmetalation reactions.

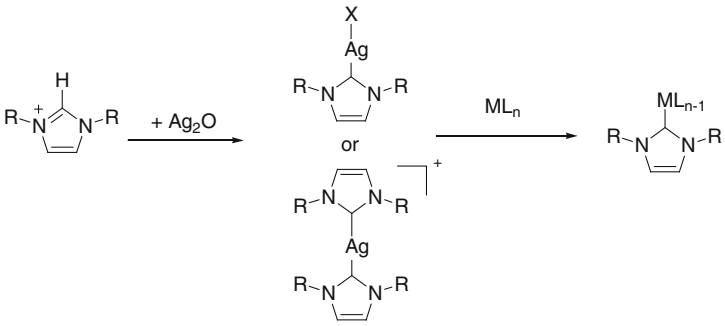

The following are the alternative methods to prepare NHC:

- Using NHC adduct is a means to protect NHC. Elimination of alcohol, chloroform, or CO_2 gives NHCs in situ:

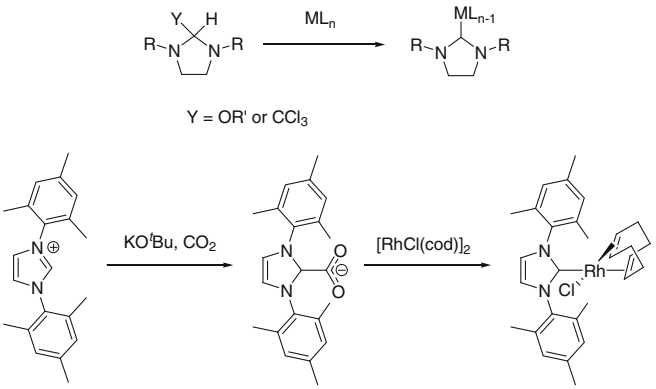

- Oxidative addition at the C2–X bond by using low-valent metal complexes.

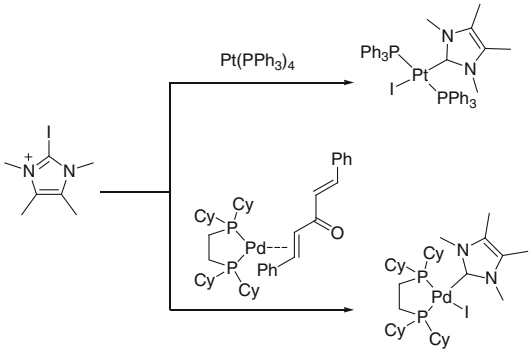

- Direct deprotonation reaction of imidazole.

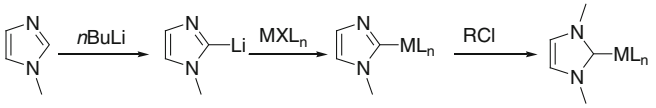

1.6 Luminescent Properties of Platinum(II) and Gold(I)/(III) Complexes

As mentioned above, platinum complexes usually display intriguing luminescent characteristics. What are the unique features of luminescent platinum(II) complexes? And what can one do to increase their emission quantum yields? In general,

for d-block transition metal complexes, three types of excited states are usually encountered: ligand-centered (IL), metal-to-ligand charge transfer (MLCT), and metal centered d–d. A typical molecular orbital diagram for square planar d^8 metal complexes is depicted below. In the d–d excited states, the antibonding $d_{x^2-y^2}$ orbital is populated. This would cause lengthening of the metal–ligand bond, leading to facile non-radiative decay via structural distortion in the excited state.

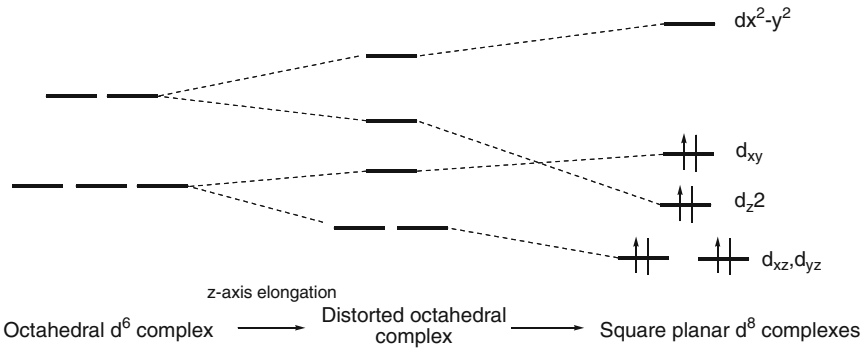

In the design of luminescent d^8 metal complexes, low-lying d–d state(s) should be avoided in order to minimize structural distortion of the emissive excited state. That is, the energy of the d–d state should be higher than that of ligand-centered or metal-to-ligand charge transfer excited states (the band gap will also be greater than kT). In this regard, strong field ligands that give a large energy gap between $d_{x^2-y^2}$ and d_{xy} orbitals are desirable. In addition, rigid, chelating ligands can minimize the structural distortion of the excited state [128].

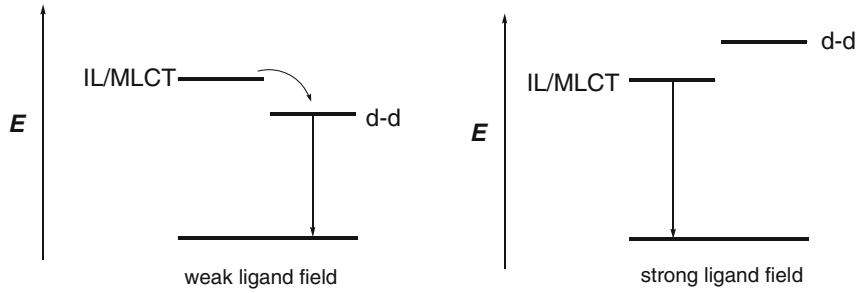

Compared to Pt(II), Au(III) has a much lower lying $d_{x^2-y^2}$, and this accounts for the fact that most of the reported gold(III) complexes to be non-emissive.

1.7 Fluorescent Thiol Probes

Cellular thiols play a pivotal role in the regulation of important biological processes including redox balance and cell apoptosis. Based on the strong nucleophilicity and high metal-binding affinity of thiols, a large number of organic, and a small number of inorganic, thiol probes have been described. Organic thiol probes can be divided into several categories with notable examples being based on maleimide-based Michael addition reactions, aldehyde-based cyclization, and cleavage reactions of sulfonamide, sulfonate, and disulfide by thiols [129]. Metal complexes have rich redox and coordination properties that can be applied as thiol probes. For example, Lam, Wong, and coworkers designed a trinuclear Ru(II)/Pt(II) complex which would release a luminescent Ru(II) complex upon reaction with thiols; this is attributed to the high binding affinity of Pt ion for soft thiols [130].

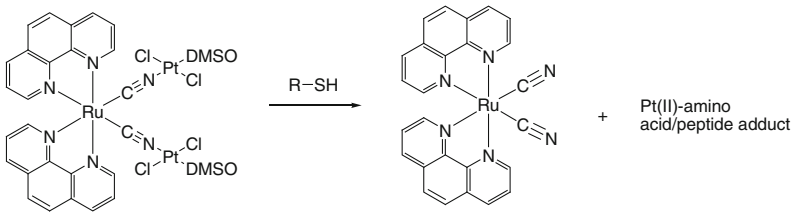

References

1. Farrer NJ, Sadler PJ (2011) Medicinal inorganic chemistry: state of the art, new trends, and a vision of the future. In: Alessio E (ed) Bioinorg Med Chem. Wiley-VCH, Germany, pp 1–37
2. Ronconi L, Sadler PJ (2007) Using coordination chemistry to design new medicines. Coord Chem Rev 251(13–14):1633–1648
3. Lo-Coco F, Avvisati G, Vignetti M, Thiede C, Orlando SM, Iacobelli S, Ferrara F, Fazi P, Cicconi L, Di Bona E, Specchia G, Sica S, Divona M, Levis A, Fiedler W, Cerqui E, Breccia M, Fioritoni G, Salih HR, Cazzola M, Melillo L, Carella AM, Brandts CH, Morra E, von Lilienfeld-Toal M, Hertenstein B, Wattad M, Lübbert M, Hänel M, Schmitz N, Link H, Kropp MG, Rambaldi A, La Nasa G, Luppi M, Ciceri F, Finizio O, Venditti A, Fabbiano F, Döhner K, Sauer M, Ganser A, Amadori S, Mandelli F, Döhner H, Ehninger G, Schlenk RF, Platzbecker U (2013) Retinoic acid and arsenic trioxide for acute promyelocytic leukemia. N Engl J Med 369(2):111–121
4. Au W-Y, Kumana CR, Kou M, Mak R, Chan GCF, Lam C-W, Kwong Y-L (2003) Oral arsenic trioxide in the treatment of relapsed acute promyelocytic leukemia 102(1). doi:10.1182/blood-2003-01-0298
5. Barry NPE, Sadler PJ (2012) Dicarba-closo-dodecarborane-containing half-sandwich complexes of ruthenium, osmium, rhodium and iridium: biological relevance and synthetic strategies. Chem Soc Rev 41(8):3264–3279

6. Abeysinghe PM, Harding MM (2007) Antitumour Bis(cyclopentadienyl) metal complexes: titanocene and molybdocene dichloride and derivatives. Dalton Trans 32:3474–3482
7. Che C-M, Sun RW-Y, Yu W-Y, Ko C-B, Zhu N, Sun H (2003) Gold(III) porphyrins as a new class of anticancer drugs: cytotoxicity, DNA binding and induction of apoptosis in human cervix epitheloid cancer cells. Chem Commun 14:1718–1719
8. Berners-Price SJ, Mirabelli CK, Johnson RK, Mattern MR, McCabe FL, Faucette LF, Sung C-M, Mong S-M, Sadler PJ, Crooke ST (1986) In vivo antitumor activity and in vitro cytotoxic properties of Bis[1,2-bis(diphenylphosphino)ethane]gold(I) chloride. Cancer Res 46(11):5486–5493
9. Ni W-X, Man W-L, Cheung MT-W, Sun RW-Y, Shu Y-L, Lam Y-W, Che C-M, Lau T-C (2011) Osmium(VI) complexes as a new class of potential anti-cancer agents. Chem Commun 47(7):2140–2142
10. Alama A, Viale M, Cilli M, Bruzzo C, Novelli F, Tasso B, Sparatore F (2009) In vitro cytotoxic activity of Tri-n-Butyltin(IV)lupinylsulfide hydrogen fumarate (IST-FS 35) and Preliminary antitumor activity in vivo. Invest New Drugs 27(2):124–130
11. Bandoli G, Dolmella A, Tisato F, Porchia M, Refosco F (2009) Mononuclear six-coordinated Ga(III) complexes: a comprehensive survey. Coord Chem Rev 253(1–2):56–77
12. Tisato F, Marzano C, Porchia M, Pellei M, Santini C (2010) Copper in diseases and treatments, and copper-based anticancer strategies. Med Res Rev 30(4):708–749
13. Magda D, Lecane P, Wang Z, Hu W, Thiemann P, Ma X, Dranchak PK, Wang X, Lynch V, Wei W, Csokai V, Hacia JG, Sessler JL (2008) Synthesis and anticancer properties of water-soluble zinc ionophores. Cancer Res 68(13):5318–5325
14. Li H, Lai CS, Wu J, Ho PC, de Vos D, Tiekink ERT (2007) Cytotoxicity, Qualitative Structure-Activity Relationship (QSAR), and anti-tumor activity of bismuth dithiocarbamate complexes. J Inorg Biochem 101(5):809–816
15. Yamase T (2005) Anti-tumor, -Viral, and -Bacterial activities of polyoxometalates for realizing an inorganic drug. J Mater Chem 15(45):4773–4782
16. Rosenberg B, Van Camp L, Krigas T (1965) Inhibition of cell division in Escherichia coli by electrolysis products from a platinum electrode. Nature 205(4972):698–699
17. Rosenberg B, Vancamp L, Trosko JE, Mansour VH (1969) Platinum compounds: a new class of potent antitumour agents. Nature 222(5191):385–386
18. Kelland L (2007) The resurgence of platinum-based cancer chemotherapy. Nat Rev Cancer 7 (8):573–584
19. Wheate NJ, Walker S, Craig GE, Oun R (2010) The status of platinum anticancer drugs in the clinic and in clinical trials. Dalton Trans 39(35):8113–8127
20. Oberoi HS, Nukolova NV, Kabanov AV, Bronich TK (2013) Nanocarriers for delivery of platinum anticancer drugs. Adv Drug Deliv Rev 65(13–14):1667–1685
21. Fichtinger-Schepman AMJ, van Oosterom AT, Lohman PHM, Berends F (1987) cis-diamminedichloroplatinum(II)-induced DNA adducts in peripheral leukocytes from seven cancer patients: quantitative immunochemical detection of the adduct induction and removal after a single dose of cis-diamminedichloroplatinum(II). Cancer Res 47 (11):3000–3004
22. Baik M-H, Friesner RA, Lippard SJ (2003) Theoretical study of cisplatin binding to purine bases: why does cisplatin prefer guanine over adenine? J Am Chem Soc 125(46): 14082–14092
23. Legendre F, Bas V, Kozelka J, Chottard J-C (2000) A complete kinetic study of GG versus AG Platination suggests that the doubly aquated derivatives of cisplatin are the actual DNA binding species. Chem Eur J 6(11):2002–2010
24. Kozelka J, Legendre F, Reeder F, Chottard J-C (1999) Kinetic aspects of interactions between DNA and platinum complexes. Coord Chem Rev 190–192:61–82
25. Legendre F, Kozelka J, Chottard J-C (1998) GG versus AG Platination: a kinetic study on hairpin-stabilized duplex oligonucleotides. Inorg Chem 37(16):3964–3967
26. Reedijk J (2003) New clues for platinum antitumor chemistry: kinetically controlled metal binding to DNA. Proc Natl Acad Sci 100(7):3611–3616

27. Reedijk J (1999) Why does cisplatin reach guanine-N7 with Competing S-donor Ligands available in the cell? Chem Rev 99(9):2499–2510
28. Mandic A, Hansson J, Linder S, Shoshan MC (2003) Cisplatin induces endoplasmic reticulum stress and nucleus-independent apoptotic signaling. J Biol Chem 278(11): 9100–9106
29. Lacour S, Hammann A, Grazide S, Lagadic-Gossmann D, Athias A, Sergent O, Laurent G, Gambert P, Solary E, Dimanche-Boitrel M-T (2004) Cisplatin-induced CD95 redistribution into membrane lipid rafts of HT29 human colon cancer cells. Cancer Res 64(10):3593–3598
30. Aris SM, Farrell NP (2009) Towards antitumor active trans-platinum compounds. Eur J Inorg Chem 10:1293–1302
31. Chen S, Xu D, Jiang H, Xi Z, Zhu P, Liu Y (2012) Trans-Platinum/Thiazole complex interferes with Sp1 Zinc-Finger Protein. Angew Chem Int Ed 51(49):12258–12262
32. Laguna A (2008) Modern supramolecular gold chemistry: gold-metal interactions and applications. Wiley-VCH Verlag GmbH & Co. KGaA, Weinheim
33. Fricker SP (2010) Cysteine proteases as targets for metal-based drugs. Metallomics 2 (6):366–377
34. de Almeida A, Soveral G, Casini A (2014) Gold compounds as aquaporin inhibitors: new opportunities for therapy and imaging. Med Chem Comm 5:1444–1453
35. Bindoli A, Rigobello MP, Scutari G, Gabbiani C, Casini A, Messori L (2009) Thioredoxin reductase: a target for gold compounds acting as potential anticancer drugs. Coord Chem Rev 253(11–12):1692–1707
36. Urig S, Fritz-Wolf K, Réau R, Herold-Mende C, Tóth K, Davioud-Charvet E, Becker K (2006) Undressing of phosphine gold(I) complexes as irreversible inhibitors of human disulfide reductases. Angew Chem Int Ed 45(12):1881–1886
37. Angelucci F, Sayed AA, Williams DL, Boumis G, Brunori M, Dimastrogiovanni D, Miele AE, Pauly F, Bellelli A (2009) Inhibition of schistosoma mansoni thioredoxin-glutathione reductase by auranofin: structural and kinetic aspects. J Biol Chem 284(42):28977–28985
38. Ilari A, Baiocco P, Messori L, Fiorillo A, Boffi A, Gramiccia M, Di Muccio T, Colotti G (2012) A cold-containing drug against parasitic polyamine metabolism: the X-Ray structure of trypanothione reductase from leishmania infantum in complex with auranofin reveals a dual mechanism of enzyme inhibition. Amino Acids 42(2–3):803–811
39. Cheng Q, Sandalova T, Lindqvist Y, Arnér ESJ (2009) Crystal structure and catalysis of the selenoprotein thioredoxin reductase 1. J Biol Chem 284(6):3998–4008
40. Karver MR, Krishnamurthy D, Kulkarni RA, Bottini N, Barrios AM (2009) Identifying potent, selective protein tyrosine phosphatase inhibitors from a library of Au(I) complexes. J Med Chem 52(21):6912–6918
41. Jeon K-I, Jeong J-Y, Jue D-M (2000) Thiol-reactive metal compounds inhibit NF-κB activation by blocking IκB kinase. J Immunol 164(11):5981–5989
42. Zhang J-J, Ng K-M, Lok C-N, Sun RW-Y, Che C-M (2013) Deubiquitinases as potential anti-cancer targets for gold(III) complexes. Chem Commun 49(45):5153–5155
43. Martins AP, Ciancetta A, de Almeida A, Marrone A, Re N, Soveral G, Casini A (2013) Aquaporin Inhibition by gold(III) compounds: new insights. Chem Med Chem 8(7): 1086–1092
44. Martins AP, Marrone A, Ciancetta A, Cobo AG, Echevarrya M, Moura TF, Re N, Casini A, Soveral G (2012) Targeting aquaporin function: potent inhibition of aquaglyceroporin-3 by a gold-based compound. PLoS ONE 7(5):e37435
45. Zou J, Taylor P, Dornan J, Robinson SP, Walkinshaw MD, Sadler PJ (2000) First crystal structure of a medicinally relevant gold protein complex: unexpected binding of $[Au(PEt_3)]^+$ to histidine. Angew Chem Int Ed 39(16):2931–2934
46. Messori L, Scaletti F, Massai L, Cinellu MA, Russo Krauss I, di Martino G, Vergara A, Paduano L, Merlino A (2014) Interactions of gold-based drugs with proteins: crystal structure of the adduct formed between ribonuclease A and a cytotoxic gold(III) compound. Metallomics 6:233–236

47. Messori L, Scaletti F, Massai L, Cinellu MA, Gabbiani C, Vergara A, Merlino A (2013) The mode of action of anticancer gold-based drugs: a structural perspective. Chem Commun 49 (86):10100–10102
48. Berners-Price SJ, Filipovska A (2011) Gold compounds as therapeutic agents for human diseases. Metallomics 3(9):863–873
49. Pillarsetty N, Katti KK, Hoffman TJ, Volkert WA, Katti KV, Kamei H, Koide T (2003) In vitro and in vivo antitumor properties of tetrakis((trishydroxymethyl) phosphine)gold(I) chloride. J Med Chem 46:1130–1132
50. Tian S, Siu F-M, Kui SCF, Lok C-N, Che C-M (2011) Anticancer gold(I)-phosphine complexes as potent autophagy-inducing agents. Chem Commun 47(33):9318–9320
51. Simon TM, Kunishima DH, Vibert GJ, Lorber A (1981) Screening trial with the coordinated gold compound auranofin using mouse lymphocytic leukemia P388. Cancer Res 41(1):94–97
52. Christopher P, Leamon JAR, Vlahov Iontcho R, Kleindl Paul J, Vetzel Marilynn, Westrick Elaine (1985) Evaluation of the in vivo antitumor activity and in vitro cytotoxic properties of auranofin, a coordinated gold compound, in murine tumor models. Cancer Res 45:32–39
53. Sadler PJ, Sue RE (1994) The chemistry of gold drugs. Met-Based Drugs 1(2–3):107–144
54. Shaw CF III (1999) Gold-Based Therapeutic Agents. Chem Rev 99(9):2589–2600
55. Kamei H, Koide T, Kojima T, Hashimoto Y, Hasegawa M (1998) Effect of gold on survival of tumor-bearing mice. Cancer Biother Radiopharm 13(5):403–406
56. Stallings-Mann M, Jamieson L, Regala RP, Weems C, Murray NR, Fields AP (2006) A novel small-molecule inhibitor of protein kinase ciota blocks transformed growth of non-small-cell lung cancer cells. Cancer Res 66(3):1767–1774
57. Baker MV, Barnard PJ, Berners-Price SJ, Brayshaw SK, Hickey JL, Skelton BW, White AH (2006) Cationic, linear Au(I) N-heterocyclic carbene complexes: synthesis. Struct Anti-Mitochondrial Act Dalton Trans 30:3708–3715
58. Hickey JL, Ruhayel RA, Barnard PJ, Baker MV, Berners-Price SJ, Filipovska A (2008) Mitochondria-targeted chemotherapeutics: the rational design of gold(I) N-heterocyclic carbene complexes that are selectively toxic to cancer cells and target protein selenols in preference to thiols. J Am Chem Soc 130(38):12570–12571
59. Rubbiani R, Kitanovic I, Alborzinia H, Can S, Kitanovic A, Onambele LA, Stefanopoulou M, Geldmacher Y, Sheldrick WS, Wolber G, Prokop A, Wölfl S, Ott I (2010) Benzimidazol-2-ylidene gold(I) complexes are thioredoxin reductase inhibitors with multiple antitumor properties. J Med Chem 53(24):8608–8618
60. Rubbiani R, Can S, Kitanovic I, Alborzinia H, Stefanopoulou M, Kokoschka M, Mönchgesang S, Sheldrick WS, Wölfl S, Ott I (2011) comparative in vitro evaluation of N-heterocyclic carbene gold(I) complexes of the benzimidazolylidene type. J Med Chem 54 (24):8646–8657
61. Meyer A, Bagowski CP, Kokoschka M, Stefanopoulou M, Alborzinia H, Can S, Vlecken DH, Sheldrick WS, Wölfl S, Ott I (2012) On the biological properties of alkynyl phosphine gold(I) complexes. Angew Chem Int Ed 51(39):8895–8899
62. Ott I, Qian X, Xu Y, Vlecken DHW, Marques IJ, Kubutat D, Will J, Sheldrick WS, Jesse P, Prokop A, Bagowski CP (2009) A gold(I) phosphine complex containing naphthalimide ligand functions as a TrxR inhibiting antiproliferative agent and angiogenesis inhibitor. J Med Chem 52(3):763–770
63. Chui CH, Wong RS-M, Gambari R, Cheng GY-M, Yuen MC-W, Chan K-W, Tong S-W, Lau F-Y, Lai PB-S, Lam K-H, Ho C-L, Kan C-W, Leung KS-Y, Wong W-Y (2009) Antitumor activity of diethynylfluorene derivatives of gold(I). Bioorg Med Chem 17 (23):7872–7877
64. Yan K, Lok C-N, Bierla K, Che C-M (2010) Gold(I) complex of N, N′-disubstituted cyclic thiourea with in vitro and in vivo anticancer properties-potent tight-binding inhibition of thioredoxin reductase. Chem Commun 46:7691–7693

65. Sun RW-Y, Li CK-L, Ma D-L, Yan JJ, Lok C-N, Leung C-H, Zhu N, Che C-M (2010) Stable anticancer gold(III)-porphyrin complexes: effects of porphyrin structure. Chem Eur J 16 (10):3097–3113
66. Lum CT, Liu X, Sun RW-Y, Li X-P, Peng Y, He M-L, Kung HF, Che C-M, Lin MCM (2010) Gold(III) porphyrin 1a inhibited nasopharyngeal carcinoma metastasis in vivo and inhibited cell migration and invasion in vitro. Cancer Lett 294(2):159–166
67. Lum CT, Yang ZF, Li HY, Wai-Yin Sun R, Fan ST, Poon RTP, Lin MCM, Che C-M, Kung HF (2006) Gold(III) compound is a novel chemocytotoxic agent for hepatocellular carcinoma. Int J Cancer 118(6):1527–1538
68. Tu SP, Sun RW-Y, Lin MCM, Cui JT, Zou B, Gu Q, Kung HF, Che C-M, Wong BCY (2009) Gold (III) porphyrin complexes induce apoptosis and cell cycle arrest and inhibit tumor growth in colon cancer. Cancer 115(19):4459–4469
69. Li W, Xie Y, Sun RWY, Liu Q, Young J, Yu WY, Che CM, Tam PK, Ren Y (2009) Inhibition of Akt sensitises neuroblastoma cells to gold(III) porphyrin 1a, a novel antitumour drug induced apoptosis and growth inhibition. Br J Cancer 101(2):342–349
70. Lum CT, Huo L, Sun RW-Y, Li M, Kung HF, Che C-M, Lin MCM (2011) Gold(III) porphyrin 1a prolongs the survival of melanoma-bearing mice and inhibits angiogenesis. Acta Oncol 50(5):719–726
71. Lum CT, Wong A, Lin MC, Che C-M, Sun RW-Y (2013) Gold(III) porphyrin complex as an anti-cancer candidate to inhibit growth of cancer-stem cells. Chem Commun 49:4364–4366
72. Sun RW-Y, Lok C-N, Fong TT-H, Li CK-L, Yang ZF, Zou T, Siu AF-M, Che C-M (2013) A dinuclear cyclometalated gold(III)-phosphine complex targeting thioredoxin reductase inhibits hepatocellular carcinoma in vivo. Chem Sci 4:1979–1988
73. Yan JJ, Chow AL-F, Leung C-H, Sun RW-Y, Ma D-L, Che C-M (2010) Cyclometalated gold(III) complexes with N-heterocyclic carbene ligands as topoisomerase I poisons. Chem Commun 46(22):3893–3895
74. Buckley RG, Elsome AM, Fricker SP, Henderson GR, Theobald BRC, Parish RV, Howe BP, Kelland LR (1996) Antitumor properties of some 2-[(Dimethylamino)methyl]phenylgold(III) complexes. J Med Chem 39(26):5208–5214
75. Parish RV, Howe BP, Wright JP, Mack J, Pritchard RG, Buckley RG, Elsome AM, Fricker SP (1996) Chemical and biological studies of dichloro(2-((dimethylamino)methyl) phenyl)gold(III). Inorg Chem 35(6):1659–1666
76. Zhu Y, Cameron BR, Mosi R, Anastassov V, Cox J, Qin L, Santucci Z, Metz M, Skerlj RT, Fricker SP (2011) Inhibition of the cathepsin cysteine proteases B and K by square-planar cycloaurated gold(III) compounds and investigation of their anti-cancer activity. J Inorg Biochem 105(5):754–762
77. Messori L, Marcon G, Cinellu MA, Coronnello M, Mini E, Gabbiani C, Orioli P (2004) Solution chemistry and cytotoxic properties of novel organogold(III) compounds. Biorg Med Chem 12(23):6039–6043
78. Gabbiani C, Mastrobuoni G, Sorrentino F, Dani B, Rigobello MP, Bindoli A, Cinellu MA, Pieraccini G, Messori L, Casini A (2011) Thioredoxin reductase, an emerging target for anticancer metallodrugs: enzyme inhibition by cytotoxic gold(III) compounds studied with combined mass spectrometry and biochemical assays. Med Chem Comm 2(1):50–54
79. Shaik N, Martínez A, Augustin I, Giovinazzo H, Varela-Ramírez A, Sanaú M, Aguilera RJ, Ma Contel (2009) synthesis of apoptosis-inducing iminophosphorane organogold(III) complexes and study of their interactions with biomolecular targets. Inorg Chem 48 (4):1577–1587
80. Vela L, Contel M, Palomera L, Azaceta G, Marzo I (2011) Iminophosphorane–Organogold (III) complexes induce cell death through mitochondrial ROS production. J Inorg Biochem 105(10):1306–1313
81. Zhang J-J, Sun RW-Y, Che C-M (2012) A dual cytotoxic and anti-angiogenic water-soluble gold(III) complex induces endoplasmic reticulum damage in hela cells. Chem Commun 48 (28):3388–3390

82. Messori L, Abbate F, Marcon G, Orioli P, Fontani M, Mini E, Mazzei T, Carotti S, O′ Connell T, Zanello P (2000) Gold(III) complexes as potential antitumor agents: solution chemistry and cytotoxic properties of some selected gold(III) compounds. J Med Chem 43 (19):3541–3548
83. Nobili S, Mini E, Landini I, Gabbiani C, Casini A, Messori L (2010) Gold compounds as anticancer agents: chemistry, cellular pharmacology, and preclinical studies. Med Res Rev 30 (3):550–580
84. Gabbiani C, Scaletti F, Massai L, Michelucci E, Cinellu MA, Messori L (2012) Medicinal gold compounds form tight adducts with the copper chaperone Atox-1: biological and pharmacological implications. Chem Commun 48:11623–11625
85. Milacic V, Chen D, Ronconi L, Landis-Piwowar KR, Fregona D, Dou QP (2006) A novel anticancer gold(III) dithiocarbamate compound inhibits the activity of a purified 20S Proteasome and 26S proteasome in human breast cancer cell cultures and xenografts. Cancer Res 66(21):10478–10486
86. Saggioro D, Rigobello MP, Paloschi L, Folda A, Moggach SA, Parsons S, Ronconi L, Fregona D, Bindoli A (2007) Gold(III)-dithiocarbamato complexes induce cancer cell death triggered by thioredoxin redox system inhibition and activation of ERK pathway. Chem Biol 14(10):1128–1139
87. Ronconi L, Aldinucci D, Dou QP, Fregona D (2010) Latest insights into the anticancer activity of gold(III)-dithiocarbamato complexes. Anti-Cancer Agents Med Chem 10:283–292
88. Dhar S, Liu Z, Thomale J, Dai H, Lippard SJ (2008) targeted single-wall carbon nanotube-mediated Pt(IV) prodrug delivery using folate as a homing device. J Am Chem Soc 130(34):11467–11476
89. Muller P, Schroder B, Parkinson JA, Kratochwil NA, Coxall RA, Parkin A, Parsons S, Sadler PJ (2003) Nucleotide cross-linking induced by photoreactions of platinum(IV)-azide complexes. Angew Chem Int Ed 42(3):335–339
90. Farrer NJ, Woods JA, Salassa L, Zhao Y, Robinson KS, Clarkson G, Mackay FS, Sadler PJ (2010) A potent trans-diimine platinum anticancer complex photoactivated by visible light. Angew Chem Int Ed 49(47):8905–8908
91. Zhao Y, Farrer NJ, Li H, Butler JS, McQuitty RJ, Habtemariam A, Wang F, Sadler PJ (2013) De novo generation of singlet oxygen and ammine ligands by photoactivation of a platinum anticancer complex. Angew Chem Int Ed 52(51):13633–13637
92. Min Y, Li J, Liu F, Yeow EK, Xing B (2013) Near-infrared light-mediated photoactivation of a platinum antitumor prodrug and simultaneous cellular apoptosis imaging by upconversion-luminescent nanoparticles. Angew Chem Int Ed 53(4):1012–1016
93. Dai Y, Xiao H, Liu J, Yuan Q, Pa Ma, Yang D, Li C, Cheng Z, Hou Z, Yang P, Lin J (2013) In vivo multimodality imaging and cancer therapy by near-infrared light-triggered trans-platinum pro-drug-conjugated upconverison nanoparticles. J Am Chem Soc 135 (50):18920–18929
94. Pathak RK, Marrache S, Choi JH, Berding TB, Dhar S (2014) The prodrug platin-A: simultaneous release of cisplatin and aspirin. Angew Chem Int Ed 53(7):1963–1967
95. Chin CF, Yap SQ, Li J, Pastorin G, Ang WH (2014) Ratiometric delivery of cisplatin and doxorubicin using tumour-targeting carbon-nanotubes entrapping platinum(IV) prodrugs. Chem Sci 5:2265–2270
96. Jennette KW, Lippard SJ, Vassiliades GA, Bauer WR (1974) Metallointercalation reagents. 2-hydroxyethanethiolato(2,2′,2″-terpyridine)-platinum(II) monocation binds strongly to DNA by intercalation. Proc Natl Acad Sci USA 71(10):3839–3843
97. Wang AHJ, Nathans J, van der Marel G, van Boom JH, Rich A (1978) Molecular Structure of a double helical DNA fragment intercalator complex between deoxy CpG and a terpyridine platinum compound. Nature 276(5687):471–474
98. Cummings SD (2009) Platinum complexes of terpyridine: interaction and reactivity with biomolecules. Coord Chem Rev 253(9–10):1495–1516

99. Liu H-Q, Peng S-M, Che C-M (1995) Interaction of a luminescent platinum(II) Complex of Substituted 2,2′-bipyridine with DNA. spectroscopic and photophysical studies. J Chem Soc Chem Commun 5:509–510
100. Liu H-Q, Cheung T-C, Che C-M (1996) Cyclometallated platinum(II) complexes as luminescent switches for calf-thymus DNA. Chem Commun 1039–1040
101. Che C-M, Yang M, Wong K-H, Chan H-L, Lam W (1999) Platinum(II) complexes of dipyridophenazine as metallointercalators for DNA and potent cytotoxic agents against carcinoma cell lines. Chem Eur J 5(11):3350–3356
102. Ma D-L, Che C-M (2003) A bifunctional platinum(ii) complex capable of intercalation and hydrogen-bonding interactions with DNA: binding studies and cytotoxicity. Chem Eur J 9 (24):6133–6144
103. Chan H-L, Ma D-L, Yang M, Che C-M (2003) Bis-intercalative dinuclear platinum(II) 6-phenyl-2,2′-bipyridine complexes exhibit enhanced DNA affinity but similar cytotoxicity compared to the mononuclear unit. J Biol Inorg Chem 8(7):761–769
104. Ma D-L, Shum TY-T, Zhang F, Che C-M, Yang M (2005) Water soluble luminescent platinum terpyridine complexes with glycosylated acetylide and arylacetylide ligands: photoluminescent properties and cytotoxicities. Chem Commun 37:4675–4677
105. Wang P, Leung C-H, Ma D-L, Sun RW-Y, Yan S-C, Chen Q-S, Che C-M (2011) Specific blocking of CREB/DNA binding by cyclometalated platinum(II) complexes. Angew Chem Int Ed 50(11):2554–2558
106. Suryadi J, Bierbach U (2012) DNA metalating-intercalating hybrid agents for the treatment of chemoresistant cancers. Chem Eur J 18(41):12926–12934
107. Ding S, Qiao X, Suryadi J, Marrs GS, Kucera GL, Bierbach U (2013) Using fluorescent post-labeling to probe the subcellular localization of DNA-targeted platinum anticancer agents. Angew Chem Int Ed 52(12):3350–3354
108. Wheate NJ, Brodie CR, Collins JG, Kemp S, Aldrich-Wright JR (2007) DNA intercalators in cancer therapy: organic and inorganic drugs and their spectroscopic tools of analysis. Mini-Rev Med Chem 7(6):627–648
109. Garbutcheon-Singh KB, Leverett P, Myers S, Aldrich-Wright JR (2013) Cytotoxic platinum (II) intercalators that incorporate 1R, 2R-diaminocyclopentane. Dalton Trans 42(4):918–926
110. Whan RM, Messerle BA, Hambley TW (2009) Binding of $[Pt(1C3)(dien)]^{2+}$ to the Duplex DNA Oligonucleotide 5′-d(TGGCCA)-3′: the effect of an appended positive charge on the orientation and location of anthraquinone intercalation. Dalton Trans 6:932–939
111. Duskova K, Sierra S, Fernández M-J, Gude L, Lorente A (2012) Synthesis and DNA interaction of ethylenediamine platinum(II) complexes linked to DNA intercalants. Bioorg Med Chem 20(24):7112–7118
112. Ma D-L, Che C-M, Yan S-C (2009) Platinum(II) complexes with dipyridophenazine ligands as human telomerase inhibitors and luminescent probes for G-quadruplex DNA. J Am Chem Soc 131(5):1835–1846
113. Wu P, Ma D-L, Leung C-H, Yan S-C, Zhu N, Abagyan R, Che C-M (2009) Stabilization of G-Quadruplex DNA with platinum(II) Schiff base complexes: luminescent probe and down-regulation of c-*myc* oncogene expression. Chem Eur J 15(47):13008–13021
114. Wang P, Leung C-H, Ma D-L, Yan S-C, Che C-M (2010) Structure-based design of platinum (II) complexes as c-*myc* oncogene down-regulators and luminescent probes for G-Quadruplex DNA. Chem Eur J 16(23):6900–6911
115. Castor KJ, Liu Z, Fakhoury J, Hancock MA, Mittermaier A, Moitessier N, Sleiman HF (2013) A platinum(II) Phenylphenanthroimidazole with an extended side-chain exhibits slow dissociation from a c-Kit G-Quadruplex Motif. Chem Eur J 19(52):17836–17845
116. Wang P, Leung C-H, Ma D-L, Lu W, Che C-M (2010) Organoplatinum(II) complexes with nucleobase motifs as inhibitors of human topoisomerase II catalytic activity. Chem Asian J 5 (10):2271–2280
117. Liu J, Leung C-H, Chow AL-F, Sun RW-Y, Yan S-C, Che C-M (2011) Cyclometalated platinum(II) complexes as topoisomerase IIα poisons. Chem Commun 47(2):719–721

118. Sun RW-Y, Chow AL-F, Li X-H, Yan JJ, Chui SS-Y, Che C-M (2011) Luminescent cyclometalated platinum(II) complexes containing N-heterocyclic carbene ligands with potent in vitro and in vivo anti-cancer properties accumulate in cytoplasmic structures of cancer cells. Chem Sci 2:728–736
119. Frezza M, Dou QP, Xiao Y, Samouei H, Rashidi M, Samari F, Hemmateenejad B (2011) In vitro and in vivo antitumor activities and DNA binding mode of five coordinated cyclometalated organoplatinum(II) complexes containing biphosphine ligands. J Med Chem 54(18):6166–6176
120. Visbal R, Gimeno MC (2014) N-heterocyclic carbene metal complexes: photoluminescence and applications. Chem Soc Rev 43:3551–3574
121. Díez-González S, Marion N, Nolan SP (2009) N-heterocyclic carbenes in late transition metal catalysis. Chem Rev 109(8):3612–3676
122. Hindi KM, Panzner MJ, Tessier CA, Cannon CL, Youngs WJ (2009) The medicinal applications of imidazolium carbene–metal complexes. Chem Rev 109(8):3859–3884
123. Poater A, Cosenza B, Correa A, Giudice S, Ragone F, Scarano V, Cavallo L (2009) SambVca: a web application for the calculation of the buried volume of N-heterocyclic carbene ligands. Eur J Inorg Chem 13:1759–1766
124. Ortiz AM, Gómez-Sal P, Flores JC, de Jesús E (2014) Learning about steric effects in NHC complexes from a 1D silver coordination polymer with Fréchet Dendrons. Organometallics 33(2):600–603
125. Benhamou L, Chardon E, Lavigne G, SP Bellemin-Laponnaz, César V (2011) Synthetic routes to N-Heterocyclic carbene precursors. Chem Rev 111(4):2705–2733
126. Furstner A, Alcarazo M, Cesar V, Lehmann CW (2006) Convenient, scalable and flexible method for the preparation of imidazolium salts with previously inaccessible substitution patterns. Chem Commun 20:2176–2178
127. Queval P, Jahier C, Rouen M, Artur I, Legeay J-C, Falivene L, Toupet L, Crévisy C, Cavallo L, Baslé O, Mauduit M (2013) Multicomponent synthesis of unsymmetrical unsaturated N-heterocyclic carbene precursors and their related transition-metal complexes. Angew Chem Int Ed 52(52):14103–14107
128. Kalinowski J, Fattori V, Cocchi M, Williams JAG (2011) Light-emitting devices based on organometallic platinum complexes as emitters. Coord Chem Rev 255(21–22):2401–2425
129. Chen X, Zhou Y, Peng X, Yoon J (2010) Fluorescent and colorimetric probes for detection of thiols. Chem Soc Rev 39(6):2120–2135
130. Chow C-F, Chiu BKW, Lam MHW, Wong W-Y (2003) A trinuclear heterobimetallic Ru(II)/Pt(II) complex as a chemodosimeter selective for sulfhydryl-containing amino acids and peptides. J Am Chem Soc 125:7802–7803

Chapter 2
Experimental Section

2.1 Materials and Instrumentation

All the synthesis starting materials were from commercially available resources, and all the solvents were of at least analytical grade. Fast atom bombardment (FAB) mass spectra were acquired on a Finnigan Mat 95 mass spectrometer. Electrospray ionization (ESI) mass spectrometry experiments were performed on a Waters Micromass Q-Tof Premier quadrupole time-of-flight tandem mass spectrometer or on an LTQ Orbitrap Velos mass spectrometer (Thermo Scientific). ^{1}H NMR spectra were recorded on DPX 400 M and 300 M Bruker FT-NMR spectrometers with tetramethylsilane as the reference. UV–Vis spectra were obtained on a Perkin-Elmer Lambda 19 UV–Vis spectrophotometer. Steady-state emission spectra were performed on a SPEX 1681 Fluorolog-3 spectrophotometer. Elemental analysis was performed by the Institute of Chemistry at the Chinese Academy of Science, Beijing. For MTT and protein assays, the absorbance was quantified using a Perkin-Elmer Fusion Reader (Packard BioScience Company). Fluorescence images were examined in an Axiovert 200 (Carl Zeiss) and in an Axio Vision Rel. 4.5 imaging system (Carl Zeiss). Dynamic light scattering (DLS) was recorded on a Malvern ZetaSizer 3000HSA. TEM analysis was performed on an FEI Tecnai G2 20 S-TWIN scanning transmission electron microscope. Most of the experimental procedures are based on our previous reports [1, 2].

2.2 X-Ray Crystallography

2.2.1 Crystal Growth

There are three common methods to grow single crystals: liquid–liquid diffusion, evaporation of mixed solvents, and vapor–liquid diffusion.

T. Zou, *Anti-Cancer N-Heterocyclic Carbene Complexes of Gold(III), Gold(I) and Platinum(II)*, Springer Theses, DOI 10.1007/978-981-10-0657-9_2

1. **Liquid–liquid diffusion** (a) Dissolve the compound with soluble solvent. (b) Slowly add the insoluble solvent. (c) Seal the bottle with a cap and then a parafilm.
2. **Evaporation of mixed solvent** (a) Dissolve the compounds into a well soluble, volatile solvent which is mixed with less soluble, less volatile solvent. (b) The bottle can be sealed with a cap or a plastic wrap to slow down the evaporation rate so as to obtain larger crystals.
3. **Vapor–liquid diffusion** (a) Place insoluble, volatile solvent (e.g., Et_2O, hexane) into a large bottle. (b) Then place a smaller tube/bottle containing the compounds, dissolved in a soluble, less volatile solvent. (c) Seal the bottle with a cap and then parafilm.

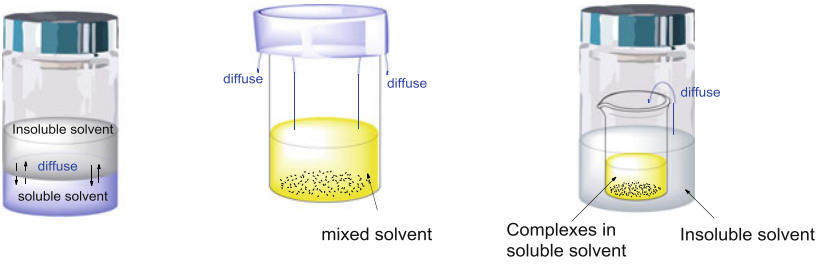

Liquid-liquid diffusion **Evaporation of mixed solvent** **Vapor-liquid diffusion**

2.2.2 *Single Crystal Analysis*

Computing program: SHELXS97 [3].
Geometry: All estimated standard deviations (esds) (except the esd in the dihedral angle between two l.s. planes) were estimated using the full covariance matrix. The cell esds are taken into account individually in the estimation of esds in distances, angles, and torsion angles; correlations between esds in cell structure report parameters were only used when they were defined by crystal symmetry. An approximate (isotropic) treatment of cell esds was used for estimating esds involving l.s. planes.
Refinement: Refinement of F^2 against ALL reflections. The weighted *R*-factor *wR* and goodness-of-fit *S* were based on F^2, and conventional *R*-factors *R* were based on *F*, with *F* set to zero for negative F^2. The threshold expression of $F^2 > 2\text{sigma}(F^2)$ was used only for calculating *R*-factors(gt) and is not relevant to the choice of reflections for refinement. *R*-factors based on *F* are statistically about twice as large as those based on *F*, and *R*-factors based on ALL data will be even larger.

2.3 Stability Testing

2.3.1 UV–Vis Absorption Measurements

2.3.1.1 Beer-Lambert Law

The law states that the absorbance is proportional to the concentration and path length of the sample.

$$A = -\lg T = -\lg \frac{I}{I_0} = \varepsilon bc$$

where A is absorbance with no unit; T is Transmittance; I is intensity of the light; ε is molar absorptivity in L mol^{-1} cm^{-1}; b is the path length of the sample in cm; and c is the concentration in mol L^{-1}.

2.3.1.2 Instrumentation

Figure [4] depicts the working principle of the UV–Vis absorption instrument. Full range light goes through the monochromator to get light of a fixed wavelength to go through the sample solution; the unabsorbed light is recorded by the detector.

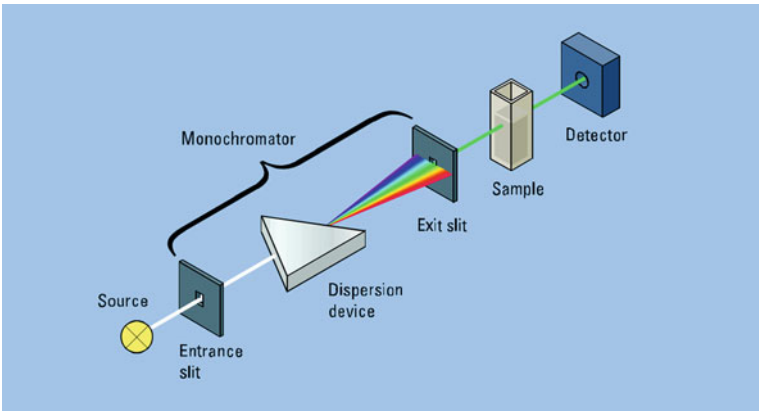

2.3.2 ESI-MS Measurements

Electrospray ionization mass spectrometry utilizes soft electrospray (where a high voltage is applied) to disperse and ionize samples in solution. The molecular weight of the sample can be quite high since multicharge can be easily produced (the *m/z*

ranges from 200 to 2000). Similar to UV–Vis absorption, the ion intensity is proportional to concentration in a given range; therefore, ESI-MS can be applied to analyze reactions both qualitatively and quantitatively.

2.3.3 ^{1}H NMR Measurements

UV–Vis changes can indicate the reactivity of the complexes in solution, and ESI-MS can reveal the possible reaction product(s) qualitatively (though in some cases can be quantitatively). ^{1}H NMR is a method that can give the reaction product both qualitatively and quantitatively. When preparing the sample reactions to mimic the biological processes, a buffer solution (phosphate buffer) should be applied. For reactions that contain air-sensitive components (e.g., thiol-containing peptides/proteins), it is necessary to degas the sample solutions by bubbling N_2 or Ar gas.

2.4 Emission Measurements

2.4.1 Emission Spectra Measurements

When a complex absorbs a photon, it will go to the high energy level (S_n) and then go to the singlet S_1 state through internal conversion (IC). The excited electron in S_1 can either go to the lower triplet T_1 state through intersystem crossing (ISC), phosphoresce to singlet S_0 state, or go directly back to S_0 giving fluorescence. The following Jablonski energy diagram shows the generation of absorption, fluorescence, and phosphorescence.

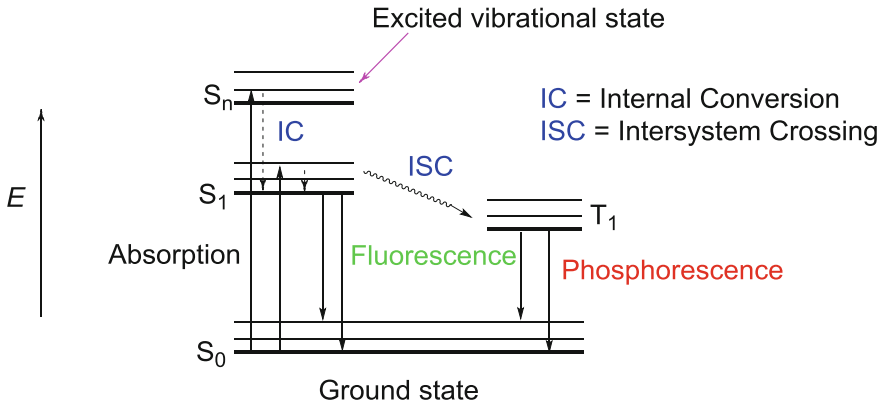

To measure the emission quantum yield (the number of photons emitted divided by the number of photons absorbed), the reference compounds $[Ru(bpy)_3](PF_6)_2$ (quantum yield of 0.062) together with the following equation were used:

$$\Phi_s = \Phi_r \times \left(\frac{B_r}{B_s}\right) \times \left(\frac{n_s}{n_r}\right)^2 \times \left(\frac{D_s}{D_r}\right)$$

where Φ_s and Φ_r are the quantum yields of the sample and reference complexes, respectively; $B = 1 - 10^{-AL}$ where A and L are the absorbance at the excitation wavelength and length of the optical path (unit cm), respectively; D_s and D_r are the integrated area of emission spectrum of sample and reference compounds, respectively.

Metal complexes usually emit phosphorescence with lifetime in the range of microseconds. Such long-lived excited states are quenched by air (oxygen); thus, the sample solution should be degassed (at least 5 freeze–pump–thaw cycles) before the measurement. Metal complexes can be highly emissive upon binding with biomolecules without degassing the solvents.

2.4.2 Emission Lifetime Measurements

The samples were prepared in the same manner as the samples for emission quantum yield measurement. Once a sample was excited with a pulse laser, the intensity at a fixed wavelength was recorded with time processing. Then, the intensity decay curve was fitted following the first exponential decay function:

$$I_t = I_0 e^{-k(t-t_0)}$$

where I_t, and I_0 are the emission intensity at time of t and t_0; $k = \frac{1}{t_0}$.

2.5 Fluorescence Microscopy

Fluorescence microscopy takes advantage of the fluorescence or phosphorescence of the compounds to generate images. Cell imaging analysis is quite useful to study the cellular localization and/or biotransformations of the compounds. Figure (left panel) [5] shows the working and basic principles of fluorescence microscopy. Samples are excited by light that passes through the excitation filter from the vertical direction; then, the emitted light goes through a dichroic mirror and emission filter and then detected by the naked eye or a camera. The right panel of the figure shows the glass bottom dishes that were used for cell imaging analysis.

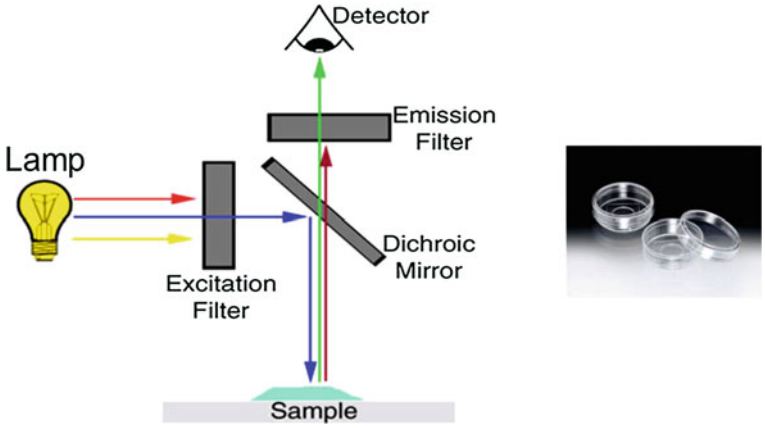

The following table summarizes the emission/excitation filters on the Axiovert 200M used in this thesis.

Name	Excitation filter (nm)	Dichroic mirror (nm)	Emission filter (nm)
New_1	340	–	510
DAPI	365	395	445 ± 25
New_2	450 ± 20	–	>580
FITC	470 ± 20	510	>515
Rhodamine	546/12	580	>590

2.6 Cell Culture and Cytotoxicity Studies

2.6.1 Cell Subculture

Subculture of cells comprises the following steps: (1) removal of the medium; (2) washing the cell monolayer once or twice with PBS; (3) addition of tryspin–EDTA (rotating the dish to cover the entire surface of the dish); (4) incubation of the cells in a 37 °C incubator or at room temperature for 2–10 min; and (5) addition of medium containing FBS to deactivate trypsin. (Centrifuging was generally used to remove all the tryspin.)

2.6.2 MTT Assay

Cytotoxicity was evaluated by means of MTT (3-(4,5-dimethylthiazol-2-yl)-2,5-diphenyltetrazolium bromide) assay [6]. MTT is a cell permeable agent that can

be reduced by intracellular reductases to form insoluble formazan. The reduced product can dissolved in solvents, such as DMSO, a solution of sodium dodecyl sulfate (SDS) in diluted HCl or acidified ethanol. Formazan (purple) has a distinguishable absorption band at 500–600 nm that can be quantified by spectrophotometry so that the viability of cells can be determined.

MTT **Formazan**

2.7 Gel Mobility Shift Assay

The gel mobility shift assay is a method often used to investigate the interaction of metal complexes with DNA (or other biomolecules). Argarose gels are commonly utilized to resolve DNA fragments. In general, mixtures of DNA and complexes containing bromophenol blue are resolved by 2 % (w/v) agarose gel electrophoresis in Tris–acetate–EDTA (TAE) buffer. After the electrophoresis is finished (the blue dye runs to the end of the gel), the gel is stained with an ethidium bromide (EB) solution, and the fluorescence is visualized by UV transillumination.

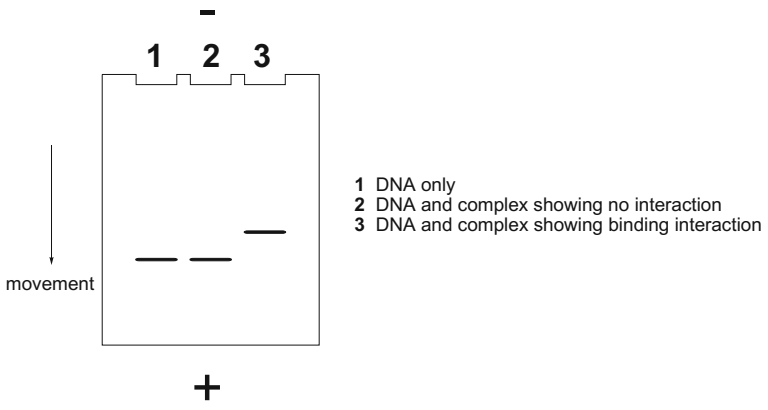

2.8 Spectroscopic Binding Studies

2.8.1 Determination of DNA-Binding Constants

DNA-binding constants were determined by absorption titration experiments [7]. The absorption spectra of a series of solutions containing a fixed concentration of complex and varied concentrations of DNA were assessed. The binding constant was determined using the Scatchard equations

$$[\mathrm{DNA}]/\Delta\varepsilon_{\mathrm{ap}} = [\mathrm{DNA}]/\Delta\varepsilon + 1/(\Delta\varepsilon \times K_{\mathrm{b}}),$$

where $\Delta\varepsilon_{\mathrm{ap}} = |\varepsilon_A - \varepsilon_F|$ ($\varepsilon_A = A_{\mathrm{obs}}/[\mathrm{complex}]$) and $\Delta\varepsilon = |\varepsilon_B - \varepsilon_F|$ (ε_B and ε_F) are extinction coefficients of the DNA-bound and DNA-unbound complex, respectively.

2.8.2 Binding with Proteins

The binding of complexes with protein (e.g., BSA) was determined by fluorescence quenching experiments [8]. The emission spectrum of a solution containing a fixed concentration of protein and varied concentrations of complex was recorded at a suitable excitation wavelength. The binding constant was determined using the following equation:

$$\log[(I_0 - I)/I] = \log K + n\log[Q]$$

where I_0 and I are the fluorescence intensities of the initial protein without complex and the protein after adding the complex, respectively; $[Q]$ is complex (quencher) concentration.

2.9 Transfection

Transfection is a biological technology to introduce cell-impermeant nucleic acids to the intracellular environment. The widely used vehicles to transfect nucleic acids are nanocarriers, including liposomes and cationic polymers. Lipofectamine 2000, (LP2000) developed by Invitrogen, contains a cationic liposome formulation. It can readily form liposomes that are capable of carrying anionic nucleic acids and can recognize anionic cell membranes.

2.10 Western Blot

Western blot is an efficient and standard method to analyze or detect a specific protein based on electrophoretic resolution of proteins. The procedures can generally be divided into the following steps:

1. **Cell lysate from cell culture**. The cells treated with drugs are washed 2–3 times with PBS and treated with RIPA lysis buffer (1 % Trition X-100, 10 % deoxycholate, 50 mM Tris-HCl, pH 7.5, 150 mM NaCl, 0.1 % SDS, 0.1 mm phenylmethanesulfonyl fluoride [PMSF, serine protease inhibitor], 10 μg/mL leupeptin [cysteine, serine and threonine protease inhibitor], and 10 μg mL^{-1} aprotinin [trypsin inhibitor]) on ice for 5–10 min. Then, the sample is centrifuged at 13,500 rpm for 10 min, and the supernatant is collected.
2. **Determination of protein concentration**. The protein concentration was quantified by DC Protein Assay (Bio-Rad). The color change is based on the below reaction: The protein reduces Cu^{2+} to Cu^{+} that can be reoxidized by Mo^{VI} in Folin reagent, forming molybdenum blue. The protein concentration can then be measured by the absorbance at 595 nm.

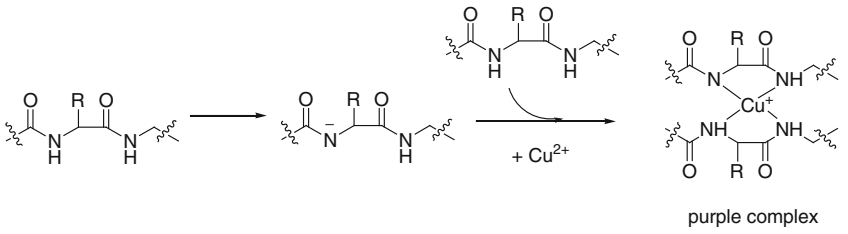

3. **Preparing samples for loading into gels**. Loading buffer (2 % SDS, 10 % 2-mercaptoehtanol, 10 % glycerol, 0.002 % bromophenol blue in 62.5 mM Tris-HCl) is added to protein lysate which is incubated at 100 °C for 5 min. After cooling, the samples are centrifuged.
4. **PAGE gels**. SDS–PAGE (sodium dodecyl sulfate polyacrylamide gel electrophoresis) was used to resolve the proteins. The gel is based on the polymerization reaction

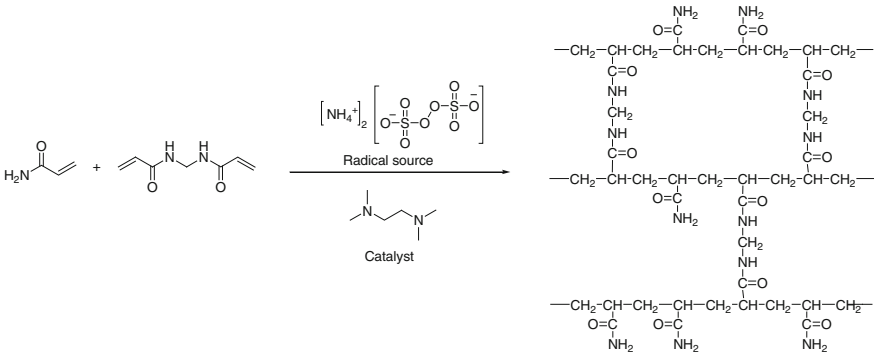

where ammonium persulphate (APs) is the radical source, and the reaction is catalyzed by N,N,N′,N′-Tetramethylethylenediamine (TEMED). The separating gel is prepared in Tris, pH 8.8, whereas the stacking gel is prepared in Tris, pH 6.8.

5. **Sample loading and gel running**. The sample (20–40 μg) was loaded by special pipette tips that have a long sharp head. The sample volume was smaller than that of the well. After loading, the gels were run at a low voltage for ~15 min to condense the protein and then at a high voltage to condense the protein separation. A protein marker was used to estimate the size of the target protein bands.
6. **Protein transfer to membrane**. The protein on gel is transferred to polyvinylidene difluoride (PVDF) membrane by a sandwich of (−)/filter paper × 2/gel/membrane/filter paper × 2/(+). The membranes were activated in 100 % methanol for 1–2 min before the transferring.

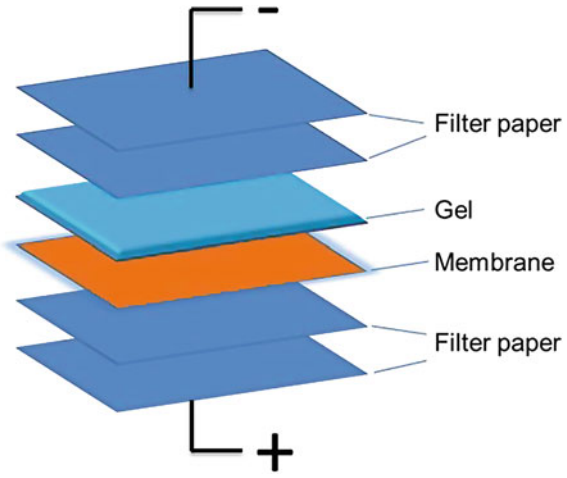

7. **Block the membrane**. The membrane needs to be blocked to prevent the non-specific binding interactions of antibodies with the membrane. BSA (5 % w/v) in TBST was used to block the membranes overnight at 4 °C.
8. **Incubation with primary antibodies**. Primary antibodies were diluted in the blocking buffer (usually 1:1000 v/v) and then incubated with the membranes at room temperature for 1–2 h with gentle shaking.
9. **Incubation with secondary antibodies**. Before adding secondary antibodies, the membranes were washed at least three times in TBST (each for 10 min) to remove excess primary antibody. The secondary antibodies were diluted by 1:5000 (v/v) and incubated with the membranes at room temperature for 1–2 h with gentle shaking.
10. **Development by chemiluminescence**. Extra secondary antibodies were washed out by TBST (three times, each for 10 min). Then, the membranes were incubated with the chemiluminescence agent which can give luminescence only in the presence of secondary antibody (conjugated to horseradish peroxidase [HRP]). The signal was detected by photographic film.

2.11 Inductively Coupled Plasma Mass Spectrometry

Inductively coupled plasma mass spectrometry (ICP-MS) is one kind of mass spectrometry for detecting metals (and some nonmetals) at ultralow concentrations (below ppb level). It is a powerful method that is particularly suitable for the measurement of cellular uptake and protein-bound metal contents. For ICP-MS analysis, the samples were fully digested before the assay. Nitric acid is usually used for digestion together with heating.

2.12 Tube Formation Assay

Tube formation was followed by an In Vitro Angiogenesis Kit (Cayman Chemical). Briefly, the diluent buffer (10×) was mixed with ECMatrix solution at 0 °C. Then, the mixture was transferred to a 96-well plate (each sample containing 50 μL) and was incubated at 37 °C for 1 h to promote polymerization. Afterward, MS1 cells (5×10^4) in DMEM containing drugs/complexes are added to the top of the polymerized matrix and incubated for a given time, until the tubes in the control growth were formed. The cell viability was verified to ascertain all the drug-treated cells remained alive.

2.13 In Vivo Antitumor Study

The animals were cared for according to the guidelines of the Laboratory Animal Unit of the University of Hong Kong (HKU). All animal experiments were conducted under the guidelines approved by the Committee on the Use of Live Animals in Teaching and Research of HKU. The following figure is a summary of the key steps for the in vivo antitumor experiments.

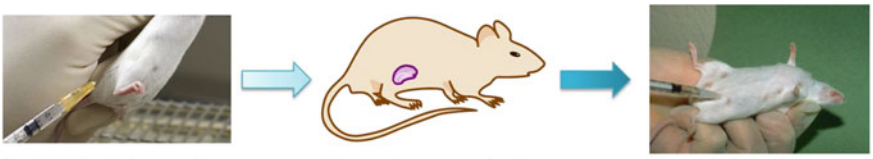

Drug administration and preliminary toxicity studies. Drug administration methods were intraperitoneal injection (i.p.), intratumoral injection (i.t.), intravenous injection (i.v.), and subcutaneous injection (s.c.), and this method sometimes cannot be distinguished from i.t. if the tumor was planted by s.c. Preference was given to i.p. due to the ease of administration compared to the other systemic injection methods (e.g., i.v). I.t. is a kind of local injection method that is not commonly used.

The drugs/complexes were first dissolved in the excipient (most commonly PET with 60 % polyethylene glycol 400, 30 % ethanol, and 10 Tween-80) and then diluted with PBS (if using DMSO as excipient, it should be below 2 % and PET could be 10 %). The treatment dosage/frequency was carefully considered. The injection volume needed to be lower than 0.5 mL (usually 0.1–0.2 mL was used). Tumor-free mice were used to test the drug toxicity in order to determine the drug treatment dosage.

Establishment of tumors models. A sufficient number of cancer cells were prepared before the establishment of the tumors in mice. For each mouse, around 2–5 × 10^6 cells. After harvesting all the cancer cells, the medium and trypsin were removed by centrifugation, and the cells were immersed in PBS at 0 °C before injection. Then, the cancer cells in 0.1 mL PBS were injected (s.c.) into the right back flanks of the mice.

Drug treatment. Once the tumors became palpable (volumes ~50 mm^3, 2–3 days after tumor inoculation), the mice were randomly divided into different treatment groups (5–7 mice for each group). The mice bearing tumors were injected with drug or vehicle control at the dosages/frequencies derived from the preliminary toxicity studies. The longest (*a*) and shortest (*b*) diameters were used to determine

the tumor volumes in the formula $V = 0.52 \times ab^2$. The body weight of the mice was recorded to track side effects.

Sacrifice of mice bearing tumors. According to the guidelines of HKU, the tumor volume must remain lower than 10 % of the body volume. After the tumors exceeded these limits, the mice were sacrificed by lethal anesthesia. The tumors were then collected and immersed in 10 % formalin (a dilution of ~40 % formaldehyde stock) in PBS. After 12 h, the tumors were resuspended in 70 % ethanol and stored at 4 °C.

Tumor growth inhibition was calculated as a ratio of tumor volume increases in the drug-treated group to that in the control group:

$$\text{Inhibition} = \left(1 - \frac{V_t - V_0}{V_t' - V_0'}\right) \times 100\ \%$$

where V_t and V_t' are the tumor volumes of drug treatment and solvent control group, respectively. V_0 and V_0' are the tumor volumes at day 0 of treatment in the drug treatment and solvent control groups, respectively.

References

1. Sun RW-Y, Li CK-L, Ma D-L, Yan JJ, Lok C-N, Leung C-H, Zhu N, Che C-M (2010) Stable anticancer gold(III)-porphyrin complexes: effects of porphyrin structure. Chem Eur J 16 (10):3097–3113
2. Sun RW-Y, Chow AL-F, Li X-H, Yan JJ, Chui SS-Y, Che C-M (2011) Luminescent cyclometalated platinum(II) complexes containing N-Heterocyclic carbene ligands with potent in vitro and in vivo anti-cancer properties accumulate in cytoplasmic structures of cancer cells. Chem Sci 2:728–736
3. Sheldrick GM (2008) A short history of SHELX. Acta Cryst A64(1):112–122
4. http://faculty.sdmiramar.edu/fgarces/LabMatters/Instruments/UV_Vis/Cary50.htm
5. Source: http://www.jic.ac.uk/microscopy/more/t5_6.htm
6. Mosmann T (1983) Rapid colorimetric assay for cellular growth and survival: application to proliferation and cytotoxicity assays. J Immunol Methods 65(1–2):55–63
7. Kumar CV, Asuncion EH (1993) DNA binding studies and site selective fluorescence sensitization of an anthryl probe. J Am Chem Soc 115(19):8547–8553
8. Samari F, Hemmateenejad B, Shamsipur M, Rashidi M, Samouei H (2012) Affinity of two novel five-coordinated anticancer Pt(II) complexes to human and bovine serum albumins: A spectroscopic approach. Inorg Chem 51(6):3454–3464

Chapter 3
Gold(III) Complexes Containing N-Heterocyclic Carbene Ligand Serve as Dual Fluorescent Thiol "Switch-On" Probe and Anticancer Agent

3.1 Introduction

Cellular thiol level is associated with cellular redox balances that are linked up with various diseases such as cancers and AIDS [1–6]. Due to the high binding affinity toward thiols, soft metal ions and their complexes are usually utilized in the design of metal-based thiol probes as well as new anticancer drug leads which could specifically target thiol-/selenol-containing proteins/enzymes [7–11]. Au(I) is one kind of soft metal ions having high binding affinity toward-SH groups and can be generated by the reduction of Au(III) with thiols. Most reported Au(III) complexes are known to be readily reduced to Au(I) and/or Au(0) by cellular thiols (e.g., glutathione, GSH) [7, 12–14]. In view of the fact that Au(III) is 4-coordinated, whereas Au(I) is usually 2-coordinated, reduction of Au(III) to Au(I) is accompanied by the release of coordinated ligand(s). In this regard, Au(III) complexes containing ligands which are strongly fluorescent in free form are envisioned to be potential biological probes. Upon coordination to Au(III), the ligand emission is usually quenched due to the low-energy lying $5d_{x2-y2}$ orbital of Au(III). Upon reduction of Au(III) to Au(I) by thiols, the fluorescent ligand(s) will be released resulting in light emission switching on effect.

It is known that Au(III) complexes are anticancer active. Examples of anticancer gold(III) complexes targeting proteins/enzymes other than DNA and which can overcome cisplatin resistance can be found in the literatures [5, 12–18]. Though the anticancer properties of numerous Au(III)/Au(I) complexes are ascribed to come from Au(I) [12–14, 16, 18–25], simple Au^+ ion is not stable and tends to undergo disproportionation under physiological conditions [7]. Recent works by various groups [23, 24, 26–33] and our own studies indicate that N-heterocyclic carbene

T. Zou, *Anti-Cancer N-Heterocyclic Carbene Complexes of Gold(III), Gold(I) and Platinum(II)*, Springer Theses, DOI 10.1007/978-981-10-0657-9_3

(NHC) ligand(s) is able to stabilize Au^+ ion against reduction to Au(0) and/or demetalation under physiological conditions.

In this chapter, a class of cationic Au(III) complexes containing both N^N^N (H_2N^N^N = 2,6-bis(imidazol-2-yl)pyridine, H_2IPI; or 2,6-bis(benzimidazol-2-yl) pyridine, H_2BPB) and NHC ligands are described. The free H_2N^N^N ligands are strongly emissive in solutions and display low cytotoxicity, and many compounds bearing imidazolyl/benzimidazolyl groups have good water solubility and are widely utilized in biological studies [34–36]. NHC ligand is able to stabilize the potentially anticancer active Au(I) formed upon reduction of these Au(III) complexes by physiological thiols. With appropriate substituent(s), substituted NHC ligands can improve the water solubility of gold complexes. In this work, the Au (III) complexes were found to act as fluorescent switch-on probe for thiols originated from the emission of the released H_2N^N^N ligand upon reduction of Au(III) to Au(I), and one of the Au(III) complexes was observed to display in vivo antitumor activity to suppress the tumor growth in mice HeLa xenograft model.

3.2 Experimental Section

3.2.1 Materials and Instrumentation

All starting materials were used as received from commercial sources unless otherwise indicated. 2,6-bis(imidazol-2-yl)pyridine (H_2IPI) [37], 2,6-bis (benzimidazol-2-yl)pyridine (H_2BPB) [34], and [Ag(NHC)X] [38–40] (X = Br, I; except mono[(1-methyl-3-(3-(triphenylphosphonio)propyl)-1*H*-imidazol-2(3H)-ylidene)silver(I) monobromide]) were synthesized according to the literature procedures. All of the solvents used were of analytical grade.

Fast atom bombardment (FAB) mass spectra were obtained on a Finnigan Mat 95 mass spectrometer. ^{1}H NMR spectra were obtained on Bruker DPX 300 and 400 M FT-NMR spectrometers with the reported chemical shifts relative to the signals of tetramethylsilane. Elemental analyses were performed at the Institute of Chemistry of the Chinese Academy of Sciences, Beijing. UV–visible absorption spectra were recorded on a Perkin-Elmer Lambda 19 spectrophotometer. Steady-state emission spectra were recorded on a SPEX 1681 Fluorolog-3 spectrophotometer. Fluorescence microscopy was performed by using Axiovert 200 (Carl Zeiss) and in an Axio Vision Rel. 4.5 imaging system (Carl Zeiss). For MTT and protein assays, the absorbance was quantified using Perkin-Elmer Fusion Reader (Packard BioScience Company).

3.2.2 Synthesis and Characterization of Gold Complexes

3.2.2.1 Synthesis of Gold Complexes

- $[Au^{III}(IPI)Cl]$

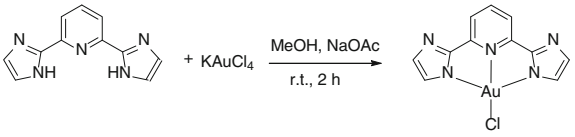

A mixture of H_2IPI (251.5 mg, 1.19 mmol), $KAuCl_4$ (300 mg, 0.794 mmol), and sodium acetate (325 mg, 3.97 mmol) was stirred in methanol (10 mL) at room temperature; a red solid was obtained after several seconds. After 2 h, the product was filtered and washed with methanol and diethyl ether. Yield 90 %; ^{1}H NMR (400 MHz, DMSO-d_6, 25 °C): δ = 8.22 (t, J = 7.9 Hz, 1 H), 7.63 (d, J = 7.9 Hz, 2 H), 7.33 (d, J = 0.72 Hz, 2 H), 7.31 (d, J = 0.70 Hz, 2 H); FAB-MS: m/z 442 $[M + H]^+$; elemental analyses calcd (%) for $C_{11}H_7AuClN_5$: C, 29.92; H, 1.60; N, 15.86; found: C, 30.19; H, 1.77; N 15.71.

- $[Au^{III}(BPB)Cl]$

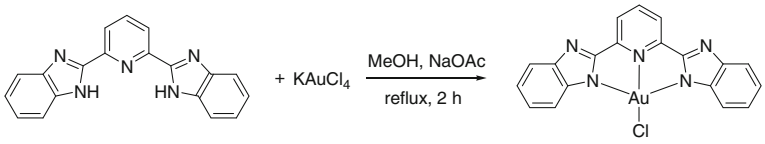

A mixture of H_2BPB (165 mg, 0.53 mmol), $KAuCl_4$ (300 mg, 0.794 mmol), and sodium acetate (325 mg, 3.97 mmol) in methanol (25 mL) was heated to reflux for 2 h. The product was filtered and washed with methanol followed by diethyl ether. Yield 95 %; ^{1}H NMR (400 MHz, DMSO-d_6, 25 °C): δ = 8.51 (t, J = 7.9 Hz, 1H), 8.18 (d, J = 7.9 Hz, 2H), 8.14 (d, J = 8.1 Hz, 2H), 7.78 (d, J = 8.0 Hz, 2H), 7.37 (m, 2H), 7.28 (m, 2H); FAB-MS: m/z 542 $[M + H]^+$; elemental analyses calcd (%) for $C_{19}H_{11}AuClN_5 \cdot H_2O$: C, 40.77; H, 2.34; N, 12.51; found: C, 40.29; H, 2.18; N, 12.39.

- **3.1** [Au^{III}(IPI)(NHC^{2Me})]

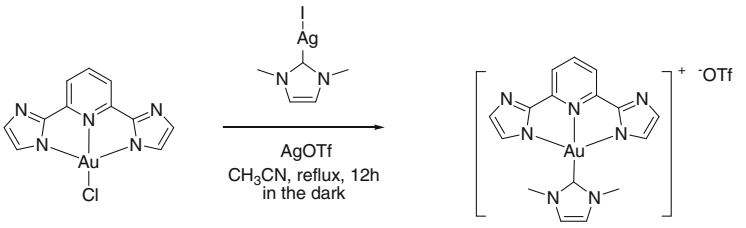

A mixture of [Au^{III}(IPI)Cl] (80 mg, 0.181 mmol), silver triflate (55.7 mg, 0.217 mmol), and (1,3-dimethyl-1*H*-imidazol-2(3H)-ylidene)silver(I) iodide (71.9 mg, 0.217 mmol) in acetonitrile (10 mL) was heated to reflux for 12 h in the dark. After cooling to room temperature, the reaction mixture was filtered, and the filtrate was purified by chromatography on an alumina column with CH_3CN/CH_2Cl_2 as eluent. A yellow solid was obtained. Yield 45 %; ^{1}H NMR (300 MHz, CD_3CN, 25 °C): δ = 8.24 (t, J = 7.9 Hz, 1H), 7.72 (d, J = 8.0 Hz, 2H), 7.57 (s, 2H), 7.25 (d, J = 0.9 Hz, 2H), 7.01 (d, J = 0.9 Hz, 2H), 3.93 (s, 6H); FAB-MS: m/z 502 $[M\text{-}OTf]^+$; elemental analyses calcd (%) for $C_{17}H_{15}AuF_3N_7O_3S$: C, 31.35; H, 2.32; N, 15.05; found: C, 31.51; H, 2.45; N, 15.22.

- **3.2** [Au^{III}(IPI)($NHC^{Me,C4}$)]

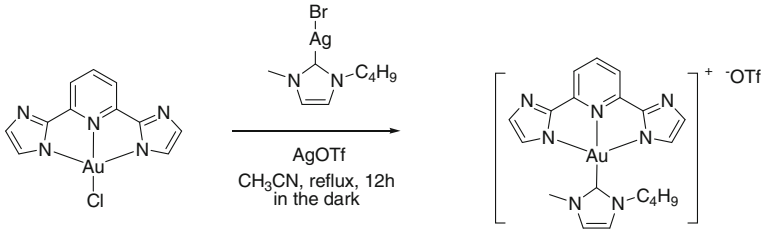

The procedure was similar to that for **3.1**. Yield 60 %; ^{1}H NMR (400 MHz, CD_3CN, 25 °C): δ = 8.24 (t, J = 8.0 Hz, 1H), 7.72 (d, J = 8.0 Hz, 2H), 7.62 (d, J = 2.1 Hz, 1H), 7.59 (d, J = 2.1 Hz, 1H), 7.25 (d, J = 0.9 Hz, 2H), 6.98 (d, J = 0.9 Hz, 2H), 4.25 (t, J = 7.3 Hz, 2H), 3.93 (s, 3H), 1.78 (m, 2H), 1.24 (m, 2H), 0.81 (t, J = 7.4 Hz, 3H); FAB-MS: m/z 544 $[M\text{-}OTf]^+$; elemental analyses calcd (%) for $C_{20}H_{21}AuF_3N_7O_3S{\cdot}H_2O$: C, 33.76; H, 3.26; N, 13.78; found: C, 33.87; H, 3.24; N, 13.87.

- **3.3** $[Au^{III}(IPI)(NHC^{Me,C8})]$

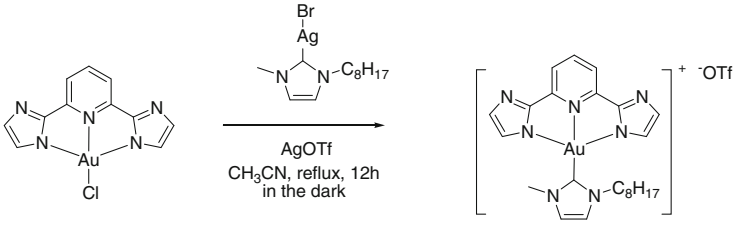

The procedure was similar to that for **1a**. Yield 45 %; ^{1}H NMR (400 MHz, CD_3CN, 25 °C): δ = 8.23 (t, J = 8.0 Hz, 1H), 7.71 (d, J = 8.0 Hz, 2H), 7.62 (d, J = 2.1 Hz, 1H), 7.60 (d, J = 2.1 Hz, 1H), 7.25 (d, J = 0.9 Hz, 2H), 6.99 (d, J = 0.9 Hz, 2H), 4.26 (t, J = 7.1 Hz, 2H), 3.94 (s, 3H), 1.80 (m, 2H), 1.17 (m, 6H), 1.11 (m, 4H), 0.82 (t, J = 7.2 Hz, 3H); FAB-MS: m/z 600 $[M\text{-}OTf]^+$; elemental analyses calcd (%) for $C_{24}H_{29}AuF_3N_7O_3S$: C, 38.46; H, 3.90; N, 13.08; found: C, 38.45; H, 3.99; N, 13.00.

- **3.4** $[Au^{III}(IPI)(NHC^{Me,C10})]$

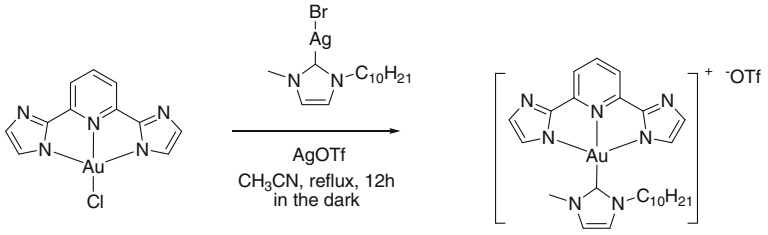

The procedure was similar to that for **3.1**. Yield 48 %; ^{1}H NMR (300 MHz, CD_3CN,25 °C): δ = 8.24 (t, J = 8.0 Hz, 1H), 7.72 (d, J = 7.9 Hz, 2H), 7.62 (d, J = 2.7 Hz, 1H), 7.59 (d, J = 2.7 Hz, 1H), 7.25 (d, J = 0.9 Hz, 2H), 6.99 (d, J = 0.9 Hz, 2H), 4.25 (t, J = 7.1 Hz, 2H), 3.93 (s, 3H), 1.82 (m, 2H), 1.27–1.10 (m, 14H), 0.85 (t, J = 6.9 Hz, 3H); FAB-MS: m/z 628 $[M\text{-}OTf]^+$; elemental analyses calcd (%) for $C_{26}H_{33}AuF_3N_7O_3S$: C, 40.16; H, 4.28; N, 12.61; found: C, 40.28, H, 4.42, N, 12.78.

- **3.5** [Au^{III}(IPI)($NHC^{Me,C16}$)]

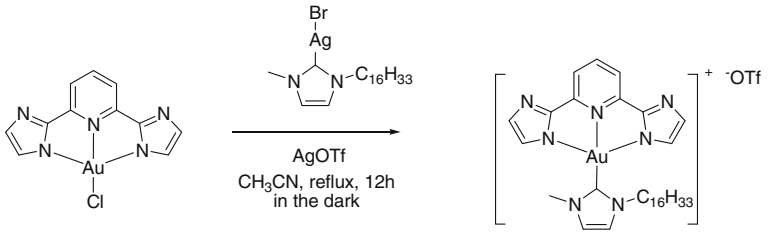

The procedure was similar to that for **3.1**. Yield 45 %; ^{1}H NMR (300 MHz, CD_3CN, 25 °C): δ = 8.23 (t, J = 8.0 Hz, 1H), 7.72 (d, J = 8.0 Hz, 2H), 7.63 (d, J = 2.0 Hz, 1H), 7.61 (d, J = 2.0 Hz, 1H), 7.23 (d, J = 0.9 Hz, 2H), 6.99 (d, J = 0.9 Hz, 2H), 4.26 (t, J = 7.1 Hz, 2H), 3.94 (s, 3H), 1.80 (m, 2H), 1.17–1.32 (m, 26H), 0.87 (t, J = 7.2 Hz, 3H); FAB-MS: m/z 712 $[M\text{-}OTf]^+$; elemental analyses calcd (%) for $C_{32}H_{45}AuF_3N_7O_3S{\cdot}H_2O$: C, 43.69; H, 5.38; N, 11.14; found: C, 44.00; H, 5.50; N, 11.16.

- **3.6** [Au^{III}(IPI)(NHC^{2C4})]

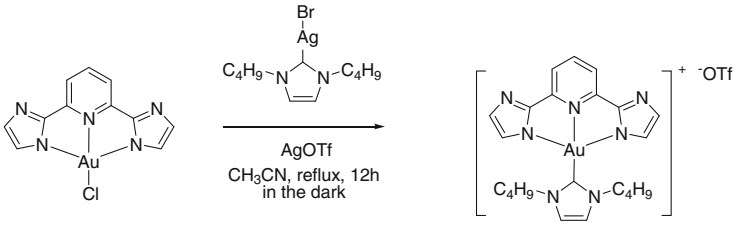

The procedure was similar to that for **3.1**. Yield 52 %; ^{1}H NMR (400 MHz, CD_3CN, 25 °C): δ = 8.23 (t, J = 7.9 Hz, 1H), 7.71 (d, J = 8.0 Hz, 2H), 7.66 (s, 2H), 7.24 (d, J = 1.0 Hz, 2H), 6.95 (d, J = 1.0 Hz, 2H), 4.28 (t, J = 7.3 Hz, 4H), 1.79 (m, 4H), 1.25 (m, 4H), 0.81 (t, J = 7.4 Hz, 6H); FAB-MS: m/z 586 $[M\text{-}OTf]^+$; elemental analyses calcd (%) for $C_{23}H_{27}AuF_3N_7O_3S$: C, 37.56; H, 3.70; N, 13.33; found: C, 38.04; H, 3.92; N, 13.09.

- **3.7** [Au^{III}(IPI)(NHC^{2C6})]

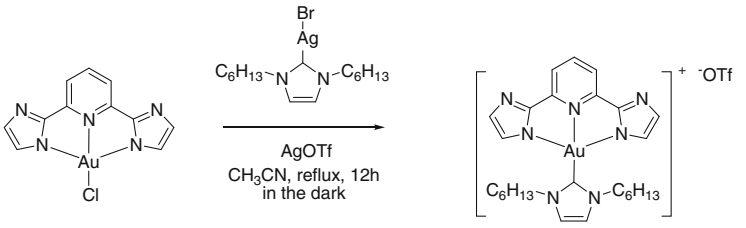

The procedure was similar to that for **3.1**. Yield 55 %; ^{1}H NMR (400 MHz, CD_3CN, 25 °C): δ = 8.24 (t, J = 8.0 Hz, 1H), 7.72 (d, J = 8.0 Hz, 2H), 7.65 (s, 2H), 7.24 (d, J = 0.8 Hz, 2H), 6.96 (d, J = 0.8 Hz, 2H), 4.26 (t, J = 7.2 Hz, 4H), 1.79 (m, 4H), 1.20–1.15 (m, 12H), 0.76 (t, J = 6.9 Hz, 6H); FAB-MS: m/z 642 $[M\text{-}OTf]^+$; elemental analyses calcd (%) for $C_{27}H_{35}AuF_3N_7O_3S$: C, 40.96; H, 4.46; N, 12.39; found: C, 41.26; H, 4.51; N, 12.48.

- **3.8** [Au^{III}(IPI)($NHC^{Me,C3PPh3}$)]

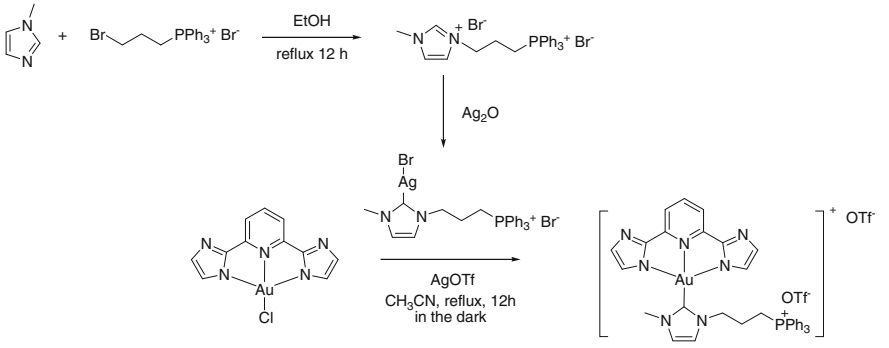

1-Methyl-3-(3-(triphenylphosphonio)propyl)-1*H*-imidazol-3-ium bromide was synthesized by refluxing a mixture of 1-methyl-1*H*-imidazole and (3-bromopropyl)triphenylphosphonium bromide (1:1) in ethanol for 12 h. After cooling to room temperature, the solvent was removed and the crude product was washed with ethyl acetate. Then, the white product was treated with silver (I) oxide in CH_2Cl_2 for 12 h; the crude Ag–NHC product was filtered and washed with CH_2Cl_2 followed by diethyl ether and was used for the next step directly. The procedure for the synthesis of **3** was similar to that for **3.1**. Total yield 32 %; ^{1}H NMR (400 MHz, CD_3CN, 25 °C): δ = 8.21 (t, J = 8.0 Hz, 1H), 7.82 (m, 3H), 7.69–7.72 (m, 3H), 7.66 (d, J = 2.0 Hz, 1H), 7.63–7.55 (m, 12H), 7.17 (d, J = 0.9 Hz, 2H), 6.98 (d, J = 0.9 Hz, 2H), 4.57 (t, J = 7.1 Hz, 2H), 3.94 (s, 3H), 3.27 (m, 2H), 2.11 (m, 2H); FAB-MS: m/z 940 $[M\text{-}OTf]^+$; elemental

analyses calcd (%) for $C_{38}H_{33}AuF_6N_7O_6PS_2 \cdot H_2O$: C, 41.20; H, 3.18; N, 8.85; found: C, 41.25; H, 3.29; N 8.72

- **3.9** [Au^{III}(BPB)(NHC^{2Me})]

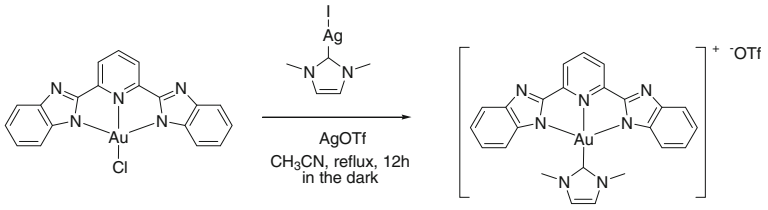

The procedure was similar to that for **3.1** except that [Au^{III}(IPI)Cl] was replaced by [Au^{III}(BPB)Cl]. Yield 43 %; ^{1}H NMR (400 MHz, CD_3CN, 25 °C): δ = 8.51 (t, J = 7.9 Hz, 1H), 8.24 (d, J = 7.9 Hz, 2H), 7.85 (s, 2H), 7.80 (d, J = 8.2 Hz, 2H), 7.31–7.23 (m, 4H), 5.99 (d, J = 7.9 Hz, 2H), 4.01 (s, 6H); FAB-MS: m/z 602 $[M\text{-}OTf]^+$; elemental analyses calcd (%) for $C_{25}H_{19}AuF_3N_7O_3S \cdot H_2O \cdot CH_2Cl_2$: C, 36.55; H, 2.71; N, 11.48; found: C, 36.46; H, 2.57; N, 11.34.

- **3.10** [Au^{III}(BPB)(NHC^{2C4})]

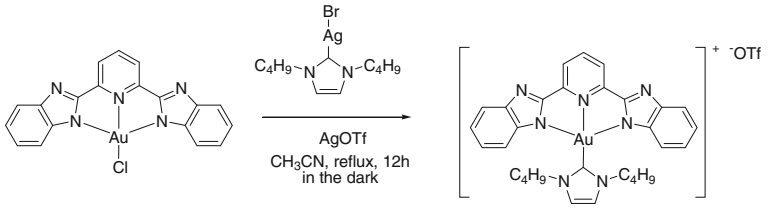

The procedure was similar to that for **3.1** except that [Au^{III}(IPI)Cl] was replaced by [Au^{III}(BPB)Cl]. Yield 51 %; ^{1}H NMR (300 MHz, CD_3CN, 25 °C): δ = 8.49 (t, J = 7.9 Hz, 1H), 8.24 (d, J = 7.9 Hz, 2H), 7.92 (s, 2H), 7.80 (d, J = 7.4 Hz, 2H), 7.31–7.20 (m, 4H), 5.91 (d, J = 8.6 Hz, 2H), 4.35 (t, J = 7.3 Hz, 4H), 1.71 (m, 4H), 1.24 (m, 4H), 0.59 (t, J = 7.3 Hz, 6H); FAB-MS: m/z 686 $[M\text{-}OTf]^+$; elemental analyses calcd (%) for $C_{31}H_{31}AuF_3N_7O_3S$: C, 44.56; H, 3.74; N, 11.73; found: C, 44.16; H, 3.84; N, 11.62.

- **3.11** [Au^{III}(BPB)(NHC^{2C6})]

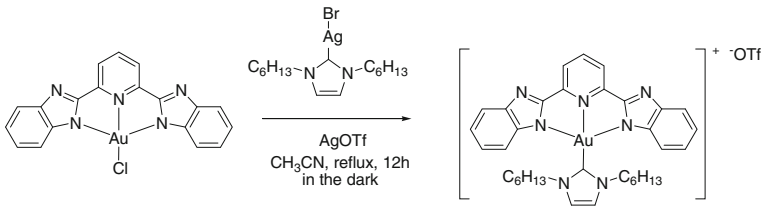

The procedure was similar to that for **3.1** except that [Au^{III}(IPI)Cl] was replaced by [Au^{III}(BPB)Cl]. Yield 55 %; ^{1}H NMR (300 MHz, CD_3CN, 25 °C): δ = 8.50 (t, J = 7.9 Hz, 1H), 8.24 (d, J = 8.0 Hz, 2H), 7.93 (s, 2H), 7.80 (d, J = 7.5 Hz, 2H), 7.31–7.20 (m, 4H), 5.93 (d, J = 7.0 Hz, 2H), 4.35 (t, J = 7.2 Hz, 4H), 1.73 (m, 4 H), 1.15 (m, 4 H), 0.89 (m, 8 H), 0.56 (t, J = 7.1 Hz, 6 H); FAB-MS: m/z 742 $[M\text{-}OTf]^+$; elemental analyses calcd (%) for $C_{35}H_{39}AuF_3N_7O_3S$: C, 47.14; H, 4.41; N, 10.99; found: C, 47.00, H, 4.46, N, 10.78.

3.2.2.2 X-Ray Crystallographic Analysis

Diffraction-quality crystals of **3.1** and **3.9** were obtained by the diffusion of Et_2O to CH_3CN solutions. The data were collected at 100 K on a BRUKER X8 PROTEUM diffractometer equipped with microfocus MicroStar rotating anode Cu X-ray generator (Cu-Kα λ = 1.54178 Å). Structure solution and refinement were performed by using SHELX-97 suite program [41] on PC platform. In the final stage of least-squares refinement, non-hydrogen atoms were refined anisotropically. H atoms were generated by the program SHELXL-97. The positions of H atoms were calculated based on riding mode with thermal parameters equal to 1.2 times that of the associated C atoms and participated in the calculation of final R-indices.

3.2.3 Reactions with GSH

3.2.3.1 UV–Visible Spectroscopic Experiments

Complexes **3.1** and **3.9** were separately dissolved in PBS (containing 5 % DMSO, v/v) solutions, and the UV–Vis absorption spectra of the solution mixture at different time points were measured. No significant spectral change was found within 72 h. Then, GSH was added to the solution (final concentration: 2 mM) followed by mixing for 30 s; the UV–Visible absorption spectra of the resultant solution mixture at different time intervals were recorded.

3.2.3.2 ESI-MS Experiments

Complex **3.1** and GSH were dissolved in milli-Q H_2O separately; the two stock solutions were then mixed together at a molar ratio of 1:6. After 30 min, the solution mixture was analyzed by ESI-MS.

3.2.3.3 ^{1}H NMR Experiments

The reaction between **3.2** and GSH was examined by ^{1}H NMR measurements on a Bruker 400 MHz spectrometer. GSH was dissolved in D_2O containing 0.1 M $NaNO_3$, with pH* adjusted to 7.4 by using sodium hydroxide. The final concentration of GSH was 10 mM. Complex **3.2** was dissolved in D_2O (pH* 7.4–7.6) with final concentration being 5 mM. Then, 100 μL of **3.2**, 350 μL of GSH, and 150 μL of D_2O were mixed. The NMR spectra of the solution mixture at different time intervals were recorded. Reactions with different ratios of **3.2** and GSH were performed by using different volumes of **3.2** and/or GSH.

3.2.4 Luminescent Properties of 3.9

3.2.4.1 In the Presence of Different Analysts

Solutions of $MgCl_2$, $CaCl_2$, amino acids (Ser, Pro, Leu, Ile, His, Ala, Cys), DTT, and GSH in 1 × PBS: DMSO = 9:1 (v/v) were freshly prepared. Stock solution of **3.9** in DMSO (10 mM) was prepared. Then, 10 μL of stock solution of **3.9** was added to 5 ml of PBS: DMSO = 9:1 (v/v) solutions containing different analytes, respectively. The resulting solution was shaken well for 5 min, and its emission spectrum was recorded. There was no significant change in emission intensity after the resulting solution was left standing for 2 and 12 h, respectively. For all of the measurements, the excitation wavelength was set at 340 nm. The intensity of emission of the solutions obtained by the reaction of **3.9** and the analytes under the aforementioned conditions were recorded and compared.

Solution of HSA at concentration of 5 mg/mL (∼75 μM) was prepared; then, 10 μL of a stock solution of **3.9** was added to 5 mL of this HSA solution. The resulting solution mixture was shaken well. After 2 min, the emission spectra at different time intervals were recorded.

3.2.4.2 Fluorescence Microscopic Examination

HeLa cells (2×10^5 cells) were seeded in a one chamber slide (Nalgene; Nunc) with culture medium (2 mL/well) and incubated at 37 °C in a humidified atmosphere of 5 % CO_2/95 % air for 24 h. After treatment with **3.9** (20 μM, 1 mL MEM) for 10 min, cells were directly exposed for fluorescent imaging without changing the old medium. The bright-field and fluorescent images (ex: 365 and 546 nm) were examined by using Axiovert 200 (Carl Zeiss) and in an Axio Vision Rel. 4.5 imaging system (Carl Zeiss). Correlation analysis was done by using ImageJ following a reported procedure [42].

3.2.5 Anticancer Properties

3.2.5.1 Cell Lines and Growth Inhibitory Assay

Human hepatocellular carcinoma (HepG2) and human cervical cancer (HeLa) cell lines were obtained from American Type Culture Collection (MD, USA). Human nasopharyngeal carcinoma cells (SUNE1) were generously provided by Prof. S. W. Tsao (Department of Anatomy, The University of Hong Kong). The cell lines were maintained in cell culture media (minimum essential medium for HepG2, HeLa, MCF-7; and RPMI-1640 medium for SUNE1, NCI-H460, and B16) supplemented with 10 % fetal bovine serum, 100 U/mL penicillin, and 100 μg/mL streptomycin at 37 °C humidified atmosphere with 5 % CO_2. Cell growth inhibitory effects of the anticancer gold(III) complexes and cisplatin were determined by MTT cytotoxicity assays. Briefly, the metal complex-treated cells were incubated with MTT (0.5 mg/mL) for 4 h at 37 °C in a humidified atmosphere of 5 % CO_2 and were subsequently lysed in solubilizing solutions. Cells were then maintained in a dark, humidified chamber overnight. The formation of formazan was measured by using a microtitre plate reader at 580 nm. Growth inhibition by metal complex was evaluated by IC_{50} (concentration of metal complex causing 50 % inhibition of cell growth). Each growth inhibition experiment was repeated at least three times, and results were expressed as means ± standard deviation (SD).

3.2.5.2 Cellular Activities of Thioredoxin Reductase (TrxR)

Cells were seeded at 2×10^5/well in 6-well plates and incubated for 24 h. Complexes **3.1**, **3.2**, **3.5** and **3.9** were serially diluted and added to the cells (final DMSO concentrations ≤1 %). After incubation for 1 h, the cells were washed three times with PBS, and 100 μL of ice-cold lysis buffer (50 mM phosphate buffer, pH 7.4, 1 mM EDTA, 0.1 % Triton-X 100) was added to the cell layer. Cell lysis was carried on ice for 5 min, and the cell lysates were collected and stored at−80 °C or assayed immediately. Afterward, cell lysates (10 μg proteins) were added to a buffer solution (100 μL) containing 50 mM potassium phosphate, pH 7.4, 1 mM EDTA, and 0.2 mM NADPH. The reaction was initiated by adding 5,5′-dithiobis (2-nitrobenzoic acid) (DTNB, 3 mM final), and the TrxR activities were determined as increases in O.D.410 nm in 10 min.

3.2.5.3 Lipophilicity Measurement

Lipophilicity was determined following a reported procedure [43]. In general, a mixture of saturated *n*-octanol with sodium chloride was mixed with equal volume of aqueous solution with 0.9 % NaCl (w/v), and then, the mixture was added with each gold(III) complex and was further shaken for 1 h at 45 rpm on the shaker.

Samples were centrifuged and the content of gold(III) complex in each phase was determined by measuring the absorbance at the appropriate wavelength for each complex. LogP was calculated as the logarithmic ratio of the concentrations of the gold(III) complex in the *n*-octanol and aqueous phases.

3.2.5.4 Cellular Uptake Experiments

In general, HeLa cells (2×10^5 cells) were seeded in 6-well tissue culture dishes with minimum essential medium (2 mL/well) and incubated at 37 °C in a humidified atmosphere of 5 % CO_2/95 % air for 24 h. The culture medium was removed and replaced with medium containing 100 μM of each complex. After exposure to the drug complexes for 10 min, the medium was removed and the cell monolayer was washed four times with ice-cold PBS. Then, 500 μL of milli-Q water was added, and the cell monolayer was scraped off from the culture dish. 300 μL of samples was digested in 300 μL 70 % HNO_3 at 70 °C for 2 h and room temperature overnight and then diluted 1:10 or 1:100 in water for inductively coupled plasma mass spectrometry (ICP-MS) analysis.

3.2.5.5 Western Blot Analysis

HeLa cells (1×10^6 cells) were seeded in 10-cm tissue culture dishes with culture medium (10 mL/well), incubated at 37 °C in a humidified atmosphere of 5 % CO_2/95 % air for 24 h, and then treated with **3.9** for 48 h. After washing with cold PBS for three times, cells were lysed in radioimmunoprecipitation assay (RIPA) buffer (500 μL, 1 % Trition X-100, 10 % deoxycholate, 50 mM Tris-HCl, pH 7.5, 150 mM NaCl, 0.1 % SDS, 0.1 mm PMSF, 10 μg/mL leupeptin, 10 μg mL^{-1} aprotinin) at 0 °C. After centrifugation, the supernatants were collected. The cellular protein content was quantified by the DC Protein Assay (Bio-Rad). For detection, samples (15–45 μg/lane) were fractionated on a 12.5 % SDS–PAGE in a Tris-glycine running buffer and blotted on polyvinylidene fluoride (PVDF) membranes. The PVDF membranes were blocked overnight at room temperature in TBST (20 mM Tris-HCl, pH 7.6, 0.1 % Tween 20 v/v) containing 5 % BSA powder (w/v). Afterward, the blots were incubated at room temperature for an hour with the primary antibody, which was diluted in TBST containing 5 % BSA powder (w/v). After washing with TBST three times, the membranes were then incubated with the respective secondary antibody for 2 h. Detection was performed by using the chemiluminescence procedure (ECL, Amersham).

3.2.5.6 In Vivo Tumor Growth Inhibition Experiments

Female BALB/cAnN-nu (Nude) mice, 5–7 weeks old, were purchased from the Charles River Laboratories (Wilmington, MA) and cared for according to the

guidelines of the Laboratory Animal Unit of the University of Hong Kong (HKU). All animal experiments were conducted under the guidelines approved by the Committee on the Use of Live Animals in Teaching and Research of HKU. To establish the HeLa xenograft model, 4×10^6 HeLa cells suspended in 100 μl of PBS were inoculated into the right back flanks of the mice by subcutaneous injection. When the tumor volumes reached about 50 mm^3 (3 days after tumor inoculation), the mice were randomly divided into different treatment groups (3 mg/kg of **3.5** or solvent control). Complex **3.5** was reconstituted in PET diluent (60 % polyethylene glycol 400, 30 % ethanol, 10 % Tween 80). Complex **3.5** dissolved in PET diluent and then diluted in PBS or PBS supplemented with equal amount of PET was injected into the mice by intratumoral injection 3 times per week until the mice were sacrificed. The volume of PET diluent injected into each mouse was ≤1.2 μL. Tumor sizes were measured 3 times per week, and tumor volume (V) was calculated by the formula $V = ab^2 \times 0.52$, where a and b were the longest and the shortest diameters of the xenografted tumor. Data were presented as mean ± SD from 5 mice per group. The tumor inhibition was calculated according to the following formula:

$$\text{Inhibition percentage} = \left(1 - \frac{V - V_0}{V' - V_0'}\right) \times 100C\%$$

where V and V' are the tumor volumes of **3.5** treatment and solvent control, respectively. V_0 and V_0' are the initial tumor volumes of the **3.5** treatment and solvent control, respectively.

3.3 Results and Discussion

3.3.1 Synthesis and Characterization

The reaction of H_2IPI or H_2BPB with $KAuCl_4$ in alcohol gave [Au^{III}(N^N^N)Cl] (where N^N^N = IPI or BPB). Complexes **3.1**–**3.8** (N^N^N = IPI) and **3.9**–**3.11** (N^N^N = BPB) were obtained (Fig. 3.1) by refluxing a mixture of [Au^{III}(N^N^N)

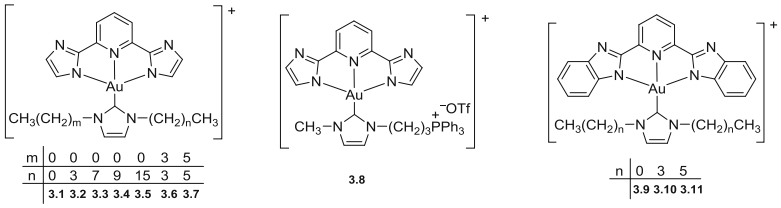

Fig. 3.1 [Au^{III}(N^N^N)(NHC)]OTf complexes 3.1–3.8 based on ligand IPI and 3.9–3.11 based on ligand BPB (anion OTf^- is not shown)

Cl], AgOTf, and [Ag(NHC)X] (X = Br or I) in acetonitrile in dark conditions (Fig. 3.1). All the complexes were characterized by ^{1}H NMR, mass spectrometry, and elemental analyses. These Au(III)–NHC complexes are soluble in CH_3OH, CH_3CN, DMF, and DMSO. Notably, **3.1** shows a considerable water solubility (>7 mg/mL); its 1D ^{1}H NMR, 2D ^{1}H-^{1}H COSY, and NOESY NMR spectra in D_2O are depicted in Figs. 3.2, 3.3, and 3.4. Complexes **3.4** and **3.5** display amphiphilic properties. Change of both *N*-methyl groups of **3.1** to longer alkyl groups to give **3.6** and **3.7,** respectively, or replacement of the imidazolyl with benzimidazolyl groups (to form **3.9**–**3.11**) renders the resultant Au(III)–NHC complexes to be insoluble in water.

The structures of **3.1** and **3.9** have been determined by X-ray crystallography (Figs. 3.5 and 3.6; Table 3.1). In both crystal structures, the molecules are paired through π–π interactions of the coordinated N^N^N ligands (interplane distance: ca. 3.3 Å for **3.1** and 3.5 Å for **3.9**). The NHC plane has an angle of 64.9° with the IPI ligand plane (**3.1**) and 78.8° with the BPB ligand plane (**3.9**), similar to related angles in $[Au^{III}(C^N^C)(NHC)]^+$ ($H_2C^N^C$ = 2,6-diphenylpyridine) (53.6°–82.0°) [45]. The Au(III)-C_{NHC} distance is 2.048 Å for **3.1** and 2.033/1.978 Å for **3.9**, comparable to those of $[Au^{III}(C^N^C)(NHC)]^+$ (1.967–2.017 Å) [45], $[Au^{III}(NHC)Cl_3]$ (1.975–2.013 Å) [46], $[Au^{III}(NHC)Br_3]$ (2.009–2.052 Å) [47], and *trans*-$[Au^{III}(NHC)_2I_2]BF_4$ (2.048 Å) [48].

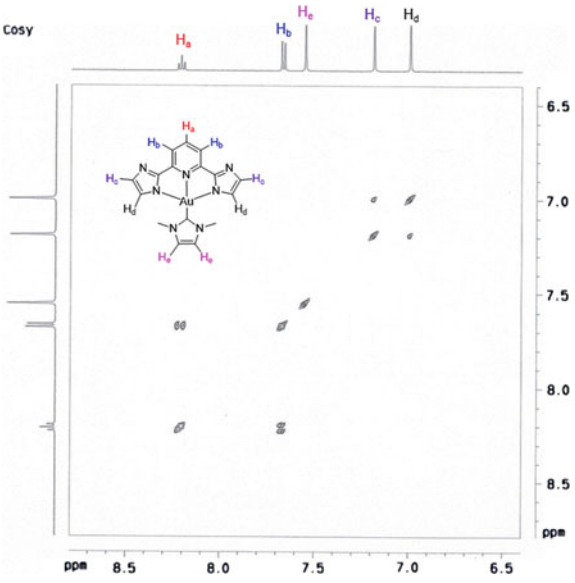

Fig. 3.2 500 MHz ^{1}H-^{1}H COSY NMR spectrum of **3.1** in D_2O at 298 K. Reproduced with permissions [44]. Copyright © 2013 WILEY-VCH Verlag GmbH & Co. KGaA, Weinheim

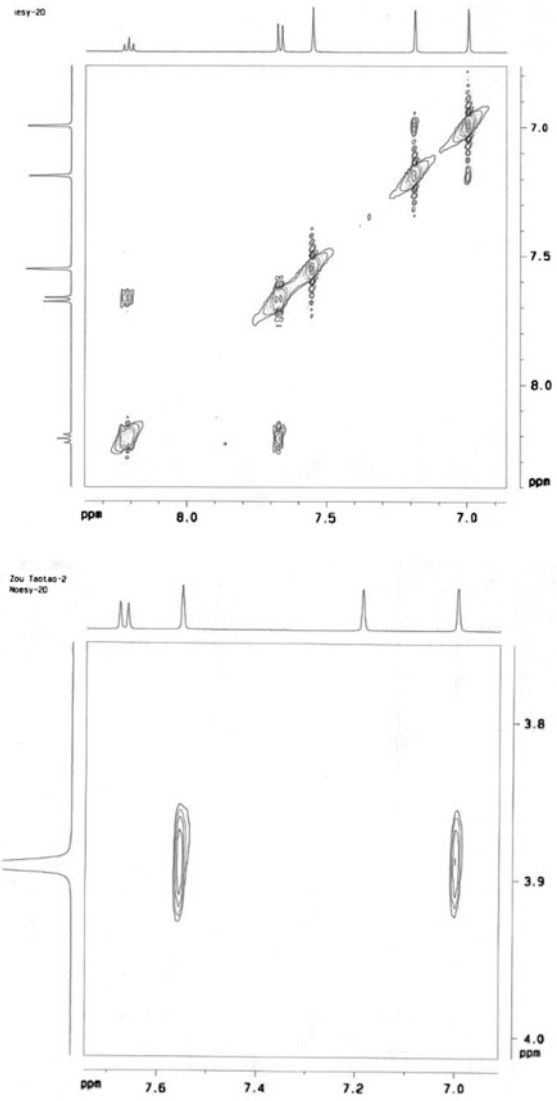

Fig. 3.3 500 MHz ^{1}H-^{1}H NOESY NMR spectrum of **3.1** in D_2O at 298 K. Reproduced with permissions [44]. Copyright © 2013 WILEY-VCH Verlag GmbH & Co. KGaA, Weinheim

3.3.2 Reactions with GSH

Complexes **3.1**–**3.11** are stable in buffer solutions. For example, complex **3.1** or **3.9** (20 μM) displays no change in its UV−Vis absorption spectrum in phosphate-buffered saline (PBS, 10 mM, containing 5 % of DMSO, v/v, pH 7.4, 25 °C) after 72 h as shown in Figs. 3.7 and 3.8, respectively. Upon addition of GSH (2 mM) to the solution, the absorption at 340–470 nm for **3.1** or 370–460 nm for **3.9** vanished

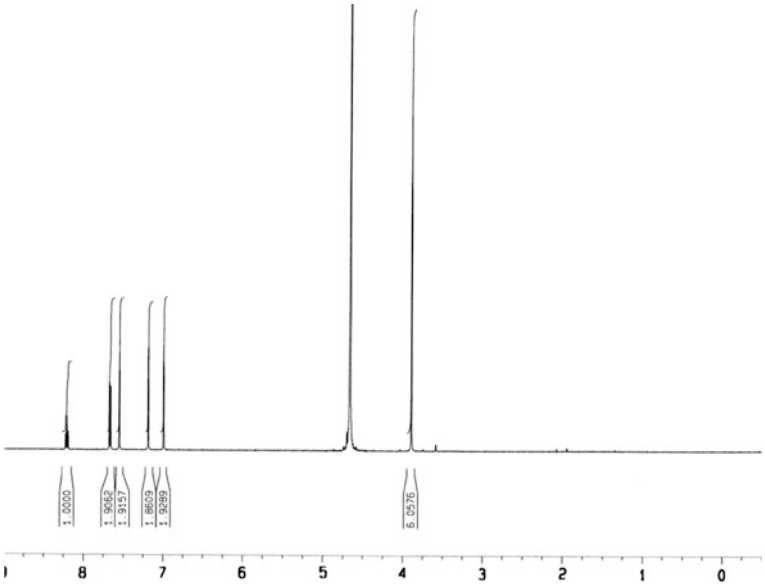

Fig. 3.4 500 MHz ^{1}H NMR spectrum of **3.1** in D_2O at 298 K. Reproduced with permissions [44]. Copyright © 2013 WILEY-VCH Verlag GmbH & Co. KGaA, Weinheim

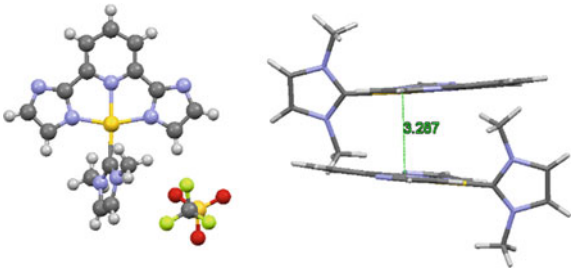

Fig. 3.5 Crystal structure of **3.1**. Reproduced with permissions [44]. Copyright © 2013 WILEY-VCH Verlag GmbH & Co. KGaA, Weinheim

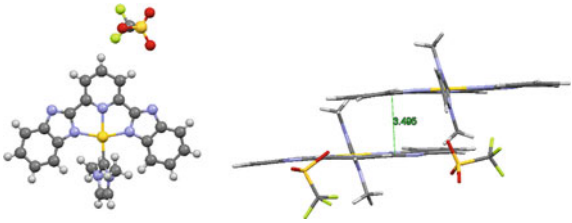

Fig. 3.6 Crystal structure of **3.2**

Table 3.1 Crystal data and structure refinement data for 3.1 and 3.9

	3.1	**3.9**
Empirical formula	$C_{17}H_{15}N_7O_3F_3SAu$	$C_{50}H_{42}Au_2F_6N_{14}O_9S_2$
Formula weight	651.39	1555.03
Temperature (K)	100(2)	100(2)
Crystal system	Orthorhombic	Monoclinic
Space group	Pbca	$P2_1/c$
a (Å)	11.1891(12)	12.8212(8)
b (Å)	14.2482(15)	15.9019(9)
c (Å)	25.338(3)	26.9453(17)
α (°)	90.00	90.00
β (°)	90.00	93.058(3)
γ (°)	90.00	90.00
Volume ($Å^3$)	4039.5(7)	5485.8(6)
Z	8	4
ρ_{calc} (mg/mm^3)	2.142	1.883
μ (mm^{-1})	15.25	11.405
F(000)	2496.0	3024.0
Crystal size (mm^3)	0.15 × 0.10 × 0.04	0.15 × 0.02 × 0.02
2θ range for data collection	6.98 to 132.36°	6.56 to 132.42°
Index ranges	$-11 \le h \le 12$, $-16 \le k \le 16$, $-30 \le l \le 29$	$-15 \le h \le 11$, $-18 \le k \le 18$, $-31 \le l \le 31$
Reflections collected	24,889	35,228
Independent reflections	3460[R(int) = 0.0633]	8705[R(int) = 0.0973]
Data/restraints/parameters	3460/0/289	8705/6/740
Goodness of fit on F^2	1.170	1.018
Final R indexes [$I >= 2\sigma(I)$]	R_1 = 0.0505, wR_2 = 0.1539	R_1 = 0.1050, wR_2 = 0.2707
Final R indexes [all data]	R_1 = 0.0519, wR_2 = 0.1563	R_1 = 0.1269, wR_2 = 0.2924
Largest diff. peak/hole [e $Å^{-3}$]	4.71/−1.77	5.92/−3.93

Reproduced with permissions [44]. Copyright © 2013 WILEY-VCH Verlag GmbH & Co. KGaA, Weinheim

<1 min, respectively. Electrospray ionization mass spectrometry (ESI-MS) analysis indicated that free H_2N^N^N ligand, [Au^I(NHC)(GS)], and GSSG were formed (Fig. 3.9).

^{1}H NMR spectroscopy (400 MHz, in D_2O, pH* = ∼7.4, [$NaNO_3$] = 0.1 M, 298 K) was employed to investigate the reaction of **3.2** (0.83 mM) with GSH (5.83 mM). As shown in Fig. 3.10, the signals of the coordinated N^N^N ligand completely disappeared, accompanied by the formation of free H_2IPI. The peaks at 3.31 are attributed to β-CH_{cys} of GSSG; [49] the new peaks at 3.15 ppm and around 3.3 ppm are indicative of binding between GSH and Au(I), as similar chemical

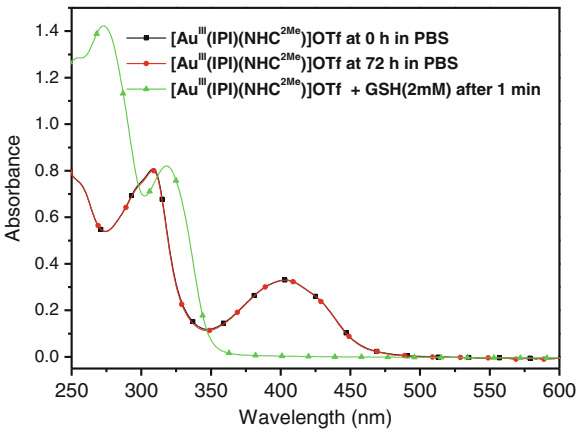

Fig. 3.7 UV–Vis absorption spectra of **3.1** (a) in PBS: DMSO = 19:1 (v/v) after 0 h (*black*), 72 h (*red*), and after addition of 2 mM GSH for 1 min. Reproduced with permissions [44]. Copyright © 2013 WILEY-VCH Verlag GmbH & Co. KGaA, Weinheim

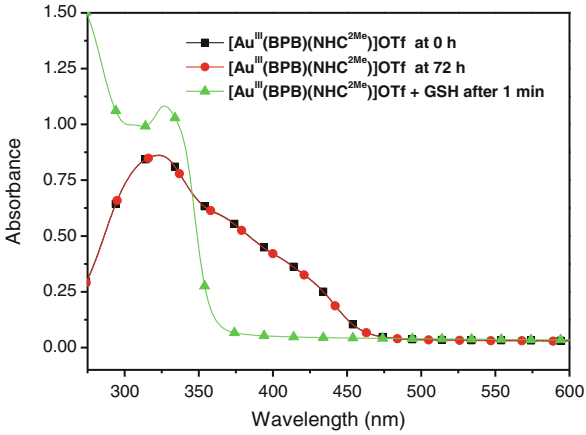

Fig. 3.8 UV–Vis absorption spectra of **3.9** (a) in PBS: DMSO = 19:1 (v/v) after 0 h (*black*), 72 h (*red*), and after addition of 2 mM GSH for 1 min. Reproduced with permissions [44]. Copyright © 2013 WILEY-VCH Verlag GmbH & Co. KGaA, Weinheim

shifts attributed to β-CH_{cys} of [Au^{I}(NHC)(Cys)] have been reported for the binding of –SH_{cys} with Au(I)–NHC complexes [27]. The signals of the NHC ligand are at 7.13 and 7.17 ppm that are similar to those reported for [Au^{I}(NHC)(Cys)] (7.15–7.30 ppm) [27]. In addition, the ^{1}H NMR spectrum did not change upon increasing the reaction time from 10 min to 60 h (Fig. 3.11), suggestive of rapid completion of the reaction and the apparently high stability of the gold(I) products toward excess GSH. The reactions of **3.2** and GSH at molar ratios of 1:3 and 1:6 were also examined, showing similar results (Fig. 3.12). Therefore, one equivalent of [Au^{III}(N^N^N)(NHC)]$^{+}$ complex reacted with three equivalents of GSH, leading to reduction of Au(III) to Au(I) and release of the coordinated N^N^N ligand. Two equivalents of GSH were oxidized to give GSSG, and the remaining one equivalent of GSH coordinated with Au(I) giving [Au^{I}(NHC)(GS)].

The stability of the Au(III)–NHC complexes toward thiol-free cellular reducing agent, ascorbic acid (2 mM), was also studied. The absorption at 340–470 nm for **3.1** did not change within 2 h, and the absorbance at 370–460 nm for **3.9** started to

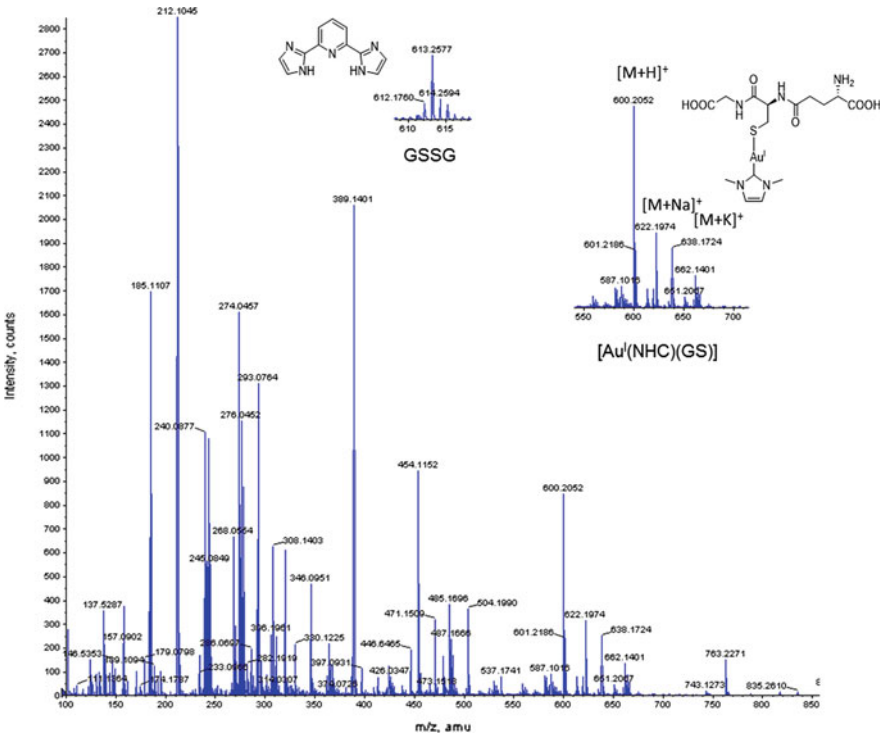

Fig. 3.9 ESI-MS-TOF spectrum of a solution mixture obtained by mixing **3.1** and GSH at 1:6 molar ratio (reaction time: 0.5 h). Reproduced with permissions [44]. Copyright © 2013 WILEY-VCH Verlag GmbH & Co. KGaA, Weinheim

notably decrease after 0.5 h; meanwhile, these absorptions did not totally vanish even after 24 h (Fig. 3.13 and Fig. 3.14). These results reveal that ascorbic acid is less effective than thiol to reduce these Au(III)–NHC complexes.

3.3.3 Emission Properties of 3.9 Toward Thiols

The $[Au^{III}(N^N^N)(NHC)]^+$ complexes **3.1–3.11** are non-emissive either in solid states or in solutions. As mentioned above, reduction of Au(III) to Au(I) by GSH is accompanied by the release of $H_2N^N^N$ which is strongly emissive. Emission spectroscopy studies showed that upon addition of thiol-containing GSH or Cys, predominant emission of $H_2N^N^N$ ligand could be switched on within <1 min; the resultant emission spectra are the same as those of the free $H_2N^N^N$ ligands (Fig. 3.15).

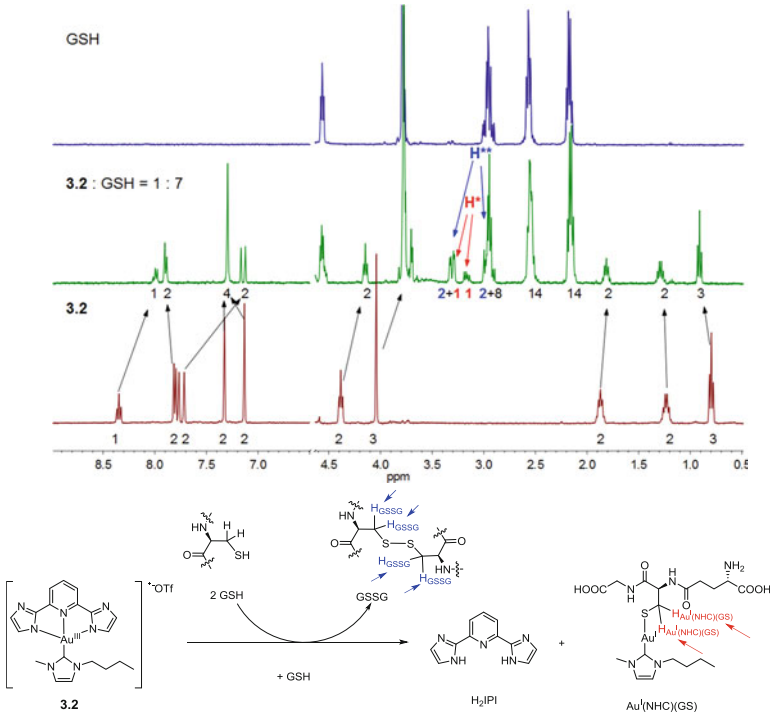

Fig. 3.10 ^{1}H NMR spectra (400 MHz) of free GSH (*top*), a mixture of GSH and **3.2** in a 7:1 molar ratio after mixing for 10 min (*middle*), and **3.2** (*bottom*); intensity ratios are shown. Reproduced with permissions [44]. Copyright © 2013 WILEY-VCH Verlag GmbH & Co. KGaA, Weinheim

Complex **3.9** containing the highly fluorescent BPB ligand with emission wavelength in visible region was chosen for further investigation. It was shown that release of the H_2BPB ligand upon treatment of **3.9** with GSH resulted in >200-fold elevation in emission intensity (Fig. 3.16a) which is much better than that of the literature reported Ru(II)-poly(1,10-phenanthroline) [50] and Cd(II)-8-hydroxyquinoline-5-sulfonic acid [51] thiol probes. No fluorescence was detected when **3.9** was treated with Ca^{2+}, Mg^{2+}, or thiol-free amino acids including Ser, Ala, Leu, Pro, His, and Ile. Complex **3.9** is particularly sensitive to thiol-containing compounds such as GSH, Cys, and the widely used reducing agent dithiothreitol (DTT) (Fig. 3.16a).

The responses of **3.9** (20 μM) toward thiol-containing human serum albumin (HSA, 5 mg/mL, ~75 μM) were further examined. As shown in Fig. 3.16b, the emission intensity increased slowly and gradually levelled off after 2 h, and the maximal response was only 20 % compared to that toward GSH under similar conditions. As each HSA molecule contains only one free thiol group, Cys34, that is, surrounded by side chains of Pro35, Asp38, His39, Val77, and Tyr84 [52, 53],

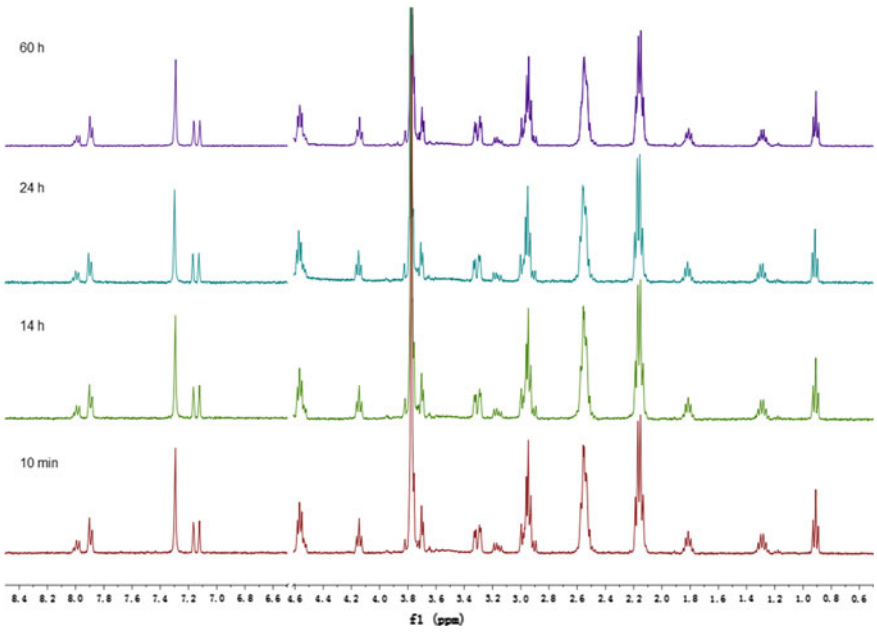

Fig. 3.11 ^{1}H NMR spectra (400 MHz, D_2O, 298 K) of **3.2** (0.83 mM) and GSH (5.83 mM) after mixing for 10 min, 14 h, 24 h, and 60 h; no significant changes were found. Reproduced with permissions [44]. Copyright © 2013 WILEY-VCH Verlag GmbH & Co. KGaA, Weinheim

these side chains could possibly hamper the interaction between –SH group and Au (III)–NHC complexes.

3.3.4 Anticancer Properties

In view of the favorable emission "switch-on" property of **3.9** toward GSH, the cellular uptake and intracellular distribution of **3.9** in cancer cells were investigated by using fluorescence microscope. After incubation of human cervical epithelioid carcinoma (HeLa) cells with **3.9** (20 μM in minimum essential medium containing 10 % fetal bovine serum, v/v) for only 10 min, a significant blue fluorescence was detected in cytoplasm but not in nucleus or extracellular environment (Fig. 3.17), suggestive of the stability of **3.9** toward cell culture media and efficient cellular uptake as well as transformation of the Au(III)–NHC complex to Au(I) complexes in cytoplasm. The specific intracellular location of the fluorescence was further studied by colocalization analysis with organelle-specific commercial dyes. It was found that a distinct portion of the blue fluorescence in the **3.9**-treated cells was localized in mitochondria which is specifically stained with MitoTracker Red® (Pearson's correlation coefficient $R = 0.74$, Fig. 3.17c). Notably, this result indicates

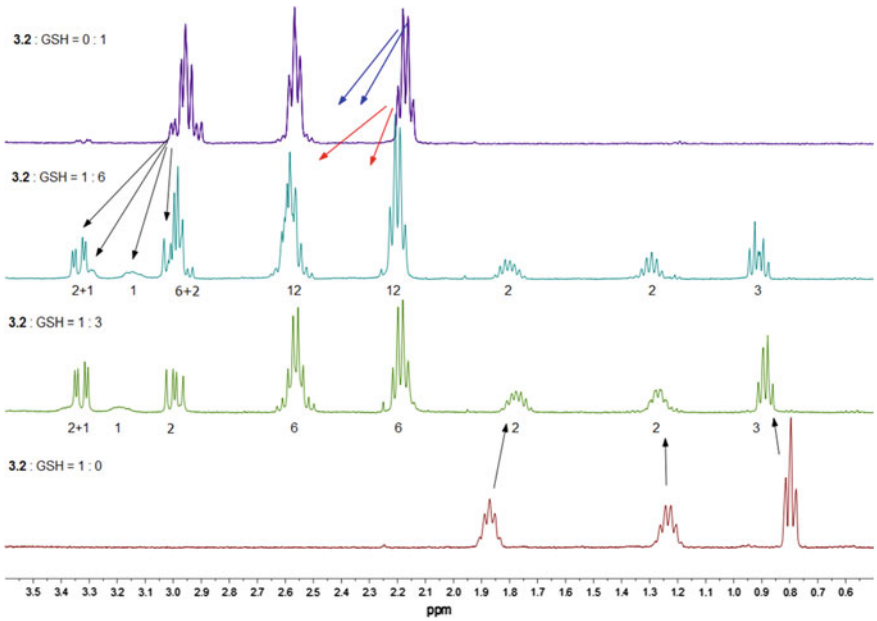

Fig. 3.12 ^{1}H NMR spectra (400 MHz, D_2O, 298 K) of **3.2** and GSH at different molar ratios after mixing for 10 min. Fig. shows the region of 3.6–0.5 ppm. Reproduced with permissions [44]. Copyright © 2013 WILEY-VCH Verlag GmbH & Co. KGaA, Weinheim

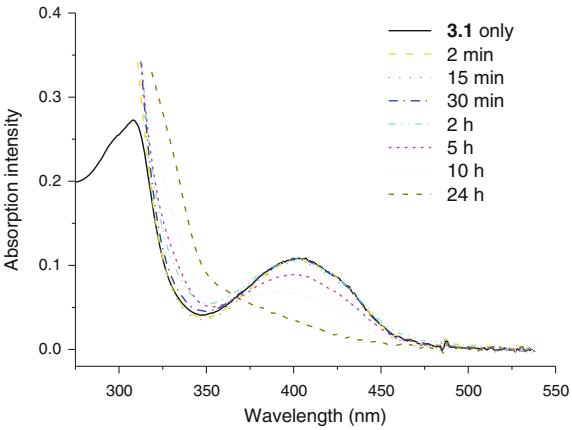

Fig. 3.13 UV–Vis absorption spectra of **3.1** in PBS: DMSO = 19:1 (v/v) containing 2 mM of ascorbic acid at different time intervals. Reproduced with permissions [44]. Copyright © 2013 WILEY-VCH Verlag GmbH & Co. KGaA, Weinheim

cellular uptake of **3.9** and intracellular reduction altogether took place within 10 min. As described above, reduction of **3.9** by ascorbic acid became notable only after 30 min, and the reaction of **3.9** with large molecular weight serum albumin was much slower; i.e., only 20 % reaction was observed after a reaction time of 2 h. As a result, both ascorbic acid and serum albumin would not pose hurdle for **3.9** to

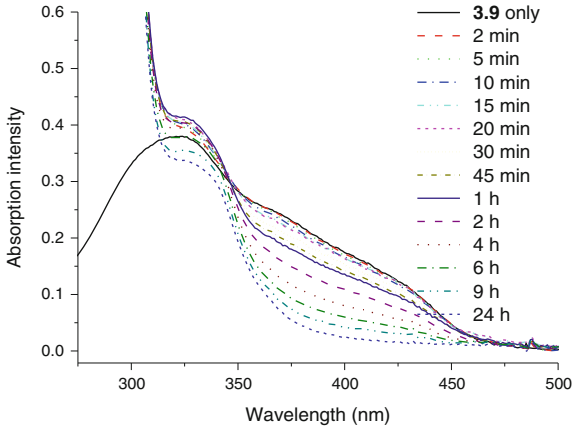

Fig. 3.14 UV–Vis absorption spectra of **3.9** in PBS:DMSO = 19:1 (v/v) containing 2 mM of ascorbic acid at different time intervals. Reproduced with permissions [44]. Copyright © 2013 WILEY-VCH Verlag GmbH & Co. KGaA, Weinheim

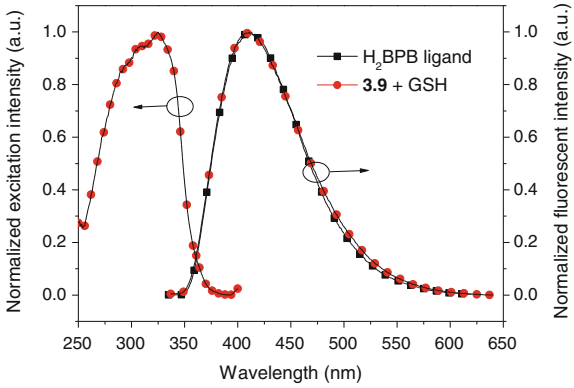

Fig. 3.15 Emission/excitation spectra for H_2BPB and **3.9** + GSH. Reproduced with permissions [44]. Copyright © 2013 WILEY-VCH Verlag GmbH & Co. KGaA, Weinheim

efficiently enter into cancer cells for tracing the intracellular thiols and for delivering the $[Au(NHC)]^+$ moiety to its molecular target thioredoxin reductase (TrxR) as described below.

Based on the above findings, the Au(III)–NHC complexes **3.1–3.11** could be reduced by intracellular GSH to form Au(I)–NHC complexes. This reaction is reminiscent of the activation process of Pt(IV) prodrugs, where Pt(IV) is reduced to Pt(II) through intracellular reduction by GSH, forming GSSG (see examples in Chap. 1) [54]. Therefore, in a cellular pharmacological context, these Au(III)–NHC complexes can be conceived as precursors/prodrugs of anticancer Au(I)–NHC

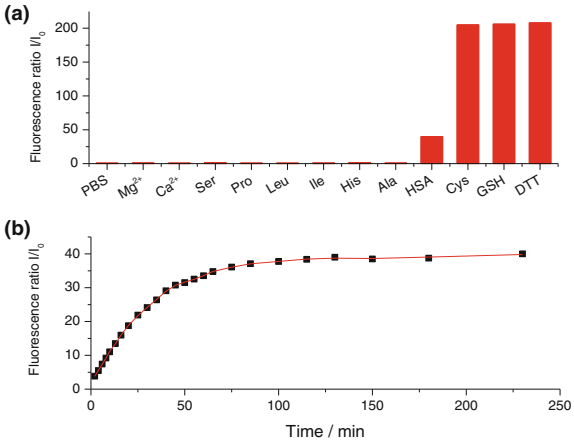

Fig. 3.16 **a** Fluorescence intensity ratio I/I_0 of **3.9** toward different analytes (2 mM, except for HSA 5 mg/mL) after mixing within 5 min (except for HSA, 2 h). I_0 and I denote the intensity before and after treatment of the analyte, respectively. No change of fluorescence was found after 12 h. **b** Time course of fluorescence intensity ratio I/I_0 of **3.9** toward HSA. Reproduced with permissions [44]. Copyright © 2013 WILEY-VCH Verlag GmbH & Co. KGaA, Weinheim

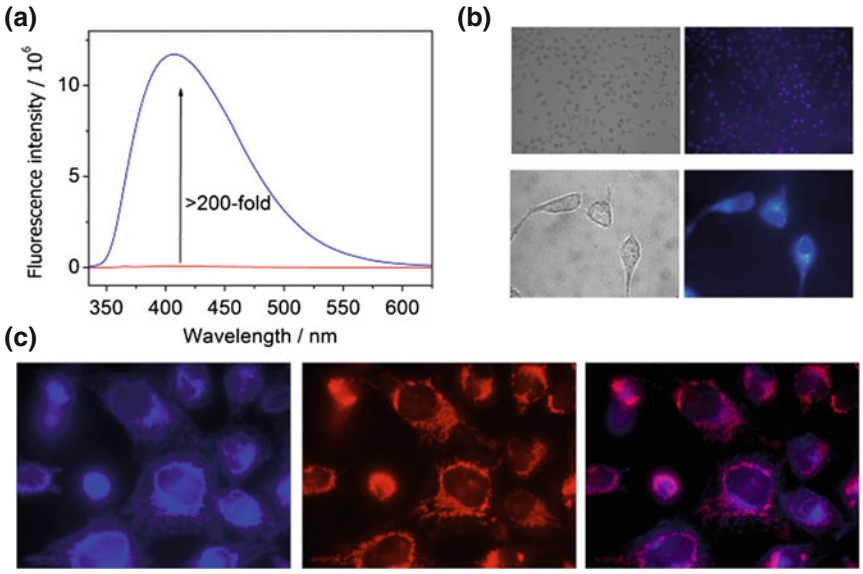

Fig. 3.17 **a** Emission intensity before (*red*) and after (*blue*) addition of GSH (2 mM) to **3.9** (20 μM) in PBS containing 10 % DMSO (v/v). **b** Fluorescence microscopic images (*up* 10× and *down* 40×) of HeLa cells after treatment with 20 μM **3.9** for 10 min. Images were taken without fixing or washing the cells. **c** Fluorescence images of **3.9** (left, ex: 365 nm), mitochondria-specific MitoTracker Red® stain (*middle*, ex: 546 nm) and the merged image (*right*). Reproduced with permissions [44]. Copyright © 2013 WILEY-VCH Verlag GmbH & Co. KGaA, Weinheim

Table 3.2 Cytotoxic IC_{50} values (μM) of **3.1–3.11** toward cancer cell lines HeLa, HepG2, NCI-H460, MCF-7, SUNE1, and B16, 72 h

Complex	HeLa	HepG2	NCI-H460	MCF-7	SUNE1	B16
3.1	32.9 ± 1.3	36.2 ± 2.2	55.0 ± 8.5	18.4 ± 0.3	28.7 ± 7.3	30.6 ± 0.3
3.2	16.5 ± 1.4	33.2 ± 1.8	11.0 ± 0.3	17.2 ± 0.6	9.9 ± 0.1	5.0 ± 0.2
3.3	14.0 ± 0.3	14.7 ± 1.5	17.3 ± 0.3	8.5 ± 0.2	8.9 ± 0.6	3.8 ± 0.1
3.4	8.8 ± 1.4	11.8 ± 1.2	9.7 ± 0.4	6.5 ± 0.5	5.5 ± 0.3	1.6 ± 0.1
3.5	1.4 ± 0.2	3.3 ± 0.5	1.4 ± 0.1	2.9 ± 0.2	–	2.2 ± 0.1
3.6	13.0 ± 1.6	28.7 ± 5.9	7.9 ± 1.1	12.9 ± 2.0	9.9 ± 0.2	8.3 ± 0.2
3.7	8.8 ± 0.6	9.1 ± 0.3	34.6 ± 3.1	8.6 ± 0.1	36.8 ± 1.6	7.7 ± 1.0
3.8	77.4 ± 1.8	–	65.4 ± 1.1	49.7 ± 3.0	47.3 ± 6.2	36.8 ± 0.9
3.9	14.4 ± 2.2	18.0 ± 0.5	11.2 ± 0.7	11.9 ± 1.0	11.2 ± 0.6	12.4 ± 0.1
3.10	9.2 ± 0.4	14.7 ± 1.1	5.5 ± 0.3	8.7 ± 0.2	5.2 ± 1.6	5.2 ± 0.2
3.11	8.4 ± 0.1	2.6 ± 0.4	5.0 ± 0.1	4.0 ± 0.1	3.1 ± 0.3	5.5 ± 0.1
Cisplatin	6.4 ± 0.6	10.8 ± 0.8	1.6 ± 0.3	21.8 ± 6.9	11.6 ± 2.2	12.3 ± 0.7

complexes. As demonstrated by Berners-Price, Filipovska, and coworkers [27], Au(I)–NHC complexes are able to induce apoptosis of cancer cells presumably through inhibition of TrxR, a SH- and SeH-containing flavoenzyme which reduces thioredoxin (Trx) and plays a pivotal role in regulating cancer cell progressions [13]. The cytotoxicity MTT assays showed that the Au(III)–NHC complexes (**3.1–3.11**) inhibited the growth of different cancer cell lines, including HeLa, hepatocellular carcinoma (HepG2), non-small cell lung carcinoma (NCI-H460), breast cancer (MCF-7), nasopharyngeal carcinoma (SUNE1), and mouse melanoma (B16) with IC_{50} ranging from 1.4 ± 0.2 to 77.4 ± 1.8 μM (Table 3.2). The cytotoxic IC_{50} values of these Au(III)–NHC complexes (**3.1–3.5**) were observed to decrease with increasing lipophilicity (Fig. 3.18). The free $H_2N^N^N$ ligand (e.g., H_2IPI) did not

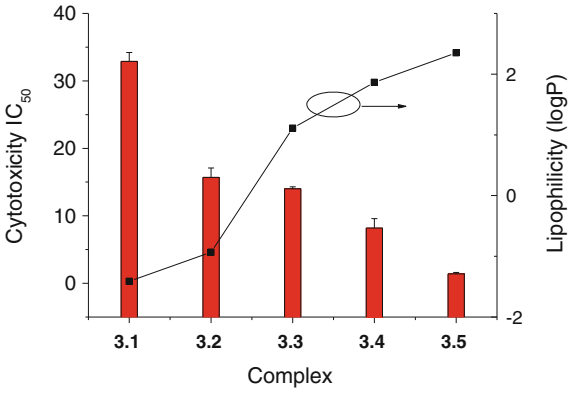

Fig. 3.18 Relationship between cytotoxicity and lipophilicity of complexes **3.1–3.5.** Reproduced with permissions [44]. Copyright © 2013 WILEY-VCH Verlag GmbH & Co. KGaA, Weinheim

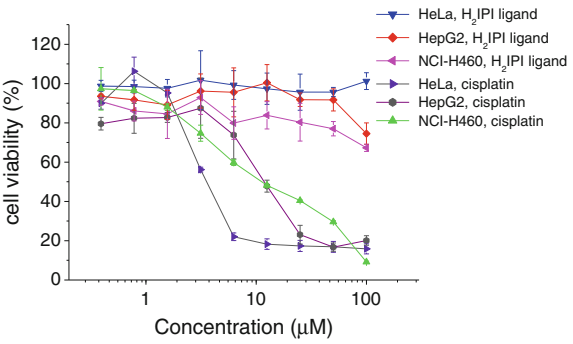

Fig. 3.19 MTT results of H_2IPI ligand and cisplatin toward HeLa, HepG2, and NCI-H460 cell lines for 72 h treatment. Reproduced with permissions [44]. Copyright © 2013 WILEY-VCH Verlag GmbH & Co. KGaA, Weinheim

exert obvious cytotoxicity even at a concentration of 100 μM (Fig. 3.19). The cytotoxicity mechanism of **3.9** was investigated in the context of expression of apoptotic proteins using Western blot analysis. Upon treating HeLa cells with 15 μM of **3.9** for 48 h, cleaved apoptotic poly(ADP-ribose) polymerase (PARP) caspases 3, 7, and 9 were activated (Fig. 3.20), revealing that the **3.9** treatment induced apoptotic cell death.

The effects of the Au(III)–NHC complexes on TrxR activity in cancer cells were studied by using DTNB as substrate. After treating HeLa cells with **3.1**, **3.2**, **3.5,** or **3.9** for 1 h, significant inhibition of the TrxR activity in the cell lysates was identified, with IC_{50} values of 14.3, 7.7, 3.8, and 5.5 μM, respectively (Table 3.3). The cytotoxic IC_{50} values for 72-h treatment with **3.1**, **3.2**, **3.5,** and **3.9** were 32.9, 16.5, 1.4, and 14.4 μM, respectively (Table 3.3). In this regard, the inhibitory potency of these complexes on TrxR could be reasonably correlated with their cytotoxicity. Notably, the 72-h cytotoxic IC_{50} of **3.5** (1.4 μM) is comparable to that of auranofin (1.8 μM), a potent TrxR inhibitor that can induce apoptotic cell death [13]. The weaker inhibition of the cellular TrxR by **3.5** compared to that by auranofin may be due to the lower cellular uptake rate of **3.5** (Table 3.3). As TrxR is an important biomolecular target of Au(I)–NHC and is abundant in cytoplasm and mitochondria [33], the specific cytoplasmic localization according to the above-mentioned findings supports that **3.9** is able to deliver anticancer active Au(I)–NHC to this biomolecular tar**get**.

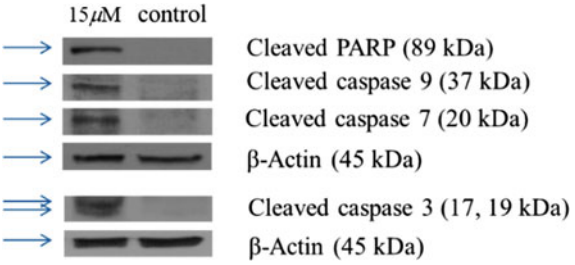

Fig. 3.20 Western blot experiments of HeLa cells treated with 15 μM of **3.9** for 48 h. Reproduced with permissions [44]. Copyright © 2013 WILEY-VCH Verlag GmbH & Co. KGaA, Weinheim

Table 3.3 Cytotoxicity, TrxR inhibition, cellular uptake, and lipophilicity of **3.1**, **3.2**, **3.5**, **3.9,** and auranofin

	Cytotoxicity IC_{50} (μM)[a]	TrxR inhibition IC_{50} (μM)[b]	Uptake (μg/g)[c]	Lipophilicity logP[d]
3.1	32.9	14.3	12.3	−1.41
3.2	16.5	7.7	22.3	−0.93
3.5	1.4	3.8	129.9	2.35
3.9	14.4	5.5	12.1	−0.05
Auranofin	1.8	0.57	1189.3	nd[e]

[a]Cytotoxicity (72-h treatment) was determined by MTT assay. IC_{50} was calculated as the average of at least 3 independent assays. [b]TrxR activity in lysates from cells treated with gold complex for 1 h. [c]Cellular uptake was determined by the gold content (μg) in cell proteins (g) after treating HeLa cells with each complex for 10 min. [d]Lipophilicity was determined by measuring λ_{max} for each complex in *n*-octanol and water-containing sodium chloride (0.9 % w/v). [e]nd = not determined. Reproduced with permissions [44]. Copyright © 2013 WILEY-VCH Verlag GmbH & Co. KGaA, Weinheim

The in vivo antitumor activity of the most potent **3.5** was further investigated. Upon treatment of nude mice bearing HeLa xenografts with **3.5** at dosage of 3 mg/kg for 3 times/week, significant inhibition in tumor growth (volume) was identified at day 11 ($p < 0.05$) and day 14 ($p < 0.01$) since the first treatment at day 0, with volume of tumor reduced by 60 and 76 %, respectively (Figs. 3.21a and 3.22). It is noteworthy that there was no mouse death or body weight loss in the treatment group (Fig. 3.21b). The slight increase in body weight of mice in the solvent control group might be attributed to faster growth of the tumors in this group.

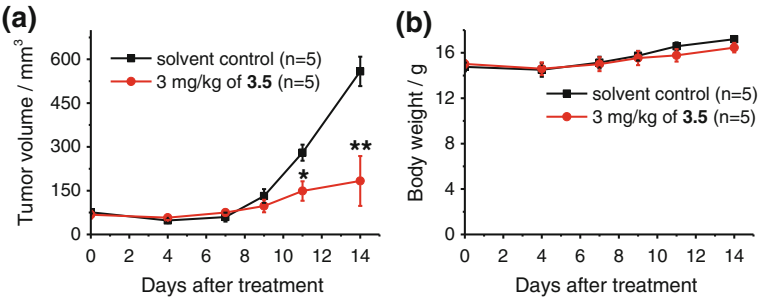

Fig. 3.21 **a** Representation of the average tumor volumes of nude mice bearing HeLa xenografts after treatment with 3 mg/kg of **3.5** or solvent only through intratumoral injection. Reproduced with permissions [44]. Copyright © 2013 WILEY-VCH Verlag GmbH & Co. KGaA, Weinheim. **b** Body weight of mice bearing HeLa xenografts in different groups

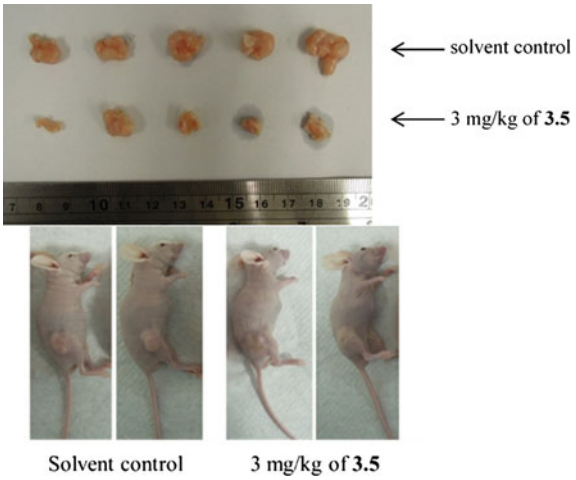

Fig. 3.22 Photographs of mouse tumors obtained from mice of different groups after treatment for 14 days. $^{*}p < 0.05$, $^{**}p < 0.01$ compared to solvent control. Reproduced with permissions [44]. Copyright © 2013 WILEY-VCH Verlag GmbH & Co. KGaA, Weinheim

3.4 Conclusion

To conclude, a new panel of Au(III) complexes bearing N-heterocyclic carbene and 2,6-bis(imidazol-2-yl)pyridine or 2,6-bis(benzimidazol-2-yl)pyridine ligands have been synthesized, and their reactions with thiols (e.g., GSH) have been examined by UV–Vis absorption spectroscopy, ESI-MS, ^{1}H NMR, emission spectrophotometry, and fluorescent microscopic analysis. The findings altogether reveal that these Au(III)–NHC complexes would react with thiols resulting in the liberation of the fluorescent $H_2N^N^N$ ligand, thus serving as a "switch-on" probe for thiols in biological system. These Au(III) complexes are also effective in suppressing the tumor growth of mice bearing HeLa xenografts. The antitumor effect possibly arises from the formation of Au(I)–NHCs upon Au(III) reduction. As the emission properties of the released $H_2N^N^N$ ligand and the Au(I) product arising from the reduction of Au(III) can be modulated and systematically tuned by ligand modification, these Au(III)–NHC complexes are useful scaffold in the design of novel "switch-on" bioprobes for thiols and anticancer agents.

References

1. Herzenberg LA, De Rosa SC, Dubs JG, Roederer M, Anderson MT, Ela SW, Deresinski SC, Herzenberg LA (1997) Glutathione deficiency is associated with impaired survival in hiv disease. Proc Natl Acad Sci USA 94(5):1967–1972
2. Rahman I, MacNee W (2000) Regulation of redox glutathione levels and gene transcription in lung inflammation: therapeutic approaches. Free Radical Biol Med 28(9):1405–1420

3. Escobedo J, Rusin O, Wang W, Alptürk O, Kim KK, Xu X, Strongin R (2006) Detection of biological thiols. In: Geddes C, Lakowicz J (eds) Reviews in fluorescence 2006, vol 2006. Springer, US, pp 139–162. doi:10.1007/0-387-33016-X_6
4. Zhang M, Yu M, Li F, Zhu M, Li M, Gao Y, Li L, Liu Z, Zhang J, Zhang D, Yi T, Huang C (2007) A highly selective fluorescence turn-on sensor for cysteine/homocysteine and its application in bioimaging. J Am Chem Soc 129(34):10322–10323
5. Bindoli A, Rigobello MP, Scutari G, Gabbiani C, Casini A, Messori L (2009) Thioredoxin reductase: a aarget for gold compounds acting as potential anticancer drugs. Coord Chem Rev 253(11–12):1692–1707
6. Zhao Q, Huang C, Li F (2011) Phosphorescent heavy-metal complexes for bioimaging. Chem Soc Rev 40(5):2508–2524
7. Sadler PJ, Sue RE (1994) The chemistry of gold drugs. Met-Based Drugs 1(2–3):107–144
8. Chow C-F, Chiu BKW, Lam MHW, Wong W-Y (2003) A trinuclear heterobimetallic Ru(II)/Pt(II) complex as a chemodosimeter selective for sulfhydryl-containing amino acids and peptides. J Am Chem Soc 125(26):7802–7803
9. Shao N, Jin JY, Cheung SM, Yang RH, Chan WH, Mo T (2006) A spiropyran-based ensemble for visual recognition and quantification of cysteine and homocysteine at physiological levels. Angew Chem Int Ed 45(30):4944–4948
10. Yang Y-K, Shim S, Tae J (2010) Rhodamine-sugar based turn-on fluorescent probe for the detection of cysteine and homocysteine in water. Chem Commun 46(41):7766–7768
11. Chen X, Zhou Y, Peng X, Yoon J (2010) Fluorescent and colorimetric probes for detection of thiols. Chem Soc Rev 39(6):2120–2135
12. Shaw CF III (1999) Gold-Based Therapeutic Agents. Chem Rev 99(9):2589–2600
13. Nobili S, Mini E, Landini I, Gabbiani C, Casini A, Messori L (2010) Gold compounds as anticancer agents: chemistry, cellular pharmacology, and preclinical studies. Med Res Rev 30 (3):550–580
14. Berners-Price SJ, Filipovska A (2011) Gold compounds as therapeutic agents for human diseases. Metallomics 3(9):863–873
15. Messori L, Abbate F, Marcon G, Orioli P, Fontani M, Mini E, Mazzei T, Carotti S, O'Connell T, Zanello P (2000) Gold(III) complexes as potential antitumor agents: solution chemistry and cytotoxic properties of some selected Gold(III) compounds. J Med Chem 43(19):3541–3548
16. Pizarro AM, Habtemariam A, Sadler PJ (2010) Activation mechanisms for organometallic anticancer complexes. Top Organomet Chem 32 (Medicinal Organometallic Chemistry):21–56
17. Che C-M, Siu F-M (2010) Metal Complexes in Medicine with a Focus on Enzyme Inhibition. Curr Opin Chem Biol 14(2):255–261
18. Che C-M, Sun RW-Y (2011) Therapeutic applications of gold complexes: lipophilic Gold(III) cations and Gold(I) complexes for anti-cancer treatment. Chem Commun 47(34):9554–9560
19. Berners-Price SJ, Mirabelli CK, Johnson RK, Mattern MR, McCabe FL, Faucette LF, Sung C-M, Mong S-M, Sadler PJ, Crooke ST (1986) In vivo antitumor activity and in vitro cytotoxic properties of Bis[1,2-bis(diphenylphosphino)ethane]gold(I) chloride. Cancer Res 46 (11):5486–5493
20. Urig S, Fritz-Wolf K, Réau R, Herold-Mende C, Tóth K, Davioud-Charvet E, Becker K (2006) Undressing of phosphine Gold(I) complexes as irreversible inhibitors of human disulfide reductases. Angew Chem Int Ed 45(12):1881–1886
21. Meggers E (2009) Targeting proteins with metal complexes. Chem Commun 9:1001–1010
22. Ott I, Qian X, Xu Y, Vlecken DHW, Marques IJ, Kubutat D, Will J, Sheldrick WS, Jesse P, Prokop A, Bagowski CP (2009) A Gold(I) phosphine complex containing naphthalimide ligand functions as a TrxR inhibiting antiproliferative agent and angiogenesis inhibitor. J Med Chem 52(3):763–770
23. Rubbiani R, Kitanovic I, Alborzinia H, Can S, Kitanovic A, Onambele LA, Stefanopoulou M, Geldmacher Y, Sheldrick WS, Wolber G, Prokop A, Wölfl S, Ott I (2010) Benzimidazol-2-ylidene Gold(I) complexes are thioredoxin reductase inhibitors with multiple antitumor properties. J Med Chem 53(24):8608–8618

24. Rubbiani R, Can S, Kitanovic I, Alborzinia H, Stefanopoulou M, Kokoschka M, Mönchgesang S, Sheldrick WS, Wölfl S, Ott I (2011) Comparative in vitro evaluation of N-heterocyclic carbene Gold(I) complexes of the benzimidazolylidene type. J Med Chem 54 (24):8646–8657
25. Meyer A, Bagowski CP, Kokoschka M, Stefanopoulou M, Alborzinia H, Can S, Vlecken DH, Sheldrick WS, Wölfl S, Ott I (2012) On the biological properties of Alkynyl phosphine Gold (I) complexes. Angew Chem Int Ed 51(39):8895–8899
26. Ray S, Mohan R, Singh JK, Samantaray MK, Shaikh MM, Panda D, Ghosh P (2007) Anticancer and antimicrobial metallopharmaceutical agents based on palladium, gold, and silver N-heterocyclic carbene complexes. J Am Chem Soc 129(48):15042–15053
27. Hickey JL, Ruhayel RA, Barnard PJ, Baker MV, Berners-Price SJ, Filipovska A (2008) Mitochondria-targeted chemotherapeutics: the rational design of gold(I) N-heterocyclic carbene complexes that are selectively toxic to cancer cells and target protein selenols in preference to thiols. J Am Chem Soc 130(38):12570–12571
28. Teyssot M-L, Jarrousse A-S, Manin M, Chevry A, Roche S, Norre F, Beaudoin C, Morel L, Boyer D, Mahiou R, Gautier A (2009) Metal-NHC complexes: a survey of anti-cancer properties. Dalton Trans 35:6894–6902
29. Lemke J, Pinto A, Niehoff P, Vasylyeva V, Metzler-Nolte N (2009) Synthesis, structural characterisation and anti-proliferative activity of NHC gold amino acid and peptide conjugates. Dalton Trans 35:7063–7070
30. Weaver J, Gaillard S, Toye C, Macpherson S, Nolan SP, Riches A (2011) Cytotoxicity of Gold(I) N-heterocyclic carbene complexes assessed by using human tumor cell lines. Chem Eur J 17(24):6620–6624
31. Wang C-H, Shih W-C, Chang HC, Kuo Y-Y, Hung W-C, Ong T-G, Li W-S (2011) Preparation and characterization of amino-linked heterocyclic carbene palladium, gold, and silver complexes and their use as anticancer agents that act by triggering apoptotic cell death. J Med Chem 54(14):5245–5249
32. Sivaram H, Tan J, Huynh HV (2012) Syntheses, characterizations, and a preliminary comparative cytotoxicity study of Gold(I) and Gold(III) complexes bearing benzimidazole— and pyrazole-derived N-heterocyclic carbenes. Organometallics 31:5875–5883
33. Schuh E, Pflüger C, Citta A, Folda A, Rigobello MP, Bindoli A, Casini A, Mohr F (2012) Gold(I) carbene complexes causing thioredoxin 1 and thioredoxin 2 oxidation as potential anticancer agents. J Med Chem 55(11):5518–5528
34. Li G, Huang J, Zhang M, Zhou Y, Zhang D, Wu Z, Wang S, Weng X, Zhou X, Yang G (2008) Bis(benzimidazole)pyridine derivative as a new class of G-quadruplex inducing and stabilizing ligand. Chem Commun 38:4564–4566
35. Boča M, Jameson RF, Linert W (2011) Fascinating variability in the chemistry and properties of 2,6-bis-(benzimidazol-2-yl)-pyridine and 2,6-bis-(benzthiazol-2-yl)-pyridine and their complexes. Coord Chem Rev 255(1–2):290–317
36. Serratrice M, Edafe F, Mendes F, Scopelliti R, Zakeeruddin SM, Grätzel M, Santos I, Cinellu MA, Casini A (2012) Cytotoxic gold compounds: synthesis, biological characterization and investigation of their inhibition properties of the zinc finger protein PARP-1. Dalton Trans 41(11):3287–3293
37. Hashiguchi BG, Young KJH, Yousufuddin M, Goddard WA III, Periana RA (2010) Acceleration of nucleophilic CH activation by strongly basic solvents. J Am Chem Soc 132 (36):12542–12545
38. Lin IJB, Vasam CS (2007) Preparation and application of N-heterocyclic carbene complexes of Ag(I). Coord Chem Rev 251(5–6):642–670
39. Baker MV, Barnard PJ, Berners-Price SJ, Brayshaw SK, Hickey JL, Skelton BW, White AH (2005) Synthesis and structural characterization of linear Au(I) N-heterocyclic carbene complexes: new analogues of the Au(I) phosphine drug auranofin. J Organomet Chem 690 (24–25):5625–5635
40. Lee CK, Vasam CS, Huang TW, Wang HMJ, Yang RY, Lee CS, Lin IJB (2006) Silver(I) N-heterocyclic carbenes with long N-Alkyl chains. Organometallics 25(15):3768–3775

41. Sheldrick GM (2008) A short history of SHELX. Acta Cryst A64(1):112–122
42. Schneider CA, Rasband WS, Eliceiri KW (2012) NIH Image to ImageJ: 25 Years of image analysis. Nat Methods 9(7):671–675
43. Sun RW-Y, Li CK-L, Ma D-L, Yan JJ, Lok C-N, Leung C-H, Zhu N, Che C-M (2010) Stable Anticancer Gold(III)-porphyrin complexes: effects of porphyrin structure. Chem Eur J 16 (10):3097–3113
44. Zou T, Lum CT, Chui SS-Y, Che C-M (2013) Gold(III) complexes containing N-heterocyclic carbene ligands: thiol "switch-on" fluorescent probes and anti-cancer agents. Angew Chem Int Ed 52(10):2930–2933
45. Au VK-M, Wong KM-C, Zhu N, Yam VW-W (2009) Luminescent cyclometalated N-heterocyclic carbene-containing Organogold(III) complexes: synthesis, characterization, electrochemistry, and photophysical studies. J Am Chem Soc 131(25):9076–9085
46. Gaillard S, Slawin AMZ, Bonura AT, Stevens ED, Nolan SP (2010) Synthetic and structural studies of [$AuCl_3$(NHC)] complexes. Organometallics 29(2):394–402
47. de Frémont P, Singh R, Stevens ED, Petersen JL, Nolan SP (2007) Synthesis, characterization and reactivity of N-heterocyclic carbene Gold(III) complexes. Organometallics 26(6):1376–1385
48. Jothibasu R, Huynh HV, Koh LL (2008) Au(I) and Au(III) complexes of a sterically bulky benzimidazole-derived N-heterocyclic carbene. J Organomet Chem 693(3):374–380
49. Petzold H, Sadler PJ (2008) Oxidation induced by the antioxidant glutathione (GSH). Chem Commun 37:4413–4415
50. Ji S, Guo H, Yuan X, Li X, Ding H, Gao P, Zhao C, Wu W, Wu W, Zhao J (2010) A highly selective OFF-ON red-emitting phosphorescent thiol probe with large stokes shift and long luminescent lifetime. Org Lett 12(12):2876–2879
51. Wang H, Wang W-S, Zhang H-S (2001) Spectrofluorimetic determination of cysteine based on the fluorescence inhibition of Cd(II)–8-hydroxyquinoline-5-sulphonic acid complex by cysteine. Talanta 53(5):1015–1019
52. Sugio S, Kashima A, Mochizuki S, Noda M, Kobayashi K (1999) Crystal structure of human serum albumin at 2.5 a resolution. Protein Eng 12(6):439–446
53. Bhattacharya AA, Grüne T, Curry S (2000) Crystallographic analysis reveals common modes of binding of medium and long-chain fatty acids to human serum albumin. J Mol Biol 303 (5):721–732
54. Dhar S, Gu FX, Langer R, Farokhzad OC, Lippard SJ (2008) Targeted delivery of cisplatin to prostate cancer cells by aptamer functionalized Pt(IV) prodrug-PLGA-PEG nanoparticles. Proc Natl Acad Sci USA 105(45):17356–17361

Chapter 4
A Binuclear Gold(I) Complex with Mixed Bridging Diphosphine and Bis(N-Heterocyclic Carbene) Ligands Shows Favorable Thiol Reactivity and Effectively Inhibits Tumor Growth and Angiogenesis In Vivo

4.1 Introduction

By virtue of appealing features such as strong σ donors to allow formation of stable metal–carbon (M-C) bond(s), stable N-heterocyclic carbenes (NHCs) have demonstrated profound impact in diverse areas of chemistry [1–13]. Less developed but with burgeoning interests in recent years is the medicinal application of metal–NHC complexes in the treatment of cancer [1, 2, 4, 5, 14–20]. The side effects and/or lack of in vivo activity of a variety of reported anticancer metal complexes including the classical Pt(II)-based anticancer drugs can be related to their instability under physiological conditions [21]. NHC ligand(s) is capable of stabilizing metal ion against precipitation into metal aggregates as well as facile ligand exchange reactions under physiological conditions and meanwhile can serve to deliver bioactive metal ions to the cellular target(s) [14, 17–19]. Indeed, there are many recent reports showing that metal complexes containing NHC ligands display potent anticancer properties with proteins as cellular targets and are potential drug candidates for drug-resistant cancers with mechanisms of anticancer action different from that of cisplatin [14–20].

Gold(I) complexes are well-known to be anticancer active [22–35]. Mirabelli and coworkers first described the in vivo antitumor activities of the apparently thiol-unreactive 4-coordinated $[Au^{I}(dppe)_2]^+$ (dppe = 1,2-bis(diphenylphosphinyl) ethane) in several solid tumor models [36], but toxicity was identified in in vivo studies with large animals (rats and rabbits) [37, 38]. Recent studies by various groups revealed that the SH/SeH-containing thioredoxin reductase (TrxR) is one of

T. Zou, *Anti-Cancer N-Heterocyclic Carbene Complexes of Gold(III), Gold(I) and Platinum(II)*, Springer Theses, DOI 10.1007/978-981-10-0657-9_4

the critical cellular targets of Au^+ ion, and the latter is capable of blocking C-terminal redox active site, –Cys–Sec– (–C–U–), of TrxR via covalent binding interactions to form Au–S/Au–Se bond(s) [22, 24–35]. However, TrxR inhibition requires facile ligand exchange reaction with thiols (i.e., the more labile Au(I) complex tends to be more potent in TrxR inhibition), but the high thiol affinity/reactivity of gold(I) complexes may lead to off-target covalent binding interactions with serum thiols including albumin and blood glutathione (GSH), resulting in limited bioavailability to tumor tissue hence no in vivo activity [30, 33, 39, 40]. In recent years, despite a large number of gold(I) complexes (mostly the mononuclear ones) with demonstrated potent TrxR inhibition as well as antiproliferative properties known in the literature, examples of Au(I) complexes showing in vivo solid tumor inhibition are sparse [36, 41–43]. It is conceived that tuning/balancing the thiol reactivity to minimize off-target binding in blood, while maintaining enough reactivity to inhibit cellular thiol-containing proteins/enzymes (e.g., TrxR) is a guiding principle in the design of new anticancer gold(I) complexes.

Au(I)–Au(I) interaction can be used to stabilize Au(I) ion for medicinal application. In literature, a dinuclear gold(I) complex, $[Au_2(Ph_3P)_2(\mu\text{-DTE})]$ (DTE = 1,4-dimercaptobutane-2,3-diol), could increase life span of mice bearing Ehrlich ascites tumors though it has severe toxicity [44]; several dinuclear gold(I) complexes with bridging bidentate bis(NHC) ligands, $[Au_2(bis(NHC))_2]^{2+}$, are inert toward thiols and could serve as biological probes [45]. It was reported that replacing one NHC of mononuclear $[Au^I(NHC)_2]^+$ with phosphine ligand would lead to stronger TrxR inhibition though increase in serum protein bindings [46]. In this chapter, a novel binuclear gold(I) complex (**4.1**-PF_6, Fig. 4.1) containing mixed diphosphine and bis(NHC) bridging ligands is described. This complex shows favorable stability in the presence of blood concentration of serum thiols (i.e., BSA and GSH), potently inhibits TrxR activity through a tight-binding mode and effectively inhibits tumor growth in two independent animal models; meanwhile, to the best of knowledge, this is the first gold(I) complex that was observed to inhibit cancer stem cell (CSC) activity in vitro and to inhibit angiogenesis in tumor models.

4.2 Experimental Section

4.2.1 Materials and Instrumentation

All starting materials were used as received from commercial sources. [Au_2bis(NHC)Cl_2] [48] and complex **4.5** (Fig. 4.1) [49] were synthesized according to a reported procedure. All the solvents were of analytical grade. Fast atom bombardment (FAB) mass spectra were obtained on a Finnigan Mat 95 mass spectrometer.

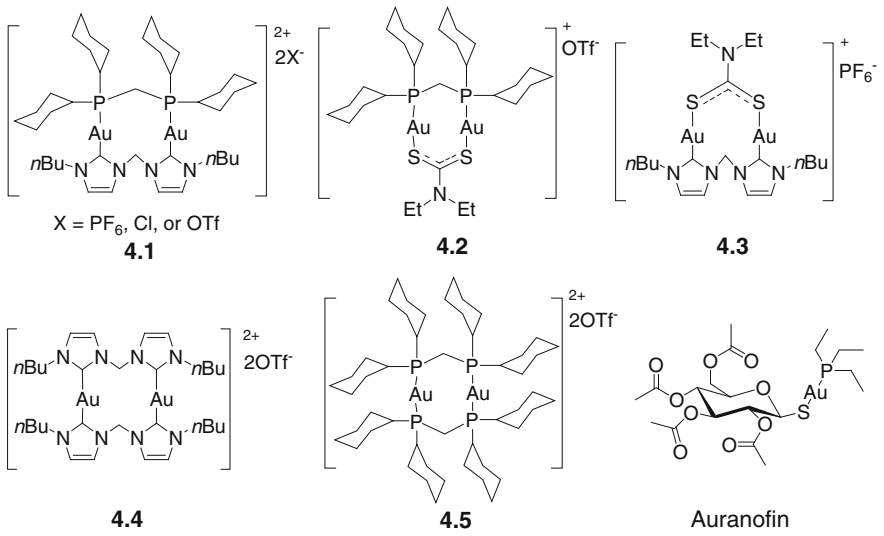

Fig. 4.1 Chemical structures of the dinuclear gold(I) complexes **4.1**–**4.5** and auranofin. Reproduced with permissions [47]. Copyright © 2014 WILEY-VCH Verlag GmbH & Co. KGaA, Weinheim

^{1}H NMR spectra were obtained on DPX 400 M Bruker FT-NMR spectrometers relative to the signal of tetramethylsilane. UV–Vis spectra were recorded on a Perkin-Elmer Lambda 19 UV/Vis spectrophotometer. Elemental analysis was performed by the Institute of Chemistry at the Chinese Academy of Sciences, Beijing. For MTT and protein assays, the absorbance was quantified using Perkin-Elmer Fusion Reader (Packard BioScience Company). Dynamic light scattering was recorded on Malvern ZetaSizer 3000HSA. TEM analysis was performed on FEI Tecnai G2 20 S-TWIN Scanning Transmission Electron Microscope. ESI-MS for stability test toward GSH was performed on Waters Micromass Q-Tof Premier quadrupole time-of-flight tandem mass spectrometer. High-resolution ESI-MS for interaction of **4.1**-PF_6 with GCUG peptide was performed on LTQ Orbitrap Velos mass spectrometer (Thermo Scientific).

4.2.2 Synthesis and Characterization of Complexes

4.2.2.1 Synthesis of Complexes

Synthesis of **4.1**

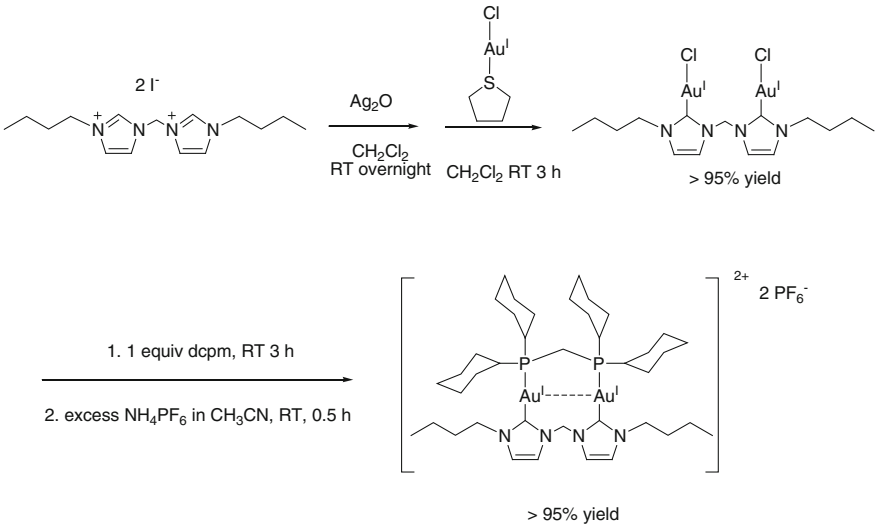

To a CH_2Cl_2 (10 mL) solution of [Au_2bis(NHC)Cl_2] (50 mg, 0.069 mmol) was added 28.2 mg of dcpm (0.069 mmol). After 2 h of stirring at room temperature, the mixture was evaporated to give **4.1**-Cl, or excess NH_4PF_6 (or LiOTf) solid was added and stirred for another 0.5 h. Then, the mixture was evaporated, and the solid was dissolved in water and extracted with CH_2Cl_2. After evaporating the organic layer and recrystallizing the solid, pure white solid **4.1**-PF_6 (or **4.1**-OTf) was obtained. Crystals of **4.1**-PF_6 were obtained by diffusing diethyl ether into a solution of the complex in CH_2Cl_2/EtOH (2:1 v/v). Yield > 95 %. **4.1**-Cl: ^{1}H NMR (400 MHz, $CDCl_3$, 298 K): δ = 9.03 (s, 2 H), 7.48 (d, 1 H, *J* = 13.3 Hz), 7.01 (s, 2 H), 6.90 (d, 1 H, *J* = 13.4 Hz), 4.25 (m, 2 H), 4.10 (m, 2 H), 3.52 (m, 1 H), 3.02 (m, 1 H), 2.52 (m, 4 H), 2.23–1.22 (m, 48 H), 0.97 (t, 6 H, *J* = 7.5 Hz). ^{31}P NMR (162 MHz, d_4-MeOH, 298 K): δ = 51.76 (s). MS-FAB(+): *m/z* 1098 $[M\text{-}Cl]^+$, 531 $[M\text{-}2Cl]^{2+}$. Anal calcd for $C_{40}H_{70}Au_2Cl_2N_4P_2{\cdot}3H_2O$: C, 40.45; H, 6.45; N, 4.72; found: C 40.30; H, 6.24; N, 4.88. **4.1**-OTf: ^{1}H NMR (400 MHz, d_6-DMSO, 298 K): δ = 7.98 (s, 2 H), 7.70 (s, 2 H), 6.55 (d, 1 H, *J* = 14.3 Hz), 6.35 (d, 1 H, *J* = 14.7 Hz), 4.15 (m, 4 H), 2.88 (m, 2 H), 2.45 (m, 2 H), 2.01-1.24 (m, 50 H), 0.88 (t, 6 H, *J* = 7.3 H). ^{31}P NMR (162 MHz, d_6-DMSO, 298 K): δ = 52.49 (s). ^{19}F NMR (377 MHz, d_6-DMSO, 298 K): δ = −77.7. MS-FAB(+): *m/z* 1211 $[M\text{-}OTf]^+$, 531 $[M\text{-}2OTf]^{2+}$. Anal calcd for $C_{42}H_{70}Au_2F_6N_4O_6P_2S_2$: C, 37.06; H, 5.18; N, 4.12; found: C, 37.01; H, 5.25; N, 4.06; **4.1**-PF_6: ^{1}H NMR (400 MHz, d_4-MeOH, 298 K): δ = 7.78 (d, 2 H, *J* = 1.6 Hz), 7.49 (d, 2 H, *J* = 1.5 Hz), 7.06 (d, 1 H, *J* = 14.3 Hz), 6.23 (d, 1 H, *J* = 14.3 Hz), 4.25 (m, 4 H), 1.36–2.69 (m, 54 H), 0.97 (t, 6 H, *J* = 7.4 H). ^{31}P NMR (162 MHz, d_4-MeOH, 298 K): δ = 50.12 (s). ^{19}F NMR (377 MHz, d_4-MeOH, 298 K): δ = −75.5 (d, *J* = 775.2 Hz). MS-FAB(+): *m/z* 1207 $[M\text{-}PF_6]^+$, 531 $[M\text{-}2PF_6]^{2+}$. Anal calcd for $C_{40}H_{70}Au_2F_{12}N_4P_4$: C, 35.51; H, 5.22; N, 4.14; found: C, 35.21; H, 5.23; N, 4.19.

Synthesis of **4.2** (Fig. 4.1)

The synthesis is similar to a reported procedure [50]. To an acetone (10 mL) solution of $Au_2(dcpm)Cl_2$ (50 mg, 0.057 mmol) was added 19.4 mg of sodium diethylcarbamodithioate ($Et_2NCS_2Na\ 3H_2O$, 0.086 mmol, 1.5 equiv). After stirring at room temperature overnight, the mixture was evaporated and washed with water. Then, the solid was redissolved in CH_3CN, followed by the addition of excess of lithium trifluoromethanesulfonate (LiOTf) and stirred for another 0.5 h at room temperature. Then, the solution was evaporated and extracted with CH_2Cl_2 and recrystallized with CH_2Cl_2/Et_2O. White yellow solid was obtained. Yield: 60 %. ^{1}H NMR (400 MHz, $CDCl_3$, 298 K): δ = 3.94 (q, 4 H, *J* = 1.6 Hz), 2.61 (t, 2 H, *J* = 10.9 Hz), 2.26 (m, 4 H), 2.02 (m, 8 H), 1.90 (m, 8 H), 1.74 (m, 4 H), 1.52-1.20 (m, 26 H). MS-FAB(+): *m/z* 950 $[M\text{-}OTf]^+$. Anal calcd for $C_{31}H_{56}Au_2F_3NO_3P_2S_3$: C, 33.85; H, 5.13; N, 1.27; found: C, 33.69; H, 5.24; N, 1.37.

Synthesis of **4.3** (Fig. 4.1)

Complex **4.3** was synthesized by a procedure similar to that for **4.1**-PF_6 except that dcpm was replaced by NaDEDT. Yield: 85 %. ^{1}H NMR (400 MHz, $CDCl_3$, 298 K): δ = 7.86 (d, 2 H, *J* = 2.0 Hz), 7.02 (d, 2 H, *J* = 2.0 Hz), 6.85 (d, 1 H, *J* = 14.1 Hz), 6.22 (d, 1 H, *J* = 14.1 Hz), 4.23 (m, 2 H), 4.10 (m, 2 H), 3.99 (m, 4 H), 1.83 (m, 4 H), 1.44 (m, 6 H), 1.37 (m, 4 H), 0.97 (t, 6 H, *J* = 7.3 Hz). MS-FAB(+): *m/z* 802 $[M\text{-}PF_6]^+$. Anal calcd for $C_{20}H_{34}Au_2F_6N_5PS_2$: C, 25.35; H, 3.62; N, 7.39; found: C, 25.22; H 3.82; N, 7.41.

Synthesis of **4.4** (Fig. 4.1)

The procedure is similar to a reported one [51]. ^{1}H NMR (400 MHz, d_6-DMSO, 298 K): 7.85 (s, 4 H), 7.68 (d, 4 H, *J* = 1.1 Hz), 7.14 (d, 2 H, *J* = 13.7 Hz), 6.32 (d, 2 H, *J* = 13.9 Hz), 4.18 (m, 8 H, 1.74 (m, 8 H), 1.20 (m, 8 H), 0.82 (t, 12 H, *J* = 7.3 Hz). ^{19}F NMR (377 MHz, d_6-DMSO, 298 K): δ = −77.7. MS-FAB(+): *m/z* 457.1 $[M\text{-}2OTf]^{2+}$. Anal calcd for $C_{32}H_{48}Au_2F_6N_8O_6S_2 \cdot H_2O$: C, 31.23; H, 4.09; N, 9.10; found: C, 31.31; H, 4.00; N, 9.18.

4.2.2.2 X-ray Crystallographic Analysis

Program(s) used to solve structure: SHELXS97; program(s) used to refine structure: SHELXL97 [52]. A white crystal of dimensions 0.06 × 0.02 × 0.02 mm inside a glass capillary was used for data collection at 296 K on a MAR diffractometer with a 300-mm image plate detector using graphite monochromatized Mo-Kα radiation (λ = 0.71073 Å). An approximate (isotropic) treatment of cell esds is used for estimating esds involving LS planes. Refinement of F^2 is performed against all reflections. The weighted R-factor wR and goodness-of-fit S are based on F^2; conventional R-factors R are based on F, with F set to zero for negative F^2. The threshold expression of $F^2 > 2\text{sigma}(F^2)$ is used only for calculating R-factors(gt),

etc., and is not relevant to the choice of reflections for refinement. R-factors based on F are statistically about twice as large as those based on F, and R- factors based on all data will be even larger.

4.2.3 Biological Application

4.2.3.1 Characterization of Reaction with Thiols

ESI-MS (Q-TOF) Experiment of Reaction of **4.1**-PF_6 with GSH

Preliminary analysis: Complex **4.1**-PF_6 (0.3 mM in MeOH, solution A) and GSH (1 mM in H_2O containing 5 mM NH_4HCO_3, solution B) were freshly prepared. Then, 250 µL of solution A + 250 µL of H_2O (containing 5 mM NH_4HCO_3), or 250 µL of solution B + 250 µL of MeOH was measured by ESI-MS. Afterward, 250 µL of solution A + 250 µL of solution B was measured at 0 and 1 h.

Linear response of intensity with concentration: MS intensity of different concentrations of **4.1**-PF_6 or auranofin in MeOH/H_2O (1:1 v/v, with 5 mM NH_4HCO_3) was measured at *m/z* 531.2 or 679.1, respectively, to find the linear intensity–concentration response.

*MS intensity changes of reaction of **4.1**-PF_6 with GSH*: 3×10^{-6} M of **4.1**-PF_6 or auranofin with 1.5×10^{-5} M or 5×10^{-5} M of GSH in MeOH/H_2O (1:1 v/v, with 5 mM NH_4HCO_3) was freshly mixed and the intensity of **4.1**-PF_6 or auranofin was measured every 1 s for 45 min.

Data analysis: For each time point, 10 scans of MS intensity were combined. Unreacted compound percentage was calculated by dividing each 10 scans by predetermined MS intensity (10 scans) at proper *m/z* of initial concentration.

Interaction with Bovine Serum Albumin

The binding with bovine serum albumin (BSA) was determined by a modified procedure [46]. In general, a 280 mg amount of BSA was dissolved in 7 mL of minimal essential medium. Complex **4.1–4.5** or auranofin was added to the BSA-containing medium with final concentration of 3 µM and was shaken at 50 rpm. After 1 and 5 h, 100 µL of the solution was taken, treated with 500 µL of cold (−20 °C) acetone, and stored at −20 °C for 30 min to allow precipitation of the protein fraction. Afterward, the solution was centrifuged at 13,500 rpm for 1 min at 4 °C, and the supernatant was taken and the left protein was treated with 500 µL of 60 % HNO_3 **(*)** at 60–70 °C for 2 h and at room temperature for 12 h. The final volume was adjusted to 10 mL for inductively coupled plasma mass spectrometry (ICP-MS) analysis. The total gold content was measured by the digested solutions of gold and BSA mixture without precipitation. The percentage of bound gold was

determined by the gold contents in precipitated proteins divided by the total gold contents, and the unbound gold was calculated from the bound gold content.

(*) Caution: concentrated HNO_3 is highly reactive with acetone, causing explosion. The acetone should be evaporated before adding HNO_3, and the digestion needs to be handled carefully!

ESI-MS (LTQ Orbitrap) Experiment of Reaction of **4.1**-PF_6 with Tetrapeptide GCUG

1 mM of **4.1-PF_6** in MeOH was mixed with equal volume of 1 mM tetrapeptide GCUG in H_2O (containing 10 mM NH_4HCO_3) and was analyzed at different time points.

^{1}H NMR Experiment of Reaction of **4.1**-PF_6 with GCUG

^{1}H NMR measurement for the reaction between **4.1**-PF_6 with GCUG peptide was performed on a Bruker 400 MHz spectrometer. Briefly, solution A (GCUG, 2 mM, 300 μL, in D_2O, phosphate buffer, pH* 7.4) was mixed with solution B (**4.1**-PF_6, 2 mM, 300 μL, in d_6-DMSO); or solution A was mixed with 300 μL d_6-DMSO; or solution B was mixed with 300 μL D_2O (phosphate buffer, pH* 7.4). Then, the spectra of the obtained mixture were recorded at 25 °C after 24 h.

4.2.3.2 Anticancer Properties

Cell Lines and Growth Inhibitory Assay

Human nasopharyngeal carcinoma cells (SUNE1) were generously provided by Prof. S.W. Tsao (Department of Anatomy, The University of Hong Kong). Other cancer cell lines were obtained from American Type Culture Collection (MD, USA). The cell lines were maintained in cell culture media (minimum essential medium for MCF-7 and HeLa; Dulbecco's Modified Eagle's Medium for B16-F10, RPMI-1640 medium for SUNE1 and H1975) supplemented with 10 % fetal bovine serum, 100 U/mL penicillin, and 100 μg/mL streptomycin at 37 °C humidified atmosphere with 5 % CO_2. Cell growth inhibitory effects of all the complexes were determined by MTT cytotoxicity assay. Briefly, drug-treated cells were incubated with MTT for 4 h at 37 °C in a humidified atmosphere of 5 % CO_2 and were subsequently lysed in solubilizing solution. Cells were then maintained in a dark, humidified chamber overnight. The formation of formazan was measured by using a microtitre plate reader at 590 nm. Growth inhibition by a drug was evaluated by IC_{50} (concentration of a drug causing 50 % inhibition of cell growth). Each growth inhibition experiment was repeated at least three times.

Inhibition of Purified Thioredoxin Reductase (TrxR)

Determination of inhibitory constant (K_i') derived from residual activities of pre-formed enzyme–inhibitor complexes. Recombinant rat TrxR1 (ICMO Corp, Sweden; 2 nM) was reduced with NADPH (0.2 mM) and then incubated with **4.1**-PF_6 (20–600 nM) for 2 h in a 50 mM phosphate buffer, pH 7.2, and 1 mM EDTA. The residual activities (slope) were measured using 3 mM DTNB (Fig. 4.9). The data were fit into Eq. 4.1:

$$v_i/v_o = \left([E_t] - K_i - [I] + \left(([I] + K_i - [E_t])^2 + (4K_i[E_t])\right)^{0.5}\right)/(2[E_t]) \quad (4.1)$$

wherein v_i, v_0 are the steady-state velocity (slope) with and without **4.1**-PF_6, respectively. $[E_t]$ is the total enzyme concentration, and $[I]$ is the inhibitor concentration.

Determination of K_i by progress curve analysis. Complex **4.1**-PF_6 (20 μM) was serially diluted to 0.3125 μM in 100 μL of 50 mM phosphate buffer, pH 7.4 (containing 1 mM EDTA, 0.2 mM NADPH, 2 nM TrxR1, and 3 mM DTNB). The progress curves were each fit into Eq. 4.2:

$$P = v_t t + ((v_0 - v_t)/k_{app})(1 - e^{(-k_{app}t)}) \quad (4.2)$$

where P is the product concentration (absorbance at 412 nm), and v_0 and v_t are the initial and final steady-state velocities, respectively. The k_{app} obtained from fitting results is the apparent first-order rate constant for establishment of the final steady-state inhibition. A plot of the obtained k_{app} against the inhibitor concentrations followed slow onset which is not linear, indicative of a two-step, tight-binding inhibition mechanism:

$$\overbrace{\underbrace{E + I \underset{k_2}{\overset{k_1}{\rightleftharpoons}} EI}_{K_i} \underset{k_4}{\overset{k_3}{\rightleftharpoons}} EI^*}^{K_i^*}$$

k_3 is the forward isomerization rate, and k_4 is the reverse isomerization rate. The k_3, k_4, and the dissociation constant (K_i) of the initial collision complex EI were obtained by fitting the data to Eq. 4.3:

$$k_{app} = k_4 + k_3[I]/([I] + K_i(1 + S/K_m)) \quad (4.3)$$

where $[I]$ is the inhibitor concentration, S is the substrate (DTNB) concentration, and K_m is the Michaelis–Menten constant for reduction of DTNB by TrxR.

Inhibition of Purified Glutathione Reductase (GR)

Glutathione reductase (Sigma-Aldrich; 0.01 U) was reduced with NADPH (0.2 mM) and then incubated with **4.1**-PF_6 (0.3125-20 μM, series dilution) for 2 h in a 50 mM phosphate buffer, pH 7.2 and 1 mM EDTA. Then, GSSG (1 mM) and DTNB (3 mM) were added to initiate the reaction. The GR activities were determined as increases in $O.D_{0.412\ nm}$ for 10 min.

TrxR Inhibition on Trx System

Recombinant rat TrxR1 (ICMO Corp, Sweden; 20 nM) was reduced with NADPH (0.2 mM) and then incubated with **4.1**-PF_6 (0–20 μM) for 2 h in a 50 mM phosphate buffer, pH 7.2 and 1 mM EDTA. Then 2 μM of Trx and 160 μM of insulin were added to the solution, and the OD_{340nm} was followed. TrxR activity was calculated by the initial OD_{340nm} increase rate.

Sphere Formation Assay [53]

HeLa or U-87 MG/SKOV-3 cells (3×10^3) in 0.5 mL DMEM/F12 (containing 20 ng/ml EGF, 20 ng/ml bFGF and 1 × B-27 Supplement) with or without **4.1**-PF_6 were seeded in a 24-well Ultra Low Cluster Plate (Costar). The cells were incubated at 37 °C for 3 days (HeLa) or 6 days (U-87). Then, photographs of spheres were taken under an inverted microscope at 50× magnification. The occupied areas of the spheres in the photographs were measured using ImageJ [54]. The experiments were repeated at least 3 times.

In Vivo Tumor Growth Inhibition Experiments

Female BALB/cAnN-nu (Nude) and female C57BL/6N mice, 5–7 weeks old, were purchased from the Charles River Laboratories (Wilmington, MA) and cared for according to the guidelines of the Laboratory Animal Unit of the University of Hong Kong (HKU). All animal experiments were conducted under the guidelines approved by the Committee on the Use of Live Animals in Teaching and Research of HKU. To establish the HeLa xenograft model, 4×10^6 HeLa cells suspended in 100 μL of PBS were inoculated into the back flanks of female BALB/cAnN-nu (Nude) mice by subcutaneous injection. When the tumor volumes reached about 50 mm^3 (3–4 days after tumor inoculation), the mice were randomly divided into different treatment groups (0.6–15 mg/kg of **4.1**-PF_6**, 4.1**-Cl, **4.1**-OTf, **4.2**, **4.3**, **4.5**; or solvent control). All the complexes were reconstituted in PET diluent (60 % polyethylene glycol 400, 30 % ethanol, 10 % Tween 80). The complexes dissolved

in PET diluent and then diluted in PBS or PBS supplemented with equal amount of PET injected into the mice by intraperitoneal injection once every 2–3 days (**4.1**-PF_6**, 4.2**, **4.3**, **4.5**) or everyday (**4.1**-Cl, **4.1**-OTf) until the mice were killed. To establish the mouse melanoma model, 4×10^5 B16-F10 melanoma cells were inoculated into the right back flanks of female C57BL/6N mice by subcutaneous injection. Five days after tumor inoculation, the mice were randomly divided into different treatment groups (solvent control or 15 mg/kg of **4.1**-PF_6). Solvent control or 15 mg/kg of **4.1**-PF_6 dissolved in PET diluent and then diluted in PBS was injected into the mice by intraperitoneal injection once every 2–3 days until the mice were sacrificed. In both models, the volume of PET diluent injected into each mouse was ≤6 μL. Tumor sizes were measured once every 2–3 days, and tumor volume (V) was calculated by the formula $V = ab^2 \times 0.52$, where a and b were the longest and the shortest diameters of the xenografted tumor. The tumor inhibition was calculated according to the following formula:

$$\text{Inhibition percentage} = \left(1 - \frac{V - V_0}{V' - V_0'}\right) \times 100C\%$$

where V and V' are the tumor volumes of **4.1**-PF_6 treatment and solvent control, respectively. V_0 and V_0' are the initial tumor volumes of the **4.1**-PF_6 treatment and solvent control, respectively.

In Vivo Toxicology Studies

The safety pharmacological studies were performed in a State Food and Drug Administration (China)-approved laboratory (Tianjin Institute of Pharmaceutical Research). The acute toxicity was firstly tested by using Chinese Kun Ming (KM) mice (10 female and 10 male) through intravenous (i.v.) injection. Single dose of **4.1**-PF_6 (0.8 mg/kg) treatment resulted in some adverse symptom such as cyanosis and hypokinesis. One male mouse died 40 min after injection. The remaining mice recovered from the adverse symptom after 1 h. The female mice showed less adverse reaction than male mice. No other mouse death was found during the following 14 days of recovery period, and no abnormal changes were found after gross anatomy. This result indicates the minimal lethal dosage of **4.1**-PF_6 upon i.v. injection is 0.8 mg/kg and female mice showed better tolerance than male mice. The treatment dosage on larger animals was based on the results of i.v. acute toxicity studies. Hartley guinea pigs were used to test all system anaphylaxis. Guinea pigs were randomly divided into 4 groups (each group contains 3 male and 3 female ones) and were treated with 0.9 % saline injection (negative control), 10 % PET solvent, 1 % ovalbumin in saline (positive control) and 0.12 mg/kg of **4.1**-PF_6 in PET solvent, respectively, through i.p. injection every other day for 5 times; after 14 days, forelimbs of guinea pigs were injected intravenously (i.v.) with twofold

dosage to see anaphylaxis reaction. Rabbits (n = 4) were used to test blood vessel irritation. Complex **4.1**-PF_6 (0.12 mg) and saline were directly injected into the left and right auricular veins, respectively, for comparison; each two rabbits were sacrificed for histopathology after 4 and 14 days of treatment.

Determination of Blood Vessel Density in the Tumor Tissues

Blood vessel density was determined by immunohistochemical detection of CD31 (cluster of differentiation 31, a platelet endothelial cell adhesion molecule) in the tumor tissues of HeLa xenograft-bearing mice in different treatment groups. Antibody against CD31 was purchased from Novus Biologicals (Littleton, CO). Xenografted tumors were fixed in 4 % paraformaldehyde for 16 h. The fixed tissues were embedded in paraffin and sectioned into slices of 5 μm thick. The tissue sections were then dewaxed and rehydrated, before they were gone through the antigen retrieval processes. The tissue sections were blocked and then incubated with anti-CD31 antibody for 1 h, washed with PBS, and further incubated with horse radish peroxidase-conjugated secondary antibody for 30 min. The sections were finally counterstained with hematoxylin, mounted under glass coverslips, and observed under an inverted microscope at 200× magnification. Ten microscopic fields were randomly chosen and the number of microvessels per field was counted. Data were calculated as mean ± SEM of 4–6 mice per treatment group.

Tube Formation Assay

The tube formation assay was conducted using a modified In Vitro Angiogenesis Kit (Cayman Chemical). 10× Diluent Buffer and ECMatrix solution were mixed in a ratio of 1:9. The mixture (50 μL) was transferred to each well of a 96-well plate and incubated at 37 °C for 1 h to allow for polymerization. MS1 cells (50,000) premixed with different concentrations of **4.1**-PF_6 in 100 μL of DMEM medium (containing 5 % FBS) were then added to the top of the polymerized matrix. After incubation at 37 °C for 2 h, tube formation in each case was examined under an inverted microscopy at a 50× magnification. The cell viability at these conditions was determined by MTT assay: MS1 cells (50000) premixed with different concentrations of **4.1**-PF_6 in 100 μL of DMEM (containing 5 % FBS) were added to a 96-well plate. After incubation at 37 °C for 2 h, the medium was extracted and fresh medium with 10 % MTT (v/v, 5 mg/mL in PBS) was added to each well and the cells were further incubated for 3 h and were lysed with SDS (sodium dodecyl sulfate, 0.5 g/mL, with 0.01 mol/L HCl). Cells were then maintained in a dark, humidified chamber overnight. The formation of formazan was measured by using a microtitre plate reader at 580 nm. Each growth inhibition experiment was repeated at least three times, and results were expressed as means ± standard deviation (SD).

4.3 Results and Discussion

4.3.1 Synthesis and Characterization

The binuclear gold(I)-diphosphine/bis(NHC) complex (**4.1**) was synthesized by the reaction of $[Au_2bis(NHC)Cl_2]$ with dcpm [dcpm = bis(dicyclohexylphosphine) methane] to give **4.1**-Cl, which underwent metathesis reaction with NH_4PF_6 or LiOTf to afford **4.1**-PF_6 and **4.1**-OTf. The synthesis of **4.1**-PF_6 has an overall yield of >90 % without heating or using moisture/air-sensitive technique during reaction. Complexes **4.2**–**4.5** (Fig. 4.1) were synthesized and auranofin was used for comparative study. The crystal structure of **4.1**-PF_6 obtained by diffusing diethyl ether into a solution of the complex in $EtOH/CH_2Cl_2$ (1:2, v/v) (Fig. 4.2; Table 4.1) shows that the Au(I)–Au(I) distance is 3.083 Å, which is slightly longer than that of **4.5** (2.926–3.013 Å) [49] but 0.46 Å shorter than that of the analogue of complex **4.4** $[Au_2(NHC–C_1–NHC)_2]^{2+}$ (3.5425 Å) [51].

4.3.2 Stability Toward Blood Thiols and In Vitro Cytotoxicity

The stability of **4.1**–**4.5** and auranofin toward bovine serum albumin (BSA) was examined by analysis of the unbound (non-covalent) gold content in the supernatant obtained from acetone precipitation of the albumin using inductively coupled plasma mass spectrometry (ICP-MS). For **4.4**, more than 90 % of gold was left unbound after incubation of **4.4** with BSA for 5 h. Complexes **4.2**, **4.3**, **4.5,** and auranofin all resulted in <30 % of unbound gold. Complex **4.1**-PF_6 showed stability with >70 % free gold content at the same incubation condition (Fig. 4.3).

Electrospray ionization quadrupole time-of-flight mass spectrometry (ESI-QTOF-MS) was applied to investigate the reaction of **4.1**-PF_6 with GSH. Mixtures of 3×10^{-6} M of **4.1**-PF_6 or auranofin (both had a linear response of MS

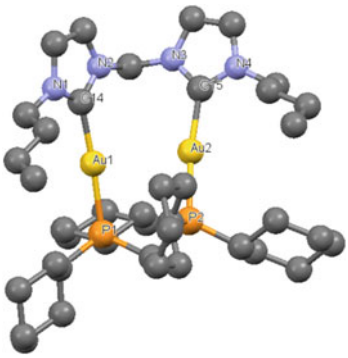

Fig. 4.2 Crystal structure of **4.1**-PF_6. The hydrogen atoms and the counteranion PF_6^- are omitted for clarity. Reproduced with permissions [47]. Copyright © 2014 WILEY-VCH Verlag GmbH & Co. KGaA, Weinheim

Table 4.1 Crystal data and structure refinement for **4.1**-PF_6

Empirical formula	$C_{40}H_{70}Au_2N_4P_2 \cdot 2(F_6P) \cdot C_2H_6O$
Formula weight	1398.88
Temperature (K)	566(2)
Crystal system	Monoclinic
Space group	$P2_1/c$
a (Å)	12.9700(9)
b (Å)	19.8499(13)
c (Å)	21.9703(14)
α (°)	90.00
β (°)	99.991(2)
γ (°)	90.00
Volume (Å^3)	5570.5(6)
Z	4
ρ_{calc} (mg/mm^3)	1.668
m (mm^{-1})	11.497
F(000)	2760.0
Crystal size (mm^3)	0.06 × 0.02 × 0.02
2θ range for data collection	6.04–131.72°
Index ranges	−15 ≤ h ≤ 14 −22 ≤ k ≤ 23 −21 ≤ l ≤ 25
Reflections collected	56,706
Independent reflections	9449[R(int) = 0.0682]
Data/restraints/parameters	9449/74/603
Goodness of fit on F^2	1.080
Final R indexes [I ≥ 2σ (I)]	R_1 = 0.0742, wR_2 = 0.1941
Final R indexes [all data]	R_1 = 0.0835, wR_2 = 0.2047
Largest diff. peak/hole (e Å^{-3})	2.60/−1.37

Reproduced with permissions [47]. Copyright © 2014 WILEY-VCH Verlag GmbH & Co. KGaA, Weinheim

intensity versus concentrations, Fig. 4.4) with fivefold excess of GSH (1.5×10^{-5} M) at pH 8.0, were freshly prepared, and the ion intensities of the two gold complexes were recorded (Fig. 4.5). After mixing with GSH, there was a rapid decrease in the ion intensity of auranofin (*m/z* 679.1) with 20 % remaining after 45 min. Furthermore, an intermediate with *m/z* value consistent with glutathione–gold–phosphine adduct GS–Au–PEt_3 (*m/z* 622.1) appeared initially and gradually decreased (Fig. 4.6). On the contrary, no significant change of the ion intensity of **4.1**$^{2+}$ (*m/z* 531.2) was found during the first 45-min incubation with GSH (Fig. 4.5), indicating that **4.1**-PF_6 was not reactive toward GSH at this concentration. When a higher concentration of GSH (5×10^{-5} M) was used, the ion intensity of auranofin decreased with a faster rate, while that of **4.1**$^{2+}$ was retained at approximate initial

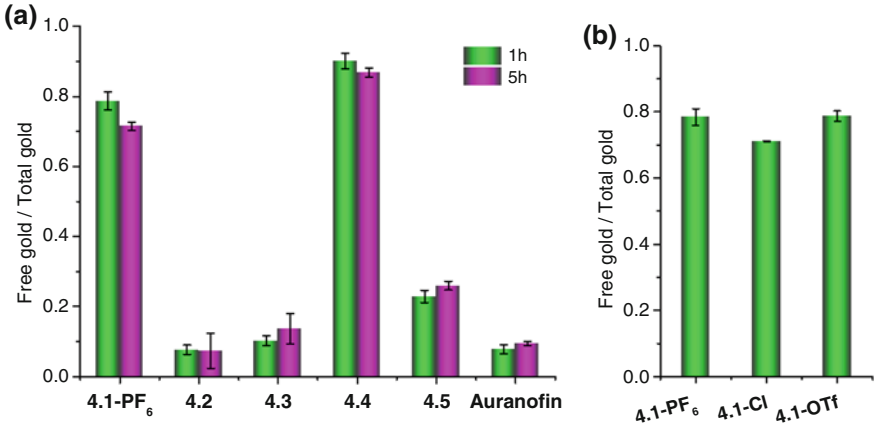

Fig. 4.3 **a** Unbound gold content (%) after incubation of different gold(I) complexes with bovine serum albumin (BSA) for 1 and 5 h based on ICP-MS analysis. **b** Free gold content after incubation of complexes with BSA for 1 h. Reproduced with permissions [47]. Copyright © 2014 WILEY-VCH Verlag GmbH & Co. KGaA, Weinheim

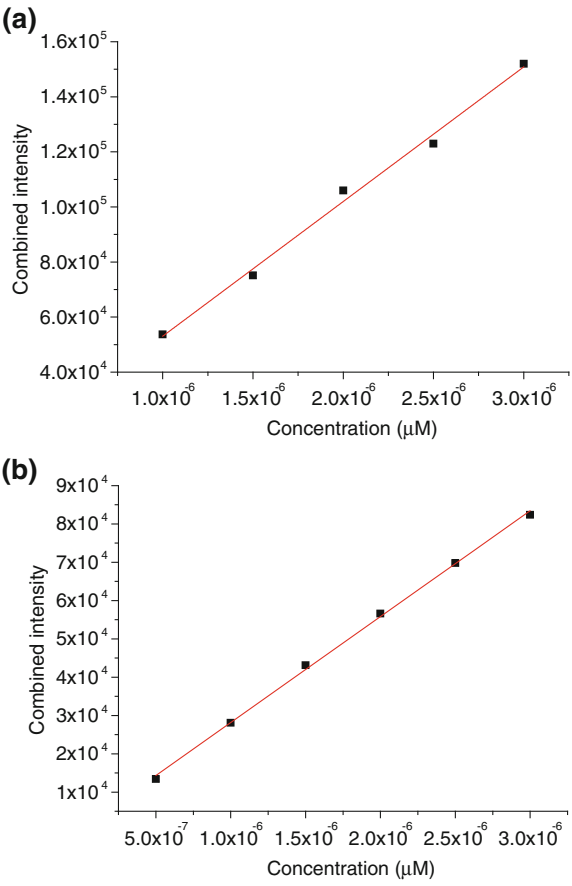

Fig. 4.4 MS ion intensity (combined 60 scans) of **a** **4.1**-PF_6 (m/z = 631.2) and **b** auranofin (m/z = 679.1) at different concentrations. Reproduced with permissions [47]. Copyright © 2014 WILEY-VCH Verlag GmbH & Co. KGaA, Weinheim

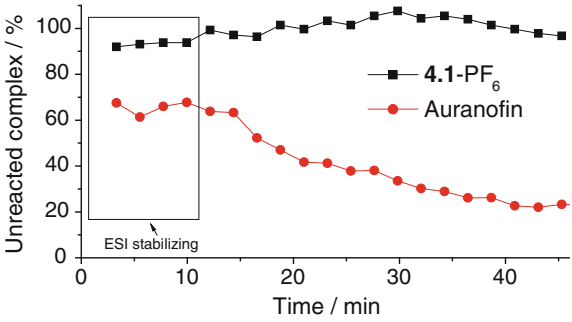

Fig. 4.5 Reaction of **4.1**-PF_6 (*black*) and auranofin (*red*) with GSH as determined by ESI-QTOF-MS. The amount of residual gold(I) complex was determined as percentage of initial ion intensity before GSH addition. Reproduced with permissions [47]. Copyright © 2014 WILEY-VCH Verlag GmbH & Co. KGaA, Weinheim. Reproduced with permissions [47]. Copyright © 2014 WILEY-VCH Verlag GmbH & Co. KGaA, Weinheim

level (Fig. 4.7). As GSH (1–10 μM) and serum albumin (35–50 mg/mL) are the major thiol-containing compounds present in blood [55], the binuclear gold(I) complex **4.1**-PF_6 appears to show favorable stability toward blood thiols.

The interaction of **4.1**-PF_6 with GSH was further studied by ESI-QTOF-MS analysis upon further increasing the concentrations of **4.1**-PF_6 and GSH. When 1.5×10^{-4} M of **4.1**-PF_6 was incubated with excess GSH (5×10^{-4} M) for 1 h, small but distinct peaks of *m*/*z* at 764.3 ($z = +1$), 684.8 ($z = +2$), and 605.3 ($z = +2$) appeared, which are attributed to $[Au(NHC\text{-}Im)(GS)]^+$, $[Au_2(dcpm)(NHC\text{-}Im)(GS)]^{2+}$ (Im = imidazolium), and $[Au_2(dcpm)_2]^{2+}$, respectively (Fig. 4.8).

The effects of serum albumin on the cytotoxicity of the gold(I) complexes were then tested. After preincubation of these complexes in minimal essential medium (MEM) with/without BSA (40 mg/mL) for 1 h, and then adding the medium containing different complexes into HeLa cells for further 24-h incubation, the cell viability was determined by means of MTT assay. As shown in Table 4.2, BSA can significantly suppress the cytotoxicity of the gold(I) complexes. The cytotoxicity of **4.1**-PF_6 was less affected compared to the other more thiol-reactive **4.2**, **4.3**, **4.5,** and auranofin. The thiol–inert complex **4.4** is less cytotoxic in both serum-containing and serum-free medium. Although **4.4** is inert toward thiols, serum albumin has a big impact on its cytotoxicity; the presence of BSA rendered **4.4** to be almost non-toxic ($IC_{50} > 300$ μM).

Complex **4.1**-PF_6 is also cytotoxic toward breast adenocarcinoma (MCF-7), nasopharyngeal carcinoma (SUNE1), lung adenocarcinoma (H1975), and mouse melanoma (B16-F10) with IC_{50} ranging from 1.3 ± 0.2 to 3.2 ± 1.0 μM; these IC_{50} values are up to 13.5-fold more cytotoxic than that of cisplatin (Table 4.3). Complexes **4.1**-Cl and **4.1**-OTf showed cytotoxicity similar to that of **4.1**-PF_6 in the in vitro cytotoxicity studies.

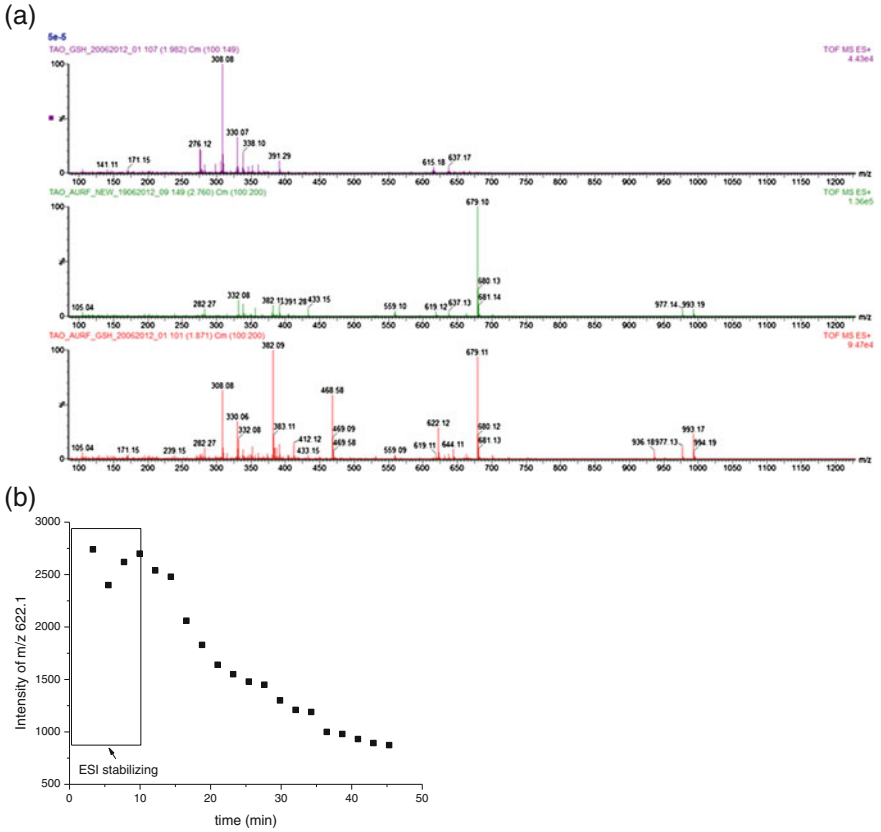

Fig. 4.6 **a** ESI-QTOF-MS spectra of GSH (*up*), auranofin (*middle*), and auranofin with GSH after mixing for 2 min (*down*). **b** MS ion intensity (combined 10 scans) of *m/z* 622.1 at different time point. Reproduced with permissions [47]. Copyright © 2014 WILEY-VCH Verlag GmbH & Co. KGaA, Weinheim

4.3.3 Inhibition of Thioredoxin Reductase

Since **4.1**-PF_6 is also thiol-reactive, the inhibition of purified TrxR activity by **4.1**-PF_6 was studied. After treating 2 nM of recombinant rat TrxR1 with 200 nM of **4.1**-PF_6 in the presence of NADPH, it showed a time-dependent decrease of TrxR activity by over 90 % in 2 h (Fig. 4.9). It is noteworthy that complex **4.1**-PF_6 inhibited TrxR more potently than the structurally related glutathione reductase (GR), with IC_{50} values of 38 nM and 10 μM, respectively, by using DTNB as the substrate (Figs. 4.10 and 4.11), which indicates the selectivity of selenol inhibition.

The TrxR inhibition was further examined by progressive curve analysis [43, 56, 57] of the time course of TrxR inhibition. As shown in Fig. 4.12a, the progress curves are nonlinear, indicating a two-phase equilibrium which is typical

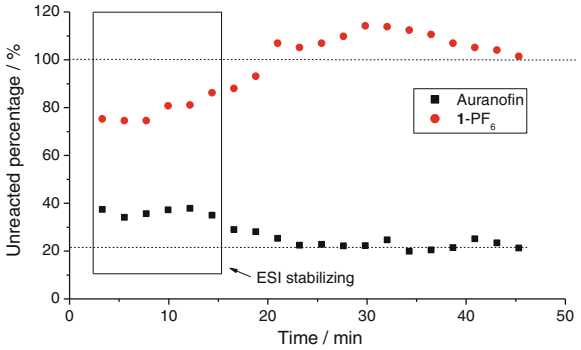

Fig. 4.7 Kinetics study of the reaction of **4.1**-PF_6 (3×10^{-6} M) and auranofin (5×10^{-5} M) with GSH by ESI-QTOF-MS analysis. Unreacted compound percentage was calculated by combined MS intensity of each 10 scans at different time point divided by initial MS intensity before GSH addition. Reproduced with permissions [47]. Copyright © 2014 WILEY-VCH Verlag GmbH & Co. KGaA, Weinheim

slow-onset tight-binding mode inhibition. Plotting the observed first-order rate constants, k_{app}, against the concentration of **4.1**-PF_6 resulted in a hyperbolic function curve (Fig. 4.12b), suggestive of a two-step binding mechanism, where the initial collision complex (denote as EI) is rapidly formed followed by a subsequent isomerization that enhances the tightness of enzyme-inhibitor complex (denote as EI*, Fig. 4.12 inset). Fitting the time course gave the values of $k_3 = 0.0260\ s^{-1}$, $k_4 = 0.0020\ s^{-1}$, $K_i = 413$ nM, $K_i^* = 28.5$ nM. Interestingly, in the presence of 2 mM GSH, the inhibitory activities on NADPH–TrxR–Trx–insulin system by **4.1**-PF_6 was found to be not attenuated but rather moderately enhanced with IC_{50} decreased from 5.56 to 3.29 μM, but the inhibition by auranofin under the same conditions was decreased (Fig. 4.13). We reasoned that GSH could assist to break the dinuclear structure of **4.1**-PF_6, thus leading to more facile ligand exchange reactions to block TrxR C-terminal, while the presence of GSH could also competitively bind gold as in the case of auranofin, thus decreasing the inhibition effect.

Several peptides that contain selenol group have been applied to mimic the binding interaction/mode of gold(I) with the active site of TrxR [33, 58, 59]. In this work, the C-terminal Gly-Cys-Sec-Gly, GCUG motif was directly used as the model. Incubating **4.1**-PF_6 (0.5 mM) with GCUG (0.5 mM) in 5 mM aqueous NH_4HCO_3 solution containing 50 % methanol (v/v) for 1, 4, or 24 h resulted in all cases a new peak at *m/z* 1187.2500 (Fig. 4.14a), which matches GCUG peptide bound with a Au_2dcpm^{2+} (*m/z* calculated: 1187.2488, error: 1.0 ppm) (Fig. 4.14b), and the isotopic pattern of this peak matches the simulated pattern. Meanwhile, the ^1H NMR signals at 6.0–8.0 ppm showed clearly the release of bis(NHC) ligand (Fig. 4.15b) and the ^1H signals of β-CH_2 of Cys and Sec were also significantly shifted, further indicating binding of S and Se with Au. Notably, auranofin was

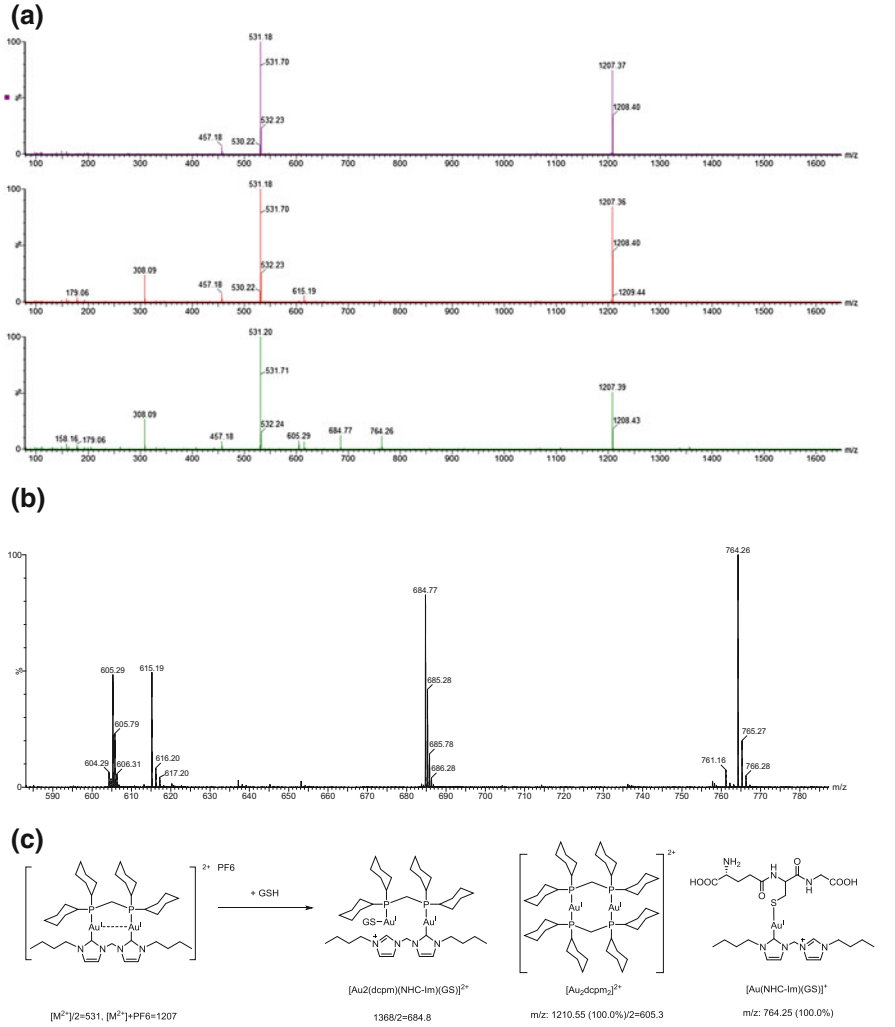

Fig. 4.8 **a** ESI-QTOF-MS spectra of **4.1**-PF_6 (*top*), freshly mixed **4.1**-PF_6 and GSH (*middle*), and **4.1**-PF_6 and GSH mixed for 1 h (*bottom*). **b** Enlarged spectrum (*m/z* 580–790) of the **4.1**-PF_6 and GSH mixture incubated for 1 h. **c** Proposed reaction of **4.1**-PF_6 with GSH according to the MS analysis. Reproduced with permissions [47]. Copyright © 2014 WILEY-VCH Verlag GmbH & Co. KGaA, Weinheim

reported to bind to the SeH of the GCUG motif via one $AuPEt_3^+$ or both SeH and SH via two $AuPEt_3^+$ [60]. In the present case, **4.1**-PF_6 is found to bind GCUG motif in 1:1 molar ratio through simultaneous coordination of the binuclear Au(I) unit to respective S and Se of the contiguous Cys and Sec residues, accompanied with the release of bis(NHC) ligand instead of dcpm. In general, it is believed that P is not as strong as NHC to serve as σ donor. It is reasoned that for complex **4.1**-PF_6, due to

Table 4.2 Cytotoxic IC_{50} (μM) of the gold(I) complexes incubated in BSA-free and BSA-containing medium for 24 h as determined by MTT assays

	4.1-PF_6	**4.2**	**4.3**	**4.4**	**4.5**	Auranofin
BSA free	13.5	3.1	1.5	46.5	0.8	1.1
BSA	46.1	16.5	7.34	>300	17.9	49.3
Ratio[a]	0.293	0.187	0.198	<0.09	0.042	0.023

Reproduced with permissions [47]. Copyright © 2014 WILEY-VCH Verlag GmbH & Co. KGaA, Weinheim

[a]Ratios were calculated by the IC_{50} of BSA free divided by IC_{50} of BSA-containing condition. All the IC_{50} values were determined from at least three independent experiments

Table 4.3 Cytotoxic IC_{50} (μM) of **4.1**-PF_6 and cisplatin in cancer cell lines upon 72-h incubation as determined by MTT assays

	HeLa	MCF-7	SUNE1	H1975	B16-F10
4.1-PF_6	1.8 ± 0.6	2.5 ± 0.4	1.3 ± 0.2	1.4 ± 0.1	3.2 ± 1.0
Cisplatin	6.6 ± 1.1	33.7 ± 7.8	9.6 ± 5.3	18.0 ± 4.4	42.9 ± 5.0

Reproduced with permissions [47]. Copyright © 2014 WILEY-VCH Verlag GmbH & Co. KGaA, Weinheim

Au(I)-Au(I) interaction, dcpm could form a favorable stable five-membered ring (–Au–P–C–P–Au–), but bis(NHC) could form less stable seven-membered ring (–Au–C–N–C–N–C–Au–), resulting in the relatively less stability for the bis(NHC) hence release of NHC ligand but not dcpm.

4.3.4 Inhibition of Cancer Stem Cell Activity

Cancer stem cells (CSCs) which carry the capability of self-renewal and differentiation are proposed to be responsible for tumor relapse and metastasis [61]. The ability to form spheres in non-adherent cultures is a characteristic of CSCs. Here, sphere formation assay was employed to study the activity of **4.1**-PF_6 on the population of HeLa and U-87 MG human glioblastoma cells. As depicted in Figs. 4.16 and 4.17, free-floating spheres were observed in the solvent-control group, and treatment of HeLa cells by 5 or 10 μM of **4.1**-PF_6 resulted in significant inhibition of the self-renewal (sphere-forming) ability of both cancer cell lines. These data revealed that **4.1**-PF_6 could inhibit the self-renewal ability of CSCs. Complex **4.1**-Cl also showed the activity to inhibit the formation of sphere in U-87 MG cells.

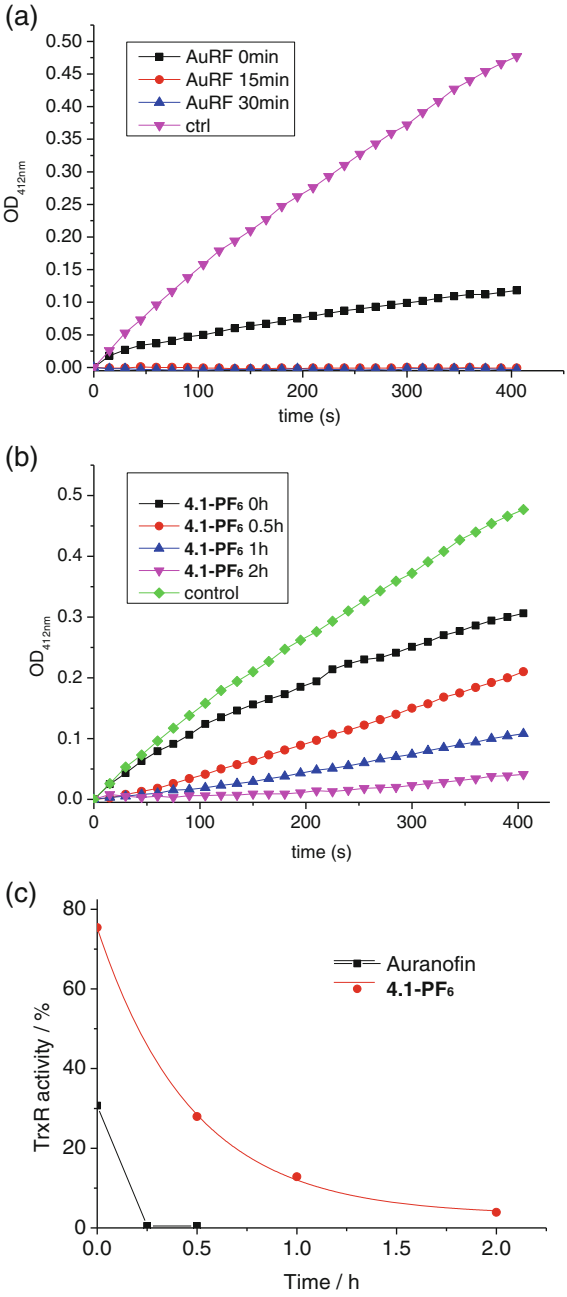

Fig. 4.9 Time-dependent TrxR inhibition by **4.1**-PF_6 and auranofin. Purified TrxR was preincubated with **a** 50 nM of auranofin or **b** 200 nM of **4.1**-PF_6 for the time indicated. The residual enzyme activities were determined as increases in absorbance at 412 nm using DTNB as substrate. **c** Plot of residual TrxR activity against preincubation time. Reproduced with permissions [47]. Copyright © 2014 WILEY-VCH Verlag GmbH & Co. KGaA, Weinheim

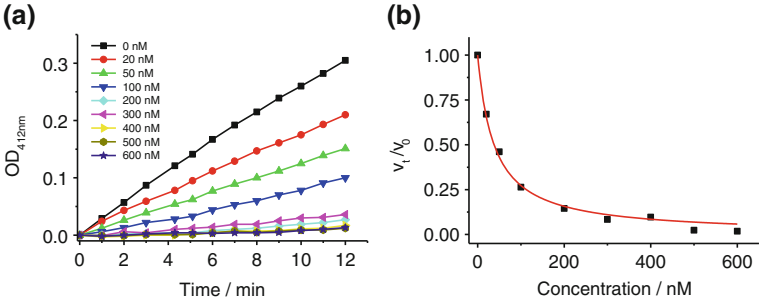

Fig. 4.10 Kinetic analysis of effect of **4.1**-PF_6 on TrxR using DTNB substrate. **a** TrxR activity after preincubating with **4.1**-PF_6 for 2 h. **b** Plot of TrxR activity against concentrations of **4.1**-PF_6 to get IC_{50} values or fit to Eq. 1 to obtain the dissociation constant. Reproduced with permissions [47]. Copyright © 2014 WILEY-VCH Verlag GmbH & Co. KGaA, Weinheim

4.3.5 In Vivo Antitumor Activities

Complexes **1**–**5** all have low solubility in water. Here, biocompatible PET (60 % polyethylene glycol 400; 30 % ethanol; 10 % Tween-80) was chosen as excipient to solubilize these complexes for in vivo study. The complexes were dissolved in PET which was then diluted by PBS with final PET content of 1.5–4 % (v/v). Complexes **4.1**-Cl and **4.1**-OTf could completely be dissolved in the buffer giving a clear solution; while complex **4.1**-PF_6 gave a finely dispersed suspension that remained stable for several hours. Dynamic light scattering (DLS) analysis showed the formation of nanoparticles with diameter size of 175 ± 81 nm. TEM measurement indicated that the particles formed from **4.1**-PF_6 solution were finely dispersed with size diameter of 144 ± 50 nm (Fig. 4.18). Complexes **4.2**, **4.3,** and **4.5** could also form similar suspensions as **4.1**-PF_6.

The in vivo antitumor effects of complexes **4.1**, **4.2**, **4.3,** and **4.5** were examined. After treating nude mice bearing HeLa xenografts by **4.1**-PF_6 with dosage of 5 mg/kg through *intraperitoneal (i.p.) injection* once every three days, statistically significant tumor volume inhibition by 79 % ($p < 0.05$, at day 6) and 81 % ($p < 0.05$, at day 9) was identified compared to those treated with control solvent (Fig. 4.19a). No mouse death or body weight loss was observed during the treatment (Fig. 4.19b). In addition, the inhibition toward the highly aggressive, poorly immunogenic mouse melanoma (B16-F10) in C57BL/6N mice model was examined. As depicted in Fig. 4.20a, despite at least three times faster tumor growth in solvent control of this model than HeLa xenograft, statistically significant tumor inhibition (62 %, $p < 0.05$, day 8) could be obtained after i.p. administration at dosage of 15 mg/kg of **4.1**-PF_6 once every 2–3 days. Importantly, the treatment at this dosage also did not cause mouse death or body weight loss (Fig. 4.20b).

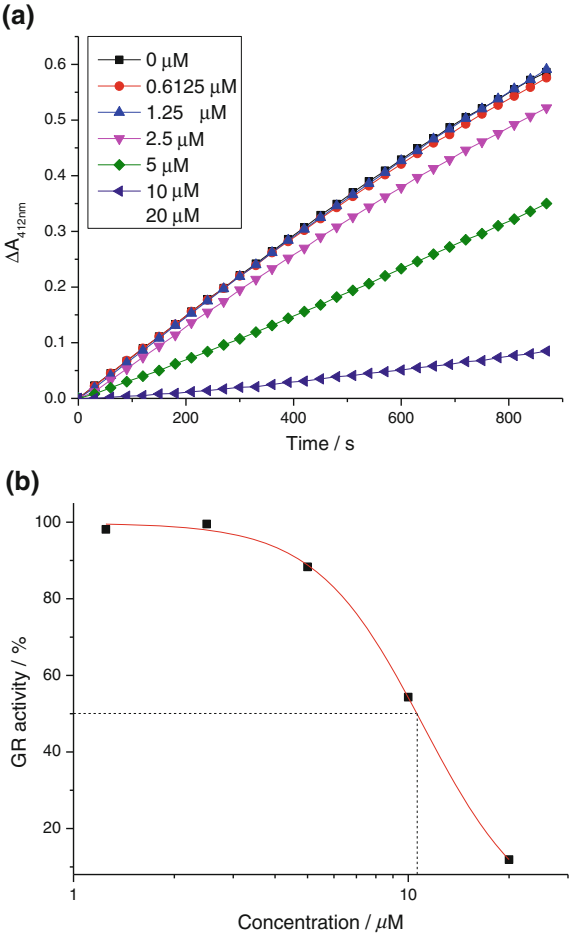

Fig. 4.11 Glutathione reductase (GR) activity: **a** purified GR was incubated with various concentrations of **4.1**-PF_6 for 2 h in the presence of NADPH and the enzyme activities were measured as increases in absorbance at 412 nm after adding DTNB and GSSG. **b** Plot of GR activity against concentrations of **4.1**-PF_6. Reproduced with permissions [47]. Copyright © 2014 WILEY-VCH Verlag GmbH & Co. KGaA, Weinheim

Complexes **4.1**-Cl and **4.1**-OTf could moderately inhibit tumor growth of mice bearing HeLa xenograft and requiring a higher treatment frequency. After administration of **4.1**-Cl or **4.1**-OTf at dosage of 5 mg/kg every day through i.p. administration, statistically significant difference could be achieved with final tumor growth inhibition of 47.7 % ($p < 0.01$) and 35.1 % ($p < 0.05$), respectively (Fig. 4.21a, c). Again, no mouse death or mouse body weight loss was found for the treatment (Fig. 4.21b, d). These results suggested that not only could the structure of the dinucelar gold cations influence the antitumor efficiency, but also the counteranion played an important role in the antitumor activities in vivo. It is

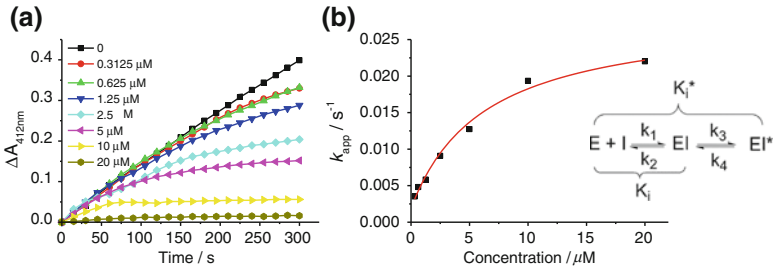

Fig. 4.12 **a** Time dependence to the onset of TrxR inhibition by **4.1**-PF_6. **b** Plot of k_{app} (determined by fitting the data in **a**) against concentrations of **4.1**-PF_6 suggests a two-step binding mechanism; inset: two-step inhibition mechanism. Reproduced with permissions [47]. Copyright © 2014 WILEY-VCH Verlag GmbH & Co. KGaA, Weinheim

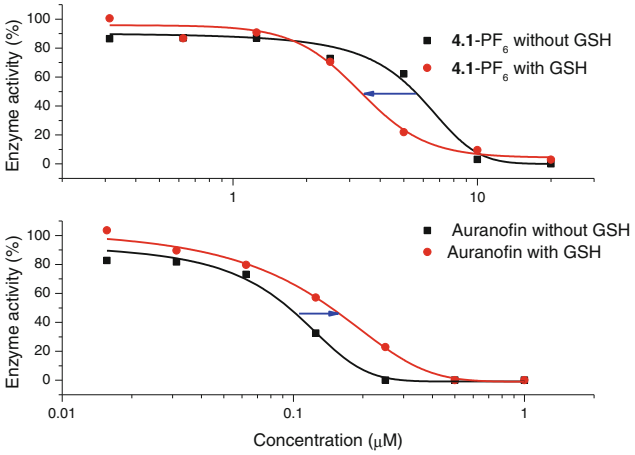

Fig. 4.13 The effects of GSH on TrxR inhibition by **4.1**-PF_6 and auranofin through NADPH–TrxR–Trx–insulin system. GSH was coincubated with NADPH, TrxR, and **4.1**-PF_6 or auranofin for 2 h; then, Trx and insulin were added to the mixture and OD_{340nm} was recorded. TrxR activity was determined by the initial rate of OD_{340nm} decrease compared to the control group. Reproduced with permissions [47]. Copyright © 2014 WILEY-VCH Verlag GmbH & Co. KGaA, Weinheim

assumed that the counteranion affects the solubility of the gold complex in the blood and hence its pharmacokinetics. A very recent report also showed that the formation of nanoparticles owing to incorporation of appropriate anions could increase the anticancer properties [62]. In this case, formation of nanoparticles could be beneficial but not sufficient to achieve in vivo antitumor activity, as complexes **4.2**, **4.3,** and **4.5** that could also form nanoparticles but have high thiol reactivity did not show antitumor activity in mice bearing HeLa xenograft (Fig. 4.22).

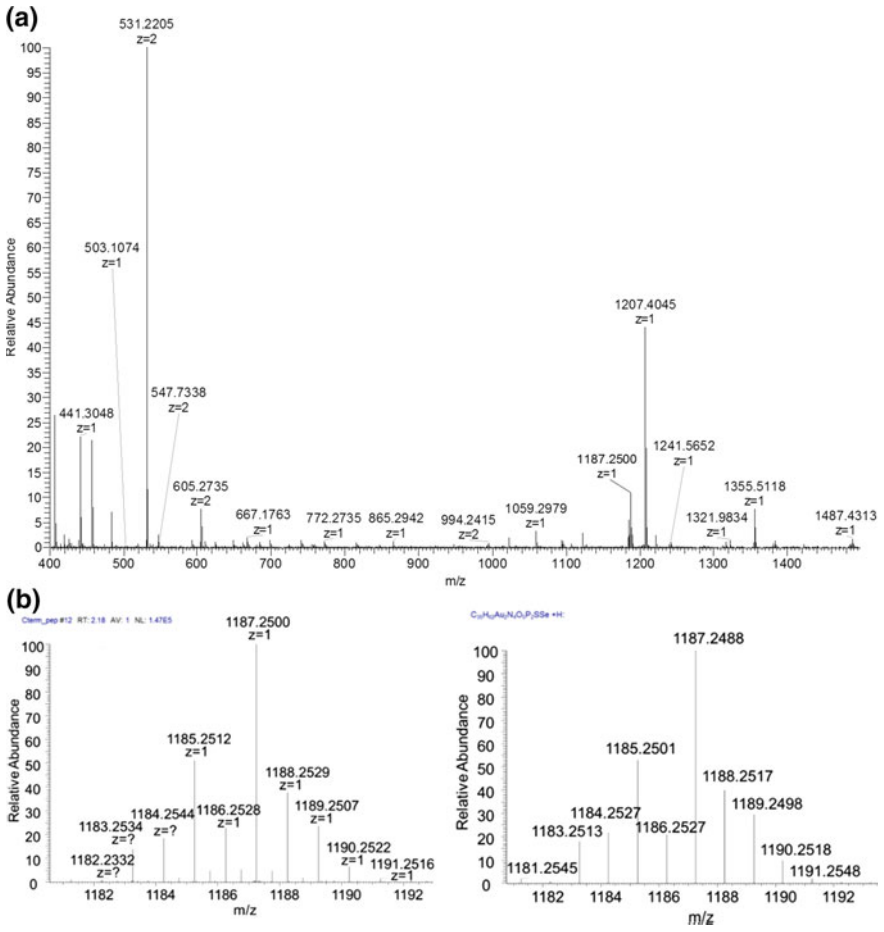

Fig. 4.14 ESI-Orbitrap-MS analysis of the reaction of **4.1**-PF_6 and GCUG: **a** MS spectrum of the mixture of **4.1**-PF_6 and tetrapeptide GCUG after incubating in 5 mM of NH_4HCO_3 (with 50 % MeOH v/v) for 24 h. **b** Enlarged peak of m/z 1187.2500 (*left*) and simulated isotopic pattern of GCUG bound with $dcpmAu_2$ (*right*). Reproduced with permissions [47]. Copyright © 2014 WILEY-VCH Verlag GmbH & Co. KGaA, Weinheim

More importantly, treatment of mice bearing HeLa xenograft by a rather low dosage, 0.6 mg/kg, of **4.1**-PF_6 through i.p. injection three times per week also resulted in statistically significant tumor growth inhibition since 6 days of treatment, with final inhibition of 59.3 % at day 14 (Fig. 4.23). Combining all these treatments, the therapeutic window of **4.1**-PF_6 could be quite large since 0.6–15 mg/kg all resulted in significant antitumor effects.

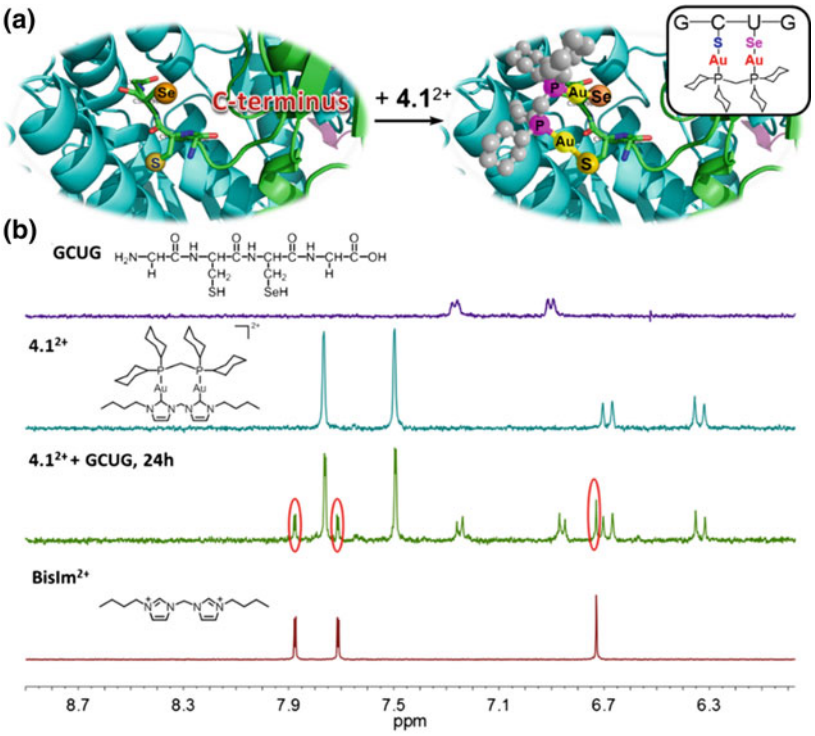

Fig. 4.15 **a** Proposed binding interaction of **4.1**-PF_6 with TrxR; inset: binding mode based on MS results. **b** ^{1}H NMR spectra (400 MHz) of GCUG (*up*), **4.1**-PF_6 (*middle up*), equal molar of **4.1**-PF_6 with GCUG (*middle down*) and $[bis(Im)]^{2+}$ ligand (*down*) in D_2O/d_6-DMSO (1:1, v/v; phosphate buffer, pH* = 7.4) after 24 h incubation. Reproduced with permissions [47]. Copyright © 2014 WILEY-VCH Verlag GmbH & Co. KGaA, Weinheim

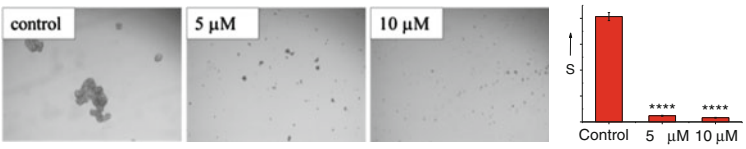

Fig. 4.16 Inhibition of sphere formation of HeLa cells by **4.1**-PF_6. *Left* Representative pictures from three independent experiments. *Right* Average area (S) occupied by spheres per microscopic field. Data are shown as mean from three independent experiments. ****$p < 0.0001$ compared to solvent control. Reproduced with permissions [47]. Copyright © 2014 WILEY-VCH Verlag GmbH & Co. KGaA, Weinheim

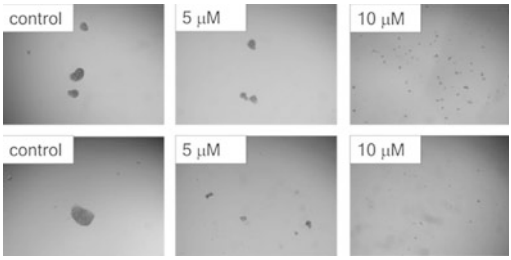

Fig. 4.17 Inhibition of sphere formation of U-87 MG human glioblastoma cells by **4.1**-Cl (*up*) and **4.1**-PF_6 (*down*). Reproduced with permissions [47]. Copyright © 2014 WILEY-VCH Verlag GmbH & Co. KGaA, Weinheim

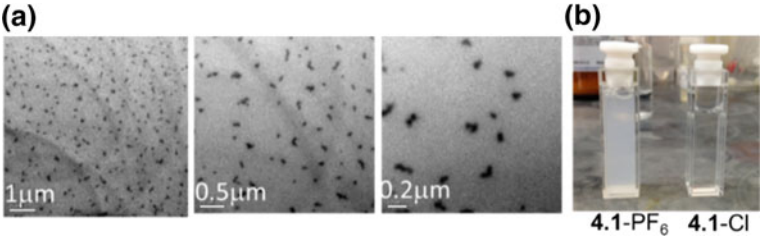

Fig. 4.18 **a** TEM analysis of **4.1**-PF_6 (1 mg/mL) particles formed in the solution of 2 % (v/v) PET in H_2O. **b** Photographs of solutions of **4.1**-PF_6 and **4.1**-Cl in 2 % (v/v) PET in PBS buffer. Reproduced with permissions [47]. Copyright © 2014 WILEY-VCH Verlag GmbH & Co. KGaA, Weinheim

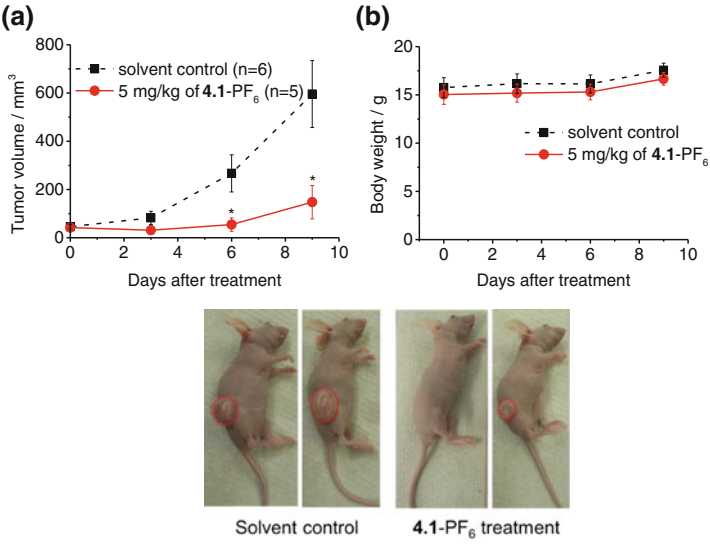

Fig. 4.19 Antitumor effect of **4.1**-PF_6 on mouse bearing HeLa xenograft. **a** Tumor volume and **b** body weight changes after treatment by **4.1**-PF_6 or solvent only. The representative pictures of mice bearing HeLa xenograft after treatment are shown. Reproduced with permissions [47]. Copyright © 2014 WILEY-VCH Verlag GmbH & Co. KGaA, Weinheim

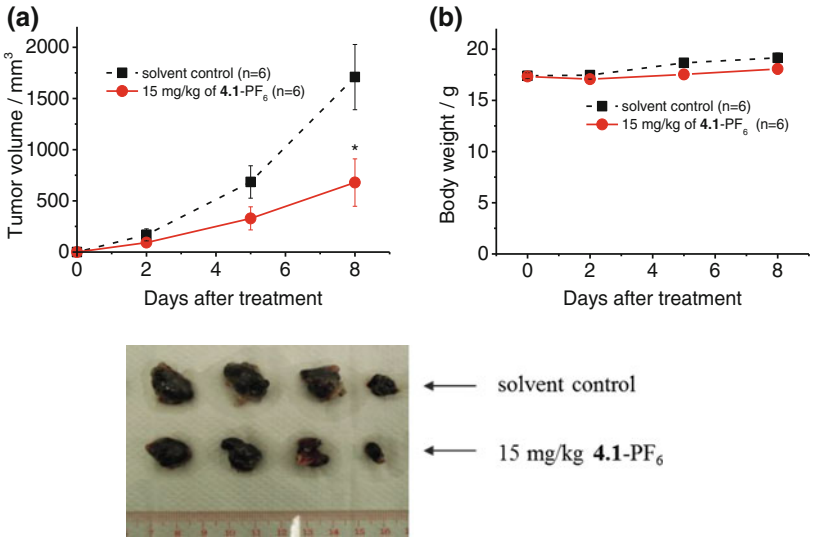

Fig. 4.20 **a** Tumor volume and **b** body weight of mouse B16-F10 melanoma model after treating with 15 mg/kg of **4.1**-PF_6 or solvent only. The slight increase of body in control group may be caused by the faster tumor growth in that group. *$p < 0.05$. Reproduced with permissions [47]. Copyright © 2014 WILEY-VCH Verlag GmbH & Co. KGaA, Weinheim

The antiangiogenic effect of gold(I) complexes in vivo has been previously reported by Ott and coworkers using zebrafish models [33, 63]. In this work, the antiangiogenic activity of **4.1**-PF_6 was investigated by immunohistochemical detection of the CD31 (cluster of differentiation 31) of the blood microvessels in the tumor tissues of mice bearing HeLa xenografts after treatment by **4.1**-PF_6 at 5 mg/kg. While the average number of microvessels per microscopic field of **4.1**-PF_6 treatment in tumor was 2.35, those treated with solvent control was 4.34 (Fig. 4.24, $p < 0.05$), suggesting that **4.1**-PF_6 could significantly inhibit angiogenesis of HeLa xenografts; this result is consistent with the result of in vitro tube formation assay as shown in Fig. 4.25.

4.3.6 Safety Pharmacology Study

To test the possible side effects of **4.1**-PF_6, some safety toxicology studies were performed in a State Food and Drug Administration of PRC (SFDA)-approved laboratory (Tianjin Institute of Pharmaceutical Research). First, all system anaphylaxis reaction was examined in guinea pigs. The animals were treated with

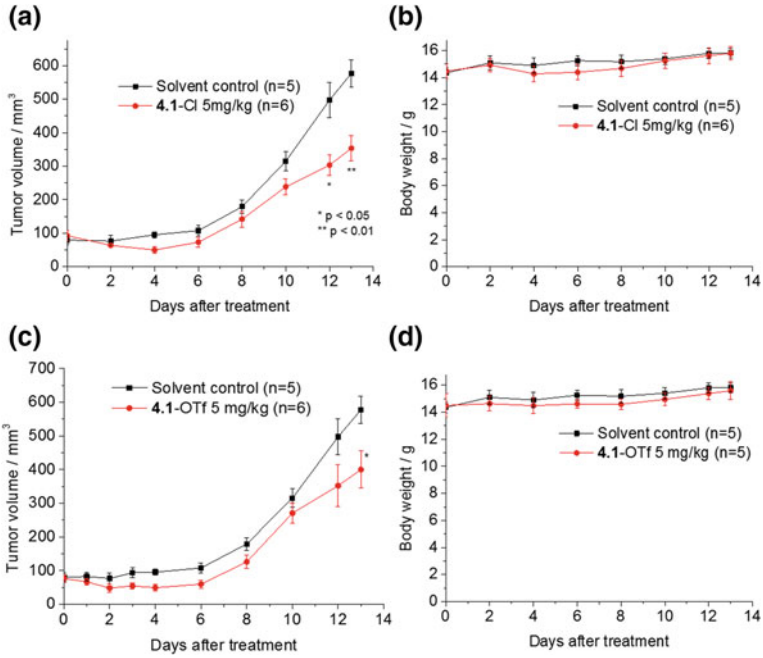

Fig. 4.21 Tumor volume of mice bearing HeLa xenograft after treating with **a** 5 mg/kg of **4.1**-Cl or **c** 5 mg/kg of **4.1**-OTf and solvent only. Body weight of mice bearing HeLa xenograft after treating with **b** 5 mg/kg of **4.1**-Cl or **d** 5 mg/kg of **4.1**-OTf and solvent only. Reproduced with permissions [47]. Copyright © 2014 WILEY-VCH Verlag GmbH & Co. KGaA, Weinheim

0.9 % saline injection (negative control), 10 % PET solvent, 1 % ovalbumin in saline (positive control), and 0.12 mg/kg of **4.1**-PF_6 in PET solvent, respectively, through i.p. injection every other day for 5 times; after 14 days, forelimbs of guinea pigs were injected intravenously (i.v.) with twofold dosage. All guinea pigs in the positive control group exhibited severe allergic reaction (eventually died), *but **4.1**-PF_6 treatment group did not show allergic reaction*. Next, blood vessel irritation test was also conducted. A 0.12 mg of complex **4.1**-PF_6 was directly injected into the auricular veins of the rabbits, and the histopathology was examined at day 4 and day 14 since the first treatment. No apparent ear–blood vessel dilatation, bleeding, swelling, or other morphological changes were identified at the administration sites upon **4.1**-PF_6 treatment. These results revealed that **4.1**-PF_6 did not show systemic anaphylaxis and localized irritation.

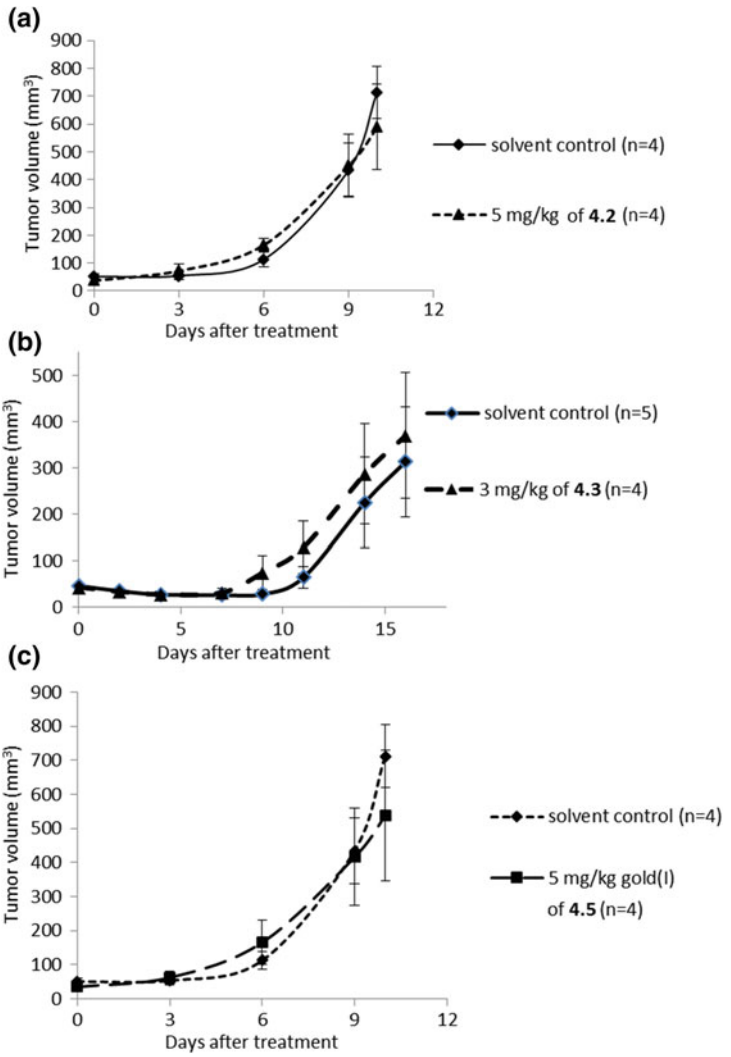

Fig. 4.22 Tumor volume of mouse bearing HeLa xenograft after treating with **a** 5 mg/kg of **4.2**, **b** 3 mg/kg of **4.3**, **c** 5 mg/kg of **4.5** or solvent only. Reproduced with permissions [47]. Copyright © 2014 WILEY-VCH Verlag GmbH & Co. KGaA, Weinheim

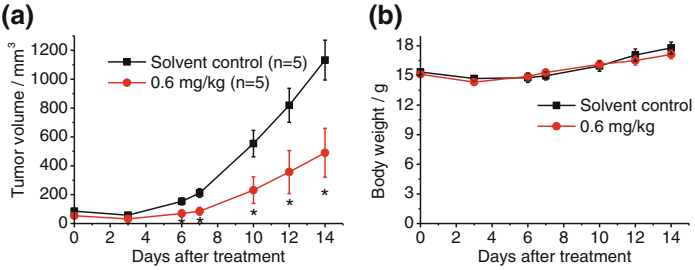

Fig. 4.23 Antitumor effect of **4.1**-PF_6 on mice bearing HeLa xenografts. **a** Tumor volume (V). **b** Body weight. *$p < 0.05$, compared to solvent control. Reproduced with permissions [47]. Copyright © 2014 WILEY-VCH Verlag GmbH & Co. KGaA, Weinheim

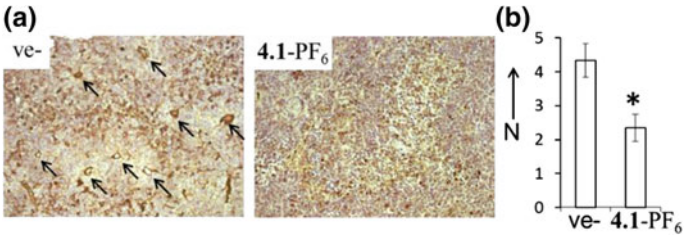

Fig. 4.24 **a** Immunohistochemical detection of CD31 in the tumor tissues after treatment by **4.1**-PF_6. *Arrows* indicate CD31 microvessels. **b** Average number of microvessels per microscopic field. *$p < 0.05$, compared to solvent control. Reproduced with permissions [47]. Copyright © 2014 WILEY-VCH Verlag GmbH & Co. KGaA, Weinheim

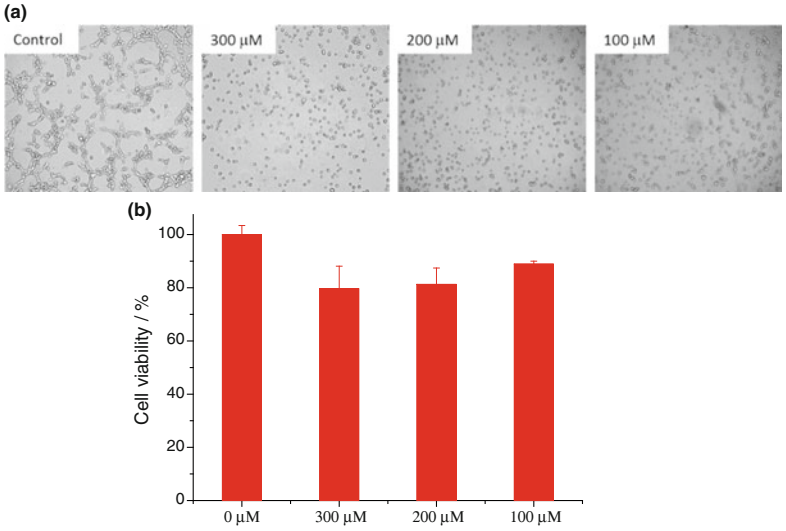

Fig. 4.25 **a** Tube formation assay on MS1 cells treated with **4.1**-PF_6 for 2 h. **b** MTT assay on MS1 cells treated with **4.1**-PF_6 for 2 h, revealing no significant cell death. Reproduced with permissions [47]. Copyright © 2014 WILEY-VCH Verlag GmbH & Co. KGaA, Weinheim

4.4 Conclusion

To conclude, the dinuclear gold(I) complex **4.1**-PF_6 shows favorable thiol stability against serum thiols in blood, and enough reactivity to serve as a tight-binding inhibitor of TrxR. It significantly inhibited tumor growth of HeLa xenografts and highly aggressive mouse B16-F10 melanoma at a wide therapeutic window with no observable side effects under different in vivo conditions. *This finding sheds lights on the clinical prospects of developing gold(I)–NHC complexes into useful anti-cancer drugs*. Future works are needed to investigate the detailed anticancer mechanism such as all the possible binding interactions of this dinuclear gold(I) complex with other thiol/selenol-containing enzymes/proteins in combination with proteomics, transcriptomics, and other advanced techniques.

References

1. Lin JCY, Huang RTW, Lee CS, Bhattacharyya A, Hwang WS, Lin IJB (2009) Coinage metal–N-heterocyclic carbene complexes. Chem Rev 109(8):3561–3598
2. Raubenheimer HG, Cronje S (2008) Carbene complexes of gold: preparation, medical application and bonding. Chem Soc Rev 37(9):1998–2011
3. Melaimi M, Soleilhavoup M, Bertrand G (2010) Stable cyclic carbenes and related species beyond diaminocarbenes. Angew Chem Int Ed 49(47):8810–8849
4. Mercs L, Albrecht M (2010) Beyond catalysis: N-heterocyclic carbene complexes as components for medicinal, luminescent, and functional materials applications. Chem Soc Rev 39(6):1903–1912
5. John A, Ghosh P (2010) Fascinating frontiers of N/O-functionalized N-heterocyclic carbene chemistry: from chemical catalysis to biomedical applications. Dalton Trans 39(31):7183–7206
6. Martin D, Soleilhavoup M, Bertrand G (2011) Stable singlet carbenes as mimics for transition metal centers. Chem Sci 2(3):389–399
7. Nolan SP (2011) The development and catalytic uses of N-heterocyclic carbene gold complexes. Acc Chem Res 44(2):91–100
8. Velazquez HD, Verpoort F (2012) N-heterocyclic carbene transition metal complexes for catalysis in aqueous media. Chem Soc Rev 41(21):7032–7060
9. Izquierdo J, Hutson GE, Cohen DT, Scheidt KA (2012) A continuum of progress: applications of N-heterocyclic carbene catalysis in total synthesis. Angew Chem Int Ed 51(47):11686–11698
10. Gaillard S, Cazin CSJ, Nolan SP (2012) N-heterocyclic carbene gold(I) and copper(I) complexes in C–H bond activation. Acc Chem Res 45(6):778–787
11. Grossmann A, Enders D (2012) N-heterocyclic carbene catalyzed domino reactions. Angew Chem Int Ed 51(2):314–325
12. Fèvre M, Pinaud J, Gnanou Y, Vignolle J, Taton D (2013) N-heterocyclic carbenes (NHCs) as organocatalysts and structural components in metal-free polymer synthesis. Chem Soc Rev 42:2142–2172
13. Gaillard S, Renaud J-L (2013) When phosphorus and NHC (N-heterocyclic carbene) meet each other. Dalton Trans 42(20):7255–7270
14. Hindi KM, Panzner MJ, Tessier CA, Cannon CL, Youngs WJ (2009) The medicinal applications of imidazolium carbene–metal complexes. Chem Rev 109(8):3859–3884

15. Yan JJ, Chow AL-F, Leung C-H, Sun RW-Y, Ma D-L, Che C-M (2010) Cyclometalated gold (III) complexes with N-heterocyclic carbene ligands as topoisomerase I poisons. Chem Commun 46(22):3893–3895
16. Sun RW-Y, Chow AL-F, Li X-H, Yan JJ, Chui SS-Y, Che C-M (2011) Luminescent cyclometalated platinum(II) complexes containing N-heterocyclic carbene ligands with potent in vitro and in vivo anti-cancer properties accumulate in cytoplasmic structures of cancer cells. Chem Sci 2:728–736
17. Oehninger L, Rubbiani R, Ott I (2013) N-heterocyclic carbene metal complexes in medicinal chemistry. Dalton Trans 42(10):3269–3284
18. Cisnetti F, Gautier A (2013) Metal/N-heterocyclic carbene complexes: opportunities for the development of anticancer metallodrugs. Angew Chem Int Ed 52(46):11976–11978
19. Liu W, Gust R (2013) Metal N-heterocyclic carbene complexes as potential antitumor metallodrugs. Chem Soc Rev 42(2):755–773
20. Zou T, Lok C-N, Fung YME, Che C-M (2013) Luminescent Organoplatinum(II) complexes containing Bis(N-heterocyclic carbene) ligands selectively target the endoplasmic reticulum and induce potent photo-toxicity. Chem Commun 49(47):5423–5425
21. Sadler PJ, Muncie C, Shipman M (2006) Metals in Medicine. In: Bertini I, Gray HB, Stiefel EI, Valentine JS (eds) Biological inorganic chemistry: structure and reactivity. University Science Books, New York, pp 95–135
22. Urig S, Fritz-Wolf K, Réau R, Herold-Mende C, Tóth K, Davioud-Charvet E, Becker K (2006) Undressing of phosphine gold(I) complexes as irreversible inhibitors of human disulfide reductases. Angew Chem Int Ed 45(12):1881–1886
23. Ray S, Mohan R, Singh JK, Samantaray MK, Shaikh MM, Panda D, Ghosh P (2007) anticancer and antimicrobial metallopharmaceutical agents based on palladium, gold, and silver N-heterocyclic carbene complexes. J Am Chem Soc 129(48):15042–15053
24. Hickey JL, Ruhayel RA, Barnard PJ, Baker MV, Berners-Price SJ, Filipovska A (2008) Mitochondria-targeted chemotherapeutics: the rational design of gold(I) N-heterocyclic carbene complexes that are selectively toxic to cancer cells and target protein selenols in preference to thiols. J Am Chem Soc 130(38):12570–12571
25. Bindoli A, Rigobello MP, Scutari G, Gabbiani C, Casini A, Messori L (2009) Thioredoxin reductase: a target for gold compounds acting as potential anticancer drugs. Coord Chem Rev 253(11–12):1692–1707
26. Ott I (2009) On the medicinal chemistry of gold complexes as anticancer drugs. Coord Chem Rev 253 (11+12):1670–1681
27. Nobili S, Mini E, Landini I, Gabbiani C, Casini A, Messori L (2010) Gold compounds as anticancer agents: chemistry, cellular pharmacology, and preclinical studies. Med Res Rev 30 (3):550–580
28. Che C-M, Siu F-M (2010) Metal complexes in medicine with a focus on enzyme inhibition. Curr Opin Chem Biol 14(2):255–261
29. Gasser G, Ott I, Metzler-Nolte N (2011) Organometallic anticancer compounds. J Med Chem 54(1):3–25
30. Berners-Price SJ, Filipovska A (2011) Gold compounds as therapeutic agents for human diseases. Metallomics 3(9):863–873
31. Che C-M, Sun RW-Y (2011) Therapeutic Applications of gold complexes: lipophilic gold(III) cations and gold(I) complexes for anti-cancer treatment. Chem Commun 47(34):9554–9560
32. Casini A, Messori L (2011) Molecular mechanisms and proposed targets for selected anticancer gold compounds. Curr Top Med Chem 11(21):2647–2660
33. Meyer A, Bagowski CP, Kokoschka M, Stefanopoulou M, Alborzinia H, Can S, Vlecken DH, Sheldrick WS, Wölfl S, Ott I (2012) On the biological properties of alkynyl phosphine gold(I) complexes. Angew Chem Int Ed 51(39):8895–8899
34. Romero-Canelón I, Sadler PJ (2013) Next-generation metal anticancer complexes: multitargeting via redox modulation. Inorg Chem 52(21):12276–12291

35. Zou T, Lum CT, Chui SS-Y, Che C-M (2013) Gold(III) complexes containing N-heterocyclic carbene ligands: thiol "switch-on" fluorescent probes and anti-cancer agents. Angew Chem Int Ed 52(10):2930–2933
36. Berners-Price SJ, Mirabelli CK, Johnson RK, Mattern MR, McCabe FL, Faucette LF, Sung C-M, Mong S-M, Sadler PJ, Crooke ST (1986) In vivo antitumor activity and in vitro cytotoxic properties of bis[1,2-bis(diphenylphosphino)ethane]gold(I) chloride. Cancer Res 46 (11):5486–5493
37. Hoke GD, Macia RA, Meunier PC, Bugelski PJ, Mirabelli CK, Rush GF, Matthews WD (1989) In vivo and in vitro cardiotoxicity of a gold-containing antineoplastic drug candidate in the rabbit. Toxicol Appl Pharmacol 100(2):293–306
38. Smith PF, Hoke GD, Alberts DW, Bugelski PJ, Lupo S, Mirabelli CK, Rush GF (1989) Mechanism of toxicity of an experimental bidentate phosphine gold complexed antineoplastic agent in isolated rat hepatocytes. J Pharmacol Exp Ther 249(3):944–950
39. Malik NA, Otiko G, Sadler PJ (1980) Control of intra- and extra-cellular sulphydryl-disulphide balances with gold phosphine drugs: 31P nuclear magnetic resonance studies of human blood. J Inorg Biochem 12(4):317–322
40. Berners-Price SJ (2011) Gold-based therapeutic agents: a new perspective. In: Bioinorganic medicinal chemistry. Wiley-VCH Verlag GmbH & Co. KGaA, pp 197–222. doi:10.1002/9783527633104.ch7
41. Pillarsetty N, Katti KK, Hoffman TJ, Volkert WA, Katti KV, Kamei H, Koide T (2003) In vitro and in vivo antitumor properties of tetrakis((trishydroxy- methyl)phosphine)gold(I) chloride. J Med Chem 46(7):1130–1132
42. Chui CH, Wong RS-M, Gambari R, Cheng GY-M, Yuen MC-W, Chan K-W, Tong S-W, Lau F-Y, Lai PB-S, Lam K-H, Ho C-L, Kan C-W, Leung KS-Y, Wong W-Y (2009) Antitumor activity of diethynylfluorene derivatives of gold(I). Bioorg Med Chem 17(23):7872–7877
43. Yan K, Lok C-N, Bierla K, Che C-M (2010) Gold(I) complex of N, N′-disubstituted cyclic thiourea with in vitro and in vivo anticancer properties-potent tight-binding inhibition of thioredoxin reductase. Chem Commun 46(41):7691–7693
44. Shaw III CF, Beery A (1986) Anti-tumor activity of two binuclear gold(I) complexes with bridging dithiolate ligands. Inorg Chim Acta 123:213–216
45. Barnard PJ, Wedlock LE, Baker MV, Berners-Price SJ, Joyce DA, Skelton BW, Steer JH (2006) Luminescence studies of the intracellular distribution of a dinuclear gold(I) N-heterocyclic carbene complex. Angew Chem Int Ed 45(36):5966–5970
46. Rubbiani R, Can S, Kitanovic I, Alborzinia H, Stefanopoulou M, Kokoschka M, Mönchgesang S, Sheldrick WS, Wölfl S, Ott I (2011) Comparative in vitro evaluation of N-heterocyclic carbene gold(I) complexes of the benzimidazolylidene type. J Med Chem 54 (24):8646–8657
47. Zou T, Lum CT, Lok C-N, To W-P, Low K-H, Che C-M (2014) A binuclear gold(I) complex with mixed bridging diphosphine and bis(N-heterocyclic carbene) ligands shows favorable thiol reactivity and inhibits tumor growth and angiogenesis in vivo. Angew Chem Int Ed 53 (23):5810–5814
48. Gil-Rubio J, Cámara V, Bautista D, Vicente J (2012) Dinuclear alkynyl gold(I) complexes containing bridging N-heterocyclic dicarbene ligands: new synthetic routes and luminescence. Organometallics 31(15):5414–5426
49. Fu W-F, Chan K-C, Miskowski VM, Che C-M (1999) The intrinsic ^{3}[dσ*pσ] emission of binuclear gold(i) complexes with two bridging diphosphane ligands lies in the near UV; emissions in the visible region are due to exciplexes. Angew Chem Int Ed 38(18):2783–2785
50. Baker MV, Barnard PJ, Berners-Price SJ, Brayshaw SK, Hickey JL, Skelton BW, White AH (2006) Cationic, linear Au(I) N-heterocyclic carbene complexes: synthesis, structure and anti-mitochondrial activity. Dalton Trans 30:3708–3715
51. Barnard PJ, Baker MV, Berners-Price SJ, Skelton BW, White AH (2004) Dinuclear gold(i) complexes of bridging bidentate carbene ligands: synthesis, structure and spectroscopic characterisation. Dalton Trans 7:1038–1047
52. Sheldrick GM (2008) A short history of SHELX. Acta Cryst A64(1):112–122

53. Lum CT, Wong A, Lin MC, Che C-M, Sun RW-Y (2013) Gold(III) porphyrin complex as an anti-cancer candidate to inhibit growth of cancer-stem cells. Chem Commun 49:4364–4366
54. Schneider CA, Rasband WS, Eliceiri KW (2012) NIH Image to ImageJ: 25 years of image analysis. Nat Methods 9(7):671–675
55. Santra S, Kaittanis C, Santiesteban OJ, Perez JM (2011) Cell-specific, activatable, and theranostic prodrug for dual-targeted cancer imaging and therapy. J Am Chem Soc 133 (41):16680–16688
56. Vathipadiekal V, Rao M (2004) Inhibition of 1,4-beta-D-xylan Xylanohydrolase by the specific aspartic protease inhibitor pepstatin: probing the two-step inhibition mechanism. J Biol Chem 279(45):47024–47033
57. Xu C, Hall R, Cummings J, Raushel FM (2006) Tight binding inhibitors of N-acyl amino sugar and N-acyl amino acid deacetylases. J Am Chem Soc 128(13):4244–4245
58. Bhabak KP, Bhuyan BJ, Mugesh G (2011) Bioinorganic and medicinal chemistry: aspects of gold(I)-protein complexes. Dalton Trans 40(10):2099–2111
59. Lee J, Jayathilaka LP, Gupta S, Huang JS, Lee BS (2012) Gold Ion-angiotensin peptide interaction by mass spectrometry. J Am Soc Mass Spectrom 23(5):942–951
60. Pratesi A, Gabbiani C, Ginanneschi M, Messori L (2010) Reactions of medicinally relevant gold compounds with the C-terminal motif of thioredoxin reductase elucidated by MS analysis. Chem Commun 46(37):7001–7003
61. Dean M, Fojo T, Bates S (2005) Tumour stem cells and drug resistance. Nat Rev Cancer 5 (4):275–284
62. Magut PKS, Das S, Fernand VE, Losso J, McDonough K, Naylor BM, Aggarwal S, Warner IM (2013) Tunable cytotoxicity of rhodamine 6G via anion variations. J Am Chem Soc 135(42):15873–15879
63. Ott I, Qian X, Xu Y, Vlecken DHW, Marques IJ, Kubutat D, Will J, Sheldrick WS, Jesse P, Prokop A, Bagowski CP (2009) A gold(I) phosphine complex containing naphthalimide ligand functions as a TrxR inhibiting antiproliferative agent and angiogenesis inhibitor. J Med Chem 52(3):763–770

Chapter 5
Luminescent Organoplatinum(II) Complexes Containing Bis(N-Heterocyclic Carbene) Ligands Selectively Target Endoplasmic Reticulum and Induce Potent Phototoxicity

5.1 Introduction

Stimulated by the success of cisplatin to combat cancers, numerous research interests have been aroused to the development of new metal-based antitumor therapeutics [1–5]. Particularly, the antitumor active platinum(II) complexes, which could either covalently bind to DNA, or non-covalently act as DNA intercalators and/or as major-/minor-groove binding agents, have emerged in the past years [6–9]. In general, DNA is conceived to be the key molecular target of the classic Pt (II) drugs despite that alternative modes of anticancer action including cisplatin-induced endoplasmic reticulum (ER) stress [10] have also been reported.

ER-stress or unfold protein response (UPR) is caused by the perturbation of protein folding and the accumulation of misfolded proteins in the lumen of ER [11]. If such stress/response cannot be released, as in the case of cells exposed to certain cytotoxic agents [12, 13], apoptotic pathway will be activated hence leading to cell death. Certain types of cancer cells including multiple myeloma are particularly sensitive to ER-stress-induced cell death due to the high ER activity [14, 15]. In this regard, developing new anticancer agents which target ER-stress pathway could be a promising therapeutic antitumor strategy [16].

Platinum(II) complexes have planar conformation. The specific target-Pt(II) complex binding interactions can be achieved through molecular design on the coordination geometry of Pt(II) complexes with appropriate chelating π-conjugated ligands having C and/or N donor atoms. Such structures allow a unique chemical scaffold for non-covalent binding interactions with biomolecules including proteins/enzymes [17]. Our group previously reported that cyclometalated [Au^{III}($^{n-Bu}$C^N)biguanide]Cl [$^{n-Bu}$HC^N=2-(4-*n*-butylphenyl)pyridine] [18], [Au_2^{III}(C^N^C)$_2$(μ-dppp)]OTf_2 [HC^N^CH=2,6-diphenylpyridine; dppp=bis(diphenylphosphino)propane] [19], and ytterbium(III) porphyrin [20] could induce ER-stress and apoptosis-independent/dependent cell death pathways. It was also reported that

T. Zou, *Anti-Cancer N-Heterocyclic Carbene Complexes of Gold(III), Gold(I) and Platinum(II)*, Springer Theses, DOI 10.1007/978-981-10-0657-9_5

luminescent $[Pt^{II}(C^N^N)(NHC)]PF_6$ (HC^N^N=6-phenyl-2,2′-bipyridine, NHC= N-heterocyclic carbene) could inhibit tumor growth in vitro and in vivo via specific cellular localization in mitochondria to target proteins instead of in nucleus to target DNA [21]. Since NHC ligands have unique electronic and steric characters, it is conceived that NHC ligands may render the Pt(II) complexes to attain stability under physiological conditions, to selectively target novel biomolecular targets, and to confer intriguing luminescent properties that can be harnessed to elicit anticancer mechanisms. In this chapter, a class of luminescent cyclometalated platinum(II)-bis (N-heterocyclic carbene) complexes which can specifically localize to ER domain and potently induce ER-stress and mitochondria dysfunction followed by cell apoptosis are described. Some of the Pt(II) complexes also displayed potent phototoxicity. Tsubomura and coworkers reported the structure and photo-physical properties of related platinum(II) complexes [22].

5.2 Experimental Section

5.2.1 Materials and Methods

All starting materials were used as received from commercial sources. All the solvents were of analytical grade. $[Pt(C^N)(\mu\text{-}Cl)]_2$ (HC^N=2-phenylpyridine, Hppy; benzo [*h*]quinolone, Hbzq; 2-(thiophen-2-yl)pyridine, Hthpy) [23] and $[bisIm]^{2+}I_2^-$ (bisIm=1,1′-methylene-3,3′-dialkylbis(imidazolium)) [24] were synthesized according to reported procedures. Fast atom bombardment (FAB) mass spectra were obtained on a Finnigan Mat 95 mass spectrometer. ^{1}H NMR spectra were obtained on DPX 400 M and 300 M Bruker FT-NMR spectrometers relative to the signal of tetramethylsilane. UV–visible spectra were recorded on a Perkin-Elmer Lambda 19 UV/Vis spectrophotometer. Steady-state emission spectra were recorded on a SPEX 1681 Fluorolog-3 spectrophotometer. Elemental analysis was performed by the Institute of Chemistry at the Chinese Academy of Sciences, Beijing. For MTT and protein assays, the absorbance was quantified using Perkin-Elmer Fusion Reader (Packard BioScience Company). Fluorescence images were examined in Axiovert 200 (Carl Zeiss) and in an Axio Vision Rel. 4.5 imaging system (Carl Zeiss).

5.2.2 Experimental Procedure and Compound Characterization

Complex **5.1** $[Pt^{II}(ppy)(bisNHC^{2Me})]OTf$

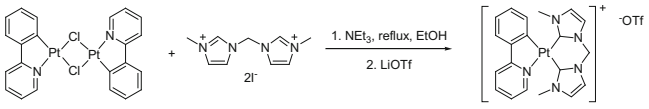

An ethanol solution (20 mL) of $[Pt(ppy)(\mu\text{-}Cl)]_2$ (60 mg, 0.078 mmol) was added with 67.4 mg of 1,1′-methylene-3,3′-dimethyllbis(imidazolium) diiodide (0.156 mmol) and Et_3N (1 mL). After refluxing the mixture for 12 h, excess of lithium triflate was added. The mixture was stirred for another 0.5 h and then evaporated. The residue was dissolved in water and extracted with CH_2Cl_2. The organic layer was evaporated to dryness. Purification of the product by column chromatography gave yellow-green solid. Yield: 80 %. ^{1}H NMR (400 MHz, $CDCl_3$, 298 K): δ = 8.62 (d, 1 H, *J* = 4.7 Hz), 8.18 (d, 1 H, *J* = 1.9 Hz), 8.14 (d, 1 H, *J* = 2.0 Hz), 7.98 (m, 1 H), 7.88 (d, 1 H, *J* = 8.0 Hz), 7.68 (m, 1 H), 7.35 (m, 2 H), 7.30 (d, 1 H, *J* = 3.7 Hz), 7.24 (d, 1 H, *J* = 1.9 Hz), 7.17–7.20 (m, 2 H), 7.10 (d, 1 H, *J* = 2.0 Hz), 6.03 (d, 1 H, *J* = 12.8 Hz), 3.88 (s, 3 H), 3.77 (s, 3 H). MS-FAB(+): *m/z* 525.1 [M-OTf]. Elemental Analysis: calcd for $C_{21}H_{20}F_3N_5O_3PtS{\cdot}H_2O$: C, 36.42; H, 3.20; N, 10.11; found: C, 36.16; H, 3.23; N, 9.97.

Complex **5.2** $[Pt^{II}(ppy)(bisNHC^{2C4})]OTf$

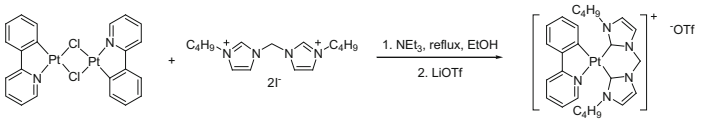

The synthesis is similar to that for **5.1**. Yield: 75 %. ^{1}H NMR (400 MHz, $CDCl_3$, 298 K): δ = 8.51 (d, 1 H, *J* = 4.9 Hz), 8.02 (d, 1 H, *J* = 2.0 Hz), 7.96–7.85 (m, 3 H), 7.68 (m, 1 H), 7.32 (m, 1 H), 7.21–7.19 (m, 3 H), 7.01 (d, 1 H, *J* = 2.0 Hz), 6.90 (m, 1 H), 6.76 (d, 1 H, *J* = 12.9 Hz), 6.10 (d, 1 H, *J* = 12.9 Hz), 4.34 (m, 1 H), 4.17 (m, 1 H), 4.05–3.93 (m, 2 H), 1.75–1.55 (m, 4 H), 1.40–0.94 (m, 4 H), 0.78 (m, 6 H). MS-FAB(+): *m/z* 609.2 [M-OTf]. Elemental Analysis: calcd for $C_{27}H_{32}F_3N_5O_3PtS{\cdot}1.5H_2O$: C, 41.27; H, 4.49; N, 8.91; found: C, 41.01; H, 4.37; N, 9.22.

Complex **5.3** $[Pt^{II}(ppy)(bisNHC^{2C6})]OTf$

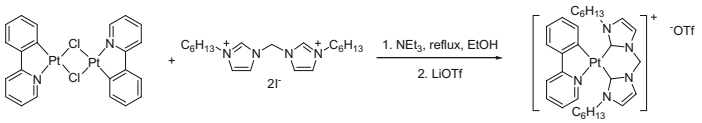

The synthesis is similar to that for **5.1**. Yield: 70 %. ^{1}H NMR (400 MHz, $CDCl_3$, 298 K): δ 8.51 (d, *J* = 5.5 Hz, 1 H), 8.00 (m, 1 H), 7.98–7.94 (m, 1 H), 7.89 (m, 2 H), 7.68 (m, 1 H), 7.33 (m, 1 H), 7.21–7.16 (m, 3 H), 7.00 (d, *J* = 1.4 Hz, 1 H), 6.96 (d, *J* = 2.1 Hz, 1 H), 6.71 (d, *J* = 13.0 Hz, 1 H), 6.10 (d, *J* = 12.7 Hz, 1 H), 4.31 (m, 1 H), 4.08 (m, 1 H), 4.00–3.90 (m, 2 H), 1.72–1.63 (m, 4 H), 1.20–1.07 (m, 12 H), 0.78 (m, 6 H). MS-FAB(+): *m/z* 665.3 (M-OTf). Elemental Analysis: calcd for $C_{31}H_{40}F_3N_5O_3PtS{\cdot}0.5H_2O$: C, 45.20; H, 5.02; N, 8.50; found: C, 45.24; H, 4.92; N, 8.51.

Complex **5.4** [Pt^{II}(bzq)(bisNHC^{2Me})]OTf

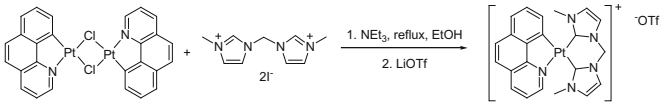

The synthesis is similar to that for **5.1**. Yield: 72 %. ^{1}H NMR (400 MHz, $CDCl_3$, 298 K): δ = 8.88 (d, 1 H, *J* = 5.3 Hz), 8.38 (d, 1 H, *J* = 8.1 Hz), 7.81–7.76 (m, 3 H), 7.65–7.52 (m, 5 H), 7.18 (d, 1 H, *J* = 1.9 Hz), 7.08 (d, 1 H, *J* = 2.1 Hz), 6.51 (d, 1 H, *J* = 13.0 Hz), 6.12 (d, 1 H, *J* = 13.0 Hz), 3.92 (s, 3 H), 3.86 (s, 3 H). MS-FAB (+): *m*/*z* 549.1 (M-OTf). Elemental Analysis: calcd for $C_{23}H_{20}F_3N_5O_3PtS{\cdot}H_2O$: C, 38.55; H, 3.09; N, 9.77; found: C, 38.23; H, 3.00; N, 9.47.

Complex **5.5** [Pt^{II}(bzq)(bisNHC^{2C4})]OTf

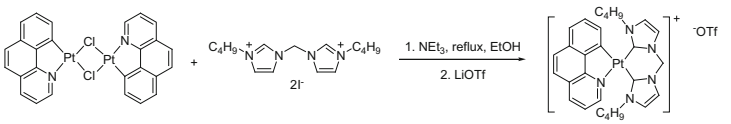

The synthesis is similar to that for **5.1**. Yield: 74 %. ^{1}H NMR (400 MHz, $CDCl_3$, 298 K): δ = 8.85 (d, 1 H, *J* = 5.3 Hz), 8.38 (d, 1 H, *J* = 8.1 Hz), 7.87 (d, 1 H, *J* = 1.9 Hz), 7.83 (m, 2 H), 7.67–7.55 (m, 5 H), 7.18 (d, 1 H, *J* = 2.0 Hz), 7.08 (d, 1 H, *J* = 2.1 Hz), 6.51 (d, 1 H, *J* = 13.0 Hz), 6.13 (d, 1 H, *J* = 12.9 Hz), 4.54 (m, 1 H), 4.35–4.12 (m, 2 H), 4.08 (m, 1 H), 1.72–1.60 (m, 4 H), 1.23–0.95 (m, 4 H), 0.78 (m, 6 H). MS-FAB(+): *m*/*z* 633.2 (M-OTf). Elemental Analysis: calcd for $C_{29}H_{32}F_3N_5O_3PtS{\cdot}H_2O{\cdot}CH_3CN$: C, 44.23; H, 4.43; N, 9.98; found: C, 44.13; H, 4.16; N, 10.01.

Complex **5.6** [Pt^{II}(thpy)(bisNHC^{2Me})]OTf

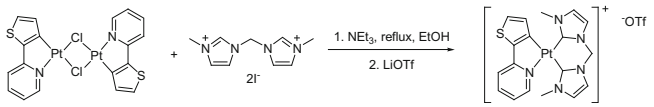

The synthesis is similar to that for **5.1**. Yield: 68 %. ^{1}H NMR (400 MHz, d_6-DMSO) δ 8.51 (d, *J* = 5.5 Hz, 1H), 8.02 (t, *J* = 7.7 Hz, 1 H), 7.70–7.72 (m, 4 H), 7.48 (d, *J* = 13.5 Hz, 2 H), 7.22 (t, *J* = 6.5 Hz, 1 H), 7.01 (d, *J* = 4.6 Hz, 1 H), 6.20 (d, *J* = 13.3 Hz, 1 H), 6.12 (d, *J* = 13.2 Hz, 1 H), 3.78 (s, 3 H), 3.75 (s, 3 H). MS-FAB(+): *m*/*z* 531.0 (M-OTf). Elemental Analysis: calcd for $C_{19}H_{18}F_3N_5O_3PtS_2{\cdot}2H_2O$: C, 31.85; H, 3.09; N, 9.77; found: C, 32.12; H, 2.89; N, 10.02.

Complex **5.7** [Pt^{II}(thpy)(bisNHC^{2C4})]OTf

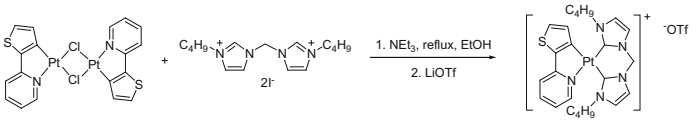

The synthesis is similar to that for **5.1**. Yield: 72 %. ^{1}H NMR (400 MHz, $CDCl_3$, 298 K): δ = 8.33 (d, 1 H, *J* = 5.1 Hz), 7.85–7.78 (m, 3 H), 7.48 (d, 1 H, *J* = 7.9 Hz), 7.40 (d, 1 H, *J* = 4.7 Hz), 7.09 (d, 1 H, *J* = 2.0 Hz), 7.06 (m, 1 H), 7.01 (d, 1 H, *J* = 2.1 Hz), 6.93 (d, 1 H, *J* = 4.6 Hz), 6.58 (d, 1 H, *J* = 13.0 Hz), 5.99 (d, 1 H, *J* = 12.9 Hz), 4.45 (m, 1 H), 4.21–3.98 (m, 2 H), 3.96 (m, 1 H), 1.79–1.59 (m, 4 H), 1.26–0.95 (m, 4 H), 0.80 (m, 6 H). MS-FAB(+): *m*/*z* 615.2 (M-OTf). Elemental Analysis: calcd for $C_{25}H_{30}F_3N_5O_3PtS_2 \cdot 3H_2O$: C, 36.67; H, 4.43; N, 8.55; found: C, 36.61; H, 4.12; N, 8.55.

Complex **5.8** [Pt^{II}(thpy)(bisNHC^{2C6})]OTf

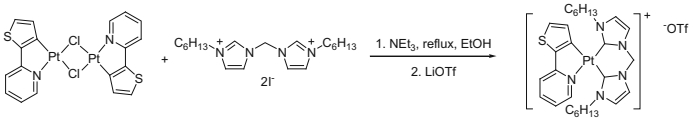

The synthesis is similar to that for **5.1**. Yield: 65 %. ^{1}H NMR (400 MHz, $CDCl_3$, 298 K): δ = 8.34 (d, 1 H, *J* = 5.2 Hz), 7.89 (d, 1 H, *J* = 2.0 Hz), 7.82 (m, 2 H), 7.49 (d, 1 H, *J* = 7.9 Hz), 7.41 (d, 1 H, *J* = 4.6 Hz), 7.08 (d, 1 H, *J* = 2.0 Hz), 7.05 (m, 1 H), 7.01 (d, 1 H, *J* = 2.1 Hz), 6.94 (d, 1 H, *J* = 4.3 Hz), 6.72 (d, 1 H, *J* = 13.0 Hz), 6.00 (d, 1 H, *J* = 12.9 Hz), 4.37 (m, 1 H), 4.15 (m, 1 H), 4.09 (m, 1 H), 3.94 (m, 1 H), 1.68 (m, 4 H), 1.25–1.02 (m, 12 H), 0.79 (m, 6 H). MS-FAB(+): *m*/*z* 671.2 (M-OTf). Elemental Analysis for $C_{29}H_{38}F_3N_5O_3PtS_2 \cdot H_2O$: calcd for C, 41.52; H, 4.81; N, 8.35; found: C, 41.81; H, 4.82; N, 8.37.

5.2.3 Stability Toward Physiological Thiols

5.2.3.1 UV–Vis Absorption Experiment

1× PBS (containing 5 % CH_3CN, v/v) was degassed with nitrogen for 5 min. Then GSH solid (final concentration 2 mM) and **5.1** (final concentration 20 μM) were dissolved in the mixed solvent and the solution was bubbled with nitrogen for another 5 min. UV–Vis absorption was detected at different time points.

5.2.3.2 ^{1}H NMR Experiment

The solution of D_2O (phosphate buffer, 10 mM, pH = 7.4, 10 % d_6-DMSO, v/v) was degassed with nitrogen. Then, **5.1** and 2-fold GSH were added to the solution and the ^{1}H NMR spectra of the mixture were recorded on a Bruker 400 MHz spectrometer at different time points.

5.2.4 Photo-physical Properties and Application in Protein Binding and Cell Imaging

5.2.4.1 Absorption and Emission

Solutions for photo-physical studies were degassed by using a high-vacuum line in a two-compartment cell with five freeze-pump-thaw cycles. The emission quantum yield was measured with $[Ru(bpy)_3](PF_6)_2$ (Φ = 0.062) as reference. The emission lifetime measurements were performed on a Quanta Ray DCR-3 pulsed Nd:YAG laser system. Errors for λ values (±1 nm), τ (±10 %), and Φ (±10 %) are estimated.

5.2.4.2 Protein Binding

Compounds **5.1**, **5.3**, **5.6**, and **5.8** were dissolved in DMSO at room temperature to afford the probe stock solution (10 mM), and then the stock solution was added to 1× PBS:DMSO = 9:1 to a final concentration of 20 μM. BSA solid was added to the diluted solution to get different molar ratios of BSA/complex solution. The resulting solution was shaken well. After 5 min, the emission spectra were recorded.

5.2.4.3 Emission Responses Toward Different Analytes

The Pt(II) complexes were first dissolved in DMSO at room temperature to afford the probe stock solution (10 mM), and then the stock solution was added to 1× PBS:DMSO = 19:1 to a final concentration of 20 μM. The stock solutions of different analytes (BSA, ctDNA, Met, Lys, Asp, Ser, $CaCl_2$, $MgSO_4$, $NaHCO_3$) were prepared to a high concentration based on their solubility. Then aliquots of the stock solutions were added into the solutions of Pt(II) complexes. The resulting solution was shaken well. After 5 min, the emission spectra were recorded. The emission quantum yields and emission lifetimes of **5.3** and **5.8** upon binding with 0.5 equivalent of BSA were measured without degassing the solvent.

5.2.4.4 Absorption-Titration Experiment

Absorption-titration experiment was performed according to a reported procedure [25]. The absorption spectrum of a solution of **5.3** in PBS (with 5 % CH_3CN) was recorded and the solution was added with the aliquots of stock solution of ctDNA (10 mM) and the absorption spectra were recorded after equilibration for 1 min per aliquot until saturation point was almost reached. The binding constant was determined by applying the Scatchard equation:

$$[\mathrm{DNA}]/\Delta\varepsilon_{\mathrm{ap}} = [\mathrm{DNA}]/\Delta\varepsilon + 1/(\Delta\varepsilon \times K_{\mathrm{b}}),$$

where $\Delta\varepsilon_{\mathrm{ap}} = |\varepsilon_{\mathrm{A}} - \varepsilon_{\mathrm{F}}|$ where $\varepsilon_{\mathrm{A}} = A_{\mathrm{obs}}/[\mathrm{complex}]$, and $\Delta\varepsilon = |\varepsilon_{\mathrm{B}} - \varepsilon_{\mathrm{F}}|$ where ε_{B} and ε_{F} correspond to the extinction coefficients of the DNA-bound and DNA-unbound complexes, respectively. Plot of $[\mathrm{DNA}]/\Delta\varepsilon_{\mathrm{ap}}$ versus [DNA] gave a slop equaling to $1/\Delta\varepsilon$ and a *y*-intercept equaling to $1/(\Delta\varepsilon \times K_{\mathrm{b}})$, and K was obtained from the ratio of the slop to the *y*-intercept.

5.2.4.5 Fluorescence Quenching Experiment

Fluorescence quenching experiment was followed with a reported procedure [26]. A solution of BSA (10 μM in PBS containing 5 % CH_3CN) was excited at $\lambda = 280$ nm and the emission spectrum was recorded. Then the solution was added with the aliquots of stock solution of **5.3** (10 mM) and the emission spectra were recorded at the same excitation wavelength after equilibration for 1 min per aliquot until saturation point was almost reached. The binding constant was determined by applying the following equation:

$$\log[(I_0 - I)/I] = \log K + \mathrm{n}\log[Q]$$

where I_0 and I are the fluorescence intensity of BSA without and with **5.3**, respectively; $[Q]$ is the concentration of **5.3**. Plot of $\log[(I_0 - I)/I]$ versus $\log[Q]$ gave the *y*-intercept equaling to $\log K$, and the binding constant can be obtained accordingly.

5.2.4.6 Fluorescence Microscopic Examination

HeLa cells (2×10^5 cells) were seeded in a one chamber slide (Nalgene; Nunc) with culture medium (2 mL per well) and incubated at 37 °C in a humidified atmosphere of 5 % CO_2/95 % air for 24 h. After treating with **5.3** or **5.8** (5 μM) and ER-Tracker™ (1 μM) or Lysotracker® (100 nM) or Mitotracker® (50 nM) for 10 min, cells were directly exposed for fluorescent imaging without removing the old medium. Correlation analysis was done by using ImageJ following a reported procedure [27].

5.2.5 *Anticancer Properties*

5.2.5.1 Cell Lines and Growth Inhibitory Assay

The cell lines were maintained in cell culture media (minimum essential medium for HeLa, MCF-7; and dulbecco's modified eagle medium for SUNE1 and HONE1, Roswell Park Memorial Institute (RPMI) 1640 medium for HCC827 and H1975) supplemented with 10 % fetal bovine serum, 100 U/mL penicillin, and 100 μg/mL streptomycin at 37 °C humidified atmosphere with 5 % CO_2. Cell growth inhibitory effects of the platinum(II) complexes and cisplatin were determined by MTT cytotoxicity assay. Briefly, drug-treated cells were incubated with MTT for 4 h at 37 °C in a humidified atmosphere of 5 % CO_2 and were subsequently lysed in solubilizing solution. Cells were then maintained in a dark, humidified chamber overnight. The formation of formazan was measured by using a microtitre plate reader at 580 nm. Growth inhibition by a drug was evaluated by IC_{50} (concentration of a drug causing 50 % inhibition of cell growth). Each growth inhibition experiment was repeated at least three times and results were expressed as means ± standard deviation (SD).

5.2.5.2 Lipophilicity Determination

Lipophilicity was determined according to a modified procedure [28]. In general, 300 μL saturated *n*-octanol with sodium chloride was mixed with 300 μL aqueous solution with 0.9 % NaCl (w/v), and then the mixture was added with each platinum complex (50 μM) and was further shaken for 1 h at 60 rpm on the shaker. Samples were centrifuged and 50 μL of each phase was added to 300 μL of 70 % HNO_3. The sample was digested overnight and diluted to 50–200-folds with mini-Q water. The content of the platinum complex in each phase was determined by inductively coupled plasma-mass spectrometry (ICP-MS). log *P* was calculated as the logarithmic ratio of the concentrations of the platinum complex in the *n*-octanol and aqueous phases.

5.2.5.3 Cell Transfection and Fluorescence Microscopic Analysis

Cell transfection was performed according to a previously reported procedure [18]. HeLa cells (2×10^5) were cultured in MEM (without antibiotics) supplemented with 10 % FBS in 35-mm glass-bottomed microwell dishes and incubated at 37 °C in a humidified atmosphere of 5 % CO_2/95 % air for 24 h. Then, plasmid DNA of RFP-ER (0.4 μg/mL) and YFP-ER (0.4 μg/mL) was separately transfected into cells following Lipofectamine 2000 protocol. After incubation at 37 °C in a humidified atmosphere of 5 % CO_2/95 % air for another 24 h, the old medium was replaced with fresh MEM containing 5 μM of **5.3**. The cells were then examined with the above-mentioned fluorescence microscopic examination procedure.

5.2.5.4 Western Blot Analysis

HeLa cells (1×10^6 cells) were seeded in 10-cm tissue-culture dishes with culture medium (10 mL per well) and incubated at 37 °C in a humidified atmosphere of 5 % CO_2/95 % air for 24 h, then treated with different concentrations of **5.3** for different time. After washing with cold PBS for three times, cells were lysed in radio-immunoprecipitation assay (RIPA) buffer (500 μL, 1 % Trition X-100, 10 % deoxycholate, 50 mM Tris-HCl, pH 7.5, 150 mM NaCl, 0.1 % SDS, 0.1 mm PMSF, 10 μg/mL leupeptin, 10 μg mL^{-1} aprotinin) at 0 °C. After centrifugation, the supernatants were collected. The cellular protein content was quantified by the DC Protein Assay (Bio-Rad). For detection, samples (15–45 μg/lane) were fractionated on a 12.5 % SDS–PAGE in a Tris-Glycine running buffer and blotted on polyvinylidene fluoride (PVDF) membranes. The PVDF membranes were blocked overnight at room temperature in TBST containing 5 % BSA powder. Afterward, the blots were incubated at room temperature for an hour with the primary antibody, which was diluted in TBST containing 5 % BSA powder. After washing with TBST three times, the membranes were then incubated with the respective secondary antibody for 2 h. Detection was performed by using the chemiluminescence procedure (ECL, Amersham).

5.2.5.5 Mitochondrial Membrane Depolarization Assay

HeLa cells (2×10^5, 2 mL MEM) were seeded in 6-well plated and incubated at 37 °C in a humidified atmosphere of 5 % CO_2/95 % air for 24 h. Then the cells were treated with **5.3** (5 or 10 μM) for 2 h. Afterward, the media were removed and the cells were washed with PBS for 3 times. The cells were stained with JC-1 (5 μM) for another 20 min. After removing the old media and washing with PBS for 3 times, the cells in PBS were observed under fluorescence microscope. For positive control, carbonyl cyanide 3-chlorophenylhydrazone (CCCP, 50 μM) and JC-1 (5 μM) were coincubated with HeLa cells for 20 min and examined with fluorescence microscope.

5.2.5.6 Determination of Phototoxicity

Phototoxicity was determined according to a modified procedure [29]. Cells were seeded in a 96-well flat-bottomed microplate at 4×10^3 cells per well in 100 μL MEM containing 10 % FBS and incubated for 24 h in a humidified atmosphere of 5 % CO_2/95 % air. Complexes **5.6**, **5.7,** and **5.8** were added to each well with serial dilution. The cells were incubated in a humidified atmosphere of 5 % CO_2/95 % air in the dark for 1 h and then exposed to broadband visible light (2.8 mW/cm^2) for 1 h. After further incubation in humidified atmosphere of 5 % CO_2/95 % air in the dark for 22 h, the cell viability was determined according to the above-mentioned MTT assay.

5.3 Results and Discussion

5.3.1 Synthesis of the Complexes

The chemical structures of the cyclometalated [Pt^{II}(C^N)bis(NHC)]OTf complexes **5.1**–**5.8** are shown in Fig. 5.1. The HC^N ligands include 2-phenylpyridine (Hppy), benzo[*h*]quinolone (Hbzq), and 2-(thiophen-2-yl)pyridine (Hthpy). The bis(NHC) ligands have alkyl substituents with varying chain length, $-(CH_2)_nCH_3$ ($n = 0, 3, 5$), aiming to adjust lipophilicity of the complexes hence tuning binding affinity with biomolecules. Complexes **5.1**–**5.8** were prepared by refluxing $[Pt(C^N)(\mu\text{-}Cl)]_2$ with bis(imidazolium) salts in the presence of base with yields of 65–80 %. The ^1H–^1H COSY and ^1H–^1H NOESY NMR spectroscopy experiments were further performed for complex **5.1** (Figs. 5.2 and 5.3). It is noteworthy that the ^1H signals of NHC ligand are concentration- and temperature dependent. Upon increase of the concentration from 0.5 to 15 mM or increase the temperature from 25 to 80 °C, the ^1H signal of methylene of bis(NHC) shifted significantly (Figs. 5.4 and 5.5). As the

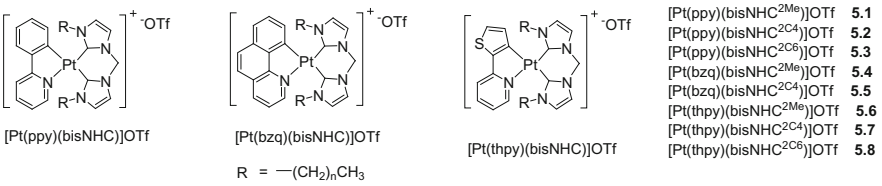

Fig. 5.1 Chemical structures of the Pt(II) complexes **5.1–5.8**

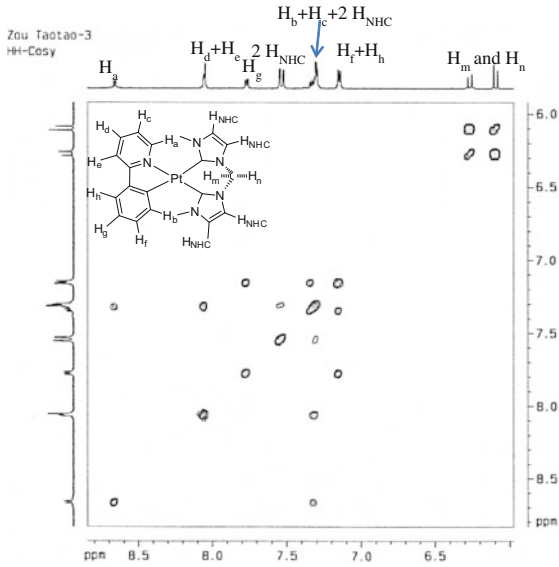

Fig. 5.2 ^1H–^1H cosy NMR (500 MHz in d_4-MeOH, 298 K) spectrum of **5.1**. Reproduced with the permission from The Royal Society of Chemistry [30]

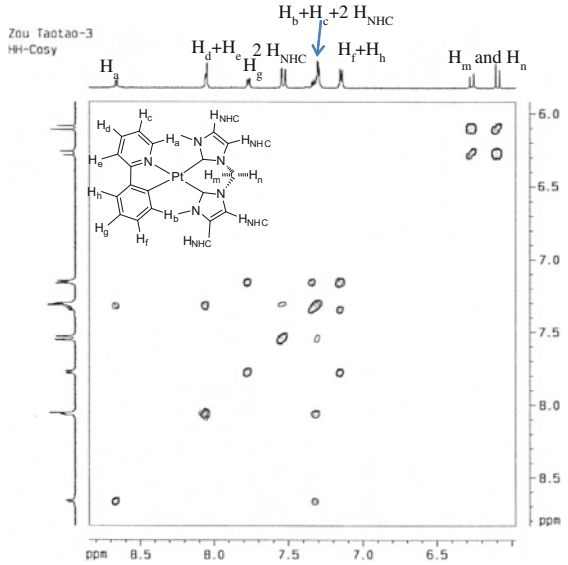

Fig. 5.3 $^{1}H–^{1}H$ noesy NMR (500 MHz in d4-MeOH, 298 K) spectrum of 5.1. Reproduced with the permission from The Royal Society of Chemistry [30]

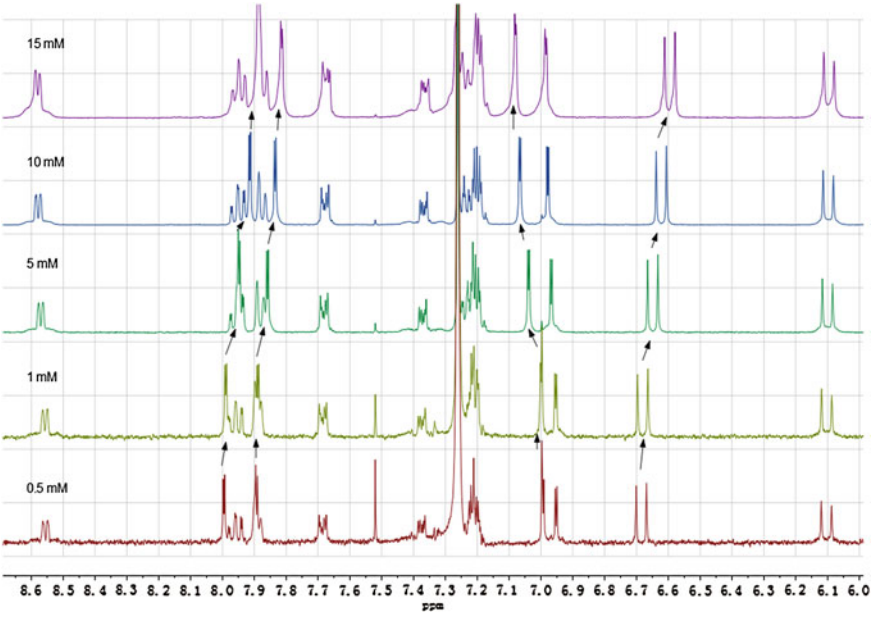

Fig. 5.4 Concentration-dependent 1H NMR (400 MHz in CDCl3, 298 K) spectrum of 5.1 at 0.5, 1, 5, 10, and 15 mM. Reproduced with the permission from The Royal Society of Chemistry [30]

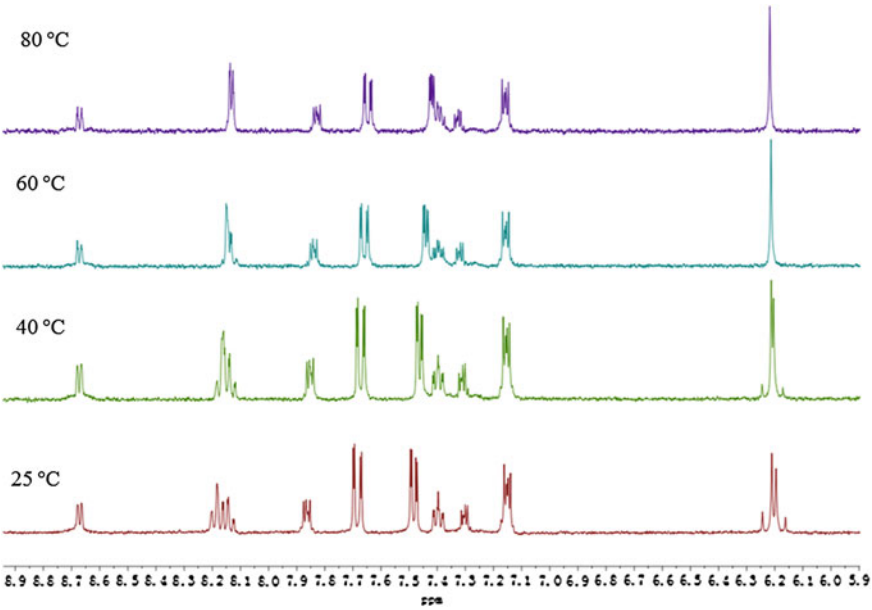

Fig. 5.5 Temperature-dependent ^{1}H NMR (400 MHz in d_6-DMSO, 298 K) spectrum of **5.1** at 25, 40, 60, and 80 °C. Reproduced with the permission from The Royal Society of Chemistry [30]

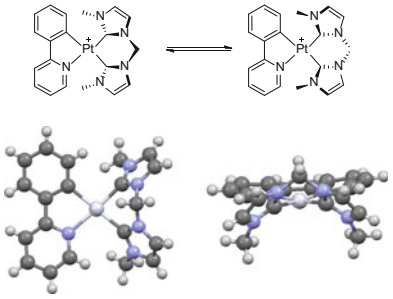

Fig. 5.6 Equilibrium of two conformations of the platinum (II) complexes. The crystal structure of $[Pt^{II}(ppy)(bisNHC^{2Me})]^{+}$ solved by Tsubomura and coworkers is shown [22]. Reproduced with the permission from The Royal Society of Chemistry [30]

two NHC planes are not parallel to the planar $[Pt(C\text{^}N)C_{NHC}\text{^}C_{NHC}]$ plane and the plane is asymmetric due to the asymmetric C^N ligand, the methylene of bisNHC could be on the upside or downside of $[Pt(C\text{^}N)C_{NHC}\text{^}C_{NHC}]$ plane (or it is an equilibrium), which could result in different ^{1}H NMR signal (Fig. 5.6). Such effects could be predominant since planar Pt(II) complexes tend to aggregate upon increase of concentration, and the higher temperature could cause faster conformation changes. The crystal structure solved by Tsubomura and coworkers further supports this explanation [22].

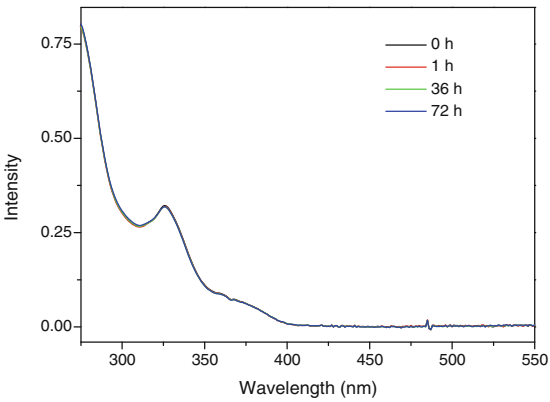

Fig. 5.7 UV–Vis absorption spectra of **5.1** (20 μM) in PBS (containing 5 % CH_3CN v/v, 2 mM GSH) at different time points. Reproduced with the permission from The Royal Society of Chemistry [30]

5.3.2 Stability Test

All the platinum(II) complexes are soluble in various organic solvents including DMF, DMSO, MeOH, CH_3CN, $CHCl_3$, and CH_2Cl_2. Their stability toward physiological thiols was investigated. For example, complex **5.1** (20 μM) in phosphate-buffered saline (PBS, containing 5 % CH_3CN, v/v) with excess glutathione (GSH, 2 mM) has no change in the UV–Vis absorption spectra in 72 h (Fig. 5.7); the ^{1}H NMR spectra of the mixture of complex **5.1** in D_2O (phosphate buffer, pH 7.4, 10 % d_6-DMSO, v/v, GSH 2-fold excess, Fig. 5.8) also did not change after 72 h of incubation.

5.3.2.1 Photo-Physical Properties and Cell Imaging Studies

The cyclometalated platinum(II) complexes **5.1**–**5.8** are luminescent in solid state and in degassed solutions. The absorption spectra of CH_2Cl_2 solutions of **5.1**, **5.4,** and **5.6** (Fig. 5.9) show intense absorptions from 250 nm to 350 nm that can be attributed to singlet intraligand (^{1}IL) transitions ($^1\pi$–π^*) of the C^N ligands [29, 31]. The absorption bands at 375 nm of **5.1** and 400 nm of **5.4** and **5.6** are assigned to intraligand transitions ^{1}LC (π–π^*) mixed with singlet metal-to-ligand charge transfer transitions (^{1}MLCT) Pt(d) → C^N (π^*) [22, 31, 32]. Complexes **5.1**, **5.4,** and **5.6** in CH_2Cl_2 display vibronic-structured emission spectra with emission maximum at 486–517 nm (Φ = 0.051, τ = 1.7 μs), 477–505 nm (Φ = 0.017, λ = 2.8 μs), and 562–605 nm (Φ = 0.24, τ = 29.2 μs), respectively (Fig. 5.9; Table 5.1). The alkyl (R) chain length of the bis(NHC) ligand does not significantly change the photo-physical properties (Table 5.1).

Complexes **5.1**, **5.3**, **5.6**, and **5.8** are weakly emissive in aerated PBS (containing 1 % DMSO, v/v). The addition of bovine serum albumin (BSA) to solutions of **5.3** and **5.8** could give a strong green emission and an orange emission, respectively, with <1 min (Figs. 5.10 and 5.11). The emission intensity starts to level off after

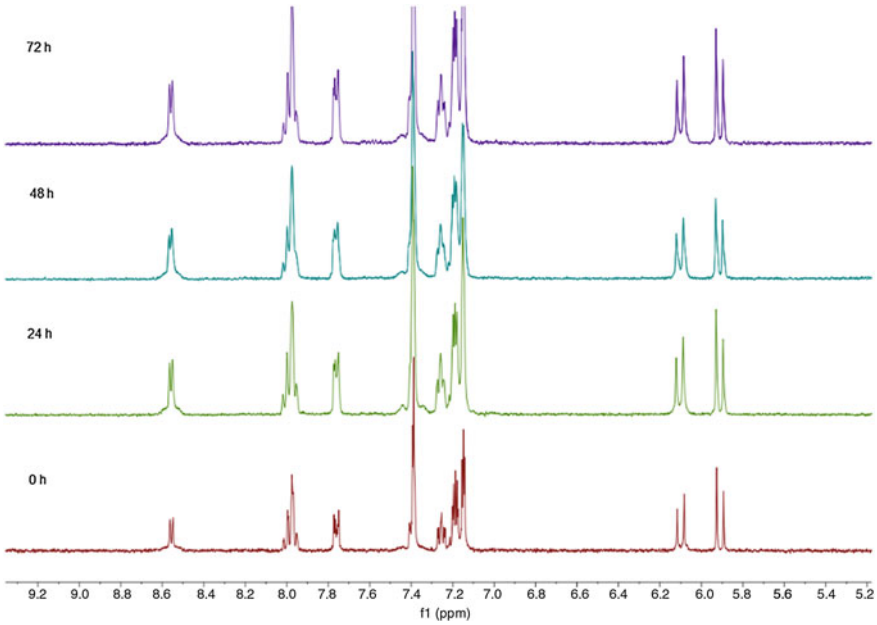

Fig. 5.8 ^{1}H NMR spectra of **5.1** in D_2O (10 mM phosphate buffer, pH 7.4, 10 % d_6-DMSO v/v) with 2 molar excess of GSH at different time points. Reproduced with the permission from The Royal Society of Chemistry [30]

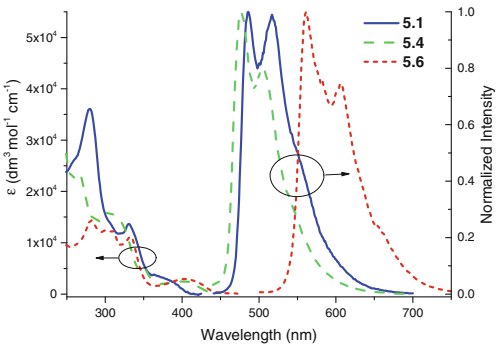

Fig. 5.9 Absorption and emission spectra of **5.1**, **5.4,** and **5.6** in degassed CH_2Cl_2. Reproduced with the permission from The Royal Society of Chemistry [30]

addition of 0.5 equivalent BSA, showing 11-fold and 12-fold elevation for complexes **5.3** and **5.8**, respectively. By contrast, only 1.3-fold and 1.5-fold elevation in emission intensity is observed for complexes **5.1** and **5.6**, respectively. It is reasoned that complexes **5.3** (log P = 2.15) and **5.8** (log P = 2.14) are more lipophilic than the corresponding **5.1** (log P = 0.69) and **5.6** (log P = 0.68), therefore the increase in the emission intensity of **5.3** or **5.8** could be attributed to the hydrophobic interactions that may restrict the vibrational motion of the Pt(II)

Table 5.1 Summary of emission data

	λ_{max} (nm)	Quantum yield	(μs)
5.1	486, 517	0.051	1.7
5.2	486, 516	0.078	2.1
5.3	485, 517	0.058	1.7
5.4	477, 505	0.017	2.8
5.5	476, 504	0.023	4.4
5.6	562, 605	0.24	29.2
5.7	561, 605	0.22	26.7
5.8	560, 604	0.22	30.3

Reproduced with the permission from The Royal Society of Chemistry [30]

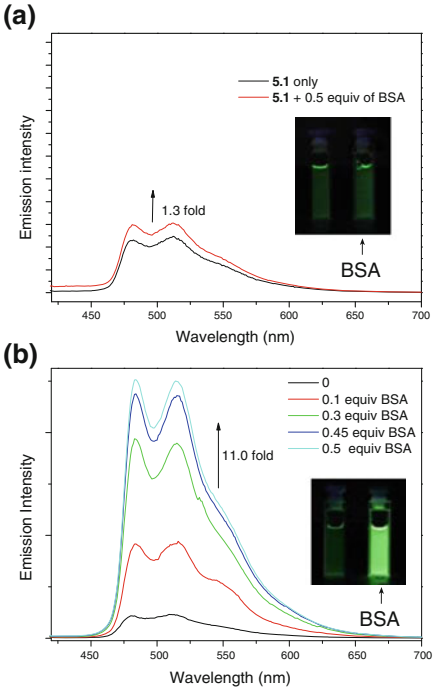

Fig. 5.10 Emission spectra of **5.1** (**a**), **5.3** (**b**), in PBS (containing 10 % DMSO, v/v) before and after adding BSA. Insets: images of the platinum (II) complexes with/without BSA under UV irritation. Reproduced with the permission from The Royal Society of Chemistry [30]

complex and/or to the shielding effect by the protein scaffold thus avoiding oxygen quenching of the platinum(II) complexes [33, 34]. No emission elevation was found in the presence of amino acids and biological ions (Fig. 5.12).

DNA has been accounted as the major target of many Pt(II) complexes in literatures. However, complex **5.3** did not show tight binding interactions with DNA. The 123 bp DNA ladder treated with equal (base pairs) molar of **5.3** did not show retarded mobility in gel mobility shift experiment (Fig. 5.13a). The binding constant of **5.3** with ctDNA was 1.4×10^4 M^{-1} as determined by Uv–Vis

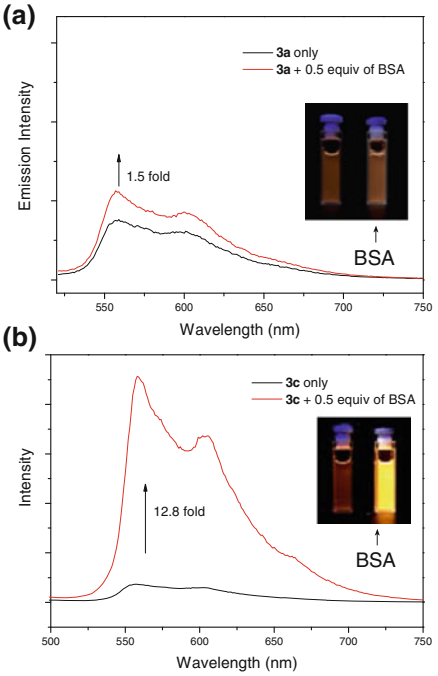

Fig. 5.11 Emission spectra of **5.6** (**a**), **5.8** (**b**), in PBS (containing 10 % DMSO, v/v) before and after adding BSA. *Insets* Images of the platinum (II) complexes with/without BSA under UV irritation. Reproduced with the permission from The Royal Society of Chemistry [30]

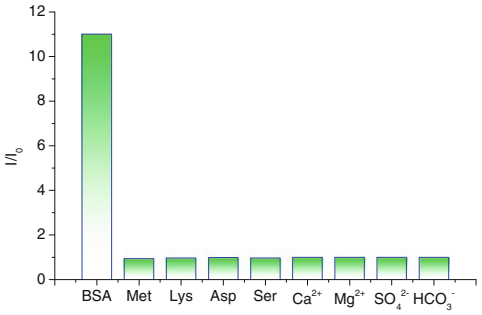

Fig. 5.12 Peak emission intensity increasing ratios of **5.3** (20 μM) toward different analytes. The concentration of BSA is 10 μM. The concentrations of other analytes are 1 mM. Reproduced with the permission from The Royal Society of Chemistry [30]

absorption-titration experiments (Fig. 5.13b), suggestive of a weak interaction of **5.3** with DNA. Emission titration experiment also indicates that the emission intensity of **5.3** was only increased by 1.6-fold even when 25 equivalents of DNA base pairs were added (Fig. 5.14). As a comparison, emission quenching experiment showed that the binding constant of **5.3** with BSA was 4.6×10^5 M^{-1} (Fig. 5.15), being much higher than that of DNA binding. As a result, complex **5.3** shows higher affinity to BSA than DNA.

In view of the favorable stability and emission elevation of the platinum(II) complexes upon binding with BSA, the subcellular localization of complexes **5.3** and **5.8** was investigated by fluorescence microscope. Upon treating human cervical

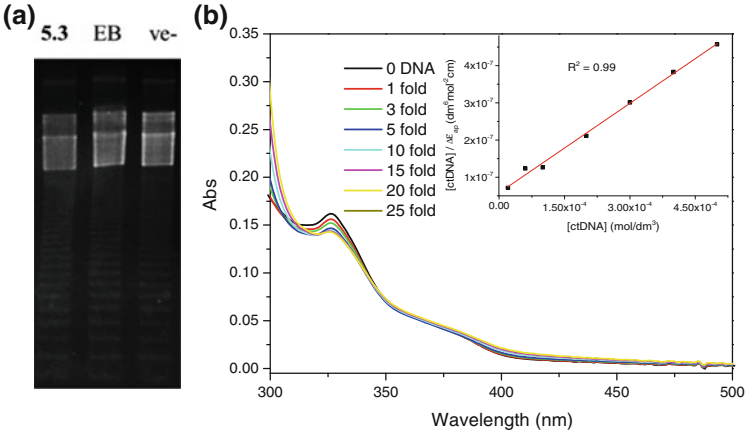

Fig. 5.13 **a** Gel electrophoresis of 123 bp DNA ladder (50 μM base pairs) in 1.5 % (w/v) agarose gel showing the mobility of the DNA in the absence (*last lane*, ve-), or the presence of **5.3** (*first lane*) and ethidium bromide (EB, *middle lane*) in a 1:1 molar ratio. **b** UV–Vis spectral changes of **5.3** in PBS (containing 5 % CH_3CN, v/v) with increasing concentration of ctDNA at 292.8 K. *Inset* Plots of [ctDNA]/$\Delta\varepsilon_{ap}$ versus [ctDNA]. Absorbance was monitored at 326 nm. Reproduced with the permission from The Royal Society of Chemistry [30]

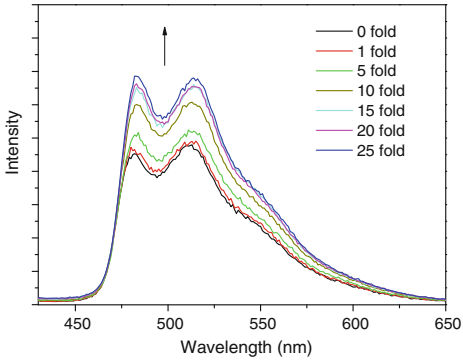

Fig. 5.14 Emission spectra of **5.3** (20 μM, in PBS containing 5 % CH_3CN, v/v) with increasing concentrations of ctDNA. Reproduced with the permission from The Royal Society of Chemistry [30]

epithelial carcinoma (HeLa) cells with **5.3** (5 μM) for only 10 min, a strong green emission in cytoplasm was developed. The specific subcellular location of **5.3** was examined by costaining the organelles with specific fluorescence probes. As shown in Fig. 5.16, complex **5.3** specifically localizes in ER where it is stained with ER-Tracker^{TM}. The Pearson's correlation coefficient *R* for colocalization of **5.3** and the ER-Tracker^{TM} is as high as 0.97. There was no background fluorescence interference in the presence of **5.3** or ER-Tracker^{TM} only at the respective excitation wavelength (Fig. 5.17). No significant colocalization was identified for **5.3** with

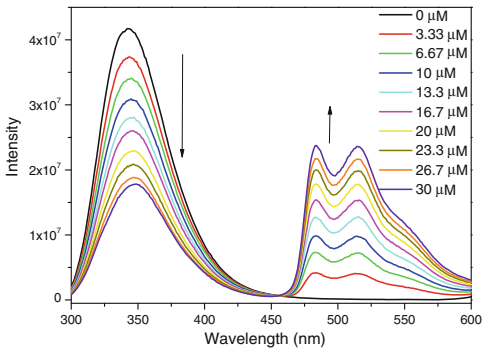

Fig. 5.15 Emission spectral changes of BSA (10 μM, in PBS containing 5 % CH_3CN, v/v) with increasing concentration of **5.3**. The concentration of **5.3** was varied from 0.0 to 30 μM. λ_{ex} = 280 nm. Reproduced with the permission from The Royal Society of Chemistry [30]

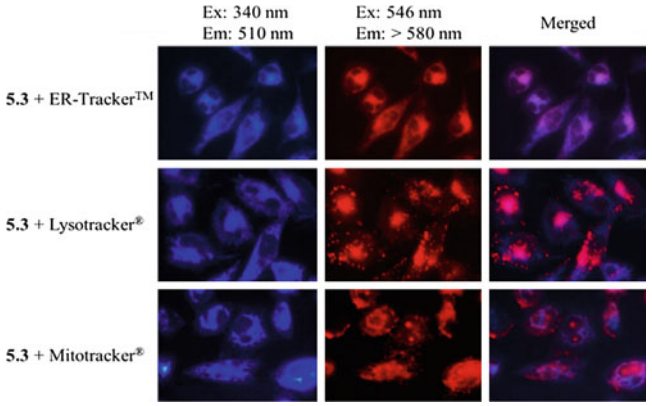

Fig. 5.16 Fluorescence microscopic analysis of **5.3** with ER-Tracker™ (*top*), Lysotracker® (*middle*), and Mitotracker® (*bottom*). Complex **5.3** was excited at 340 nm with emission filter of 510 nm (*blue pseudocolor*). ER-tracker™, Lysotracker®, and Mitotracker® were excited at 546 nm with emission filter of >580 nm. Reproduced with the permission from The Royal Society of Chemistry [30]

lysosome-specific Lysotracker® and mitochondria-specific Mitotracker® probes (Fig. 5.16). The specific subcellular location was further confirmed by using HeLa cells transfected with an ER-resident protein that is tagged with yellow fluorescent protein (YFP-ER) or monomeric red fluorescent protein (mRFP-ER). Both fluorescent proteins showed significant colocalization with **5.3** with Pearson's correlation coefficient R = 0.92 and 0.98 in YFP- and mRFP-tagged HeLa cells, respectively (Fig. 5.18). Complex **5.8** could specifically target ER according to the similar colocalization analysis (Fig. 5.19).

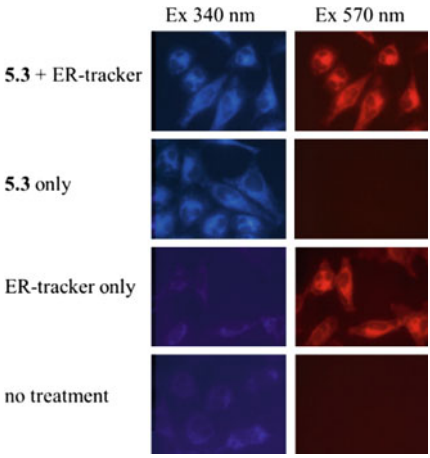

Fig. 5.17 Fluorescence microscopic images of HeLa cells incubated with **5.3** + ER-Tracker™, **5.3** only, ER-Tracker™ only, or MEM only at different excitation wavelength. Reproduced with the permission from The Royal Society of Chemistry [30]

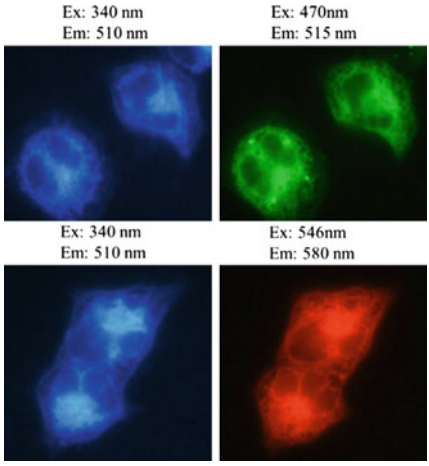

Fig. 5.18 Fluorescence microscopic images of transfected HeLa cells after being treated with 5 μM of **5.3** for 10 min. Top: images of **5.3** treated HeLa cells with an ER-resident protein tagged yellow fluorescent protein (YFP-ER); bottom: images of **5.3** treated HeLa cells with monomeric red fluorescent protein (mRFP). The respective excitation and emission condition are shown. Reproduced with the permission from The Royal Society of Chemistry [30]

5.3.3 Anticancer Properties

The complexes **5.1**–**5.8** are cytotoxic to various cancer cell lines including HeLa, nasopharyngeal carcinoma (HONE1, SUNE1), breast cancer (MCF-7), and lung carcinoma (HCC827, H1975), with IC_{50} ranging from 0.45 ± 0.11 to 52.2 ± 5.4 μM, most of which are more potent than that of cisplatin (2.75 ± 0.42 to 27.0 ± 5.0 μM). Among these platinum(II) complexes, **5.3** displayed the highest cytotoxicity toward these cancer cell lines (0.45 ± 0.11–0.72 ± 0.11 μM, Table 5.2).

As mentioned above, complex **5.3** could selectively localize to ER domain. Then experiments were performed to examine whether the accumulation of **5.3** in ER domain could induce ER-stress by Western blot assay. After treating HeLa cells by

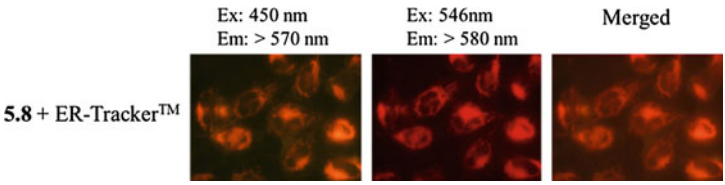

Fig. 5.19 Fluorescence microscopic images of HeLa cells incubated with **5.8** and ER-Tracker™ (R = 0.90). Reproduced with the permission from The Royal Society of Chemistry [30]

Table 5.2 72 h cytotoxicity IC_{50} values (μM) of **5.1**–**5.8** in human carcinoma cell lines of HeLa, HONE1, SUNE1, MCF-7, HCC827, and H1975

	HeLa	HONE1	SUNE1	MCF-7	HCC827	H1975
5.1	3.79 ± 1.05	2.55 ± 0.35	3.07 ± 0.99	52.2 ± 5.4	12.0 ± 1.72	5.58 ± 1.34
5.2	1.39 ± 0.10	1.15 ± 0.06	1.47 ± 0.07	3.49 ± 053	1.76 ± 0.40	1.78 ± 0.57
5.3	0.68 ± 0.30	0.52 ± 0.05	0.62 ± 0.04	0.66 ± 0.03	0.72 ± 0.11	0.45 ± 0.11
5.4	2.54 ± 0.46	1.41 ± 0.03	2.23 ± 0.13	10.8 ± 1.78	8.92 ± 2.61	4.41 ± 1.79
5.5	0.91 ± 0.10	0.83 ± 0.20	1.35 ± 0.09	1.52 ± 0.10	1.11 ± 0.15	0.64 ± 0.02
5.6	22.9 ± 4.32	2.14 ± 0.55	2.54 ± 0.78	51.2 ± 8.8	21.2 ± 5.4	22.5 ± 0.5
5.7	2.14 ± 0.56	1.14 ± 0.05	1.74 ± 0.56	2.91 ± 0.07	2.50 ± 0.51	1.76 ± 0.85
5.8	1.27 ± 0.32	1.10 ± 0.03	1.91 ± 0.39	1.59 ± 0.17	1.42 ± 0.04	0.80 ± 0.02
cisplatin	10.9 ± 2.3	2.75 ± 0.42	9.59 ± 5.26	17.9 ± 7.8	27.0 ± 3.2	27.0 ± 5.0

Reproduced with the permission from The Royal Society of Chemistry [30]

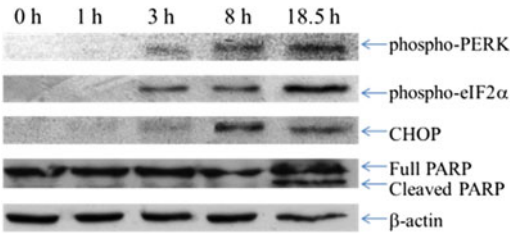

Fig. 5.20 Western blot analysis of ER-stress-related proteins after treating HeLa cells with **5.3** for different time. Reproduced with the permission from The Royal Society of Chemistry [30]

5.3 (3 μM) for 1–18.5 h, the expressions of phosphorylated RNA-dependent protein kinase-like endoplasmic reticulum kinase (PERK), phosphorylated eukaryotic initiation factor 2α (eIF2α), and C/EBP homologous protein (CHOP) all were significantly upregulated (Fig. 5.20), indicative of ER-stress [16, 35]. In addition, the apoptosis-related poly-ADP ribose polymerase (PARP) and caspases 3, 7, 9 were all cleaved (Fig. 5.21) after the cells were incubated with **5.3** for 24 h, suggesting that **5.3** could induce apoptosis of HeLa cells.

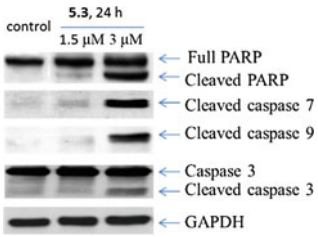

Fig. 5.21 Western blot analysis of ER-stress-related proteins after treating HeLa cells with **5.3** for different time. Reproduced with the permission from The Royal Society of Chemistry [30]

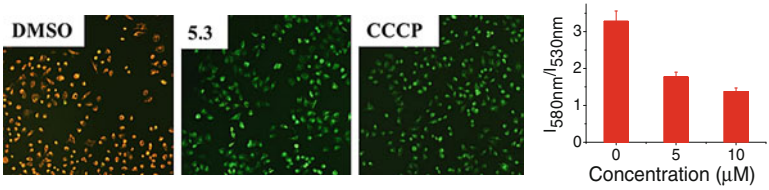

Fig. 5.22 JC-1 staining of HeLa cells. *Left* HeLa cells were treated with DMSO vehicle, **5.3** (5 μM) and CCCP (carbonyl cyanide *m*-chlorophenyl hydrazine, a mitochondrial membrane potential disrupter, 50 μM) for 2 h, and examined using fluorescence microscope with excitation at 470 nm. *Right* JC1 fluorescence intensity ratio of I_{580nm}/I_{530nm} after treatment of HeLa cells with **5.3**. Reproduced with the permission from The Royal Society of Chemistry [30]

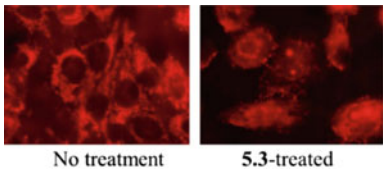

Fig. 5.23 Fluorescence microscopic images of HeLa cells treated without (*left*) or with (*right*) 5 μM of **5.3**. HeLa cells were stained with mitochondria-specific Mitotracker®. Reproduced with the permission from The Royal Society of Chemistry [30]

The disruption of active mitochondria is a distinctive feature of the early stages of apoptosis [36]. In order to confirm that whether **5.3**-induced apoptosis is associated with mitochondria dysfunction, the mitochondria membrane potential was analyzed by using JC1 staining. JC1 is a green fluorescent cationic dye which could specifically accumulate in the inner membrane of normal mitochondria with a transmembrane potential, forming orange fluorescent aggregates [37]. As depicted in Fig. 5.22, the untreated HeLa cells showed orange fluorescence after JC1 staining but cells treated with **5.3** (5 or 10 μM) for 2 h resulted in green fluorescence of JC1. The intensity ratios of orange to green fluorescence (I_{580nm}/I_{530nm}) were quantified to be 3.28 ± 0.28, 1.77 ± 0.13, and 1.37 ± 0.10 for treatment by **5.3** at 0, 5, and

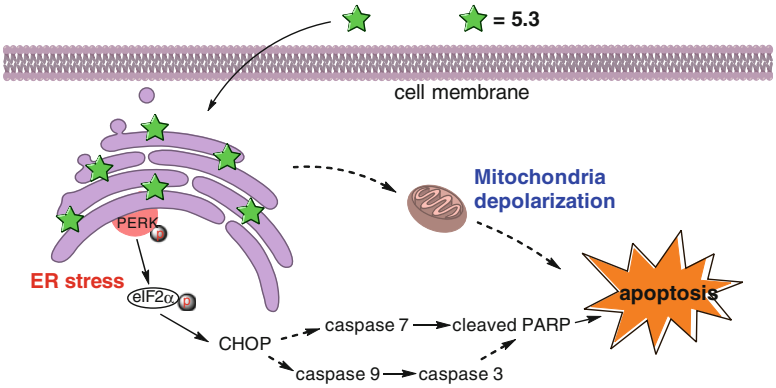

Fig. 5.24 Proposed anticancer pathway by **5.3**. Reproduced with the permission from The Royal Society of Chemistry [30]

10 μM, respectively. Furthermore, distinct mitochondria swelling could be observed after **5.3** treatment (Fig. 5.23). Therefore, complex **5.3** treatment is able to induce mitochondria dysfunction. Collectively, complex **5.3** selectively targets ER and induces ER-stress and mitochondria dysfunction, subsequently leading to apoptotic cell death (Fig. 5.24).

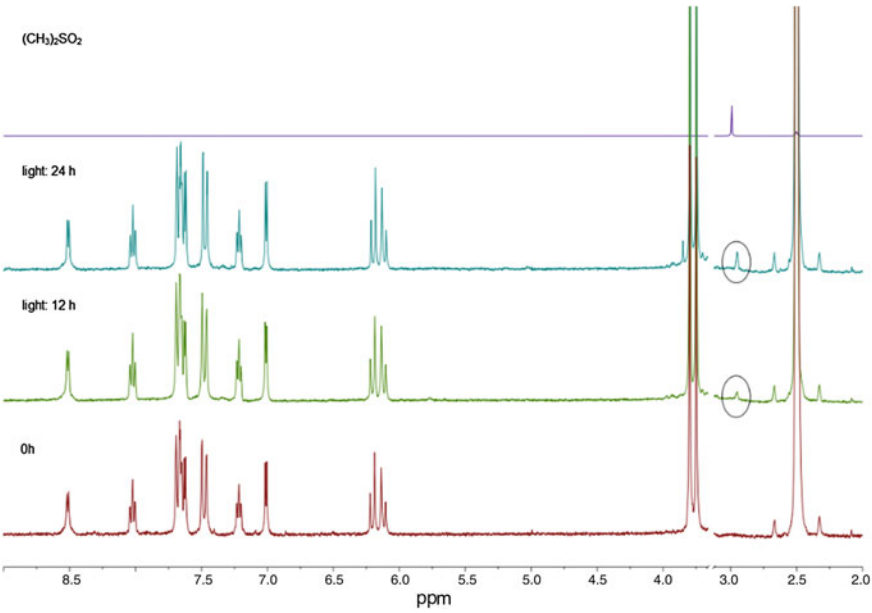

Fig. 5.25 ^{1}H NMR spectra of **5.6** in d_6-DMSO after exposing to 2.8 mW/cm^2 for different time. Reproduced with the permission from The Royal Society of Chemistry [30]

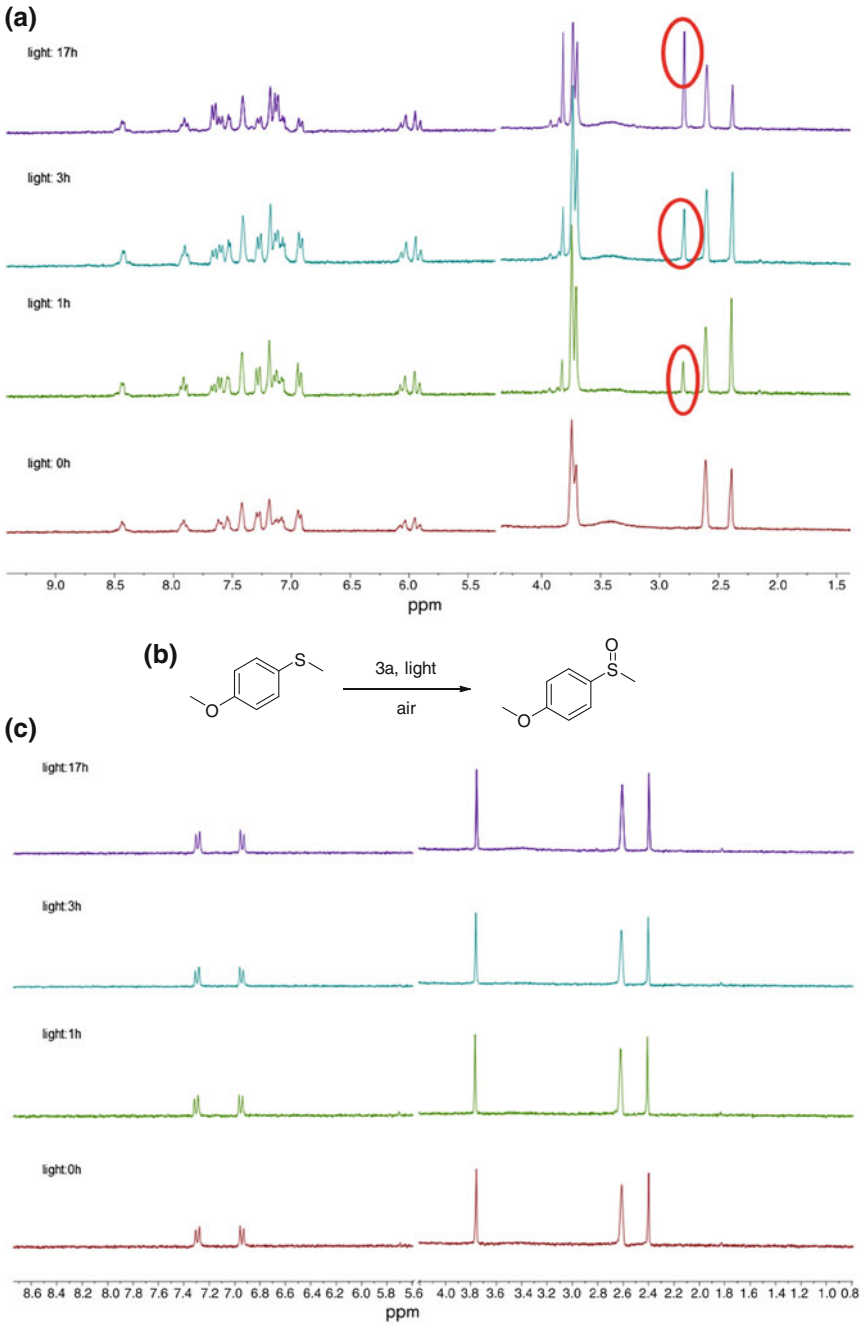

Fig. 5.26 **a** ^{1}H NMR spectra of the mixture of **5.6** and (4-methoxyphenyl)(methyl)sulfane in D_2O (pH 7.4, phosphate buffer, 10 % d_6-DMSO) after exposing to 2.8 mW/cm^2 of visible light for different time. **b** Proposed photo-oxidation reaction. **c** ^{1}H NMR spectra of (4-methoxyphenyl)(methyl)sulfane in D_2O (pH 7.4, phosphate buffer, 10 % d_6-DMSO) after exposing to 2.8 mW/cm^2 of visible light for different time. Reproduced with the permission from The Royal Society of Chemistry [30]

5.3.4 Phototoxicities

Since complexes **5.6**–**5.8** have long-lived emissive excited states and absorb visible spectral light, they could possibly induce photo-cytotoxicity to cancer cells. The photo-stability was firstly tested by using ^{1}H NMR spectrometry. After exposing **5.6** to visible light ($\lambda > 400$ nm, 2.8 mW/cm^2) in d_6-DMSO for 12 and 24 h, the chemical shifts of the initial ^{1}H signals did not change (Fig. 5.25), but a new peak at around 3.0 ppm developed with time. The peak is attributed to the oxidized product, $(CH_3)_2SO_2$. This result is suggestive of high photo-stability of **5.6** and the efficient photo-oxidation of DMSO via $^1O_2$ intermediate. It is shown that 1-methoxy-4-(methylsulfanyl)benzene could be readily oxidized to form 1-methoxy-4-(methylsulfinyl)benzene by **5.6** in D_2O (phosphate buffer, pH 7.4, containing 10 % d_6-DMSO, v/v) under the same conditions of light irritation based on ^{1}H NMR measurement (Fig. 5.26). Notably, it was found that after irradiation of low concentration of **5.6** (20 μM in PBS) under the same light condition for 24 h, the emission peak intensity gradually decreased by 58 %, and the UV–Vis absorption spectra also changed with 48 % decrease of absorbance at 400 nm (Fig. 5.27); these results reveal that the photo-oxidation was accompanied by the decomposition of **5.6** when at low micromolar concentration.

Subsequently, the photo-cytotoxicity of **5.6**–**5.8** was examined by MTT assays. After treatment of HeLa cells with these complexes at different concentrations for 1 h to allow uptake, and then exposing cells under 2.8 mW/cm^2 visible light for

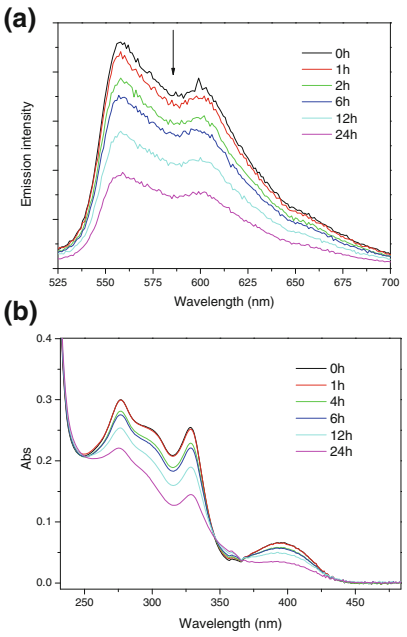

Fig. 5.27 Emission spectra (**a**) and UV–Vis absorption spectra (**b**) of **5.6** (20 μM, in PBS containing 5 % CH_3CN, v/v) after exposing to visible light ($\lambda > 400$ nm, 2.8 mW/cm^2) for 24 h. $\lambda_{ex} = 400$ nm for emission spectra. Reproduced with the permission from The Royal Society of Chemistry [30]

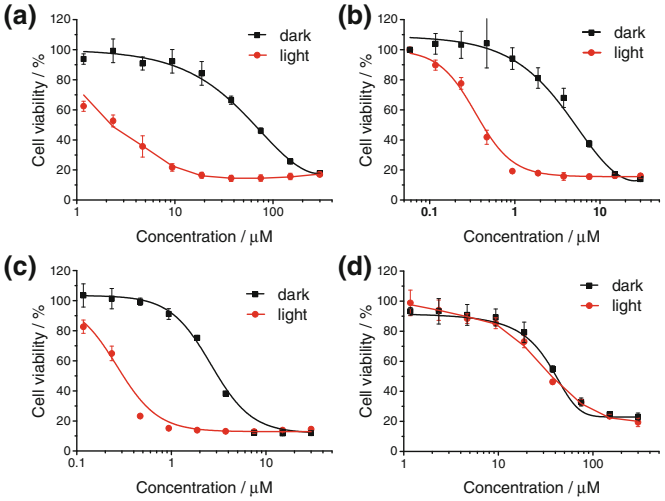

Fig. 5.28 HeLa cell viability after treatment with **5.6** (**a**), **5.7** (**b**), **5.8** (**c**), and cisplatin (**d**) under light or dark. Reproduced with the permission from The Royal Society of Chemistry [30]

another 1 h, the results of total 24-h MTT assays showed that the IC_{50} values of **5.6**, **5.7,** and **5.8** were decreased by 28.2-fold, 13.7-fold, and 10.0-fold, respectively, upon photo-irradiation in comparison with those measured under the dark conditions (Fig. 5.28a–c; Table 5.3). There was no significant difference in IC_{50} values identified for cisplatin-treated HeLa cells in the presence/absence of light under the same condition (0.84-fold, Fig. 5.28d). Complexes **5.6**–**5.8** also show photo-cytotoxicity toward other cancer cell lines of HONE1, MCF-7, and B16-F10 with IC_{50} values decreased by 5.6- to 33.1-fold upon light irradiation condition (Table 5.3).

5.4 Conclusion

To conclude, the highly luminescent cyclometalated platinum(II) complexes containing both C^N and bis(NHC) ligands were synthesized and characterized. The Pt(II) complexes can selectively bind to hydrophobic proteins such as BSA but not DNA and can specifically localize to ER domain. They are also cytotoxic to various cancer cells, which is ascribed to apoptotic cell death induced by ER-stress and mitochondria dysfunction based on Western blot analysis and mitochondria depolarization experiment. Some of these complexes with long-lived excited states and emission high quantum yield also show photo-cytotoxicity to cancer cells.

Table 5.3 24 h cytotoxicity IC_{50} (μM) of **5.6–5.8** in the absence/presence of light

	HeLa			MCF-7			HONE 1			B16-F10		
	Dark	Light	Ratio	Dark	Light	Ratio	Dark	Light	Ratio	Dark	Light	Ratio
5.6	59.6 ± 5.4	2.11 ± 0.70	28.2	152.6 ± 23.9	7.25 ± 0.99	21.0	54.0 ± 10.0	1.63 ± 0.84	33.1	59.4 ± 12.1	5.63 ± 0.45	10.6
5.7	5.33 ± 0.86	0.39 ± 0.04	13.7	10.3 ± 1.0	0.50 ± 0.05	20.6	9.70 ± 2.58	0.61 ± 0.08	15.9	3.04 ± 0.36	0.51 ± 0.07	6.0
5.8	2.92 ± 0.02	0.29 ± 0.03	10.0	5.52 ± 0.16	0.40 ± 0.01	13.8	4.45 ± 0.73	0.41 ± 0.15	10.1	2.18 ± 0.54	0.39 ± 0.03	5.6
cisplatin	31.8 ± 2.1	37.7 ± 3.8	0.84	123.1 ± 11.8	122.2 ± 17.1	1.01	39.9 ± 8.41	55.5 ± 24.7	0.72	100.1 ± 11.7	92.4 ± 12.4	1.08

The ratios of $IC_{50,\ dark}/IC_{50,\ light}$ are also shown. $IC_{50,\ dark}$ and $IC_{50,\ light}$ refer to the 24 h cytotoxicity IC_{50} in the absence and presence of light, respectively. Reproduced with the permission from The Royal Society of Chemistry [30]

References

1. Meggers E (2007) Exploring biologically relevant chemical space with metal complexes. Curr Opin Chem Biol 11(3):287–292
2. Haas KL, Franz KJ (2009) Application of metal coordination chemistry to explore and manipulate cell biology. Chem Rev 109(10):4921–4960
3. Liu H-K, Sadler PJ (2011) Metal complexes as DNA intercalators. Acc Chem Res 44(5):349–359
4. Gill MR, Thomas JA (2012) Ruthenium(II) Polypyridyl complexes and DNA–from structural probes to cellular imaging and therapeutics. Chem Soc Rev 41(8):3179–3192
5. Wang X, Guo Z (2013) Targeting and delivery of platinum-based anticancer drugs. Chem Soc Rev 42(1):202–224
6. Ho Y-P, Au-Yeung SCF, To KKW (2003) Platinum-based anticancer agents: innovative design strategies and biological perspectives. Med Res Rev 23(5):633–655
7. Jung Y, Lippard SJ (2007) Direct cellular responses to platinum-induced DNA damage. Chem Rev 107(5):1387–1407
8. Cummings SD (2009) Platinum complexes of terpyridine: interaction and reactivity with biomolecules. Coord Chem Rev 253(9–10):1495–1516
9. Liu H-K, Sadler PJ (2012) Interactions of metallodrugs with DNA. In: NMR of biomolecules. Wiley-VCH Verlag GmbH & Co. KGaA, pp 282–296. doi:10.1002/9783527644506.ch16
10. Mandic A, Hansson J, Linder S, Shoshan MC (2003) Cisplatin induces endoplasmic reticulum stress and nucleus-independent apoptotic signaling. J Biol Chem 278(11):9100–9106
11. Liu Y, Ye Y (2011) Proteostasis regulation at the endoplasmic reticulum: a new perturbation site for targeted cancer therapy. Cell Res 21(6):867–883
12. Dietrich A, Mueller T, Paschke R, Kalinowski B, Behlendorf T, Reipsch F, Fruehauf A, Schmoll H-J, Kloft C, Voigt W (2008) 2-(4-(tetrahydro-2H-pyran-2-yloxy)-undecyl)-propane-1,3-diamminedichloroplatinum(II): a novel platinum compound that overcomes cisplatin resistance and induces apoptosis by mechanisms different from that of cisplatin. J Med Chem 51(17):5413–5422
13. Tardito S, Bassanetti I, Bignardi C, Elviri L, Tegoni M, Mucchino C, Bussolati O, Franchi-Gazzola R, Marchiò L (2011) Copper binding agents acting as copper ionophores lead to caspase inhibition and paraptotic cell death in human cancer cells. J Am Chem Soc 133 (16):6235–6242
14. Karpas A, Harder L, Czepulkowski B, Bloxham D, Saward R, Dremucheva A, Siebert R (2005) Studies of four new human myeloma cell lines. Leuk Lymphoma 46(1):101–112
15. Kurtoglu M, Philips K, Liu H, Boise LH, Lampidis TJ (2010) High endoplasmic reticulum activity renders multiple myeloma cells hypersensitive to mitochondrial inhibitors. Cancer Chemother Pharmacol 66(1):129–140
16. Healy SJ, Gorman AM, Mousavi-Shafaei P, Gupta S, Samali A (2009) Targeting the endoplasmic reticulum-stress response as an anticancer strategy. Eur J Pharmacol 625 (1–3):234–246
17. Che C-M, Siu F-M (2010) Metal complexes in medicine with a focus on enzyme inhibition. Curr Opin Chem Biol 14(2):255–261
18. Zhang J-J, Sun RW-Y, Che C-M (2012) A dual cytotoxic and anti-angiogenic water-soluble Gold(III) complex induces endoplasmic reticulum damage in HeLa cells. Chem Commun 48 (28):3388–3390
19. Sun RW-Y, Lok C-N, Fong TT-H, Li CK-L, Yang ZF, Zou T, Siu AF-M, Che C-M (2013) A dinuclear cyclometalated Gold(III)-phosphine complex targeting thioredoxin reductase inhibits hepatocellular carcinoma in vivo. Chem Sci 4:1979–1988
20. Kwong W-L, Sun RW-Y, Lok C-N, Siu F-M, Wong S-Y, Low K-H, Che C-M (2013) An Ytterbium(III) Porphyrin induces endoplasmic reticulum stress and apoptosis in cancer cells: cytotoxicity and transcriptomics studies. Chem Sci 4:747–754

21. Sun RW-Y, Chow AL-F, Li X-H, Yan JJ, Chui SS-Y, Che C-M (2011) Luminescent cyclometalated platinum(II) complexes containing N-Heterocyclic carbene ligands with potent in vitro and in vivo anti-cancer properties accumulate in cytoplasmic structures of cancer cells. Chem Sci 2:728–736
22. Uesugi H, Tsukuda T, Takao K, Tsubomura T (2013) Highly emissive Platinum(II) complexes bearing carbene and cyclometalated ligands. Dalton Trans 42:7396–7403
23. Godbert N, Pugliese T, Aiello I, Bellusci A, Crispini A, Ghedini M (2007) Efficient, ultrafast, microwave-assisted syntheses of cycloplatinated complexes. Eur J Inorg Chem 32:5105–5111
24. Jin C-M, Twamley B, Shreeve JM (2005) Low-melting dialkyl- and bis(polyfluoroalkyl)-substituted 1,1′-methylenebis(imidazolium) and 1,1′-methylenebis(1,2,4-triazolium) bis (trifluoromethanesulfonyl)amides: ionic liquids leading to bis(N-heterocyclic carbene) complexes of palladium. Organometallics 24(12):3020–3023
25. Kumar CV, Asuncion EH (1993) DNA binding studies and site selective fluorescence sensitization of an anthryl probe. J Am Chem Soc 115(19):8547–8553
26. Samari F, Hemmateenejad B, Shamsipur M, Rashidi M, Samouei H (2012) Affinity of two novel five-coordinated anticancer Pt(II) complexes to human and bovine serum albumins: a spectroscopic approach. Inorg Chem 51(6):3454–3464
27. Schneider CA, Rasband WS, Eliceiri KW (2012) NIH Image to ImageJ: 25 years of image analysis. Nat Methods 9(7):671–675
28. Sun RW-Y, Li CK-L, Ma D-L, Yan JJ, Lok C-N, Leung C-H, Zhu N, Che C-M (2010) Stable anticancer Gold(III)-porphyrin complexes: effects of porphyrin structure. Chem Eur J 16 (10):3097–3113
29. Lai S-W, Liu Y, Zhang D, Wang B, Lok C-N, Che C-M, Selke M (2010) Efficient singlet oxygen generation by luminescent 2-(2′-Thienyl)pyridyl cyclometalated Platinum(II) complexes and their calixarene derivatives. Photochem Photobiol 86(6):1414–1420
30. Zou T, Lok C-N, Fung YME, Che C-M (2013) Luminescent Organoplatinum(II) complexes containing bis(N-heterocyclic carbene) ligands selectively target the endoplasmic reticulum and induce potent photo-toxicity. Chem Commun 49(47):5423–5425
31. Liu J, Leung C-H, Chow AL-F, Sun RW-Y, Yan S-C, Che C-M (2011) Cyclometalated Platinum(II) complexes as topoisomerase IIα poisons. Chem Commun 47(2):719–721
32. Díez Á, Forniés J, Fuertes S, Lalinde E, Larraz C, López JA, Martín A, Moreno MT, Sicilia V (2009) Synthesis and luminescence of cyclometalated compounds with nitrile and isocyanide ligands. Organometallics 28(6):1705–1718
33. Tong GS-M, Che C-M (2009) Emissive or nonemissive? A theoretical analysis of the phosphorescence efficiencies of cyclometalated platinum(II) complexes. Chem Eur J 15 (29):7225–7237
34. Lo KK-W, Choi AW-T, Law WH-T (2012) Applications of luminescent inorganic and organometallic transition metal complexes as biomolecular and cellular probes. Dalton Trans 41(20):6021–6047
35. Lai E, Teodoro T, Volchuk A (2007) Endoplasmic reticulum stress: signaling the unfolded protein response. Physiology 22:193–201
36. Green DR, Reed JC (1998) Mitochondria and apoptosis. Science 281(5381):1309–1312
37. Smiley ST, Reers M, Mottola-Hartshorn C, Lin M, Chen A, Smith TW, Steele GD, Chen LB (1991) Intracellular heterogeneity in mitochondrial membrane potentials revealed by a J-aggregate-forming lipophilic cation JC-1. Proc Natl Acad Sci U S A 88(9):3671–3675

Chapter 6
Summary and Evaluation

Small molecules–biomacromolecules interactions represent one of the most important biological interactions in living organisms. This thesis is focused on the design, synthesis, and anticancer properties of small gold(III), gold(I), and platinum (II) molecules. Importantly, N-heterocyclic carbene ligands have been introduced to optimize the thermodynamic stability and reaction kinetics of these metal complexes with biomolecules. The Au(III)–NHC complexes described in Chap. 3 selectively reacted with thiol-containing biomolecules and thus act as dual thiol "switch-on" probes and anticancer agents. The dinuclear gold(I)–bisNHC–diphosphine complex described in Chap. 4 shows a favorable stability (reactivity) and is a promising drug candidate to be further developed for cancer treatment. The highly luminescent Pt(II)–bisNHC complex (Chapter 5) selectively targets the endoplasmic reticulum and induces potent cytotoxicity.

In recent years, anticancer gold complexes have attracted increasing attention, especially since the discovery of anticancer gold(III) porphyrin complexes 10 years ago. Stability is a key concern in the design of both gold(III)- and gold(I)-based medicines. For gold(III) complexes, strong chelating ligands (such as porphyrin) should be utilized to avoid facile reduction by cellular reducing agents. Alternatively, taking advantage of the intrinsic reducing properties in physiological solutions, and the associated coordination number change from 4 of Au^{3+} to 2 of Au^{+}, gold(III) complexes have been developed as prodrugs/precursors of anticancer gold(I) complexes and luminescent thiol "switch-on" probes. This novel concept may have lasting impact on the design of gold-based anticancer agents and delivery systems. For gold(I) complexes, despite that the past 10 years have witnessed burgeoning outputs on gold(I) complexes' anticancer properties, such studies mainly describe in vitro studies (cell-based) but seldom examples of in vivo (whole animal-based) investigation. One possible reason for the lack of in vivo anticancer activity is the high reactivity with off-target blood thiols (e.g., serum albumin) of these compounds. Thus, the development of gold(I) complexes with enough stability to avoid binding with blood thiols, while possessing sufficient reactivity to inhibit cellular thiol-containing enzymes, is of critical importance to achieve in vivo

T. Zou, *Anti-Cancer N-Heterocyclic Carbene Complexes of Gold(III), Gold(I) and Platinum(II)*, Springer Theses, DOI 10.1007/978-981-10-0657-9_6

active drugs. The dinuclear gold(I) complex containing a bisNHC and a diphosphine ligand constitutes an important scaffold showing favorable thiol reactivity to achieve in vivo antitumor activity. Future studies will investigate the detailed mechanisms of action and the efficacy of these compounds in large animals.

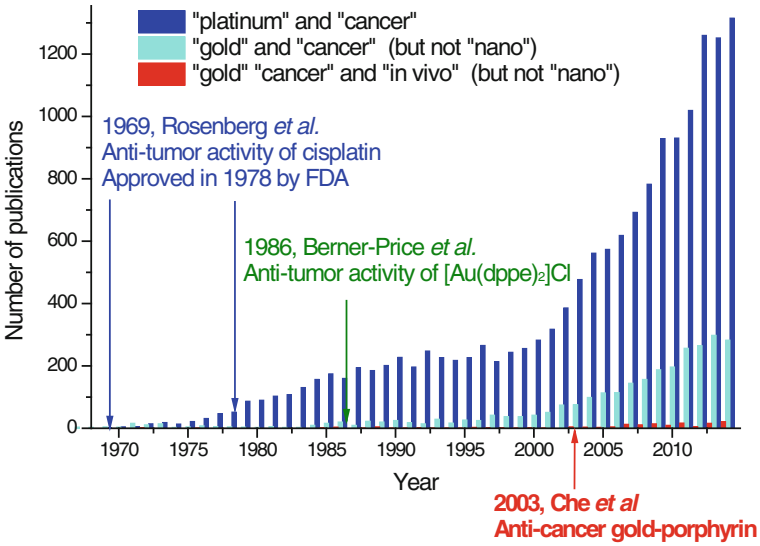

Unlike the gold complexes which are reactive in biological systems (Chaps. 3 and 4), the platinum(II) complexes described in Chapter 5 are stable in physiological conditions. In view of the intrinsic emission properties of these Pt(II) complexes, their anticancer action mechanism can be easily elucidated by fluorescence microscopy. More importantly, these phosphorescent metal complexes have long-lived excited states that generate reactive oxygen species which could contribute to their potent photo-cytotoxicity.

Collectively, the NHC complexes of gold(III), gold(I), and platinum(II) in this thesis have shown potent anticancer activities in vitro and in vivo. By fine-tuning the reactivity of these metal complexes with biomolecules, in connection with more in-depth biological studies, the metal–NHC complexes will potentially make impactful contributions to clinical cancer treatment.